TECHNISCHE UNIVERSITÄT MÜNCHEN
TUM Campus Straubing für Biotechnologie und Nachhaltigkeit

Exploring enzyme promiscuity to unlock new-to-nature reactions for biocatalysis

Samed Güner

Vollständiger Abdruck der von der promotionsführenden Einrichtung TUM Campus Straubing für Biotechnologie und Nachhaltigkeit der Technischen Universität München zur Erlangung des akademischen Grades eines

Doktors der Naturwissenschaften (Dr. rer. nat.)

genehmigten Dissertation.

Vorsitz:	Prof. Dr. Marc Ledendecker
Prüfer*innen der Dissertation:	1. Prof. Dr. Volker Sieber
	2. Prof. Dr. Wilfried Schwab

Die Dissertation wurde am 06.10.2022 bei der Technischen Universität München eingereicht und von der promotionsführenden Einrichtung TUM Campus Straubing für Biotechnologie und Nachhaltigkeit am 07.02.2023 angenommen.

“Science is hard, there is nothing easy about being a scientist, but that’s exactly why it’s so much fun and why it’s worth working at.” – *Frances H. Arnold*

ABSTRACT

The transition to a sustainable global society is a major challenge. The key requirements for the chemical industry are decarbonization, defossilization and plastic pollution control. Biocatalysis can be an important factor on this journey, since it is usually a green and sustainable technology. Despite the tremendous achievements in this field, the biocatalytic *de novo* synthesis of complex compounds based on simple building blocks is still a difficult task. This derives from the shortcomings of the biocatalytic toolbox, as the availability of sophisticated biocatalysts remains limited. Thus, tailoring and expansion of the biocatalytic toolbox is crucial, especially with respect to oligomerization of C_1 synthons and access to novel reaction mechanisms.

The first part of this study was focused on the biocatalytic assembly of a C_4 carbon skeleton derived from formaldehyde, a sustainable C_1 building block. For this, the enzyme formolase was tailored by advanced protein engineering methods from a three-carbon producer to sets of variants with enhanced two-carbon ($C_1 + C_1$) or four-carbon ($C_2 + C_2$) activity. The establishment of a high-throughput combinatorial screening enabled the evaluation of each single variant in terms of glycolaldehyde (C_2), dihydroxyacetone (C_3) and erythrulose (C_4) activity. This facilitated the targeted identification of variants with desired properties. By applying variants from both sets in a synthetic enzyme cascade, the hitherto fixation of formaldehyde was extended by a C_1 unit and the functional C_4 sugar erythrulose was produced. Recently, glycolaldehyde has been recognized as a promising C_2 platform molecule that can be provided in the future by technical fixation of carbon dioxide. To this end, the potential of the most promising variant (>30-fold lower K_m value; >10-fold increased catalytic efficiency) was demonstrated in a fully atom-economical biocatalytic process. Starting from 25.0 g L^{-1} glycolaldehyde, 24.6 g L^{-1} erythrulose (98% theoretical yield) was produced, the highest concentration achieved *in vitro* to date.

In the second part of this study, the development of new-to-nature biocatalysts was explored by targeting alkylsulfatases as a platform to unlock novel reaction mechanisms. For this, the inverting *sec*-alkylsulfatase PISA1, which catalyzes the hydrolysis of alkyl sulfate esters (via S_N2), was identified as an appropriate protein scaffold. In addition, the new alkylsulfatases CmAS, FtAS and VpAS were identified using a sequence-driven approach with emphasis on conserved protein motifs. Several methods for the preparation of metal-free alkylsulfatase scaffolds were presented. Coordination of Ni(II) by PISA1 allowed the utilization of ammonia as a nucleophile, resulting in a primary aliphatic amine instead of the corresponding alcohol. However, different functional properties were observed depending on the enzyme preparation, which made reproducibility a challenge. Metal ion screening with 18 multivalent metal cations using the protein scaffolds of CmAS and VpAS showed the impact of metal ions on the substrate scope. The use of Eu(II) for the natural hydrolysis of a sulfate ester bond was one of the highlights. In addition, a second non-natural reaction was discovered that produced unbranched alkenyl arenes.

ACKNOWLEDGEMENTS

Foremost, I would like to thank my doctoral advisor, Prof. Dr. Volker Sieber. Your supervision has contributed significantly to my scientific and personal development. Thank you for your trust, your great interest in my work, and for keeping me encouraged and challenged. You always gave me the right balance between individual freedom and scientific support. Even on the busiest days, you made time for constructive discussions. I am grateful for the opportunity to work and grow under your guidance.

Many thanks to Prof. Dr. Wilfried Schwab for reviewing and examining this thesis. I would also like to thank Prof. Dr. Marc Ledendecker, the chair of my thesis committee, who ensured my defense went smoothly. Special thanks to my mentor Dr. Stefan Gilch (Evonik Industries AG), for his commitment and for helping me better to access science from an industrial point of view. Not to forget Prof. Bastian Blombach, who encouraged me to start the writing process.

I am very grateful for all the cross-chair collaborations that have added depth to this work. Prof. Dr. Iris Antes and Dr. Okke Melse with QM/MM simulations. Prof. Dr. Arne Skerra and Dr. Christian Deuschle with protein mass spectrometry. Prof. Dr. Johannes Buchner with access to the CD spectrometer, and Dr. Annika Strauch with guidance during the measurement. Prof. Dr. Gerhard Schenk *via* insightful discussions on metallo-β-lactamases.

Furthermore, I would like to express my gratitude to the permanent staff of the chair. Elisabeth Aichner, who guided me through all the administrative challenges and shared her wisdom in all aspects. Dr. Broder Rühmann and Petra Lommes for their advice and help with the analytics. Dr. Doris Schieder for organizing the lecturers. Magdalena Haslbeck, Manuel Döring, Anja Schmid, and Lena Würstl for their technical support in the lab.

As a graduate student, I worked with many talented scientists, including those not mentioned here. Therefore, I thank CBR's past and present members for their scientific input, enjoyable working atmosphere, and all the favors. In particular, Dr. Samuel Sutiono and Ioannis Zachos. Our daily lab interactions, creative discussions about science, and your engagement in my projects are priceless, from coworkers to true friends. Further, it was a great pleasure to share my hands-on experience with Vannesa Wegat and push together the utilization of C_1 carbon sources. The regular practice for our team marathon (Torben Hüsing, Korbinian Sinzinger, and Robert Genth) was a crucial physical challenge for me. The now traditional game nights have entertained me and enhanced my strategic thinking—thanks to all who participated.

My sincere gratitude to my family and especially to my parents. Ihr wart immer für mich da und habt mir ein wunderbares Leben ermöglicht. Eure Unterstützung und der sichere Hafen, den Ihr mir geboten habt, haben all das erst möglich gemacht.

TABLE OF CONTENTS

ABBREVIATIONS

°C	Degree Celsius
3D	Three-dimensional
Å	Angstrom (1 x 10^{-10} m)
AA	Amino acid
AI	Autoinduction
APS	Ammonium persulfate
bp	Base pairs
BSA	Bovine serum albumin
C	Carbon
CO_2	Carbon dioxide
Da	Dalton
DA-64	N-(carboxymethylamino-carbonyl)-4.4'-bis-(dimethylamino)-diphenylamine
DHA	Dihydroxyacetone
DMSO	Dimethyl sulfoxide
DNA	Deoxyribonucleic acid
DNase	Deoxyribonuclease
dNTPs	Deoxyribonucleotides
EDTA	Ethylenediaminetetraacetic acid
ERY	Erythrulose
FALD	Formaldehyde
FLS	Formolase
g	Gram
GALD	Glycolaldehyde
h	Hour
HEPES	4-(2-hydroxyethyl)-1-piperazineethane sulfonic acid
HOMO	Highest occupied molecular orbital
HPLC	High performance liquid chromatography
HTS	High-throughput screening
IMAC	Immobilized metal affinity chromatography
IPTG	Isopropyl β- d-1-thiogalactopyran
kb	Kilo base pairs
k_{cat}	Turnover number
k_{cat}/K_m	Catalytic efficiency
K_m	Michaelis-Menten constant
L	Liter
LB	Lysogeny broth
m	Meter
M	Molar

MBL	Metallo-β-lactamase
mg	Milligram
min	Minute
mL	Milliliter
mM	Millimolar
MOPS	3-(N-morpholino)propanesulfonic acid
MQ-H_2O	Milli-Q® pure water
N	Nitrogen
NAD^+	Nicotinamide adenine dinucleotide (oxidized)
NADH	Nicotinamide adenine dinucleotide (reduced)
OD	Optical density
rpm	Rotation per minute
RT	Room temperature
s	Second
SDS-PAGE	Sodium dodecyl sulfate – polyacrylamide gel electrophoresis
SEC	Size exclusion chromatography
SOC	Super optimal broth with catabolite repression
TAE	TRIS acetic acid EDTA buffer
TB	Terrific broth
TEMED	N,N,N,N-Tetramethylethane-1,2-diamine
ThDP	Thiamine diphosphate
T_m	Melting temperature
TRIS	Tris(hydroxymethyl)aminomethane
UV	Ultraviolet
V	Volt
x g	Earth´s gravitational force (10 N/kg)

LIST OF PUBLICATIONS

1. **Güner, S.**, Wegat, V., Pick, A. & Sieber, V. (2021). Design of a synthetic enzyme cascade for the *in vitro* fixation of a C_1 carbon source to a functional C_4 sugar. *Green Chemistry*, 23(17), 6583-6590.

2. **Güner, S.,** Lommes, P., Schenk, G. & Sieber, V. (2023). Exploring novel alkylsulfatases as a platform for artificial metalloenzymes to access new-to-nature reactions. (submitted)

3. Zachos, I., **Güner, S.**, Essert, A., Lommes, P. & Sieber, V. (2022). Boosting artificial nicotinamide cofactor systems. *Chemical Communications*, 58(85), 11945-11948

4. Sinzinger, K., Obst, U., **Güner, S.**, Schieder, D. & Sieber, V. (2023). *Pichia pastoris* enzyme production platform: from combinatorial library screening to bench-top fermentation on residual cyanobacteria biomass. (submitted)

5. Wegat, V., **Güner, S.**, Döring, M., Fabarius, J., Roth, A. & Sieber, V. (2023). Robot-aided high-throughput engineering of FLS enzyme for *in vivo* application. (submitted)

LIST OF TABLES

Page

LIST OF FIGURES

Page

LIST OF EQUATIONS

Page

1. INTRODUCTION

1.1 Biocatalysis

The field of biocatalysis has undergone tremendous development in recent decades and nowadays exhibits a significant impact on chemical synthesis – both in industry and academia.[1,2] Central to this is the ongoing tailoring of biocatalysts and the expansion of the accessible chemical reactions for the targeted synthesis of pharmaceuticals, chemicals and food ingredients.[3] These are based on biological transformations facilitated by partially purified enzymes or enzyme containing cells, so-called biocatalysts.[4] In the early days, biocatalytic processes had to be designed around the limitations of the respective biocatalysts, whereas today key developments enable the adaptation of biocatalysts to the manufacturing process.[5] This evolution in the field of biocatalysis progressed in several waves.[6]

1.1.1 The potential of biocatalytic processes

The emergence of two requirements for organic synthesis contributed decisively to the increased use of biocatalysts in industrial processes. First, in the mid-1980s, the importance of stereoisomerism for drug action became evident. In response, the FDA (U.S. Food and Drug Administration) introduced regulations that both enantiomers of chiral drugs must be tested separately.[4] The need for cost-effective catalysts suitable for enantioselective synthesis ultimately led to the recognition that enzymes were promising catalysts.[1] Second, in the 1990s, the impact of industrial manufacturing on the environment, including global warming, as well as the deterioration of the natural habitat and its biodiversity, became apparent.[7,8] Thereupon, the approach of green chemistry with stronger environmental responsibility was developed in chemical synthesis. The 12 principles of green chemistry[9] defined by Anastas and Warner in 1998, aimed at preventing waste, cleaner processes and the extensive use of renewable resources, are receiving more attention today than ever before. Biocatalytic processes fulfill 10 of the 12 principles of green chemistry, making it a truly green and sustainable technology (Table 1.1).[10]

Table 1.1: Green chemistry and biocatalysis.

	Green chemistry principle	Biocatalysis
01	Waste prevention instead of remediation	Significantly reduced waste
02	Atom economy	More atom- and step-economical
03	Less hazardous syntheses	Generally low toxicity
04	Design for safer products	Not relevant (product not process)
05	Safer solvents and auxiliaries	Usually performed in water
06	Energy efficiency	Mild conditions/energy efficient
07	Renewable feedstocks	Enzymes are renewable
08	Shorter synthesis (avoid derivatization)	Avoids protection/deprotection steps
09	Catalytic rather than stoichiometric reagents	Enzymes are catalysts
10	Design products for degradation	Not relevant (product not process)
11	Real-time analysis	Applicability to biocatalytic processes
12	Inherently safer processes	Mild and safe conditions

Adapted from “Role of Biocatalysis in Sustainable Chemistry” by Sheldon and Woodley, *Chem. Rev.* 2018.[10]

In the development of new production processes, sustainability is now increasingly prioritized.[11] In this context, it is widely recognized that biocatalysts possess important advantages over conventional chemical catalysts (Table 1.2).[12,13] A biocatalyst is produced from renewable resources and is biocompatible, biodegradable and essentially harmless and non-toxic. In addition, enzymatic reactions are generally highly selective catalyzed allowing regio- and stereoisomers as well as different functional groups (chemoselectivity) to be discriminated. This avoids costly activation, protection and deprotection steps, resulting in routes that are more economical and generate less waste than conventional organic syntheses. Moreover, these reactions are usually carried out under mild conditions in aqueous solution at ambient temperature, physiological pH and atmospheric pressure.[14] This renders biocatalytic processes more environmentally friendly, cost-effective and therefore sustainable, while also allowing the combination of several biocatalysts to establish attractive cascade processes.[15] In short, biocatalysis is a genuine alternative to chemical catalysis, even from an industrial point of view.[16] Despite these sophisticated properties, there are still drawbacks associated with biocatalysis. For example, the lack of commercially available, well-characterized biocatalysts is a persistent concern.[17] The suggested advantage of mild reaction conditions also provides challenges. On the one hand, this creates a narrow operating window, so that variations in temperature, solvent, pH, ionic strength and salt type can lead to deactivation of an enzyme.[12] On the other hand, the high water solubility implies that proteins are not easily recovered and recycled. However, both of these problems can be addressed by developing effective methods to immobilize biocatalysts on solid supports or by retention through membranes to enable stabilization and multiple recycling for a cost-effective, environmentally friendly process.[18] Although many enzymes are sufficiently flexible to accept non-natural substrates, this is not true for the dependence on natural cofactors. Most of them are relatively unstable, expensive and often not replaceable by cheaper, artificial alternatives.[19] However, in recent years, impressive progress was achieved in the regeneration of natural cofactors and the use of artificial alternatives.[20–22]

Table 1.2: Key requirements of sustainable industrial catalysts.

Requirement	Metal-based catalysis	Fermentation (growing cells)	Biocatalysis (resting cells)	Biocatalysis (isolated enzymes)
High selectivity operation	🟡	🟡	🟡	🟢
Under mild conditions	🔴	🟢	🟢	🟢
Tunable properties	🟡	🟢	🟢	🟢
Renewable catalyst	🔴	🟢	🟢	🟢
Degradable catalyst	🔴	🟢	🟢	🟢
Operation at high product conc.	🟢	🟡	🟡	🟡
High catalyst stability	🟢	🟡	🟡	🟡
Catalytic rate	🟢	🔴	🟡	🟢

Adapted from "Ensuring the Sustainability of Biocatalysis" by Woodley, *ChemSusCem* 2022.[13]
🟢 Required performance in the majority of cases
🟡 Performance requires improvement in the majority of cases
🔴 Performance does not meet the requirement

In addition, substrate and/or product inhibition can lead to a decrease in reaction rate, which can limit the efficiency of the process.[23] Major achievements in bioinformatics, combined with next-generation sequencing technologies and advances in protein engineering, enable biocatalysts to be tailored to the ideal process today.[24–26] This provides the ability to tune the properties of the biocatalyst more readily, compared to traditional chemical catalysts.[13] Key characteristics such as activity, stability and selectivity can be tailored to fulfill important industrial process parameters such as substrate and product concentration, yield, catalyst and volume productivity (space-time-yields) and reaction time.[27] In addition, new biocatalysts can be engineered to possess non-native catalytic functions.[28] This means that modern tools, including computational protein design and machine learning are used to engineer enzymes that catalyze reactions that are not found in nature (new-to-nature biocatalysis).[29] In fact, the industrial application of biocatalysis enables a biobased circular economy, whereby chemicals, pharmaceuticals or food additives are produced from renewable resources.[8] However, for already established traditional processes, it is essential that biocatalysis outperforms such processes before the industry will consider replacing an existing plant with a biocatalytic solution.

1.1.2 The evolution of the biocatalysis landscape

The cornerstone of modern biocatalysis was the discovery that living cells are not necessarily required for biological transformations.[30] The catalytic components (enzymes) present in cell extracts are sufficient to perform chemical reactions, as Eduard Buchner proved more than a century ago.[31] Expanding on this, Ludwig Rosenthaler reported the first enantioselective organic synthesis by producing (*R*)-mandelonitrile from benzaldehyde and hydrogen cyanide using an extract of bitter almonds.[32] In the following decades, the focus was on identification and application of suitable, naturally occurring enzymes, respecting all shortcomings of poorly defined biocatalysts.[33] The invention and greater accessibility of key technologies in the 1970s and 1980s, such as recombinant DNA technology,[34] DNA sequencing,[35] polymerase chain reaction (PCR),[36] X-ray crystallography,[37] and the founding of the Protein Data Bank (PDB),[38] enabled much more efficient production of proteins with recombinant expression hosts, as well as a deeper understanding of enzymatic functions and mechanisms. Together with the development of rational design of proteins based on site-directed mutagenesis, introduced by Michael Smith in 1978,[39] the way was paved for tailoring of protein structures and catalytic properties. This allowed biocatalysts to be optimized for non-natural substrates to synthesize unusual synthetic intermediates.[5] However, the engineering of an enzyme required knowledge of the respective protein structure and mechanism. Typically, this process took years to complete. The invention of directed evolution in the 1990s, a process for the laboratory evolution of proteins, greatly accelerated the engineering of an enzyme.[40] This process comprises iterative cycles of random changes in a protein's amino acid sequence, followed by screening (or selection) of the resulting libraries for variants with desired properties.[41] Methods for the preparation of such

libraries are usually based on random mutagenesis[42,43] or *in vitro* recombination.[44,45] However, large libraries are generated and usually only a few variants display the targeted improvements, therefore a high-throughput and appropriate screening is essential. In order to reduce the screening effort, attention was shifted to smarter libraries, which are significantly smaller and cover the functional space (active site) more effectively.[46] Thereby, the constantly advancing knowledge of protein sequences, structures and functions, as well as computer-assisted prediction algorithms, *in silico* engineering and docking studies are utilized to select promising target sites.[47] By using a semi rational approach in which the selected positions are randomized individually or in combination by site saturation mutagenesis, the size of the library can be significantly reduced while the functional content is increased.[48] The progressive establishment of technological innovations nowadays renders powerful tools for rational design and directed evolution, greatly advancing the development of novel biocatalysts. This opens up new synthetic routes as well as simplifying existing pathways for the production of complex compounds. Machine learning tools[49] for artificially evolved enzymes, highly accurate prediction of three-dimensional protein structures by the deep learning algorithm AlphaFold2[50] and microfluidics[51] as an ultra-high-throughput screening platform should be emphasized here. Thus, it seems that the field of biocatalysis is entering the next evolutionary stage.[33]

1.2 Biocatalytic *de novo* synthesis of complex compounds

Tremendous efforts in the field of biocatalysis and associated research areas have matured it into an attractive technology that is gaining importance for the transition to sustainable industrial chemistry.[52] These include biocatalytic solutions to decarbonization (carbon-negative production), defossilization (production from renewable resources), and plastic pollution control (recycling of plastics and use of biobased alternatives).[8] Recently, more and more efforts are devoted to biocatalytic *de novo* synthesis (total synthesis) of complex compounds based on simple building blocks, so-called synthons (Figure 1.1), targeting a more sustainable, resource efficient and step economical synthesis. Here, advances in protein engineering and the ability to implement novel catalytic functions are used to modify existing pathways or design artificial enzymatic routes.[53,54] In this context, the selective formation of carbon–carbon (C–C) bonds, the incorporation of functional groups and the catalysis of reactions not found in nature's repertoire are of great benefit.[1] The scope of chemical reactions accessible *via* biocatalysis increased dramatically in recent years driven by the discovery and development of novel biocatalysts. However, the availability of sophisticated biocatalytic tools for the assembly of synthetic compounds remains limited, which is also a major barrier to the routine use of enzymes in organic synthesis. To this end, continuous expansion and tailoring of the biocatalytic toolbox is crucial, especially with respect to the formation of non-natural C–C bonds and access to novel enzymatic reaction mechanisms.[3,55] This will allow increased use of one-carbon (C_1) building blocks for the synthesis of complex compounds in the future, thus driving the decarbonization and defossilization of the chemical industry and ensuring a broader range of accessible products.

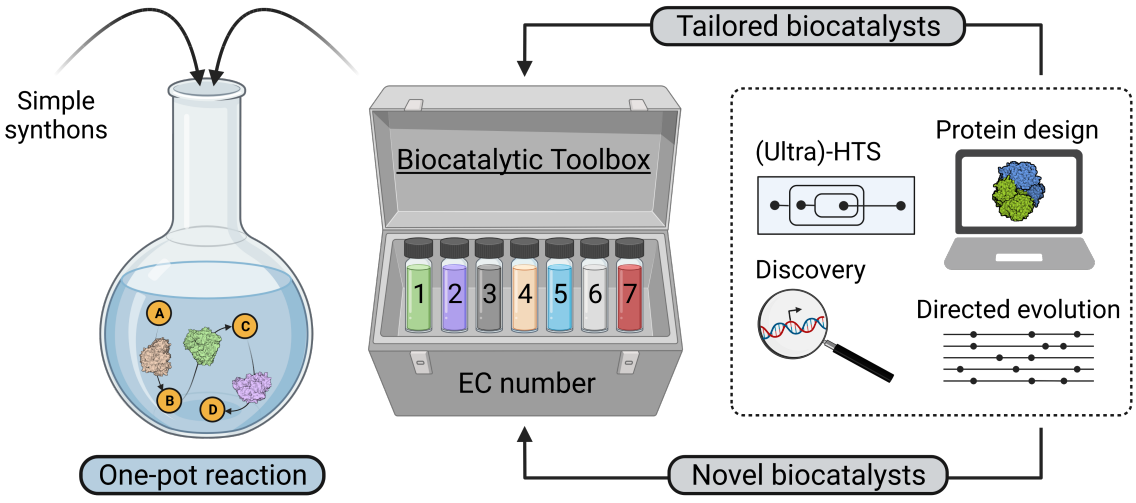

Figure 1.1: Biocatalytic *de novo* synthesis of a target compound. The biocatalytic toolbox is composed of a variety of accessible enzymatic reactions, which are catalyzed by a range of enzymes. The scope of the current biocatalytic toolbox enables the targeted synthesis of various complex compounds from relatively simple starting materials. For the synthesis, appropriate biocatalysts are selected and combined in powerful cascade processes, which are performed either *in vitro* in a one-pot reaction or *in vivo*. Advanced technologies in protein engineering will enable the further expansion of this biocatalytic toolbox through the tailoring of biocatalysts and the discovery and development of novel enzymes. This will broaden the range of compounds accessible by biocatalytic *de novo* synthesis in the future.

1.2.1 Biocatalytic toolbox for C–C bond formation

The biocatalytic tools already available facilitated the development of powerful enzymatic cascades for an efficient synthesis of target molecules. To assemble the core structure, the selective formation of C–C bonds is essential to enable *de novo* synthesis from simple and inexpensive building blocks. The biocatalytic toolbox features numerous enzymes that perform the formation of these bonds to build natural primary and secondary metabolites.[3] This is often mediated by a nucleophilic attack on an aldehyde. From the perspective of biocatalytic retrosynthesis,[56] the use of hydrogen cyanide as a nucleophile or the umpolung of a second aldehyde leads to 1,2 disconnections. In contrast, the use of enols or enolates results in 1,3 disconnections.[1] However, the availability of biocatalysts suitable for the formation of synthetic C–C bonds is limited due to insufficient enzyme promiscuity. Therefore, industrial applications are typically restricted to a small subset of lyases to perform aldol reaction, cyanohydrin formation and acyloin condensation.[55]

1.2.1.1 Aldol reaction

The aldol reaction is a key biochemical process for the formation of naturally occurring metabolites. During this aldol addition, the coupling of an enol or enolate with a carbonyl compound is catalyzed, producing β-hydroxyketones. A high degree of control is required to define which carbonyl compound acts as a donor (nucleophile) and which as an acceptor (electrophile). Nature optimized this type of stereospecific C–C bond formation in the form of aldolases.[57] However, when two or more stereocenters are created, the preferred configuration can be biased by kinetics (when differences in activation energy are large) or by thermodynamic stability of the stereoisomers (when differences in activation energy are small).[58] This effect was also observed for non-enzymatic catalyzed reactions.[59] Aldolases are ubiquitous enzymes that can be divided into 4 groups according on the accepted donor or into 3 types depending on the activation mode of the donor carbonyl group (Figure 1.2).

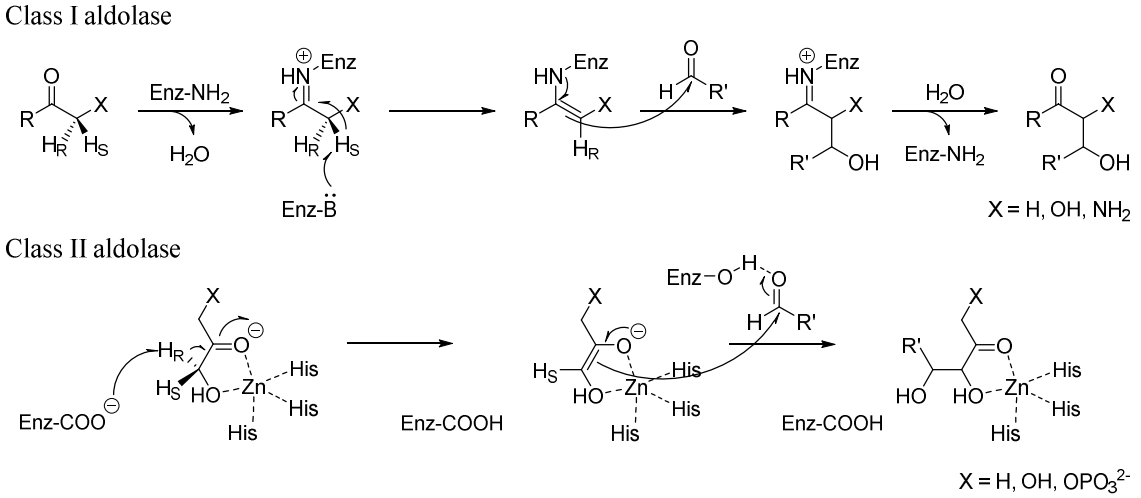

Figure 1.2: Proposed mechanism of class I and class II aldolases. Adapted from "C–C Bond-Forming Lyases in Organic Synthesis" by Brovetto *et al*., *Chem. Rev.* 2011.[60]

Class I aldolases activate the donor by forming an imine (Schiff base) *via* a conserved lysine in the active site. The activated donor attacks then the acceptor with high selectivity, forming an enamine.[61] Class II aldolases, on the other hand, are found mainly in microorganisms and generally demonstrated higher stability. These are metalloenzyme that usually use Zn(II) as a cofactor, although Co(II) and Fe(II) can also be active. The coordinated transition metal ion acts as a Lewis acid and supports the activation of the donor.[62,63] In addition, some aldolases are dependent on the cofactor pyridoxal phosphate (PLP), which is essential for donor activation *via* quinoide aldimine intermediate.[64] Regardless of the type of activation, which implies an enolizable donor (C_2 or higher), only a few aldolases demonstrated to tolerate C_1 compounds as acceptors.[65] The aldol addition is an important reaction from an industrial point of view. A well-characterized example is represented by 2-deoxyribose-5-phosphate aldolases (DERA), which catalyze the reversible condensation of acetaldehyde and glyceraldehyde-3-phosphate (G3P) producing 2-deoxyribose-5-phosphate. The formation of a stable hemiacetal then leads to the shift of the reaction equilibrium to the aldol side.[66] Sensitivity to high acetaldehyde concentrations presented a challenge that was addressed by protein engineering while also expanding the scope for non-natural substrates.[67,68] DERA is used in various industrial production processes, especially for the side chains of statins.[69] Whereas, the production of non-phosphorylated ketoses and aldoses was enabled by the discovery of D-fructose-6-phosphate aldolase (FSA). This was the first aldolase that accepted non-phosphorylated ketones and aldehydes as donor, such as dihydroxyacetone, hydroxyacetone and glycolaldehyde.[70] Subsequently, the biocatalyst was tailored for various substrate.[71] For example, variant A129S showed a 17-fold increase in catalytic efficiency when using the C_3 ketose dihydroxyacetone as a donor.[72] FSA^{A129S} in resting cells (30 g L^{-1}) was applied for the synthesis of L-erythrulose from dihydroxyacetone and formaldehyde, achieving a yield of 252 g L^{-1}.[73]

1.2.1.2 Cyanohydrin formation

Hydroxynitrile lyases, which catalyze the reversal decomposition of cyanohydrins, are used by a variety of organisms, plants and animals to release hydrogen cyanide (HCN) as a defense mechanism. The reverse reaction is applied industrially to produce (*R*)- or (*S*)-α-hydroxy nitriles by enantioselective condensation of HCN with aldehydes or ketones (Figure 1.3A). The industrial synthesis of these 1,2 difunctional cyanohydrins, which are used as versatile building blocks, is usually performed at low pH in a two-phase system.

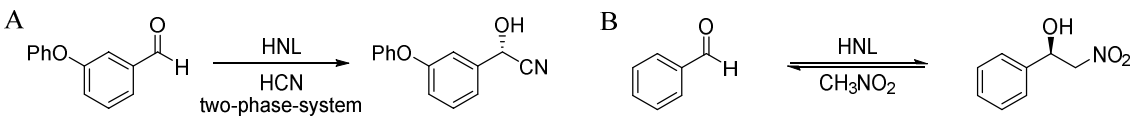

Figure 1.3: Hydroxynitrile lyase. (**A**) HNL are employed industrially in two-phase-systems and (**B**) equally the enantioselective Henry reaction can be performed. Adapted from "Biocatalysis making waves in organic chemistry" by Hanefeld *et al*., *Chem. Soc. Rev.* 2022.[1]

Thus, undesired background reactions are suppressed and high substrate loadings are achieved.[74] Recently, immobilized hydroxynitrile lyases were applied in flow biocatalysis,[75] where high space-time yields of up to 1.2 kg L^{-1} h^{-1} were achieved by using a single-phase organic solvent.[76] Moreover, this enzyme class showed sufficient promiscuity to utilize also nitromethane for nucleophilic attack (biocatalytic Henry reaction), allowing the formation of abiotic C–C bonds (Figure 1.3B).[77]

1.2.1.3 ThDP dependent umpolung

Thiamine diphosphate (ThDP) dependent enzymes are found in most organisms and catalyze a wide range of reactions. A subset of these biocatalysts can be used for the selective formation of C–C bonds.[78] The catalytic activity is based on a sophisticated mechanism mediated by the cofactor. The active site of the biocatalyst, on the other hand, is responsible for the selectivity of the reaction, defining accepted molecules and stereochemistry.[79] This provided an excellent platform for the catalysis of synthetic C–C bonds,[80] which is otherwise mainly dominated by non-enzymatic carbene catalysts.[81] The reaction mechanism is based on umpolung of carbonyl functions, allowing the generated nucleophilic carbon to be added to an electrophilic carbon center (Figure 1.4). For this, the ThDP cofactor is coordinated in the active site in a configuration in which its pyrimidine and thiazolium rings take an angle of 90 degrees to each other. The amino group of the aminopyrimidine ring is arranged in such a way that it can deprotonate the C2 atom of the thiazolium ring, thus forming a ylide that can also be considered a tautomeric carbene. A carbonyl compound (acceptor or electrophile) is coordinated by the active site to ideally position the ylide for nucleophilic attack, resulting in covalent bond. This can be either an aldehyde, a ketone (very rare due to steric hindrance) or an α-ketoacid (requires decarboxylation). Subsequently, an umpolung of the linked acceptor takes place, shifting the negative charge to the carbon of the carbonyl group. Thus, a reactive carbanion is generated, which can attack a second carbonyl compound (donor or nucleophile) and a new carbon–carbon bond is formed. The product is then released from the cofactor.[82]

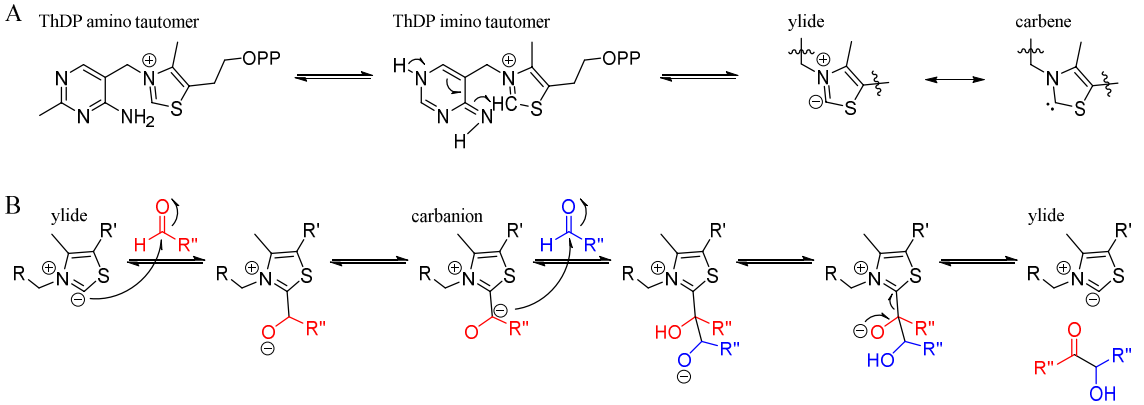

Figure 1.4: ThDP dependent carboligation of aldehydes *via* umpolung. (**A**) ThDP is coordinated by the enzyme so that the two aromatic rings are at close to 90° to each other. The amino group can then deprotonate the thiazole ring. (**B**) The resulting ylide then attacks an aldehyde. This results in a carbanion that attacks another carbonyl compound as donor. The new C–C bond is formed and the product released. This reaction is kinetically controlled. Adapted from "Biocatalysis making waves in organic chemistry" by Hanefeld *et al*., *Chem. Soc. Rev.* 2022.[1]

For the formation of C–C bonds, this is a powerful method.[60] However, the mechanism of the reaction is reversible, which is also true for the decarboxylation step.[83] Recently, this was exploited for the biocatalytic carboxylation of an abundant industrial intermediate (methional) to enable the synthesis of the essential amino acid L-methionine.[84] Moreover, this reaction mechanism indicated a promising potential for the realization of biocatalytic C_1 chemistry to enable the assembly of complex compounds from simple C_1 carbon sources.[65] Such synthetic routes necessitate direct coupling of two C_1 units, which is chemically challenging since the generation of C_1 nucleophiles is difficult, as opposed to C_1 electrophiles (for instance: CO_2 or formaldehyde).[85] As described above, the ThDP dependent umpolung can be used to invert the reactivity of a carbonyl compound, which also includes the C_1 compound formaldehyde. In recent years, a handful of ThDP dependent enzymes were engineered for the direct combination of formaldehyde molecules. The most prominent of these is a computationally redesigned enzyme called formolase, which catalyzes the new-to-nature carboligation of three molecules of formaldehyde.[86] Two additional ThDP dependent enzymes were similarly evolved to catalyze the selective combination of two formaldehyde molecules.[87,88] However, these biocatalysts showed low catalytic efficiencies, rendering the development of efficient synthetic routes challenging. The design of novel and the optimization of existing biocatalytic tools is indispensable to exploit the synthetic opportunities in this field.

1.2.2 Biocatalytic toolbox for ammonia based amination

In 2018, approximately 35% of the 200 top-selling small molecule drugs contained at least one chiral amine subunit in their structure.[89] Accordingly, the industrial demand for amine containing synthons is unabated. The pharmaceutical, agrochemical and chemical industries showed particular interest in primary chiral amines, which are applied as versatile building blocks for the synthesis of complex compounds.[90,91] However, chemical catalysis of these compounds is costly and requires the use of unsustainable transition metal catalysts and harsh reaction conditions.[92] Whenever chemocatalysis reaches its limits, the competitiveness of biocatalysis for industrial processes is strengthened. Biocatalysts such as ω-transaminases, amine dehydrogenases, reductive aminases and ammonia lyases, are promising tools for the synthesis of primary chiral amines (Figure 1.5). Nevertheless, the synthesis using inexpensive ammonia remains a challenge in synthetic chemistry.[93]

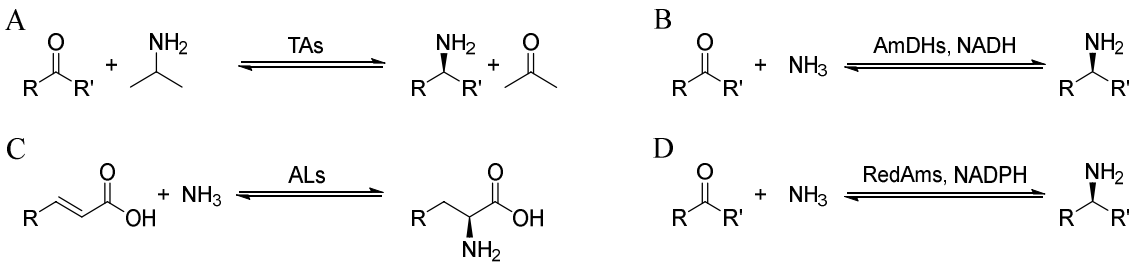

Figure 1.5: Biocatalytic toolbox to chiral primary amines. (**A**) Transaminases (TAs). (**B**) Amine dehydrogenases (AmDHs). (**C**) Ammonia lyases (ALs). (**D**) Reductive aminases (RedAms). Chirality presented only exemplary. Adapted from "A reductive aminase from *Aspergillus oryzae*" by Aleku *et al.*, *Nature Chem* 2017.[94]

1.2.2.1 ω-transaminases

Transaminases (TAs) are pyridoxal phosphate dependent enzymes and catalyze the reversible transfer of an amino group from a suitable donor (via pyridoxamine intermediate) to a carbonyl acceptor.[95] Here, donor, acceptor, product and co-product are in equilibrium, which often requires an excess of donor, *in situ* recycling or a follow-up reaction to shift the reaction to the product side.[91] TAs are divided into α-transaminases (substrate spectrum limited to α-ketoacids) and ω-transaminases (virtually any ketone or aldehyde functionality).[96,97] However, wild type enzymes often showed a limited substrate scope, as often only substrates with at least one small substituent (typically methyl or ethyl) were accepted. This issue was addressed by protein engineering to increase the capacity of the active site and to broaden the substrate range.[98] Hence, ω-TAs were applied industrially for the asymmetric synthesis of amines (up to 100% yield) or for the kinetic resolution of racemic amines.[99] Scientists from Codexis and Merck successfully tailored an (*R*)-selective ω-TA (ATA-117) for the synthesis of the antidiabetic drug sitagliptin phosphate. Semi-rational design and directed evolution were used to engineer the binding pocket of the enzyme for the target molecule.[100] By switching from a rhodium catalyst to the biocatalyst, total yield and productivity increased by 10% and 53%, respectively, while total waste decreased by 19%.[101]

1.2.2.2 Amine dehydrogenases

Advanced protein engineering methods enabled the tailoring of amine dehydrogenases (AmDHs) to catalyze the NAD(P)H dependent reductive amination of ketones to primary chiral amines. For this purpose, substrate specificities of amino acid dehydrogenases were successfully engineered. Unlike ω-TAs, which require a sacrificial amine source and release a co-product, these biocatalysts demonstrated to utilize ammonia directly.[102–104] This facilitates an increase in atom efficiency, under the condition that the use of a sacrificial substrate based cofactor regeneration system can be omitted.[105] Scientists demonstrated that a simultaneous inter-connected redox-neutral cascade overcomes this challenge. Here, an alcohol dehydrogenase is combined with an AmDH to convert alcohols into amines. The reducing equivalents released during the oxidation of the alcohol are directly used for the reductive amination of the ketone.[106] However, only a limited number of artificial AmDHs were developed so far, which furthermore showed a narrow substrate range (small aliphatic or aromatic ketones).[107,108] The recently discovered enzyme family of natural AmDHs provides greater diversity with the potential to facilitate substrate scope expansion in the future.[109] Although the number of characterized AmDHs is growing, industrial scalability of the catalyzed reductive amination is not achieved so far.[110]

1.2.2.3 Reductive aminases

Reductive aminases (RedAms) are reported as a subgroup of the imine reductases[111] (IRED) and catalyze in addition to the reduction of prochiral imines also the NAD(P)H dependent reductive amination of ketones.[94] However, such enzymes were mainly involved in the production of secondary and tertiary amines. Following the discovery of new RedAms, it was demonstrated that ammonia can also be used as an amine source. Thus, providing access to the synthesis of primary amines. Although this is the same reductive amination performed by amine dehydrogenases, RedAms offer a broader substrate range.[112]

1.2.2.4 Ammonia lyases

The family of ammonia lyases (ALs) is well studied and consists of structurally and mechanistically diverse enzymes that catalyze the reversible addition of ammonia to C=C double bonds (biocatalytic hydroamination).[113] However, ALs aminate only α,β-unsaturated carboxylic acids, leading mainly to the synthesis of α- and β-amino acids. This narrow substrate range severely limited the synthetic applicability of such biocatalytic tools.[114]

1.2.3 Biocatalytic toolbox for new-to-nature reactions

Although the scope of reactions accessible by biocatalysis has steadily expanded with the discovery of new classes of enzymes, limitations in C–N bond formation, C–C bond formation, halogenation, carbonylation, ether formation, as well as functionalization and reduction of C=C double bonds persist. To close this gap and expand the synthetic applicability of the biocatalytic toolbox, enzymes that catalyze non-natural reactions are required.[115] Accordingly, a strong demand has emerged for biocatalysts with novel properties for the synthesis of a broader range of molecules.[116] For the preparation of so-called new-to-nature biocatalysts, various approaches are pursued, such as the exploitation of natural enzymatic promiscuities, advanced protein engineering of enzymes with novel functions and the use of protein backbones as chiral carriers for abiotic cofactors.[117] These approaches have allowed researchers to identify numerous non-natural catalytic functions, providing a solid starting point for further protein optimization.[118]

1.2.3.1 Identification of the natural enzyme promiscuities

A number of natural biocatalysts exhibited a certain degree of catalytic flexibility, which describes the ability to perform a side reaction in addition to the main reaction. Enzymatic promiscuity can be related to both the acceptance of non-natural substrates and the type of reaction catalyzed. This property of a catalyst is referred to as versatile in other fields and offers the potential to drive the discovery of novel catalytic functions.[12] Moreover, the promiscuity of a biocatalyst can be unlocked by using special reaction conditions. For example, flavin dependent ene reductases natively catalyze the asymmetric reduction of activated alkenes. Upon excitation of the flavin with blue light, a new-to-nature intermolecular radical cyclization reaction was achieved.[119]

1.2.3.2 Protein engineering of novel catalytic functions

Beyond the optimization of enzymatic promiscuities using advanced protein engineering methods to elevate them to a synthetically useful level, tailoring of biocatalysts for a specific new-to-nature reaction emerged as an efficient tool. Enzyme classes with a natural broad reaction scope, such as the cytochrome P450 family, are often selected for this. These biocatalysts are known for heme-dependent regioselective C–H oxyfunctionalization, but also perform a variety of other reactions.[120] Most of these reactions are based on the formation of a highly valent iron(IV) oxo-cation radical species.[121] The electronic structure of carbenes and nitrenes feature strong similarities to this oxene species, which suggested a putative catalytic function.[122,123] Both are important intermediates for the synthesis of complex compounds. However, no suitable carbene or nitrene transferase was discovered in nature.[124] Accordingly, cytochrome P450 enzymes have been identified as a sophisticated starting point for tailoring new-to-nature biocatalysts *via* protein engineering to implement these functionalities.[125,126]

1.2.3.3 Artificial metalloenzymes

Artificial metalloenzymes assembled from a protein scaffold and a transition metal catalyst offer unique potential for novel features. While the protein scaffold provides the required stereocontrol and function under mild reaction conditions, abiotic metal cofactors allow access to a wide range of reaction mechanisms that cannot be achieved by natural enzymes.[127] Since initial attempts to generate artificial metalloenzymes, the research field has expanded dramatically over the past 60 years to cover at present a range of reaction classes.[128]

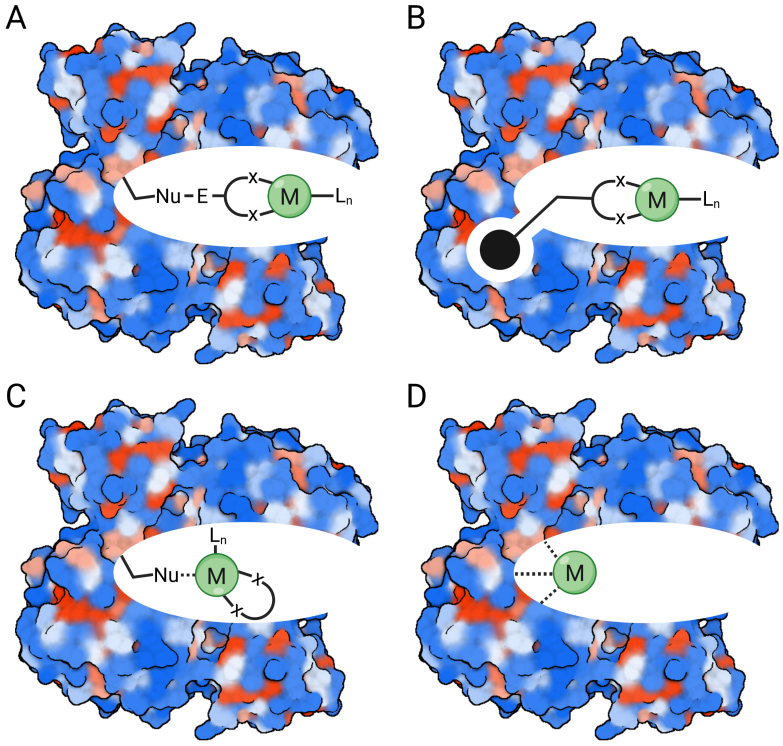

Figure 1.6: Four anchoring strategies for artificial metalloenzyme assembly. (**A**) Covalent immobilization. (**B**) Supramolecular anchoring. (**C**) Dative coordination. (**D**) Metal substitution. Adapted from "Artificial Metalloenzymes: Challenges and Opportunities" by Davis and Ward, *ACS Cent. Sci.* 2019.[129]

Meanwhile, four complementary anchoring strategies have been established to incorporate non-native metal cofactors in the active site of a protein scaffold and access new-to-nature reactions (Figure 1.6). (A) Covalent immobilization, achieved by an irreversible reaction between functional groups of the metal ligand and the protein backbone. (B) Supramolecular anchoring, where a metal cofactor is attached in linkage with a high-affinity inhibitor, substrate or cofactor. (C) Dative coordination, based on the interaction of a Lewis-basic amino acid with a coordinately unsaturated metal center. (D) Metal substitution, in which the metal of a native metalloenzyme is exchanged for a non-native metal.[129] Among the known proteins, numerous incorporate a metal ion binding site for structural or catalytic purposes, offering broad access to protein scaffolds with well-tailored active sites.[130] Sophisticated coordination environments of native metalloenzymes facilitate the modulation of the unique reactivity of metal ions.[131] In fact, several of these binding sites display a similar affinity for different metal ions, including those not typically used by nature for catalysis. This renders metal substitution as the straightforward strategy to access new-to-nature activities that are otherwise associated with abiotic catalysts.[132] An example of this can be illustrated by the Zn(II) dependent carbonic anhydrase. The metal-free protein scaffold obtained by treatment with a cheating agent can be used as a platform for loading with various non-native metal ions to unlock different reaction types. Coordination of Mn(II) allowed the catalysis of epoxidation,[133] while hydrogenation and hydroformylation reactions were performed using Rh(II).[134,135] However, such novel reactions are often catalyzed with low activity, requiring an optimization by protein engineering.

1.3 Oligomerization of formaldehyde

In recent decades, as previously outlined, significant progress has been accomplished in the research field of biocatalysis. This broadened the range of complex compounds that can be synthesized *via* biocatalysis. To further drive the decarbonization and defossilization of the chemical industry, C_1 chemistry has emerged as a promising option.[136–140] Thereby, complex molecules are generated from simple one-carbon (C_1) synthons. A process that requires the direct coupling of two C_1 units and represents a challenge for chemistry.[85] However, oligomerization of the C_1 compound formaldehyde is a promising biocatalytic option.

The following section was previously published and is reproduced herein with permission from S. Güner, V. Wegat, A. Pick and V. Sieber "Design of a synthetic enzyme cascade for the *in vitro* fixation of a C_1 carbon source to a functional C_4 sugar" Green Chemistry, 2021, 23(17), 6583 – 6590.[141] Copyright 2021. The Royal Society of Chemistry.

The author, André Pick and Volker Sieber conceived and designed the study. The author performed *in silico* studies, design and cloning of the library, screening development, screening, selection of variants, characterization, applying suitable variants, determination of kinetic parameters and data analysis. Vanessa Wegat produced library supernatant and performed GDH assay. The author wrote the initial draft of the manuscript. The co-authors critically reviewed the manuscript.

Formaldehyde (FALD), a more challenging starting compound due to its higher reactivity, has come recently into the spotlight of biocatalysis.[65] It can be easily derived from C_1 feedstocks such as methane, methanol, formate or CO_2.[142–144] Since they themselves are derived utilizing renewable resources (biomass and or energy), a green supply of FALD is possible. To control FALD's high reactivity, highly selective biocatalysts are well suited as long as they are sufficiently tolerant against aldehydes. In 1861, Butlerov described the base-catalyzed aldol condensation of FALD to a heterogeneous mixture of sugar-like compounds, better known as the formose reaction.[145,146] For a long time, no enzyme was described that could catalyze this reaction selectively. Finally, a computationally designed enzyme called formolase (FLS) was published in 2015.[86,147] In this seminal work, a thiamine diphosphate dependent benzaldehyde lyase was redesigned by means of protein engineering. The targeted reaction was the selective production of the three-carbon ketose dihydroxyacetone (DHA) from FALD. The enzymatic carbon-carbon bond formation is facilitated by the cofactor *via* an umpolung reaction.[148] However, the kinetic parameters of FLS are still insufficient. Specifically, the low affinity for FALD is a challenge for establishing efficient one-pot enzyme cascades, where catalytic activity is low and many enzymes have a lower tolerance to FALD. To bypass this, either a less harmful aldehyde was used as a substrate or stepwise approaches were established to apply FLS in *in vitro* cascades.[149,150] For the latter, a stepwise cascade was also described in which a pool of DHA

(from 0.75 g L^{-1} FALD) was first generated by FLS. Subsequently, an equimolar amount of FALD and a variant of D-fructose-6-phosphate aldolase (FSA^{A129S}) was added to generate the four-carbon sugar L-erythrulose.[73] Erythrulose (ERY) is a functional sugar and can be used as an ingredient in tanning agents as it reacts with amino groups in the upper layer of the skin.[151] Since the use of DHA alone can cause dry skin, unnatural color and allergic reactions, in most cases ERY and DHA are applied in combination. This helps overcome the disadvantages of DHA, resulting in a more natural color and a product that is gentler to the skin.[152] Optimally, a ratio of ERY to DHA in a range of 0.3 to 1 is used.[153] The industrial production of ERY is performed *via* fermentation. In this process, erythritol is oxidized to erythrulose in a single step, achieving up to 242 g L^{-1} erythrulose.[154] Erythritol itself can be used as a sweetener and is mainly produced by biotransformation of glucose with much lower yields.[155] Beyond that, continuous production of ERY has been reported. This was achieved by using a transketolase in a membrane reactor. Under CO_2 release, ERY is formed as a product of glycolaldehyde (GALD) and β-hydroxypyruvate.[156] Moreover, erythrulose can also be formed directly from two GALD molecules; however, this is a side activity of transketolases and has not found application to date.[157] This might be due to a high K_m value,[157] instability through GALD[158] or product inhibition.[159] Considering the distinct stability toward aldehydes, FLS would be a suitable biocatalyst for this reaction. In fact, we observed the combination of two GALDs to ERY in our preliminary work for FLS as well. To the best of our knowledge, this has not yet been described in literature. This discovery unlocks the opportunity to extend the fixation of the C_1 carbon source FALD by FLS and produce the functional C_4 sugar rather than the C_3 ketose. This, however, required optimizing FLS *via* protein engineering. Inspired through the first law of directed evolution, "you get what you screen for" by Frances Arnold,[41] which highlights the importance of screening design, we developed a high-throughput combinatorial screening in 96-well scale. Multiple assays were performed for screening the same library (semi-rational design) in order to evaluate each variant in terms of GALD, DHA and ERY activity. This enabled us to select suitable candidates with different properties from this library. One set of variants was tailored to convert FALD primarily to GALD and a second one to generate ERY from GALD. Suitable candidates were combined to develop a synthetic enzyme cascade for cell-free production of ERY from FALD."

1.4 Exploring alkylsulfatases to create new-to-nature biocatalysts

Artificial metalloenzymes have emerged as a viable option to expand the biocatalytic toolbox with new-to-nature functionalities to overcome its limitations.[127] Recognizing that many of the reported proteins incorporate a metal binding site, metal substitution of native metalloenzymes appeared to be the straightforward strategy for the preparation of artificial metalloenzymes.[128] Enzyme classes that are characterized by a certain catalytic flexibility in the sense of natural reaction diversity are often suitable for this application. Although members of the metallo-β-lactamase (MBL) superfamily are substantially divergent in sequence and function, scientists discovered that the catalytic functions of the different subfamilies overlap, leading to high promiscuity across the superfamily.[160] MBLs constitute class B among the β-lactamases and are subdivided into subclasses B1, B2 and B3.[161] Conserved are mainly structural features such as the αββα-fold (MBL fold) and a binuclear Zn(II) binding site. Primarily to perform hydrolysis of diverse substrates with different chemical properties.[162] The appropriate coordination of metal ion(s) required for catalytic activity is empowered by an unusual flexibility, in contrast to other metalloenzymes.[163] Accordingly, the MBL superfamily has been identified as promising target to introduce natural reactions.[28] Moreover, for some binuclear metallohydrolases, successful metal substitution has already been demonstrated.[164–166] Thus, these enzymes can offer a suitable platform for the development of new-to-nature biocatalysts.

Alkylsulfatases, the only group of sulfatases that are members of the MBL superfamily, offer an attractive substrate scope and a sophisticated reaction mechanism. These biocatalysts incorporate a conserved binuclear Zn(II) cluster and catalyze the hydrolysis of sulfate ester bonds to release the corresponding alcohol and hydrogen sulfate. Based on the accepted substrates, these enzymes are divided into primary and secondary alkylsulfatases.[167,168] No indications regarding the stereochemical preferences of *prim*-alkylsulfatases exist, since predominantly only primary alkyl sulfate esters (achiral molecules) such as the anionic surfactant SDS (sodium dodecyl sulfate) can be hydrolyzed.[169] In contrast, a broader substrate spectrum was observed for *sec*-alkylsulfatases, allowing the hydrolysis of chiral alkyl sulfate esters in which the sulfate moiety varies in relative position from C2 to C4.[170] This enabled insight into the stereo-chemical preferences.

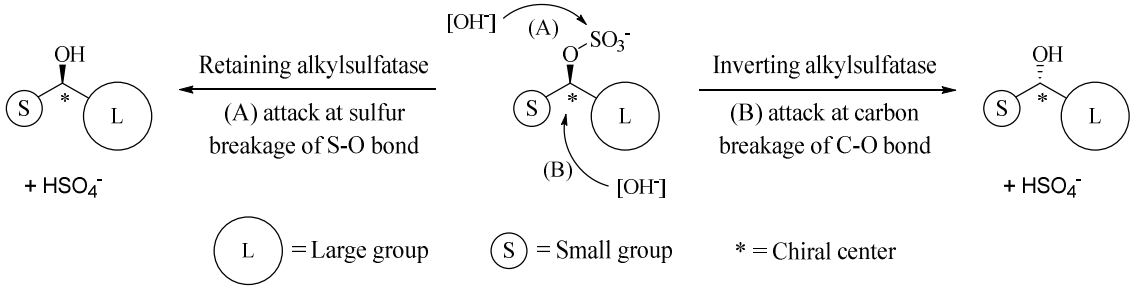

Figure 1.7: Stereochemistry of enzymatic hydrolysis of alkyl sulfate esters. Through (**A**) retention or (**B**) inversion of the configuration at the chiral carbon center. Adapted from "New enzymes for biotransformations: microbial alkyl sulfatases displaying stereo- and enantioselectivity" by Gadler and Faber, *Trends Biotechnol*. 2007.[171]

It was identified that *sec*-alkylsulfatases exhibit the rare feature of double selectivity. In addition to high enantioselectivity (discrimination of substrate enantiomers), high stereoselectivity was also observed, leading to either retention (breakage of S–O bond) or inversion (breakage of C–O bond) of configuration at the chiral carbon center (Figure 1.7).[172] Accordingly, these enzymes are well-suited for the establishment of enantioconvergent processes to overcome the 50%-yield limitation of kinetic resolution.[173] However, only a small number of alkylsulfatases were identified and heterologously expressed so far. These include the *prim*-alkylsulfatases SdsA1[174] and SdsAP[175], as well as the *sec*-alkylsulfatase PISA1[169] from *Pseudomonas* sp. DSM6611. PISA1 is an inverting *sec*-alkylsulfatase that exhibits high enantioselectivity for (*R*)-2-alkyl sulfates. While the binuclear Zn(II) cluster is mainly responsible for the supply and coordination of hydroxide, the protein scaffold ensures an appropriate substrate binding. The inversion is achieved by a nucleophilic attack (via S_N2) of [OH^-] on the chiral carbon atom of the sulfate ester, breaking the C–O bond and releasing the inverted alcohol.[176] Non-enzymatic catalysis of this reaction is very slow since sulfate is a poor leaving group from a mechanistic point of view.[177] The elimination of the sulfate moiety can be accelerated by protonation, since HSO_4^- is a good leaving group. In the case of PISA1, most likely histidine at position 317 acts as a general acid catalyst to facilitate the reaction.[176] Investigation of the substrate spectrum showed that a wide range of secondary alkyl sulfate esters could be converted, while aromatic, olefinic and acetylenic side chains were tolerated. Perfect enantioselectivity was observed for molecules that contained substituents of different sizes adjacent to the sulfate ester moiety.[170] To date, PISA1 has been studied mainly as a biocatalytic tool for enantioconvergent processes and the one-pot deracemization of secondary alcohols.[178] Nevertheless, in light of the described characteristics of PISA1 and its superfamily, it can be assumed that this protein scaffold furthermore harbors great potential for the incorporation of novel functionalities. A viable strategy to accomplish this would be to swap the nucleophile used for the reaction, thus opening up new classes of products. Enzymatic amination, especially for the synthesis of primary amines, is a persistent limitation of the biocatalytic toolbox. Existing biocatalysts, such as ammonia lyases, amine dehydrogenases and reductive aminases, suffer from the shortcomings of a narrow substrate range, dependence on costly cofactors or a reversible reaction mechanism (chapter 1.2.2). Accordingly, there is a high demand for the discovery or development of novel biocatalysts with more feasible properties. The use of ammonia instead of water by PISA1 would enable an irreversible new-to-nature route for the production of primary amines. However, from an organic chemistry perspective, bimolecular nucleophilic substitution (S_N2) reactions are extremely sensitive to the nature of the nucleophile, substrate and leaving group.[179] Based on the frontier molecular orbital theory, good nucleophiles possess high HOMO energies. This is equally true for heteronucleophiles with different central atoms, since the nucleophilicity increases with decreasing electronegativity (increasing polarizability).[180]

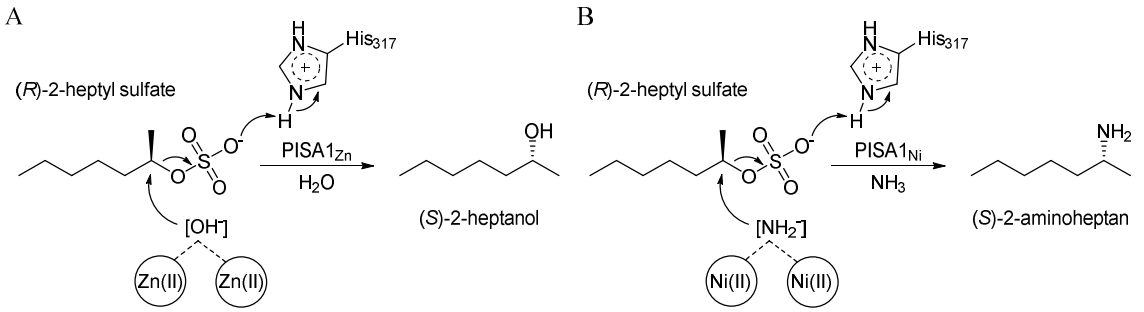

Figure 1.8: Design of study on development of a new-to-nature biocatalyst. (**A**) Natural hydrolytic reaction of PISA1 with binuclear Zn(II) cluster and water. (**B**) Envisioned new-to-nature biocatalyst for synthesis of primary aliphatic amines. Artificial metalloenzyme based on the protein scaffold of PISA1 and replacement of native Zn(II) ions with non-native Ni(II) ions. The use of ammonia as a nucleophile enables the production of primary amines instead of secondary alcohols.

As direct neighbors in the periodic table of elements, oxygen and nitrogen share rather similar electronegativities, leading to similar nucleophilic properties of [OH^-] and [NH_2^-], with slight advantages for nitrogen. The replacement of the native nucleophile by an N-nucleophile thus appears reasonable. However, nature has evolved the active site of PISA1, including the selective coordination Zn(II), to perform the hydrolytic S_N2 reaction. Hence, it can be assumed that this biocatalyst uses predominantly water even in the presence of ammonia. To shift this ratio toward ammonia and the synthesis of primary amines, metal substitution could be a viable option. The unusual flexibility of the first coordination sphere of MBLs (residues involved in the direct coordination of metal ions) appears to facilitate a metal substitution. Ni(II) seems to be suitable for this application, since despite rather similar properties to Zn(II), a higher affinity for ammonia has been described.[181–183] In addition, the applicability of other metal ions for this purpose is also to be investigated.

1.5 Aim and objectives

An essential function of academic biocatalysis research is the discovery and development of novel biocatalytic tools, which gives this research field the character of a tool factory. Despite the tremendous achievements over the past decades, the biocatalytic toolbox remains limited. These include the selective formation of C–C bonds, the incorporation of functional groups and the catalysis of reactions that do not occur in nature. The aim of this thesis is to address some of these limitations and to extend the biocatalytic toolbox by tailoring existing biocatalysts and developing new-to-nature biocatalysts.

The use of one-carbon (C_1) building blocks for the synthesis of complex compounds is gaining significance in light of the fundamental need for decarbonization and defossilization of the chemical industry. Scientists have succeeded in developing a novel biocatalyst, so-called formolase, for the specific oligomerization of formaldehyde (C_1) to dihydroxyacetone (C_3). However, the kinetic parameters of this new-to-nature biocatalyst are still insufficient. Since dihydroxyacetone is an important key intermediate, it can be easily introduced into the central metabolic pathway of many organisms and thus be used for biotechnological processes. However, for the biocatalytic *de novo* synthesis of complex compounds, it is necessary to extend the enzymatic oligomerization of C_1 synthons. Accordingly, one goal is to extend the hitherto fixation of formaldehyde by the enzyme formolase by a C_1 unit. This would allow the biocatalytic production of a C_4 carbon backbone derived from a C_1 building block.

Furthermore, the demand of biocatalytic tools for the functionalization of molecules remains unabated. In this context, amines represent one of the most important functional groups, since many target molecules contain a chiral amine subunit in their structure. In particular, the synthesis of primary chiral amines is a challenge for both organic chemistry and biocatalysis. From an atom economy perspective, biocatalytic amination using ammonia as an amine source offers a satisfying efficiency. However, biocatalysts suitable for this approach suffer from the shortcomings of poor catalytic efficiency, narrow substrate scope, dependence on costly cofactors or reversible reaction mechanism. Consequently, the establishment of biocatalytic tools with more feasible properties turns out to be essential. The development of artificial metalloenzymes that can catalyze new-to-nature reactions is a promising strategy to address this bottleneck. In this work, the inverting *sec*-alkylsulfatase PISA1 is identified as a sophisticated protein scaffold. Accordingly, this project aims to explore the potential of alkylsulfatases as a platform for artificial metalloenzymes that enable the selective production of primary aliphatic amines. In addition to broadening the scope of accessible primary amines, the major advantage of this putative biocatalyst is that the amination could be irreversibly catalyzed.

2. MATERIALS AND METHODS

2.1 Materials

All materials and devices used in this study were provided by the Chair of Chemistry of Biogenic Resources, Technical University of Munich – Campus Straubing for Biotechnology and Sustainability (TUMCS), unless otherwise stated.

2.1.1 Chemicals

Table 2.1 below lists all chemicals used, including additional information.

Table 2.1: Chemicals.

Name	Provider	Item number
Acetic acid glacial	Carl Roth GmbH, Karlsruhe, DE	6755.1
Adenosin-5′-triphosphate (ATP)	Carl Roth GmbH, Karlsruhe, DE	K054.1
Adenosin-5′-monophosphate (AMP)	Alfa Aesar, Ward Hill, USA	J61643
Agar-agar	Carl Roth GmbH, Karlsruhe, DE	5210.2
Agarose	Biozym Scientific GmbH, Oldendorf, DE	840004
Ammonia 32% (w/v)	Merck Millipore, Darmstadt, DE	1.05426.1000
Ammonium chloride	Carl Roth GmbH, Karlsruhe, DE	K298.1
Ammonium sulfate	AppliChem, Darmstadt, DE	A1032,5000
Ammonium peroxodisulfate (APS)	Merck Millipore, Darmstadt, DE	1.01201.0500
Ba(II) chloride · $2H_2O$	Sigma-Aldrich, St. Louis, USA	B0750
Bromophenol blue	Merck Millipore, Darmstadt, DE	1.08122
Ca(II) chloride · $2H_2O$	Carl Roth GmbH, Karlsruhe, DE	5239.1
Cd(II) chloride	Alfa Aesar, Ward Hill, USA	52852
Chelex100 resin	Bio-Rad Laboratories GmbH, München, DE	1432832
Ce(III) chloride · $7H_2O$	Thermo Fisher Scientific, Waltham, USA	11381079
Chloramphenicol	Sigma-Aldrich, St. Louis, USA	C0378
Co(II) chloride · $6H_2O$	Alfa Aesar, Ward Hill, USA	A16346
Co(II) sulfate · $7H_2O$	Alfa Aesar, Ward Hill, USA	A16201
Cu(II) chloride · $2H_2O$	AppliChem, Darmstadt, DE	A27870250
Cu(II) sulfate · $5H_2O$	Sigma-Aldrich, St. Louis, USA	61245
Carbenicillin disodium salt	Carl Roth GmbH, Karlsruhe, DE	6344.3
Coomassie brilliant blue G 250	SERVA GmbH, Heidelberg, DE	17524
DA-64	FUJIFILM Wako Chemicals, Neuss, DE	043-22351
Dihydroxyacetone	Sigma-Aldrich, St. Louis, USA	8.20482
Dimethyl-2,6-pyridinedicarboxylate	Alfa Aesar, Ward Hill, USA	H32251
Diphenylamine	Merck Millipore, Darmstadt, DE	8205280100
Ethyl acetate	Th. Geyer GmbH, Renningen, DE	22778
Ethylenediaminetetraacetic acid (EDTA)	Carl Roth GmbH, Karlsruhe, DE	8043.2
Ethanol absolute	VWR International GmbH, Darmstadt, DE	20821.321
L-Erythrulose (pharmaceutical standard)	Merck Millipore, Darmstadt, DE	PHR1453-1G
L-Erythrulose	Carbosynth Biosynth., Compton, GB	ME03102
Eu(II) chloride	Sigma-Aldrich, St. Louis, USA	431850
Fe(II) chloride · $4H_2O$	AppliChem, Darmstadt, DE	A35840250
Formaldehyde 37%	Carl Roth GmbH, Karlsruhe, DE	7398.1
Ga(III) chloride	Alfa Aesar, Ward Hill, USA	43879,06
α-D-Glucose · H_2O	SERVA GmbH, Heidelberg, DE	22720
Glycerol 99.5%	Carl Roth GmbH, Karlsruhe, DE	3783
Glycine	Carl Roth GmbH, Karlsruhe, DE	3790.2

Glycolaldehyde dimer	Sigma-Aldrich, St. Louis, USA	G6805
Guanosin-5'-triphosphat (GTP)	Carl Roth GmbH, Karlsruhe, DE	K056.4
H_2SO_4 96% (w/v)	Carl Roth GmbH, Karlsruhe, DE	4623.1
HCl 37 % (w/v)	Merck Millipore, Darmstadt, DE	30721
HEPES	Carl Roth GmbH, Karlsruhe, DE	HN78.3
Imidazole	Merck Millipore, Darmstadt, DE	1.04716
In(III) chloride	Sigma-Aldrich, St. Louis, USA	429414-5G
IPTG	Carl Roth GmbH, Karlsruhe, DE	CN08
Kanamycin sulfate	Carl Roth GmbH, Karlsruhe, DE	T832.3
K_2HPO_4	Carl Roth GmbH, Karlsruhe, DE	P749.3
KH_2PO_4	Carl Roth GmbH, Karlsruhe, DE	3904.3
α-Lactose · H_2O	Carl Roth GmbH, Karlsruhe, DE	6868.1
β-Mercaptoethanol	Merck Millipore, Darmstadt, DE	8,0574
Mg(II) chloride · $6H_2O$	Carl Roth GmbH, Karlsruhe, DE	2189.1
Mg(II) sulfate · $7H_2O$	Merck Millipore, Darmstadt, DE	1.05886.1000
Mn(II) chloride · $2H_2O$	Merck Millipore, Darmstadt, DE	1.05934.0100
Mn(II) sulfate · H_2O	Merck Millipore, Darmstadt, DE	1.05941.0250
MOPS	Carl Roth GmbH, Karlsruhe, DE	6979.3
NADH	Carl Roth GmbH, Karlsruhe, DE	AE12
Na_2HPO_4	Carl Roth GmbH, Karlsruhe, DE	P030
NaH_2PO_4	Sigma-Aldrich, St. Louis, USA	71496
Ni(II) chloride · $6H_2O$	AppliChem, Darmstadt, DE	A3917
Ni(II) sulfate · $6H_2O$	Merck Millipore, Darmstadt, DE	1.06727
Os(III) chloride · $3H_2O$	Thermo Fisher Scientific, Waltham, USA	11317738
Phosphoenolpyruvate	Sigma-Aldrich, St. Louis, USA	860077
Potassium acetate	Carl Roth GmbH, Karlsruhe, DE	4986.1
Potassium chloride	Carl Roth GmbH, Karlsruhe, DE	6781.1
Potassium hydroxide	Carl Roth GmbH, Karlsruhe, DE	6751.2
Pt(IV) potassium chloride	Alfa Aesar, Ward Hill, USA	11048
Rb(I) chloride	Alfa Aesar, Ward Hill, USA	12892
Rh(III) chloride · nH_2O	Thermo Fisher Scientific, Waltham, USA	10571641
Roti®-Quant	Carl Roth GmbH, Karlsruhe, DE	K015.3
Rotiphorese® Gel 30 (37.5:1)	Carl Roth GmbH, Karlsruhe, DE	3029.1
Ru(III) chloride · H_2O	Sigma-Aldrich, St. Louis, USA	463779-1G
Serva DNA Stain clear G	SERVA GmbH, Heidelberg, DE	39804
Sn(II) chloride	Alfa Aesar, Ward Hill, USA	A16202
Sodium acetate	Carl Roth GmbH, Karlsruhe, DE	X891.1
Sodium dithionite	Sigma-Aldrich, St. Louis, USA	71699
Sodium dodecyl sulfate (SDS)	SERVA GmbH, Heidelberg, DE	20760
Sodium chloride	Carl Roth GmbH, Karlsruhe, DE	P029.3
SYPRO® Orange Protein Gel Stain	Sigma-Aldrich, St. Louis, USA	S5692
TEMED	VWR International GmbH, Darmstadt, DE	M146
Thiamine diphosphate (ThDP)	Sigma-Aldrich, St. Louis, USA	C8754
TRIS	Sigma-Aldrich, St. Louis, USA	T1503
Tryptone/Peptone	Carl Roth GmbH, Karlsruhe, DE	8952.5
Tryptone/Peptone	Sigma-Aldrich, St. Louis, USA	T9410-1KG
Yeast extract	Carl Roth GmbH, Karlsruhe, DE	2363.4
Yeast extract	Sigma-Aldrich, St. Louis, USA	Y1625-1KG
Zn(II) chloride	Merck Millipore, Darmstadt, DE	1.08816.0250
Zn(II) sulfate · 7H2O	Merck Millipore, Darmstadt, DE	1.08883.1000
1,10-Phenanthroline · H_2O	Carl Roth GmbH, Karlsruhe, DE	9113
2-Aminoheptane	Alfa Aesar, Ward Hill, USA	B22863.14
8-Hydroxyquinoline-5-sulfonic acid	Thermo Fisher Scientific, Waltham, USA	121921000

2.1.2 Standards and kits

Table 2.2 below lists the protein and DNA standards as well as the kits used in this work.

Table 2.2: Standards and kits.

Application	Name	Provider
Standards		
DNA size marker	Quick-Load® Purple 2-log DNA ladder (#N0550S)	New England Biolabs, Ipswich, USA
	Quick-Load® Purple 1kb plus DNA ladder (#N0552G)	New England Biolabs, Ipswich, USA
Protein size marker	PageRuler™ Unstained Protein Ladder (#26614)	Thermo Fisher Scientific, Waltham, USA
Kits		
Plasmid DNA isolation	GeneJet™ Plasmid Miniprep Kit (#K0503)	Thermo Fisher Scientific, Waltham, USA
Gel extraction and PCR purification	NucleoSpin® Gel and PCR Clean-up (#740609.250)	Machery and Nagel, Düren, DE
Purification of genomic DNA	DNeasy UltraClean Microbial Kit (#12224-50)	QIAGEN, Hilden, DE
Blunt end cloning	CloneJET™ PCR Cloning Kit (#K1231)	Thermo Fisher Scientific, Waltham, USA

2.1.3 Enzymes

Table 2.3 summarizes all commercial enzymes used in this work.

Table 2.3: Commercial enzymes.

Name	Provider	Item number
DNase	AppliChem, Darmstadt, DE	A3778
Lysozyme	Sigma-Aldrich, St. Louis, USA	8259
T4 DNA ligase	New England Biolabs, Ipswich, USA	M0202
Taq DNA polymerase	New England Biolabs, Ipswich, USA	M0267
GoTaq G2 DNA polymerase	Promega, Madison, USA	M7845
Phusion high-fidelity DNA polymerase	New England Biolabs, Ipswich, USA	M0530
Quick CIP (calf intestinal phosphatase)	New England Biolabs, Ipswich, USA	M0525
DpnI	New England Biolabs, Ipswich, USA	R0176
NdeI	New England Biolabs, Ipswich, USA	R0111
XhoI	New England Biolabs, Ipswich, USA	R0146
BsaI	New England Biolabs, Ipswich, USA	R0535
BbsI	New England Biolabs, Ipswich, USA	R0539
Peroxidase from horseradish	Sigma-Aldrich, St. Louis, USA	P6782-50MG
Pyruvate oxidase from microorganisms	Sigma-Aldrich, St. Louis, USA	P4591-100UN

2.1.4 Bacterial strains

In this work, different *E. coli* strains were used for cloning and expression of various proteins. *E. coli* XL1-Blue, DH5α or TOP10 were used for standard plasmid generation. *E. coli* BL21 (DE3) or Rosetta (DE3) was used for protein expression. Table 2.4 provides details about the genotype and reference of each strain. The list of microorganisms used for genomic DNA isolation and cloning is shown in Table 2.5 below. Microorganisms were purchased from Leibniz Institute DSMZ (Deutsche Sammlung von Mikroorganismen und Zellkulturen GmbH) or were obtained from different groups.

Table 2.4: Bacterial strains.

E. coli strain	Genotype	Reference
XL1-Blue	*rec*A1 *end*A1 *gyr*A96 *thi*-1 *hsd*R17 *sup*E44 *rel*A1 *lac* [F′ *pro*AB *lac*I^{q} ZΔM15 *Tn*10 (Tet^{R})]	Stratagene, Heidelberg, DE
DH5α	F^{-} φ80*lac*ZΔM15 Δ(*lac*ZYA-*arg*F)U169 *rec*A1 *end*A1 *hsd*R17(r_{K}^{-}, m_{K}^{+}) *pho*A *sup*E44 λ^{-} *thi*-1 *gyr*A96 *rel*A1	Invitrogen, Carlsbad, USA
TOP10	F^{-} *mcr*A Δ(*mrr-hsd*RMS-*mcr*BC) φ80*lac*ZΔM15 Δ*lac*X74 *rec*A1 *ara*D139 Δ(*ara-leu*)7697 *gal*U *gal*K λ^{-} *rps*L(Str^{R}) *end*A1 *nup*G	Invitrogen, Carlsbad, USA
BL21 (DE3)	F^{-} *omp*T *gal dcm lon hsd*S_{B}(r_{B}^{-} m_{B}^{-}) λ(DE3 [*lac*I *lac*UV5-T7p07 *ind*1 *sam*7 *nin*5])	Novagen, Darmstadt, DE
Rosetta (DE3)	F^{-} *omp*T *gal dcm lon hsd*S_{B}($r_{B}^{-}m_{B}^{-}$) λ(DE3 [*lac*I *lac*UV5-T7p07 *ind*1 *sam*7 *nin*5]) [*mal*B^{+}]K$_{-12}$(λ^{S}) pRARE[T7p20 *ile*X *arg*U *thr*U *tyr*U *gly*T *thr*T *arg*W *met*T *leu*W *pro*L orip15A](Cm^{R})	Novagen, Darmstadt, DE

Table 2.5: Microorganisms as template for isolation of genomic DNA.

Microorganism	Strain	Reference
Fontimonas thermophila	HA-01	DMSZ 23609
Variovorax paradoxus	EPS	Obtained from Prof. Dirk Tischler (Ruhr-Universität Bochum)
Vibrio vulnificus	ATCC 27562	Obtained from Prof. Bastian Blombach (TUMCS)

2.1.5 Media and antibiotics

Heat stable cultivation media, buffers and solutions were autoclaved at 121°C and 1 bar overpressure for 20 minutes. For cultivation media consisting of various solutions, all solutions were sterilized before mixing.

Table 2.6: Media composition.

Media	Components
LB	Lysogeny broth 5.0 g L^{-1} yeast extract, 10.0 g L^{-1} tryptone, 10.0 g L^{-1} sodium chloride (NaCl) Dissolved in 1 L MQ-H_2O and autoclaved. Desired antibiotics were added prior use.
LB agar	Lysogeny broth agar LB medium with 15.0 g L^{-1} agar. After autoclaving, the agar was cooled to 55°C, the desired antibiotic was added and agar was poured into 10 cm petri plates. Plates were stored at 4°C.
TB	Terrific broth 24.0 g L^{-1} yeast extract, 12.0 g L^{-1} tryptone, 5.0 g L^{-1} glycerol Dissolved in 0.9 L MQ-H_2O. After autoclaving 0.1 L of 10x TB salts were added under sterile conditions. Desired antibiotics were added prior use.
10x TB salts	23.1 g L^{-1} monopotassium phosphate (KH_2PO_4), 125.4 g L^{-1} dipotassium phosphate (K_2HPO_4) dissolved in 1 L MQ-H_2O and autoclaved.
AI	Autoinduction 5.0 g L^{-1} yeast extract, 10.0 g L^{-1} tryptone Dissolved in 925 mL MQ-H_2O. After autoclaving 1 mL of magnesium sulfate ($MgSO_4$), 20 mL of 50x 5052 and 50 mL of 20x NPS were added under sterile conditions. Desired antibiotics were added prior use.
50x 5052	250.0 g L^{-1} glycerol, 25.0 g L^{-1} D-glucose monohydrate, 100.0 g L^{-1} lactose monohydrate dissolved in 1 L MQ-H_2O and autoclaved.
20x NPS	66.0 g L^{-1} ammonium sulfate ($(NH_4)_2SO_4$), 136.0 g L^{-1} KH_2PO_4, 142.0 g L^{-1} disodium phosphate (Na_2HPO_4) dissolved in 1 L MQ-H_2O and autoclaved.
SOC	Super optimal broth with catabolite repression 5.0 g L^{-1} yeast extract, 20.0 g L^{-1} tryptone, 0.5 g L^{-1} NaCl, 10 mM $MgSO_4$, 10 mM magnesium chloride ($MgCl_2$), 2.5 mM potassium chloride (KCl), 20 mM D-glucose

Table 2.7: Antibiotics.

Solution	Stock concentration	Final concentration	Solvent
Ampicillin	100 mg mL^{-1}	100 µg mL^{-1}	MQ-H_2O
Carbenicillin	100 mg mL^{-1}	100 µg mL^{-1}	MQ-H_2O
Kanamycin sulfate	100 mg mL^{-1}	100 or 50 µg mL^{-1}	MQ-H_2O
Chloramphenicol	34 mg mL^{-1}	34 µg mL^{-1}	100% (v/v) ethanol

Heat unstable solutions were filtered through a sterile syringe filter holder (0.22 µM, VWR International GmbH, Darmstadt, DE). All media used are listed in Table 2.6. Purified water, MQ-H_2O, (Merck Millipore, Darmstadt, DE) was used for all media, buffers and solutions. Stored at room temperature, if not otherwise specified. Stock solutions of antibiotics were filtered (syringe filter holder, 0.22 µm) and stored in aliquots of 1 mL at -20°C. For selective medium, sterile antibiotics (Table 2.7) were added.

2.1.6 Plasmids

Table 2.8 lists all plasmids used or generated in this work. The pJET1.2/blunt vector, which encodes a lethal gene when religated, can be used for blunt end cloning of gBlocks. The pET21a, pET24a and pET28a vectors can be used for protein expression. All vectors contain an N-terminal T7 tag and a C-terminal His_6 tag sequence, while pET28a also carries an N-terminal His_6 tag configuration.

Table 2.8: Plasmids.

Plasmid	Description	Reference
pJET1.2/blunt	Amp^R, rep(pMB1), eco47IR, P_{lacUV5}, T7 promotor	Thermo Fisher Scientific, Waltham, USA
pET21a	Amp^R ColE1 P_{lac} *lac*Z' *lac*I, T7 expression system under control of a lac operator	Schober *et al*., 2011[169]
pET24a	Kan^R ColE1 P_{lac} *lac*Z' *lac*I, T7 expression system under control of a lac operator	Novagen, Darmstadt, DE
pET28a	Kan^R ColE1 P_{lac} *lac*Z' *lac*I, T7 expression system under control of a lac operator	Novagen, Darmstadt, DE
pET24a_FLS	Formolase was synthesized as reported[86] by GeneArt (Regensburg, DE) cloned *via* restriction sites NdeI and XhoI	This study
pET24a_*Pfu*ADHd	Alcohol dehydrogenase ADHd[184] (PF1960) from *P. furiosus* cloned *via* restriction sites NdeI and XhoI	This study
pET28a_cysDN	Sulfate adenylyltransferase subunit 1 (cysN) and Sulfate adenylyltransferase subunit 2 (cysD) from *E. coli* cloned *via* restriction sites NdeI and XhoI	Ortiz-Tena *et al*., 2018[185]
pET28a_MET14	Adenylyl-sulfate kinase from *S. cerecisiae* S288c cloned *via* restriction sites NdeI and EcoRI	Ortiz-Tena *et al*., 2018[185]
pET28a_PPDK	Pyruvate phosphate dikinase from *P. freudenreichii* cloned *via* restriction sites NdeI and EcoRI	Ortiz-Tena *et al*., 2018[185]
pET21a_PISA1	Inverting *sec*-Alkylsulfatase from *Pseudomonas* sp. DSM 6611 cloned *via* restriction sites NheI and XhoI	Schober *et al*., 2011[169]
pET24a_PISA1	Inverting *sec*-Alkylsulfatase from *Pseudomonas* sp. DSM 6611 cloned *via* restriction sites NdeI and XhoI	This study
pET24a_CmAS	Alkyl/Aryl-sulfatase from *C. metallidurans* Ni-2 cloned *via* restriction sites NdeI and XhoI	This study
pET24a_FtAS	Alkyl sulfatase BDS1 from *F. thermophila* cloned *via* restriction sites NdeI and BbsI	This study
pET24a_VpAS	Sterol-binding domain protein from *V. paradoxus* EPS cloned *via* restriction sites NdeI and BsaI	This study

2.1.7 Single-strand oligonucleotides (primers)

All primers were ordered from Biomer (Ulm, DE) or Eurofins Genomic (Ebersberg, DE) and are listed in Table 2.9.

Table 2.9: Single-strand oligonucleotides (primers).

Name	Application	Sequence 5' → 3'
T7_fwd_mut	Forward primer to amplify a gene under T7 promotor	GAATTGTGAGCGGATAACAATTCCC
T7_rev_mut	Reverse primer to amplify a gene under T7 terminator	CTTTGTTAGCAGCCGGATCTC
*Pfu*ADHd_fwd	Forward primer to amplify PfuADHd from genomic DNA of *P. furiosus*	TATATACATATGAAAAGGGTAAATGCATTCA ACGACCTTAAGC
*Pfu*ADHd_rev	Reverse primer to amplify PfuADHd from genomic DNA of *P. furiosus*	TATATACTCGAGCACACACCTCCTTGCCATCT CTCTATCC
FtAS_fwd	Forward primer to amplify FtAS from genomic DNA of *F. thermophila*	TATATACATATGGACGTGATAGGGCGTGTCGC GC
FtAS_rev	Reverse primer to amplify FtAS from genomic DNA of *F. thermophila*	TATCTCGAGTGTGTCCTCGACGGGTACGAACA GAC
VpAS_fwd	Forward primer to amplify VpAS from genomic DNA of *V. paradoxus*	TATATACATATGACCCCTTCTTCCTTCTCCATG GCCCTG
VpAS_rev	Reverse primer to amplify VpAS from genomic DNA of *V. paradoxus*	GATCGGTCTCCTCGAGCTTCCGCGGCTCGACC ACAGGGAACATC

2.1.8 Devices and additional materials

The devices used for this work are summarized in Table 2.10 and listed in alphabetical order.

Table 2.10: Devices.

Device	Model	Manufacturer
Autoclave (steam sterilizer)	Varioklav135S	Thermo Fisher Scientific, Waltham, USA
Benchtop centrifuge	Galaxy MiniStar	VWR International GmbH, Darmstadt, DE
Benchtop centrifuge	Heraus Frisco 21	Thermo Fisher Scientific, Waltham, USA
Benchtop centrifuge	Heraus Pico 17	Thermo Fisher Scientific, Waltham, USA
CD spectrometer	Chirascan plus	Applied Photophysics, Leatherhead, UK
Centrifuge	Sorvall RC-6+	Thermo Fisher Scientific, Waltham, USA
Centrifuge rotor	F9-4x1000Y	Thermo Fisher Scientific, Waltham, USA
Centrifuge rotor	F10S-6x500Y	Thermo Fisher Scientific, Waltham, USA
Centrifuge rotor	SS-34	Thermo Fisher Scientific, Waltham, USA
Centrifuge	Sorvall Lynx 6000	Thermo Fisher Scientific, Waltham, USA
Centrifuge rotor	F9-6x1000 LEX	Thermo Fisher Scientific, Waltham, USA
Centrifuge rotor	F12-6x500 LEX	Thermo Fisher Scientific, Waltham, USA
Centrifuge rotor	A27-8x50	Thermo Fisher Scientific, Waltham, USA
Centrifuge	Rotanta 460R	Hettich Lab Technology, Tuttlingen, DE
Colony picker	CP-7200	Norgren Systems, Fairlea, USA
Dispenser	MicroFlo Select	BioTek Instruments GmbH, Winooski, USA
Electric balance	TE1502S	Sartorius AG, Göttingen, DE
Electric balance	TE6101	Sartorius AG, Göttingen, DE
Electric balance	Pioneer	Ohaus Europe GmbH, Nänikon, CH
Electric balance	AW320	Shimadzu Coporation, Kyoto, JPN
Electrophoresis (DNA)	Mini-Sub Cell GT Cell	Bio-Rad Laboratories GmbH, München, DE
Electrophoresis (DNA)	Wide Mini-Sub Cell GT Cell	Bio-Rad Laboratories GmbH, München, DE
Electrophoresis (protein)	Mini-PROTEAN Tetra Vertical Electrophoresis Cell	Bio-Rad Laboratories GmbH, München, DE
Freezer (-20°C)	Liebherr Compact	Liebherr-International S.A., Bulle, CH
Freezer (-80°C)	Forma 900 series	Thermo Fisher Scientific, Waltham, USA

Freeze-dyer (lyophilization)	Alpha2-4 LD plus	Martin Christ GmbH, Osterode am Harz, DE
FPLC	Äkta Purifier UPC 900	GE Healthcare Europe GmbH, Freiburg, DE
FPLC column	5 mL HisTrap FF Crude	GE Healthcare Europe GmbH, Freiburg, DE
FPLC column	HiPrep 26/10 Desalting	GE Healthcare Europe GmbH, Freiburg, DE
GC-FID	Trace GC 2000 with Ultra Trace	Thermo Fisher Scientific, Waltham, USA
GC-MS	Ultra Trace DSQ II	Thermo Fisher Scientific, Waltham, USA
GC column	Rxi-5Sil-MS column	Restek GmbH, Bad Homburg v. d. Höhe, DE
GC column	BPX-5	SGE Analytical Science
Gel documentation	Gel iX Imager	Intas Science GmbH, Göttingen, DE
Gel tray	Transilluminator DR 15x19	Clare Chemical Research, Dolores, USA
Heating block	Eppendorf ThermoMixer C	Eppendorf AG, Hamburg, DE
Heating block	SLG digital dry bath	Süd-Laborbedarf GmbH, Gauting, DE
Heating block	Tmix	Analytik Jena AG, Jena, DE
Homogenizer	Ultra Turrax T18 Basic	IKA-Werke GmbH, Staufen, DE
HPLC	Ultimate 3000	Dionex Corporation, Sunnyvale, USA
HPLC detector	RS Diode Array	Dionex Corporation, Sunnyvale, USA
HPLC detector	Ultimate 3000 Photodiode Array	Dionex Corporation, Sunnyvale, USA
HPLC detector	Refractive Index Detector	Shodex Showa Denko Europe, München, DE
HPLC column	Rezex ROA-Organic Acid (8%)	Phenomenex, Aschaffenburg, DE
Incubator	Heraus B12	Thermo Fisher Scientific, Waltham, USA
Incubator	Heraus Kelvitron kp	Thermo Fisher Scientific, Waltham, USA
Incubator	KBF 240	Binder, Tuttlingen, DE
Incubator shaker	Multitron Standard	Infors, Einsbach, DE
Incubator shaker	New Brunswick Innova 44/44R	Eppendorf AG, Hamburg, DE
Incubator shaker	IKA KS 4000 ic central	IKA-Werke GmbH, Staufen, DE
Liquid handling platform	FreedomEvo 200	Tecan Group Ltd., Männedorf, CH
Liquid handling platform	Multi Channel Arm MCA96	Tecan Group Ltd., Männedorf, CH
Liquid handling platform	Liquid Handling Arm LiHa	Tecan Group Ltd., Männedorf, CH
Liquid handling platform	Incubator StoreX IC	LiCONiC GmbH, Montabauer, DE
Magnetic stirrer	MR 3001 K	Heidolph Instruments GmbH, Schwabach, DE
Microplate reader	Infinite 200 pro	Tecan Group Ltd., Männedorf, CH
Microplate reader	Multiskan Spectrum	Thermo Fisher Scientific, Waltham, USA
Microplate reader	Varioskan	Thermo Fisher Scientific, Waltham, USA
Microplate reader	Epoch 2	BioTek Instruments, Vermont, USA
NMR spectrometer	JEOL ECS 400	Jeol Ltd., Akishima, JPN
PCR thermocycler	C1000 thermal cycler	Bio-Rad Laboratories GmbH, München, DE
PCR thermocycler	CFX96 optical reaction module	Bio-Rad Laboratories GmbH, München, DE
PCR thermocycler	MJ Mini	Bio-Rad Laboratories GmbH, München, DE
PCR thermocycler	My Cycler	Bio-Rad Laboratories GmbH, München, DE
pH meter	FiveEasy	Mettler-Toledo GmbH, Gieen, DE
pH meter	FiveGo	Mettler-Toledo GmbH, Gieen, DE
pH meter electrode	LE438	Mettler-Toledo GmbH, Gieen, DE
pH meter electrode	InLab Micro Pro-ISM	Mettler-Toledo GmbH, Gieen, DE
Pipettes	Transferpette, manual	Brand GmbH, Wertheim, DE
Pipettes (multichannel)	Transferpette, manual	Brand GmbH, Wertheim, DE
Pipettes (multichannel)	Research pro, electric	Eppendorf AG, Hamburg, DE
Shaker	MaxQ 2000	Thermo Fisher Scientific, Waltham, USA
Shaker (notating)	Rocking Platform	VWR International GmbH, Darmstadt, DE
Shaker (plate)	TiMix 5 control	Edmund Bühler GmbH, Hechingen, DE
Spectrophotometer	NanoPhotometer P-330	Implen, Westlake Village, USA
Sonicator	Ultrasonic technology UIS250V	Hielscher Ultrasonics GmbH, Teltow, DE
Sonotrode	LS24d10	Hielscher Ultrasonics GmbH, Teltow, DE
Sonotrode	VialTweeter	Hielscher Ultrasonics GmbH, Teltow, DE
Water bath	ED-33	Julabo Labortechnik GmbH, Seelbach DE
Water bath	CC1 Compatible Control	Huber Kältemaschinenbau, Offenburg, DE
Water bath	Microprocessor Control MPC	Huber Kältemaschinenbau, Offenburg, DE
Water purification system	Q-POD MilliQ	Merck Millipore, Darmstadt, DE

Table 2.11 contains additional material and consumables used during this work.

Table 2.11: Additional materials.

Material	Provider
Centrifugation tubes/bottles 30 mL, 500 mL, 1 L	Nalge Nunc International, Rochester, USA
Disposable cuvettes	VWR International GmbH, Darmstadt, DE
Reaction tube 15 mL, 50 mL	Sarstedt, Nümbrecht, DE
F-bottom plates (clear)	Greiner Bio/One GmbH, Frickenhausen, DE
Gel extraction tool x-tracta	VWR International GmbH, Darmstadt, DE
Glass flasks 100 mL, 200 mL, 500 mL, 1 L, 5 L	VWR International GmbH, Darmstadt, DE
Microtiter plates 96 well (polystyrol, F-ground)	Greiner Bio/One GmbH, Frickenhausen, DE
Microseal 'B' PCR Plate Sealing Film	Bio-Rad Laboratories GmbH, München, DE
PD-10 desalting columns	GE Healthcare Europe GmbH, Freiburg, DE
Petri dishes	Sarstedt, Nümbrecht, DE
PCR plate 96 well, hard shell, thin wall	Bio-Rad Laboratories GmbH, München, DE
PCR reaction tubes	VWR International GmbH, Leuven, B
Reaction tubes 1,5 mL and 2 mL	Sarstedt, Nümbrecht, DE
Syringe 60 mL	Dispomed, Gelnhausen, DE
Syringe filter holder, 0.22 µm	VWR International GmbH, Darmstadt, DE
Syringe filter holder, 0.45 µm	VWR International GmbH, Darmstadt, DE

2.1.9 Software and online tools

Table 2.12 summarizes all software and online tools used during this work.

Table 2.12: Software and online tools.

Name	Purpose	Manufacturer
BioRad CFX Manager	BioRad qPCR analysis software	Bio-Rad Laboratories GmbH
PyMol 2.4.1	3D molecular visualization system	DeLano Scientific LLC, Schrödinger
GraphPad Prism 7	Statistical analysis, including enzyme kinetics	GraphPad Software Inc.
YASARA 15.11.18	Molecular-graphics, modelling and simulation	YASARA Biosciences GmbH
BioRender	Figure preparation	https://biorender.com/
Swiss PDB viewer	Protein analyzation tool	Swiss Institute of Bioinformatics
Chromeleon	Chromatography data system	Thermo Fisher Scientific
ChemDraw Pro 17.0	Molecule editor	PerkinElmer Inc.
Chem3D Pro 17.0	3D models of chemical structures	PerkinElmer Inc.
Unicorn 7.0	Control software for Äkta (FPLC)	GE Healthcare Europe GmbH
Xcalibur	Chromatography data system	Thermo Fisher Scientific
CloneManager 9.0	*In silico* DNA manipulation	Scientific and Educational Software
Snap Gene Viewer 4.3.5	Primer design	GSL Biotech LLC
Origin 2018b	Data analysis and graphing tool	OriginLab Corporation
Gel get Imager	Gel documentation	Intas Science GmbH
Adobe CS 6 Design	Figure preparation	Adobe System Software Ireland Ltd.
Citavi 6.8	Reference management	Swiss Academic Software GmbH
AutoDock Vina 1.1.2	Protein ligand docking tool	http://vina.scripps.edu/
ProtParam	Computation of various physical and chemical parameters of proteins	Swiss Institute of Bioinformatics
Robetta	Homology modeling, structure prediction	http://new.robetta.org/
ClustalOmega	DNA alignment tool	European Bioinformatics Institute
SIM – alignment tool	Protein alignment tool	Swiss Institute of Bioinformatics
Protein Data Base	Database	https://www.rcsb.org/
UniProt	Database	http://www.uniprot.org/
PubMed	Database	http://www.ncbi.nlm.nih.gov/pubmed
KEGG	Database	http://www.genome.jp/kegg/
BRENDA	Database	http://www.brenda-enzymes.org/
BLAST	Database	https://blast.ncbi.nlm.nih.gov

2.2 Methods

Methods used in this study were derived directly or indirectly from standard operational procedure (SOP) of the Chair of Chemistry of Biogenic Resources, Technical University of Munich – Campus Straubing for Biotechnology and Sustainability (TUMCS).

2.2.1 Bioinformatics

2.2.1.1 *In silico* analysis

The thiamine diphosphate-dependent (ThDP) benzaldehyde lyase was redesigned by protein engineering for the production of DHA from FALD. Therefore, several positions within the active pocket of the FLS have already been modified. In order to identify promising target positons, the focus was on amino acid residues in the active center that had not yet been investigated. The active site of the enzyme is formed at the interface of the monomers of the homodimer. The cofactor ThDP is thereby embedded. The analysis was performed using the protein structure visualization software PyMOL, while previously studied positions were taken from the literature.

2.2.1.2 Docking studies

Docking studies were performed to identify promising target positons. The crystal structure of FLS (PDB ID: 4QQ8) was previously published with thiamine diphosphate (ThDP) as cofactor.[86] 2D structures of the ligands, such as dihydroxyethyl-ThDP, FALD, GALD, DHA and ERY were drawn by using ChemDraw™ Professional (Version 17.0). These structures were converted to 3D structures (.pdb) and energy minimized by using Chem3D™ Professional (Version 17.0). Docking studies were performed by using YASARA, which rely on AutoDock VINA to dock ligand to a receptor. The FLS as receptor (PDB ID: 4QQ8) was prepared according to YASARA standard protocol. *In silico* analysis was done by using PyMOL (Version 2.4.1).

2.2.1.3 *In silico* engineering

FLS variants were generated *in silico* by using YASARA. Amino acid residues were swapped to desired amino acid and the protein was than energy minimized. Receptor was prepared according to YASARA standard protocol and used for further docking studies.

2.2.2 Microbiological methods

2.2.2.1 Cultivation and storage of *E. coli* strains

Cultivation of *E. coli* was performed in lysogeny broth (LB) for cloning purposes. All solutions were autoclaved (121°C, 20 min, 1 bar overpressure) and stored at room temperature, if not stated otherwise. Depending on the resistance marker of the strain, respective antibiotics were added. Cultures were grown in shaking flasks (37°C, 150 rpm, 12 h) or tubes (37°C, 300 rpm, 12 h) on an orbital shaker. Long-term storage stocks (stored at -80°C) were prepared by mixing liquid cultures with a sterile glycerol solution to a final glycerol concentration of 30 % (v/v).

2.2.2.2 Determination of the optical density of *E. coli* cell suspensions

The optical density of *E. coli* cultures was measured at 600 nm in plastic cuvettes in a total volume of 1 mL. An OD_{600} of 1.0 corresponds to approximately 3.2 x 10^8 cells mL^{-1}.

2.2.2.3 Preparation of chemically competent *E. coli* cells

This procedure was adapted from the Promega *Protocols and Applications Guide* (3rd edition), p.45-46. The corresponding *E. coli* strain was plate out from a glycerol stock on a LB agar plate and incubated at 37°C overnight. A single colony was used to inoculate the pre-culture (5 mL LB medium). The pre-culture was cultivated overnight (37°C, 300 rpm). The next day, the entire cell suspension was used to inoculate the main culture, which was grown in a 5 L baffled flask containing 500 mL LB medium and 20 mM $MgSO_4$ (37°C, 90 rpm). After the main culture had reached an OD_{600} of 0.4, the cells were harvested and centrifuged in a sterile centrifugation bottle (4500 x g, 4°C, 5 min). The cell pellet was gently resuspended in 200 mL of ice-cold TFB I buffer and incubated on ice for 30 min. After a second centrifugation step, the cell pellet was gently dissolved in 20 mL of ice-cold TFB II buffer and incubated again on ice for 30 min. Finally, the cell suspension was aliquoted to 100 µL in sterile reaction tubes (pre-cooled) and flash frozen in liquid nitrogen. The competent cells were stored at -80°C prior use. The stock solutions for TBF I and TBF II buffers (Table 2.13) were prepared and autoclaved separately. The buffers were always prepared freshly.

Table 2.13: Composition of TBF I and TBF II buffers for competent cell preparation.

TBF I	TBF II
30 mM potassium acetate (CH_3COOK)	10 mM MOPS
50 mM manganese chloride ($MnCl_2$)	-
10 mM calcium chloride ($CaCl_2$)	75 mM $CaCl_2$
100 mM rubidium chloride (RbCl)	10 mM RbCl
15 % (v/v) glycerol	15 % (v/v) glycerol
Adjust pH to 5.8 with acetic acid (CH_3COOH)	Adjust pH to 6.5 with potassium hydroxide (KOH)

2.2.2.4 Transformation of chemically competent *E. coli* cells

Chemically competent cells were thawed on ice for about 10 min. Plasmid DNA (1 – 10 µL) was added and the cells were incubated on ice for 30 min. After a heat shock at 42°C for 45 s, the cells were directly cooled on ice for 5 min. After supplementation of 900 µL of SOC-medium (pre-warmed), a regeneration step was performed for 1 h at 37°C on a rotary shaker (150 rpm). Finally, the cell suspension was plated out on LB agar plates with the respective selection marker.

2.2.2.5 Calculation of transformation efficiency

To calculate transformation efficiency, the competent *E. coli* strain was transformed with 1 ng of the pET24a plasmid DNA. Different dilutions were plated out on LB agar plates and incubated overnight at 37°C. The transformation efficiency was calculated using the following formula:

$$T_E = \frac{n_{colonies} \cdot f}{m_{DNA}}$$

Equation 2.1: Calculation of transformation efficiency.

T_E	Transformation efficiency (colonies per µg DNA)
$n_{colonies}$	Number of colonies on an agar plate
f	Dilution factor
m_{DNA}	DNA used for transformation in µg

2.2.2.6 Disposal of bacteria

All used bacterial cell suspensions and with bacteria contaminated materials were sterilized by autoclaving for 20 min at 121°C and 1 bar overpressure or 20 min at 134°C and 1 bar overpressure, respectively.

2.2.3 Molecular biological methods

2.2.3.1 Isolation and purification of plasmid DNA

Plasmid DNA was produced with *E. coli* XL1-blue, TOP10 or DH5α. Isolation and purification were performed using the GeneJET™ Plasmid Miniprep Kit. The instructions of the manufacturer were followed, whereby 5 mL of cell culture was harvested by centrifugation (RT, 4000 x g, 10 min) and plasmid DNA was eluted from the column with 50 µL of provided elution buffer. The plasmids were stored at -20°C.

2.2.3.2 Isolation and purification of genomic DNA

For the isolation of genomic DNA, the DNeasy UltraClean Microbial Kit was used without any changes to the given protocol described by the manufacturer.

2.2.3.3 Determination of DNA concentrations

DNA concentration was measured photometrically at 260 nm in a nanophotometer. Calculation was done according to the Lambert-Beer Law indicating that an extinction of 1.0 at 260 nm and a thickness of 1 cm refer to double stranded DNA concentration of 50 µg mL^{-1}. A DNA solution was considered as pure when there is no extinction higher than 300 nm and the ratio of the extinction at 260 nm over 280 nm ($\frac{A_{260}}{A_{280}}$) is at least 1.8.[186]

2.2.3.4 Amplification of DNA

Polymerase chain reaction (PCR) was performed as described by Ausubel and co-workers.[187] For the amplification of genes for cloning, Phusion® high-fidelity DNA polymerase was applied. The reactions were carried out as described by the manufacturer in a volume of 50 µL each in a thermocycler. The reaction conditions are summarized in Table 2.14. This procedure was also applied for the amplification of genes from genomic DNA. Here, cells of the organism of interest were resuspended in 50 µL MQ-H_2O and 1 µL of the suspension was used (or purified genomic DNA). The initial denaturation step was prolonged to 5 min to disrupt the cells, if necessary.

Table 2.14: Conditions for the Phusion® high-fidelity DNA polymerase.

Composition		Program			
Component	Amount	Step	[s]	[°C]	Cycles
5x HF-buffer	10.0 µL	Initial denaturation	30	98	1
10 mM dNTP mix	1.0 µL	Denaturation	10	98	
10 µM Primer forward	1.0 µL	Annealing	30	64	30
10 µM Primer reverse	1.0 µL	Elongation	30/kb	72	
DNA template	20 – 100 ng	Final elongation	300	72	1
Phusion polymerase	0.5 µL	Hold		16	∞
MQ-H_2O	*ad* 50 µL				

2.2.3.5 Agarose gel electrophoresis

Agarose gel electrophoresis was used to separate DNA fragments, such as PCR amplifications or restriction digests of plasmids, according to their length (Table 2.15). For this, a 1% (w/v) suspension of agarose in 1x TAE-buffer was prepared. The solution was stored at 65°C prior to use. To perform DNA electrophoresis, 25 µL of SERVA DNA stain clear G was added to 50 mL of 1% agarose solution before pouring the gel. The hardened agarose gel was then placed in the electrophoresis chamber and the samples were mixed with the appropriate amount of loading dye. A DNA size marker was also loaded to at least one of the wells as reference. After filling the pockets, the gel was run at 120 V for 20 to 30 min. If photos were taken, the gel was monitored with the gel get imager and UV-light was applied. If the gel slices had to be cut out and used for further experiments, only the transilluminator in combination with special orange glasses was used to check the result.

Table 2.15: Solutions for DNA gel electrophoresis.

Solution	Composition
TAE buffer	TRIS-acetate-EDTA
	40 mM TRIS-HCl (pH 7.6), 20 mM acetic acid, 1 mM Ethylenediaminetetraacetic acid (EDTA)
	A 50x TAE stock solution was prepared and prior the electrophoresis the 1x TAE buffer was made
1 %	10 g L^{-1} agarose in 1x TAE
	The solution was brought microwave-assisted to a boil and stored at 65°C. A nucleic acid stain was added prior use.
5x Loading dye	0.075 mM TRIS-HCl (pH 7.6), 0.05 mM EDTA, 50% (v/v) glycerol, 0.025% (w/v) bromophenol blue, 0.025% xylene cyanol
Nucleic acid stain	20000x SERVA DNA Stain Clear G (Serva, Heidelberg, DE)

2.2.3.6 Colony PCR

In order to verify the correct insertion of DNA fragments into plasmids, the *E. coli* cells that were transformed with ligation reactions, were analyzed by colony PCR. For this, single colonies from agar plates were resuspended in 20 µL LB medium and 1 µL of this suspension was used as a template in the PCR reaction. The cells were disrupted by a prolonged initial denaturation step. The common colony PCR conditions used in this work are listed in Table 2.16.

Table 2.16: Colony PCR reaction conditions.

Composition		Program			
Component	Amount	Step	[s]	[°C]	Cycles
10x ThermoPol buffer	2.0 µL	Initial denaturation	300	95	1
10 mM dNTP mix	0.4 µL	Denaturation	20	95	
10 µM Primer forward	0.4 µL	Annealing	30	55	30
10 µM Primer reverse	0.4 µL	Elongation	60/kb	72	
DNA template	1.0 µL	Final elongation	300	72	1
Taq polymerase	0.1 µL	Hold		16	∞
MQ-H_2O	*ad* 20 µL				

2.2.3.7 QuikChange™ PCR

The QuikChange™ site directed mutagenesis principle was used to create mutant gene variants that contain a specific amino acid alteration.[188] To obtain the amino acid mutation two complementary primers, which carry the desired codon alteration, were designed and used as starting points for the amplification of the new plasmid. To inhibit secondary structure formation in primer and template, 5% of dimethyl sulfoxide (DMSO)[189] can be added, if necessary. With the help of multiple thermal cycling steps, mutated plasmids were formed, which were then treated with DpnI. The endonuclease digests methylated and hemi methylated DNA, leading to the destruction of the parental DNA. The PCR product was purified using NucleoSpin® Gel and PCR Clean-up Kit using protocol described by the manufacturer. For chemically transformation of *E. coli*, 10 µL of elution was used. The conditions for the mutagenesis are listed in Table 2.17.

Table 2.17: Conditions for QuikChange™ PCR.

Composition		Program			
Component	Amount	Step	[s]	[°C]	Cycles
5x HF-buffer	10.0 µL	Initial denaturation	180	98	1
10 mM dNTP mix	1.0 µL	Denaturation	30	98	
10 µM Primer forward	1.0 µL	Annealing	60	64	18
10 µM Primer reverse	1.0 µL	Elongation*	30/kb	72	
DNA template	20 ng	Final elongation	600	72	1
Phusion polymerase	0.5 µL	Hold		16	∞
(DMSO	5.0 µL)				
MQ-H_2O	*ad* 50 µL	*amplification of the complete plasmid			

2.2.3.8 Site-saturation mutagenesis by overlap extension PCR

Oligonucleotides used for the generation of the semi-rational double mutant library of FLS are listed in Table 2.18. Protocol for introduction of degenerate bases at multiple codon locations was performed according to Williams *et al*., 2014.[190] Template used was pET24a_FLS with a length of 1749 bp. In order to saturate both positions simultaneously, three parts were first amplified individually (148, 276 and 1456 bp) and then combined using another PCR. The total fragment had a length of 1880 bp. Oligonucleotides 3a-e and 5a-e were mixed in advance in a ratio of 8:2:3:1:1 and then used as forward primer to amplify fragments 2 and 3, respectively. After verification by sequencing, the library was digested with NdeI-XhoI and was ligated again.

Table 2.18: Oligonucleotides for overlap extension PCR.

Part	Name	Oligonucleotide sequence	DC*	Ratio
1	1_T7_fwd_mut	GAATTGTGAGCGGATAACAATTCCC	-	-
1	2_Part1_rev	CCATGCAGGCCAAACAGATG	-	-
2	3a_H29NRT_fwd	CATCTGTTTGGCCTGCATGGNRTTCATATTGACACCATTTTTC	NRT	8
2	3b_H29ATS_fwd	CATCTGTTTGGCCTGCATGGATSTCATATTGACACCATTTTTC	ATS	2
2	3c_H291VAA_fwd	CATCTGTTTGGCCTGCATGGVAATCATATTGACACCATTTTTC	VAA	3
2	3d_H29CCG_fwd	CATCTGTTTGGCCTGCATGGCCGTCATATTGACACCATTTTTC	CCG	1
2	3e_H29ACT_fwd	CATCTGTTTGGCCTGCATGGACTTCATATTGACACCATTTTTC	ACT	1
2	4_Part2_rev	CAGGGTGTTGGTTTCGTCATC	-	-
3	5a_Q113NRT_fwd	GATGACGAAACCAACACCCTGNRTGCCGGTATTGATCAGG	NRT	8
3	5b_Q113ATS_fwd	GATGACGAAACCAACACCCTGATSGCCGGTATTGATCAGG	ATS	2
3	5c_Q113VAA_fwd	GATGACGAAACCAACACCCTGVAAGCCGGTATTGATCAGG	VAA	3
3	5d_Q113CCG_fwd	GATGACGAAACCAACACCCTGCCGGCCGGTATTGATCAGG	CCG	1
3	5e_Q113ACT_fwd	GATGACGAAACCAACACCCTGACTGCCGGTATTGATCAGG	ACT	1
3	6_T7_rev-mut	CTTTGTTAGCAGCCGGATCTC	-	-

*DC = degenerated codon

2.2.3.9 Restriction of double stranded DNA with restriction endonucleases

For the specific cleavage of double stranded DNA, type IIP (palindromic specificity; one domain) and type IIS (shifted cleavage; two domains) restriction endonucleases were used. Type IIP restriction enzymes (NdeI and XhoI) recognize specific palindromic sequences and create single stranded overhangs, so called sticky ends, within these sequences. Type IIS restriction enzymes (BsaI and BbsI) in contrast recognize asymmetric DNA sequences and create sticky ends by cleavage outside of the recognition site. In order to clone genes into a vector, it is first necessary to enzymatically digest the corresponding DNA, vector and gene of interest, to create linear DNA fragments with the complementary sticky ends. This allows the gene of interest to be inserted into the vector backbone, resulting in a plasmid carrying the desired gene. To reduce self-ligation events of the backbone, different single stranded overhangs at the 3' and 5' end are created. The reaction mixture (Table 2.19) was incubated for 2 h at 37°C. After 1 h incubation, 1 µL CIP (calf intestinal phosphatase; 5 U) was added to the samples containing the vector backbone, to cleave the 3′ and 5′ phosphate group off the DNA, so self-ligation events will be reduced further. The reactions were stopped by enzyme inactivation according to the manufacturer. Finally, the samples were ready for the application on an agarose gel to separate the different DNA fragments. The correct DNA bands were excised using X-tracta gel extraction tool and purified using NucleoSpin® Gel and PCR Clean-up Kit following a standard protocol by the manufacturer.

Table 2.19: Sample components of the restriction digest.

Component	Amount
10x CutSmart buffer	4 µL
DNA	2 µg
Restriction enzyme I	1 µL (20 U)
Restitction enzyme II	1 µL (20 U)
MQ-H_2O	*ad* 40 µL

2.2.3.10 Ligation of DNA fragments with single stranded overhangs

If the DNA was enzymatically digested with restriction enzymes, usually a ligation step to insert the gene of interest into the vector backbone was carried out. Hence, a total reaction volume of 20 µL was prepared, containing 2 µL of 10x T4 ligation buffer, 1 µL of T4 ligase and the according volumes of DNA solution to apply a molar ratio of insert to backbone of 3:1. The remaining volume was filled up with MQ-H_2O. The samples were incubated overnight at 16°C and finally 10 µL of the sample was used for the transformation of *E. coli*.

2.2.3.11 Ligation of DNA fragments with blunt ends

Blunt end ligations using the vector pJET2.1/blunt were performed with the CloneJET™ PCR Cloning Kit following the instructions of the manufacturer. Inserts were double-stranded DNA fragments. Chemically competent *E. coli* cells were transformed using 1 µL of the reaction mixture.

2.2.3.12 DNA sequencing

Sequencing of DNA was performed by Eurofins Genomics (Ebersberg, DE). The TubeSeq Service of Eurofins Genomics was used, where the samples are sequenced using the Sanger method. Usually 50 to 100 ng μL^{-1} DNA were prepared in 15 µL of MQ-H_2O, followed by the addition of 2 µL of a sequencing primer.

2.2.4 Protein production and analysis

2.2.4.1 Preparation of $PISA1_{GO}$

The expression plasmid of $PISA1_{GO}$ was kindly provided by Prof. Kurt Faber (Department of Chemistry, Organic and Bioorganic Chemistry, University of Graz).[169] $PISA1_{GO}$ was expressed, purified and dialyzed by José Guillermo Ortiz Tena.[176,191] The concentration was determined using a nanophotometer. The enzyme preparation was mixed with glycerol at 20% (v/v) final concentration. $PISA1_{GO}$ (2.8 mg mL^{-1}) was aliquoted and stored at -20°C until prior to use.[191]

2.2.4.2 Expression of recombinant genes in *E. coli*

For the expression of recombinant genes, *E. coli* BL21 (DE3) or *E. coli* Rosetta (DE3) were transformed with the corresponding plasmid. For the analysis of gene expression into soluble proteins, small-scale expression tests were performed in a volume of 50 mL of various selective media in a 250 mL shaking flasks with baffles. From a single colony, a pre-culture was prepared in respective media (37°C, 150 rpm, 12 h) and used for the inoculation of the main cultures to an OD_{600} of 0.05. After the cell suspensions had reached an OD_{600} of 0.8 to 1.0 (37°C, 150 rpm), the cultures were induced with 0.5 mM isopropyl-β-D-thiogalactopyranoside (IPTG), if necessary, and were incubated either at 16°C, 20°C, room temperature, 30°C or at 37°C overnight. After 3 h expression at 30°C and 37°C samples were harvested (2 mL) and stored at -20°C. The next day samples from all conditions were then harvested (2 mL), resuspended in 1 mL of corresponding

binding buffer and disrupted by sonication (100% amplitude, 0.5 ms, 3x 45 sec pulse/45 sec cooling on ice). The soluble fraction was obtained by centrifugation (14.800 x g, 3 min, 4°C) and both the soluble and insoluble fraction were analyzed by SDS-PAGE. For preparation of recombinant proteins, expression was performed in a volume of 1 L of respective medium using a 5 L shaking flask with baffles. From a single colony, a pre-culture (20 mL in 100 mL baffled shaking flask) was prepared, which was used for inoculation (OD_{600} of 0.05) of the main cultures. The cells were incubated at 37°C and 90 rpm until an OD_{600} of 0.8 to 1.0 was reached. Then cultures were induced with 0.5 mM IPTG and were incubated overnight at room temperature. The cells were harvested by centrifugation (4.000 x g, 15 min, 20°C) and either directly used for protein purification or stored at -20 °C or -80 °C prior to the purification.

2.2.4.3 Preparation of buffers for protein purification

All buffers were filtered through 0.45 µm filter paper prior to use and are summarized in Table 2.20. Buffers were stored at room temperature.

Table 2.20: Buffers for protein purification.

Proteins	Binding buffer	Elution buffer	Desalting/Dialysis buffer
FLS	50 mM NaP_i buffer, pH 8.2 500 mM NaCl 5 mM Imidazole	50 mM NaP_i buffer, pH 8.2 500 mM NaCl 500 mM Imidazole	50 mM NaP_i buffer, pH 8.2
*Pfu*ADHd	50 mM NaPi buffer, pH 8.2	-	100 mM potassium phosphate, pH 6.0
APSk (MET14)	50 mM HEPES/K^+, pH 8.0 300 mM NaCl 10 mM Imidazole	50 mM HEPES/K^+, pH 8.0 300 mM NaCl 500 mM Imidazole	50 mM HEPES/K^+, pH 8.0
ATPs/GTPase (cysDN)	50 mM TRIS-HCl, pH 8.0 300 mM NaCl 50 mM Imidazole	50 mM TRIS-HCl, pH 8.0 300 mM NaCl 500 mM Imidazole	50 mM HEPES/K^+, pH 8.0
PPDK	50 mM KP_i buffer pH 8.0 500 mM NaCl 20 mM Imidazole 10 % (w/v) glycerol	50 mM KP_i buffer pH 8.0 500 mM NaCl 500 mM Imidazole 10 % (w/v) glycerol	50 mM HEPES/K^+, pH 8.0
PISA1	50 mM NaP_i buffer, pH 8.2 500 mM NaCl 5 mM Imidazole	50 mM NaP_i buffer, pH 8.2 500 mM NaCl 500 mM Imidazole	100 mM TRIS-HCl, pH 8.2
CmAS	100 mM TRIS-HCl, pH 7.5 500 mM NaCl 5 mM Imidazole	100 mM TRIS-HCl, pH 7.5 500 mM NaCl 500 mM Imidazole	100 mM TRIS-HCl, pH 7.5
FtAS	50 mM NaP_i buffer, pH 8.2 500 mM NaCl 5 mM Imidazole	50 mM NaP_i buffer, pH 8.2 500 mM NaCl 500 mM Imidazole	100 mM TRIS-HCl, pH 8.2
VpAS	100 mM TRIS-HCl, pH 7.5 500 mM NaCl 5 mM Imidazole	100 mM TRIS-HCl, pH 7.5 500 mM NaCl 500 mM Imidazole	100 mM TRIS-HCl, pH 7.5

2.2.4.4 Cell disruption by sonication

Harvested cells of the expression culture were dissolved (10 to 20% w/v) in corresponding binding buffer supplemented with 5 µg mL^{-1} of DNase. The cell suspension (50 mL reaction tube) was placed in ice and a sonotrode was inserted. Sonication was performed for 15 min (75% amplitude, 0.5 ms pulse). Upon sonication, the cell suspension was centrifuged at 45,000 x g for 30 min at 10°C. The supernatant was filtered through 0.45 µm syringe filter holder before His_6-tagged proteins were purified by immobilized metal ion affinity chromatography (IMAC).

2.2.4.5 Immobilized metal ion affinity chromatography

Immobilized metal ion affinity chromatography was performed using HisTrap™ FF crude columns with 5 mL column volume (CV) and the Äkta™ purifier system. All enzymes used in this study bearing His_6-tag at the N or C-terminus. The protein supernatant was loaded with 5.0 mL min^{-1} flow rate. The column was washed with the binding buffer until the online UV detector (280 nm) showed absorption <50 mAU (approximately 25 mL of the binding buffer) using 5.0 mL min^{-1} flow rate. During the chromatography, histidine residues of the His_6-tag bind to vacant positions in the coordination sphere of the immobilized nickel ions with high specificity and affinity. Other proteins will pass through the column and will be washed away. The protein of interest can then be eluted with imidazole. Higher concentration of imidazole will break the interaction between the nickel ions and the histidine residues. A single fraction was collected using elution buffer and a flowrate of 5.0 mL min^{-1}. The column was equilibrated again with binding buffer using 10.0 mL min^{-1} of flow rate for another purification run or was washed with MQ-H_2O and stored in 20% ethanol. Finally, protein purity was analyzed *via* SDS-PAGE.

2.2.4.6 Size exclusion chromatography for desalting proteins

In order to switch buffers and remove salts, size exclusion chromatography of the elution fraction was performed. Here, the Äkta™ purifier system was used with the column HiPrep 26/10 desalting with approximately 53 mL column volume. The following procedure was applied:

Flow rate:	8.0 to 15.0 mL min^{-1}	
Equilibration:	2 CV	Desalting buffer
Loading:	max. 15 mL	Elution fraction
Elution:	2 CV	Desalting buffer;
		with manual collection of the protein fraction
		(monitored by UV)
Column cleaning:	2 CV	Desalting buffer
Column storage:	2 CV	MQ-H_2O
	2 CV	20% EtOH

Equilibration, column cleaning and column storage were performed with 15.0 mL min^{-1} flow rate; protein loading and elution were performed with 8.0 mL min^{-1} flow rate.

2.2.4.7 Desalting of proteins with PD-10 column

For desalting of smaller sample volumes, PD-10 desalting columns (sephadex G-25 resin) were used. Columns were first washed with MQ-H_2O (25 mL) and then equilibrated with desired buffer (25 mL). Sample volume was 1.0 – 2.5 mL while eluting with 3.5 mL buffer (dilution factor of 1.4). The elution was collected in 0.5 mL fractions. Columns were stored in 20% ethanol (w/v).

2.2.4.8 Protein dialysis

In order to remove salts and imidazole, dialysis of alkylsulfatase preparations were performed as well. The elution fraction were dialyzed twice for 6 h against 200x excess of dialysis buffer at 4°C. A dialysis membrane made of regenerated cellulose with molecular weight cut-off of 6.0 to 8.0 kDa were used.

2.2.4.9 Heat purification of *Pfu*ADHd

The cell pellet was dissolved in binding buffer (50 mM sodium phosphate, pH 8.2) and disrupted by sonication in the presence of lysozyme in an ice bath. The resulting cell lysate was heated for 30 min at 80°C, subsequently centrifuged for 30 min at 40000 x g. The supernatant was filtered through a 0.45 µm filter before desalting (100 mM potassium phosphate, pH 6.0) using HiPrep desalting column 26/10 50 mL.

2.2.4.10 Determination of protein concentration using UV spectroscopy

The concentration of purified proteins was determined by UV spectroscopy using a nano-photometer. The absorption of aromatic amino acid such as tryptophan and tyrosine, as well as of the disulfide bridging cysteine between 250 and 300 nm are taken into account. The extinction coefficient is then calculated by the following formula[192]:

$$\varepsilon_{280} = \sum W \cdot 5500 + \sum Y \cdot 1490 + \sum C \cdot 125$$

Equation 2.2: Calculation of the extinction coefficient of proteins.

ε_{280}	Extinction coefficient [M^{-1} cm^{-1}]
W	Tryptophan
Y	Tyrosine
C	Cysteine

The protein concentration can then be assessed from the Lambert-Beer law:

$$c = \frac{A_{280}}{d \cdot \varepsilon_{280}} \cdot M_W$$

Equation 2.3: Calculation of the protein concentration using UV spectroscopy.

c	Protein concentration [mg mL^{-1}]
A_{280}	Absorption at 280 nm
d	Optical path length [cm]
ε_{280}	Extinction coefficient [M^{-1} cm^{-1}]
M_W	Molecular weight [g mol^{-1}]

Table 2.21 listed the molecular weight, extinction coefficient and GenBank ID of all enzymes used in this work. Hereby, the His_6-tag was considered for all proteins. For all alkylsulfatases it was also considered that the native N-terminal secretion tag was spliced off already. The molecular weight (M_W) as well as the extinction coefficient at 280 nm (ε_{280}) of all proteins was calculated with the ProtParam tool. Assuming all cysteine residues are reduced.

Table 2.21: Molecular weight, extinction coefficient and GeneBank ID of all enzymes used.

Enzymes	Mw [g mol^{-1}]	ε280 [M^{-1} cm^{-1}]	GenBank ID
FLS	61,378.9	53,400	-
*Pfu*ADHd	31,795.3	52,370	AAL82084.1
APSk	23,000.0	93,300	CAA41055.1
ATPS/GTPase	87,700.0	21,500	AAA23645.1/AAA23646.1
PPDK	97,680.1	53,860	CBL55854.1
PISA1	70,899.5	82,280	CCA63329.1
CmAS	70,980.1	99,240	AVA36238.1
FtAS	62,677.6	73,340	SFF55323.1
VpAS	70,165.7	82,280	ADU34375.1

2.2.4.11 Storage of Purified Proteins

ATPs/GTPase, APSk and PPDK prepared for the sulfate assay were mixed 1:1 with 40% (w/v) glycerol. This enzymes were aliquoted, flash frozen in liquid nitrogen and stored at -20°C prior to use. All other enzymes were slowly dripped into liquid nitrogen, resulting in aliquots of 20 to 50 µL. The globules were stored in a 50 mL reaction tube at -80°C prior to use.

2.2.4.12 Thermofluor assay

Protein melting points (T_m) were determined using the thermofluor assay. Here, SYPRO™ orange was used as fluorescent dye and instructions of Boivin *et al*. were followed.[193] The dye interacts with the hydrophobic core of the protein, which is exposed by unfolding under denaturing conditions. At this point, the dye becomes fluorescent, resulting in a sharp sigmoidal curve in the detection unit. The inflection point of the sigmoidal curve represents the melting temperature (T_m) at which 50 % of the protein is unfolded. An alternative representation is to plot the first derivative (dRFU dT^{-1}), where the apex equals T_m. Total well volume was 25 µL, containing 2 µL of 1 mg mL^{-1} enzyme, 2 µL of SYPRO Orange working stock and 21 µL of buffer. Everything was prepared as triplicates in Hard-Shell® 96-well PCR plates. After centrifugation step (2500 x g, 30 s) the plate was inserted into the BioRad qPCR cycler. The temperature gradient was set to begin at 5°C and rise until 95°C in steps of 0.5°C per 30 s. The Thermofluor assay allows the detection of global stability trends according to e.g. pH, salt concentration or buffer type, and can also be used to screen the effect of small molecules that can affect the folding, aggregation state and solubility of the protein construct.[193] In addition, this can be used as an evaluation tool for metal ion binding of alkylsulfatases to differentiate between holoenzymes and apoenzymes as well as to investigate aldehyde dependent protein inactivation and modification.

2.2.4.13 Sodium dodecyl sulfate-polyacrylamide gel electrophoresis (SDS-PAGE)

Sodium dodecyl sulfate–polyacrylamide gel electrophoresis (SDS-PAGE) was performed for protein separation as described by Ausubel and coworkers[187] with modifications. To prepare polyacrylamide gels, the Mini/PROTEAN® Tetra Cell Casting Stand and Clamps were used. For 2 gels, a separating gel (12% acrylamide) was prepared according to Table 2.22. The solution was swirled gently, immediately used to load the chambers and covered with isopropanol. After polymerization (RT, 60 min), the isopropanol layer was removed, the stacking gel layer (5% acrylamide) added and the desired comb inserted. After polymerization (RT, 60 min), gels were stored at 4°C until usage, wrapped in wet paper towels. For sample preparation, 40 µL protein sample was mixed with 10 µL 5x SDS loading buffer, spun down, and incubated for 5 min at 95°C. Then, 7.5 µL per sample were loaded on a 12% SDS-gel. SDS electrophoresis buffer was added to the Mini-PROTEAN® Tetra Vertical Electrophoresis Cell and the gel was run for about 45 to 60 min with 45 mA for each gel. To determine the protein size, a protein size marker was applied as reference. After the electrophoretic run, the gels were microwave-assisted stained with the coomassie-staining solution and destained with MQ-H_2O and a tissue soaked with 80% ethanol.

Table 2.22: Solutions for SDS-PAGE.

Solution	Separating gel	Stacking gel	Composition
Acrylamide	4.00 mL	0.83 mL	30.0% (v/v) acrylamide, 0.8% bisarcylamide
4x Separating gel buffer	2.50 mL	-	0.8% (w/v) SDS, 1.5 M TRIS The pH was adjusted with HCl to 8.80
4x Stacking gel buffer	-	1.25 mL	0.8% (w/v) SDS, 0.5 M TRIS The pH was adjusted with HCl to 6.80
MQ-H_2O	3.29 mL	2.77 mL	-
APS	100 µL	50 µL	10% (w/v) ammonium persulfate
TEMED	10 µL	5 µL	N,N,N',N'-tetramethylethane-1,2-diamine
5x SDS loading buffer			50.0% (v/v) glycerol, 12.5% (v/v) β-mercaptoethanol, 7.5% (w/v) SDS, 0.25 g L^{-1} bromophenol blue The pH was adjusted with HCl to 6.80
10 x SDS electrophoresis buffer			1.0% (w/v) SDS, 2.5 M TRIS, 1.92 M glycine The pH was adjusted with HCl to 8.50
1x Coomassie-staining solution			A spatula coomassie brilliant blue G 250 in MQ-H_2O with 0.1% (v/v) hydrochloric acid

2.2.5 Specific methods for formolase

2.2.5.1 GDH assay

DHA production from FALD was measured using a coupled enzyme assay. 100 µL of supernatant containing FLS wild type or variants were combined with 100 µL assay mix consisting of 100 mM phosphate buffer (pH 8.0), 1 mM $MgSO_4$, 1.6 mM NADH, 268 mM FALD, 0.1 mM TPP and 100 µg mL^{-1} glycerol dehydrogenase. NADH concentrations were measured over a 1 h period at 30°C and 340nm.

2.2.5.2 DPA assay

GALD was determined in 96-well scale in the presence of FALD and DHA by using a spectrophotometric chromogenic reagent, as previously published.[87] However, the assay also reacted equally with ERY, so that GALD and ERY were not distinguishable. Fortunately, this was not a serious issue, as GALD and ERY was distinguishable by using the *Pfu*ADHd assay. Chromogenic solution was prepared as followed: 3.0 g of diphenylamine was dissolved in 250 mL acetic acid and then 7.5 mL concentrated sulfuric acid was added. 100 µL sample was transferred to a DWP and 300 µL of chromogenic solution was added to each well. DWPs were sealed with an aluminum foil and incubated at 90°C (water bath) for 15 min. After an additional 15 min on the bench (cool down), the plates were centrifuged at 4000 x g for 10 min. Finally, 200 µL were transferred to a 96-MTP and absorption at 650 nm was measured by using a spectrophotometer.

2.2.5.3 *Pfu*ADHd assay

In order to distinguish between GALD and ERY (DPA assay), the same reaction mixture was assayed with a thermostable alcohol dehydrogenase from *Pyrococcus furiosus* (*Pfu*ADHd). Initial experiments showed specific activity of *Pfu*ADHd with 50 mM GALD in presence and absence of equimolar FALD, DHA and ERY. The reduction master mix contained *Pfu*ADHd in 100 mM potassium phosphate, pH 6.0 supplemented with 2.0 mM NADH. A total of 3 L expression culture was used to prepare 170 mL *Pfu*ADHd (heat purified). Subsequently, 2 mM NADH was weighed and added to the mixture. Finally, 100 µL of sample (FALD or GALD consumption) was transferred to 96-MTP and 100 µL of reduction master mix was added. Oxidation of NADH was monitored at 30°C for 15 min at 340 nm using a spectrophotometer.

2.2.5.4 HPLC analytics

For analysis, 50 µL of each sample was withdrawn and diluted 1:10 with 5.0 mM H_2SO_4. The mixtures were then filtered through 10 kDa filters. The filtrates were subjected to HPLC analysis. FALD, GALD, DHA and ERY were separated using an ion-exclusion column (Rezex™ ROA-organic acid H+ (8%)), run isocratically using 2.5 mM H_2SO_4 at 70°C for 20 min.

2.2.5.5 Setup of the high-throughput combinatorial screening

To evaluate the variants in terms of GALD, DHA and ERY production, the double mutant library was screened using different assays. In total, each variant was tested under six conditions. All reactions were prepared in 96-well scale using 50 mM sodium phosphate, pH 8.2 supplemented with 2.0 mM $MgSO_4$, 0.1 mM ThDP and substrate. All approaches were incubated at 30°C in a plate shaker. The following conditions were investigated: (1) Initial production of DHA started from 134 mM FALD (GDH assay). Simultaneous production of GALD and ERY based on 100 mM FALD after (2) 1 h and (3) 22 h (DPA assay). In order to distinguish between GALD and ERY formation activity, the reaction mixtures of (2) and (3) were assayed using GALD specific *Pfu*ADHd, also after (4) 1 h and (5) 22 h. The consumption of GALD was investigated as well. For this purpose, the library was incubated with 100 mM GALD and the remaining GALD was detected after (6) 22 h by *Pfu*ADHd assay.

2.2.5.6 Reaction conditions

Reactions for initial measurement of DHA were prepared separately and are described in the GDH assay section. FALD consumption was prepared as followed: 200 µL of library supernatant was transferred to a 96 DWP and 200 µL master mix (100 mM sodium phosphate, pH 8.2 with 4.0 mM $MgSO_4$, 0.1 mM ThDP and 100 mM FALD) was added. To avoid evaporation all plates were sealed. DWPs were incubated at 30°C in the plate shaker. After one hour, 100 µL of sample was taken for the DPA assay and another 100 µL for the *Pfu*AdhD assay. This was repeated after further 21 h incubation time. GALD consumption was prepared as followed: 100 µL of library supernatant was transferred to a 96 MTP and 100 µL master mix (100 mM sodium phosphate, pH 8.2 supplemented with 4.0 mM $MgSO_4$, 0.1 mM ThDP and 100 mM GALD) was added. To avoid evaporation all plates were sealed again. 96 MTPs were incubated at 30°C in the plate shaker. After 22 h, 100 µL of sample was taken for the *Pfu*AdhD assay.

2.2.5.7 Expression of the double mutant library of FLS

Electrocompetent *E. coli* BL21 (DE3) was transformed by using the double mutant library prepared as described in chapter 2.2.3.8. The obtained clones were robot-assisted transferred into individual wells of a 96 DWP using a colony picker, where each well was filled with 1 mL TB media supplemented with 50 µg mL^{-1} kanamycin. Incubation was conducted overnight at 37°C and 1000 rpm using a plate shaker. Then, the optical density (OD_{710}) was measured automatically (Tecan Freedom Evo 200, CH) and robot-assisted inoculation of the main cultures in 96 deep well plate (DWP) to an OD_{710} of 0.05 was done. To support initial cell growth, the culture plates were incubated at 37°C, 1000 rpm for 3.75 h followed by automated OD measurements. Subsequently, to induce gene expression, 1 mM IPTG was added using the 96-Multichannel-Arm (MCA) of the robot, prior to incubation for 16 h at 25°C, 1000 rpm. Following incubation, the biomass was harvested by centrifugation (15 min, 1000 rpm, 4°C) with subsequent cell lysis for 1.5 h.

2.2.5.8 Characterization of variants

Characterization of FLS variants was performed *via* HPLC to allow simultaneous detection of FALD, GALD, DHA and ERY. All variants were investigated under three conditions to evaluate their putative behavior in a synthetic enzyme cascade. Therefore, 40 µM of FLS was applied to FALD (3.0 g L^{-1}), GALD (3.0 g L^{-1}) or a mixture (1.5 + 1.5 g L^{-1}). Reactions were performed in 50 mM sodium phosphate buffer (pH 8.2) supplemented with 2 mM $MgCl_2$ and 0.1 mM ThDP for 22 h at 30°C. The template FLS was not considered here because it primarily produced DHA from FALD. Analysis was performed *via* HPLC.

2.2.5.9 Kinetic characterization

For kinetic characterization with GALD, approximately one-month-old purified FLS_wt, FLS_B1 and FLS_B2 (stored at -80°C) were thawed at room temperature. Reactions were prepared in a 96-MTP, containing 30 µM of respective FLS (1.84 mg mL^{-1}), 2 mM $MgSO_4$, 0.1 mM ThDP and varying GALD concentrations in 50 mM sodium phosphate buffer, pH 8.0. Thereby, GALD concentrations of 2.5, 5, 7.5, 10, 25, 50, 75, 100, 250, 500, 750 and 1000 mM were investigated. After pre-incubation of reaction mixture and enzymes separately for 10 min at 30°C, reactions were started with addition of enzyme. After mixing by pipetting directly t_0 samples were taken, proper diluted and prepared for HPLC analysis. After further 90 min incubation at 30°C and 750 rpm shaking in a MTP-Shaker, again samples were taken. The initial slope based on ERY production was used to determine catalytic activities. Subsequently, the data were fitted to determine the kinetic parameters.

2.2.5.10 Reaction conditions of the synthetic enzyme cascade

Reactions were performed in 1.5 mL reaction tubes with a total volume of 200 µL. A 1:1 ratio (45 µM each) of purified enzymes were applied to 3.0 g L^{-1} FALD in 50 mM sodium phosphate buffer (pH 8.2) supplemented with 2 mM $MgCl_2$ and 0.1 mM ThDP and were incubated for 22 h at 30°C. In doing so, FLS_A1, FLS_A2 or FLS_A3 was combined with FLS_B1 or FLS_B2, respectively. Analysis was performed by HPLC.

2.2.5.11 Biocatalysis of erythrulose

Biocatalysis of ERY directly from GALD was investigated using FLS_wt, FLS_B1 and FLS_B2 in comparison. Purified enzymes (stored at -80°C) were thawed at room temperature and concentrated using 10 kDa centrifugation filters (10 min, 10.000 x g). Reactions were prepared as duplicates (200 µL approach) in a 96-MTP. A aluminum sealing was used to avoid evaporation. The reaction mixture was prepared in 50 mM sodium phosphate buffer, pH 8.0 and contained 150 µM of enzyme, 25 g L^{-1} GALD, 2 mM $MgSO_4$ and 0.1 mM ThDP. After pre-incubation for 10 min at 30°C, reactions were started with additions of enzymes. Reactions were incubated at 30°C and 750 rpm shaking. Samples were taken after 0 h, 2 h, 4 h, 8 h and 16 h and were analyzed by HPLC. The 96-MTP was sealed with an aluminum sealing.

2.2.6 Specific methods for alkylsulfatases

2.2.6.1 Standard reaction conditions for PISA1

The catalytic activity of PISA1 was tested with various secondary alkyl sulfate esters as substrate, described by Schober and coworkers.[169] Here, usually 5 mg of racemic substrate was dissolved in 980 µL of 100 mM TRIS-HCl, pH 8.2. The reaction was started by adding 20 µL of PISA1 (6.5 mg mL^{-1}) and the reaction mixture was shaken at 30°C and 120 rpm for 24 h. However, initial experiments within this work revealed that both the amount of enzyme used and the reaction time can be significantly reduced. For higher accuracy, 20 mM substrate from a 200 mM stock solution was generally used and reactions were performed in 500 µL scale for 1 h at 30°C and 350 rpm.

2.2.6.2 Sulfate assay

The enzymatic hydrolysis of alkyl sulfate esters leads to the release of free sulfate (SO_4^{2-}), which can be detected calorimetrically. Here, free sulfate is coupled to the oxidation of the dye DA-64 to produce Bindschedler's green *via* an enzyme cascade, yielding a colorimetric signal at 727 nm, which is proportional to the sulfate concentration in the sample.[185] Potassium sulfate (K_2SO_4) dissolved in MQ-H_2O was used as a standard. The sulfate assay was calibrated in a linear range between 2.5 and 250.0 µM K_2SO_4. MQ-H_2O blank and standards were measured in triplicates and samples in duplicates. Samples were proper diluted with MQ-H_2O. The measurements were performed in 96-MTP scale. 50 µL of the sample, standard or blank was mixed with 50 µL of master mix 1 (Table 2.23). The plate was sealed and incubated for 45 min at room temperature, while shaking on a microtiter plate shaker. Then, 100 µL of master mix 2 (Table 2.23) was added and the plate was incubated for 30 min at 37°C, while shaking. The absorbance (A) was measured photometrically at 727 and 540 nm, and $A_{727-540}$ was computed for each sample, standard or blank. The calibration curve was then calculated from mean values by subtracting the blank absorbance from each calibration point. Linear regression was then used to calculate the sulfate concentration. The master mix components ATP, GTP, APSk, ATPs/GTPase, DA-64, PEP, AMP, ThDP, PPDK, POx and HRP were prepared for 120 reactions, aliquoted and stored at -20°C. Aliquots were thawed on ice. Both master mixes were prepared directly prior to use on ice.

Table 2.23: Master mix composition for sulfate assay.

Master mix 1 (final concentration)	Master mix 2 (final concentration)
25.0 mM HEPES/K^+, pH 8.5	200.0 mM KP_i buffer, pH 5.7
6.00 mM Magnesium chloride ($MgCl_2$)	0.10 mM Magnesium chloride ($MgCl_2$)
2.00 mM Adenosine triphosphate (ATP)	20.0 mM Ammonium chloride (NH_4Cl)
2.00 mM Guanosine triphosphate (GTP)	0.20 mM DA-64
10.0 µM APS kinase (MET14)	1.00 mM Phosphoenolpyruvate (PEP)
1.00 µM ATP sulfurylase/GTPase (cysDN)	1.00 mM Adenosine monophosphate (AMP)
	1.00 mM Thiamine diphosphate (ThDP)
	0.10 U mL^{-1} Pyruvate phosphate dikinase (PPDK)
	0.10 U mL^{-1} Pyruvate oxidase (POx)
	0.40 U mL^{-1} Horseradish peroxidase (HRP)

2.2.6.3 GC analytics

The enzymatic hydrolysis of alkyl sulfate esters leads to the release of the corresponding alcohol, which can be detected by gas chromatography. Detection can be performed either by coupling with a flame ionization detector (GC/FID) or by coupling with mass spectrometry (GC/MS). In order to detect even traces of non-natural products, the more sensitive GC/MS analysis was generally preferred. To extract aliphatic target molecules, ethyl acetate (1:1) was added to the sample and mixed well. The organic phase was carefully collected and a spatula tip of sodium sulfate was added to remove any residual water. After a centrifugation step, the dried sample was transferred into GC microvials. The standards were treated identically to the samples. The GC/MS measurement was performed using a Rxi®-5Sil-MS column (30 m, 0.25 mm, 0.25 µm film) on a ThermoQuest™ Trace™ GC 2000 ultra gas chromatograph with a quadrupole detector (Ultra Trace™ DSQ II). 1 µL of sample was injected (280°C) *via* autosampler (TriPlus™) with a split of 1:10. He carrier gas flow of 0.6 mL min^{-1} (constant), and separated on the column (50°C/hold 1.0 min, 15°C min^{-1} to 120°C, 30°C min^{-1} to 280°C/hold for 1.0 min). The transfer line and ion source were set at 250°C and the MS start time was 3.0 min.

2.2.6.4 Screening of optimal reaction conditions

In order to determine optimal reaction conditions, the kinetic stability of alkylsulfatases was investigated under various conditions. For this, 10 mM *rac*-2-octanyl sulfate/K^+ was applied as substrate and the *sec*-alkylsulfatase activity was studied in a temperature range of 30 – 75°C and a pH range of 4 – 11. For easier comparison, the applied alkylsulfatase concentration was normalized to 10 µM. To achieve the necessary throughput, the reactions were set up in 96-well PCR plates and the temperature gradient function of the BioRad qPCR cycler was used. Total well volume was 50 µL, containing 5 µL alkylsulfatase (100 µM stock), 5 µL substrate (100 mM stock) and 40 µL of the respective buffer. Buffers used: 150 mM citric acid sodium phosphate buffer (pH 4.0 and 5.5), 100 mM potassium phosphate buffer (pH 6.0), 100 mM TRIS-HCl buffer (pH 7.0, 7.5, 8.0, 8.5 and 9.0) and 100 mM ammonium buffer (pH 10.0 and 11.0). As a negative control, the respective alkylsulfatase was inactivated for 15 min at 95°C, precipitated proteins were removed by centrifugation and 5 µL of supernatant was used for the reaction. All reactions were incubated overnight at respective temperature and subsequently stopped using heat step (15 min, 95°C). Precipitated proteins were separated by centrifugation and the amount of released sulfate was determined by sulfate assay.

2.2.6.5 Optimal reaction conditions

If not stated otherwise, alkylsulfatase reactions were prepared in 100 mM TRIS-HCl (pH adjusted at room temp.) under the following conditions: PISA1 at pH 8.2/30°C, CmAS at pH 7.5/50°C, FtAS at pH 8.2/45°C, and VpAS at pH 7.5/65°C. For a GC/MS measurement, the reactions were stopped with ethyl acetate. For the sulfate assay, the reactions were inactivated *via* a heat step.

2.2.6.6 CD spectroscopy

Far UV circular dichroism spectra (FUV CD) of alkylsulfatases were recorded from 180 – 250 nm using a Chirascan™ plus CD spectrometer (Applied Photophysics, Leatherhead, UK). To obtain a better signal-to-noise ratio, all samples were measured in 20 mM sodium phosphate buffer, pH 8.2 (via PD-10 desalting column). All measurements were performed using 1 mm quartz cuvettes at protein concentrations of 0.25 – 0.35 mg mL^{-1}. Spectra were collected with a bandwidth of 1.0 nm in 1.0 nm steps and 0.5 s time per point at a temperature of 20°C. All spectra show an average of 10 individual measurements.

2.2.6.7 Preparation of metal-free buffer

In order to prepare a metal-free buffer, 100 mM TRIS-HCl, pH 8.2 was treated with a chelating ion exchange resin. For this purpose, 50 g L^{-1} Chelex® 100 was supplemented, which consists of crosslinked polystyrene beads with chelating groups that can complex polyvalent metal ions. The treatment was usually performed overnight at room temperature with stirring. Subsequently, the chelating beads were separated by filtration. The used Chelex® 100 was collected and regenerated according to the manufacturer's instructions. Removal of the metal ions from the buffer resulted in an increase in pH to 8.49, regardless of the pH value previously adjusted. Accordingly, one metal-free buffer was prepared and used for all alkylsulfatases.

2.2.6.8 Synthesis of alkyl sulfate esters

Chemical synthesis (performed by Petra Lommes, CBR) of compounds to explore the promiscuity of alkylsulfatases was performed as previously described.[185,194] The sulfur trioxide triethylamine complex was used as the sulfation agent of the sodium alkoxide (in 4-fold amount). The substrates used in this work, including their respective reactants and storage conditions, are listed in Table 2.24. The proper synthesis was confirmed by NMR spectroscopy.

Table 2.24: Synthesized substrates for alkylsulfatases.

Number	ID	Reactant	Cation	Mw [g mol^{-1}]	Storage
PL209	*rac*-2a	(±)-2-heptanol	K^+	233.35	At room temperature
PL210	*rac*-2c	(±)-2-octanol	K^+	247.38	At room temperature
PL211	*rac*-2a	(±)-2-heptanol	NH_4^+	213.39	Argon atmosphere (at -20°C)
PL212	*rac*-3a	(±)-3-heptanol	NH_4^+	213.39	Argon atmosphere (at -20°C)
PL213	*rac*-4a	(±)-4-heptanol	NH_4^+	213.39	Argon atmosphere (at -20°C)
PL214	*rac*-5a	(±)-4-phenyl-2-butanol	NH_4^+	247.29	Argon atmosphere (at -20°C)

2.2.6.9 NMR spectroscopy

Nuclear magnetic resonance (NMR) spectroscopy allows the structural analysis of compounds with NMR active nuclei. ^1H and ^{13}C spectra were measured with a JEOL ECS 400 (Jeol Ltd., Akishima, JPN). To confirm proper synthesis of the alkylsulfatase substrates, 10 – 20 mg of each compound was dissolved in 800 µL dimethylsulfoixe-d_6 (DMSO-d_6) and then analyzed by NMR (performed by Petra Lommes, CBR).

3. ENZYMATIC OLIGOMERIZATION OF FORMALDEHYDE

This work was previously published and is reproduced herein with permission from S. Güner, V. Wegat, A. Pick and V. Sieber "Design of a synthetic enzyme cascade for the *in vitro* fixation of a C_1 carbon source to a functional C_4 sugar" Green Chemistry, 2021, 23(17), 6583 – 6590.[141]

The author, André Pick and Volker Sieber conceived and designed the study. The author performed *in silico* studies, design and cloning of the library, screening development, screening, selection of variants, characterization, applying suitable variants, determination of kinetic parameters and data analysis. Vanessa Wegat produced library supernatant and performed GDH assay. The author wrote the initial draft of the manuscript. The co-authors critically reviewed the manuscript.

Realizing a sustainable future requires intensifying the waste stream conversion, such as converting the greenhouse gas carbon dioxide into value-added products. In this paper, we focus on utilizing formaldehyde as a C_1 carbon source for enzymatic C–C bond formation. Formaldehyde can be sustainably derived from other C_1 feedstocks, and in this work, we designed a synthetic enzyme cascade for producing the functional C_4 sugar erythrulose. This involved tailoring the enzyme formolase, which was optimized for fusing formaldehyde, from a three-carbon producer (dihydroxyacetone) to sets of variants with enhanced two-carbon (glycolaldehyde) or four-carbon (erythrulose) activity. To achieve this, a high-throughput combinatorial screening was developed, and every single variant was evaluated in terms of glycolaldehyde, dihydroxyacetone and erythrulose activity. By applying the two most promising variants in an enzyme cascade, we were able to show for the first time production of ERY starting from a C_1 carbon source. In addition, we demonstrated that one of our tailored formolase variants was able to convert 25.0 g L^{-1} glycolaldehyde to 24.6 g L^{-1} erythrulose (98% theoretical yield) in a fully atom-economic biocatalytic process. This represents the highest achieved *in vitro* concentration of erythrulose to date.

3.1 Concept

The ThDP-dependent benzaldehyde lyase was optimized for the stepwise fixation of a C_1 carbon source *via* C_2 to C_3. The best variant was renamed and is better known as formolase[86] (FLS "wild type"). Accordingly, FALD is converted almost exclusively to DHA by FLS. From GALD alone, we have observed for the first time that FLS can generate the C_4 sugar ERY as well. On this basis, we set the objective to fine-tune the specificity of FLS and develop a synthetic enzyme cascade for the production of ERY from FALD. To better control this stepwise reaction, we decided to generate and apply two variants of FLS (Figure 3.1). One variant to primarily produce GALD and a second variant to convert it to ERY. Both variants were also tailored to reduce the initial DHA activity.

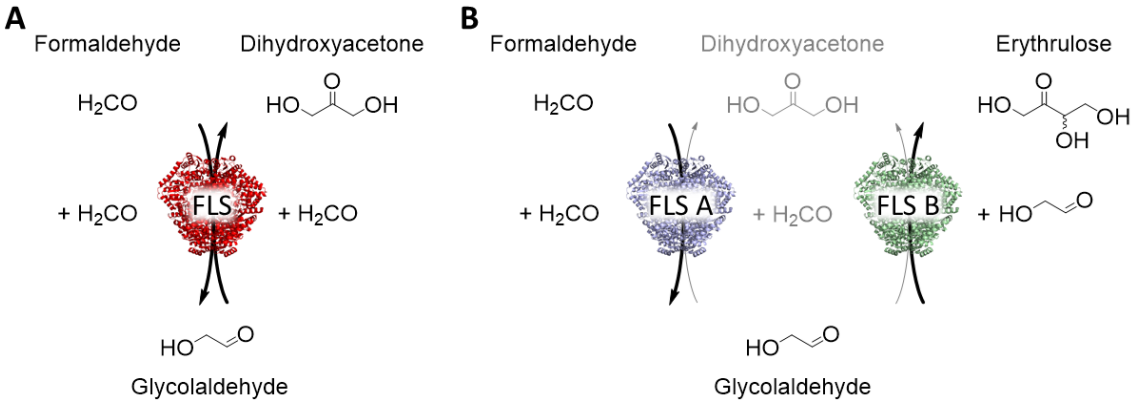

Figure 3.1: Design of study on enzymatic oligomerization of formaldehyde. Reaction catalyzed by FLS wild type (**A**) and combination of two FLS variants (**B**) for the *in vitro* fixation of formaldehyde primarily to erythrulose.

3.2 *In silico* analysis of FLS wild type

In order to optimize ERY catalysis, we performed *in silico* analysis to identify promising target positions and improve the C-C bond formation between two GALD. For a deeper understanding, docking studies were performed with FLS harboring the cofactor ThDP or dihydroxyethyl-ThDP (GALD-linked ThDP). GALD was used as the ligand in these studies, which revealed the importance of amino acids at positions 29 and 113 (Figure 3.2). Here, glutamine 113 shows strong interactions with both free GALD and with GALD linked to ThDP. Histidine 29, on the other hand, mainly defines the available space for coordinating the second GALD. As part of *in silico* engineering, alterations at these positions highlighted the importance of these positions for the targeted reaction. Both positions were selected and combined to generate a double mutant library with the aim of creating variants with desired properties.

If the library had been created using NNK (32 codons, 20 amino acids), a total of 1024 variants would have been generated. To achieve >95% library coverage, an oversampling factor of three must be applied. This would have required the screening of 35 plates (96-well). Taking all conditions into consideration, 210 plates would have had to be assayed. Therefore, we searched for possibilities to reduce library size, without reducing the number of allowed amino acids too strongly. It was important to include the template amino acids histidine and glutamine. This ensured that single mutations were also considered. Using NDT (12 codons, 12 amino acids) would not include glutamine. For this, it could be combined with VMA (6 codons, 6 amino acids). For using NDT/VMA (18 codons, 18 amino acids), 88 plates would still have had to be measured. Therefore, we decided to employ an individual library design that include histidine and glutamine. The aim was to generate the same number of variants at the DNA and amino acid level and to include as many amino acids as possible. Therefore, a total of 15 codons and amino acids were allowed for both positions (29 and 113), resulting in 225 variants. As controls, FLS wild type, empty vector (pET24a) and medium were measured on each plate as well. Thus, a total of 704 colonies (plus controls) were investigated on 8 plates. From this, a coverage of 95.7% can be calculated. Accordingly, 48 plates were measured.

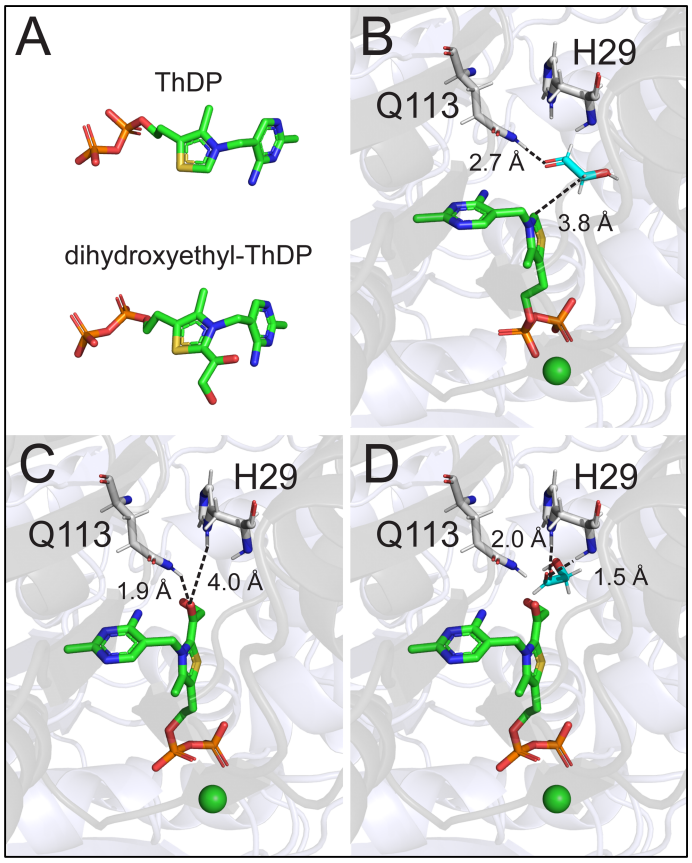

Figure 3.2: FLS wild type docking studies. The active site is formed at the interface of two monomers that coordinates ThDP (sticks) and a Mg^{2+} (green sphere). (**A**) ThDP and dihydroxyethyl-ThDP are illustrated as sticks. (**B**) FLS wild type with ThDP was used to dock GALD. It was stabilized by Q113 (distance 2.7 Å) and the distance to the ylide of ThDP was 3.8 Å (suitable distance for umpolung reaction[87]). (**C**) Dihydroxyethyl-ThDP was docked into the active site of FLS. Hydroxyl group was stabilized by Q113 again (distance 1.9 Å). H29 defined the space for coordinating a second aldehyde. (**D**) Here (C) was used to dock GALD into the active center. GALD was successfully coordinated near the cofactor (dihydroxyethyl-THDP) only in very rare events. The aldehyde group was stabilized this time by H29 (distances of 2.0 Å and 1.5 Å).

3.3 Development of a high-throughput combinatorial screening

The double mutant library was robot-assisted produced on a 96-well scale, enabling a fast analysis. To evaluate each variant in terms of GALD, DHA and ERY activity, several assays were performed (Table 3.1). The combination of the individual information allowed us to select suitable candidates with targeted features. The initial DHA production starting from FALD was determined by a coupled enzyme assay (GDH assay[86]). Here, DHA is reduced to glycerol by the NADH-dependent enzyme glycerol dehydrogenase (GDH) and the consumption of NADH is monitored spectrophotometrically. The specific detection of GALD in presence of FALD and DHA has already been described using diphenylamine (DPA) as a chromogenic reagent.[87,195] Since we observed an as yet undescribed cross activity with ERY, we had to develop a way to distinguish both. No suitable candidate has been identified from our in-house enzyme collection that is specifically active on ERY in presence of FALD, GALD and DHA. Fortunately, we found a suitable candidate to specifically detect GALD. The alcohol dehydrogenase from *Pyrococcus furiosus* (*Pfu*ADHd[184]) enabled us to distinguish between GALD and ERY. It also allowed us to evaluate GALD consumption.

Table 3.1: Overview of the conditions tested for high-throughput combinatorial screening.

Substrate	Monitoring	Time	Assay
FALD	Production of DHA	initial	GDH
FALD	Production of GALD	1 h	*Pfu*ADHd
FALD	Production of ERY	1 h	DPA – *Pfu*ADHd
FALD	Production of GALD	22 h	*Pfu*ADHd
FALD	Production of ERY	22 h	DPA – *Pfu*ADHd
GALD	Consumption of GALD	22h	*Pfu*ADHd

In total, each variant was tested under six conditions (varying substrate, time and measurement principle), which provided information about four different activities.

3.4 FLS variants with enhanced four-carbon activity

During the screening, we first focused on the second reaction of the cascade – the C–C bond formation between two GALD. Here, we identified variants with increased ERY (from GALD) and reduced DHA (from FALD) production. Among them, the two most promising variants were FLS_B1 (H29I/Q113G) and FLS_B2 (H29I/Q113S), which share the same substitution toward isoleucine at position 29 but with varying substitution at position 113. This was a strong indication that at position 29, isoleucine is essential to shift the FLS to a stronger erythrulose synthase character. The rather bulky glutamine was exchanged for smaller amino acids such as glycine and serine.

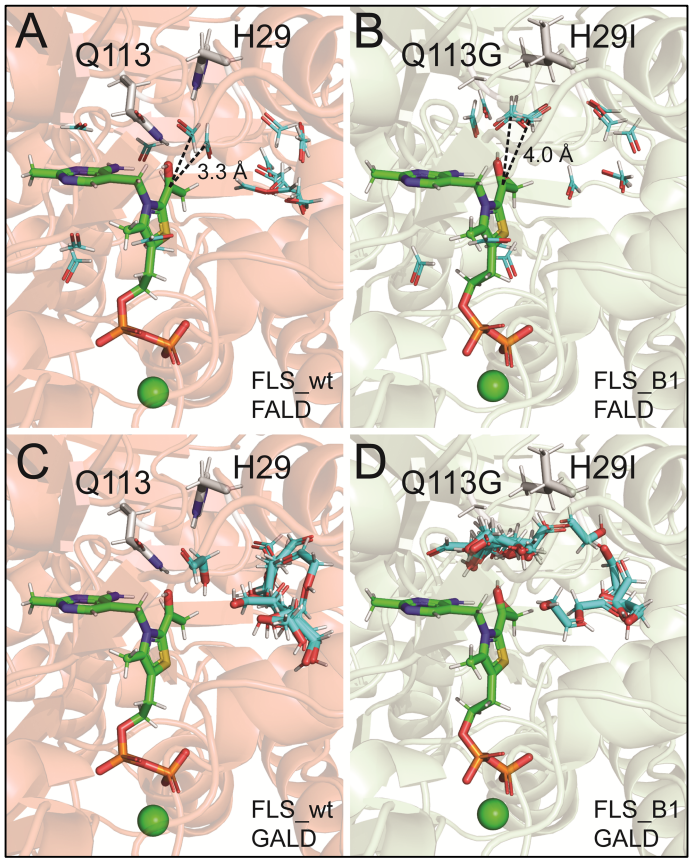

Figure 3.3: FLS wild type and FLS_B1 docking studies. Docking studies of (**A**/**C**) FLS wild type (light red) and (**B**/**D**) FLS_B1 (light green) with dihydroxyethyl-ThDP (dark green) as cofactor and (**A**/**B**) FALD or (**C**/**D**) GALD as ligand. The active site is formed at the interface of the homodimer. Residues at positions 29 and 113 are illustrated as sticks in gray.

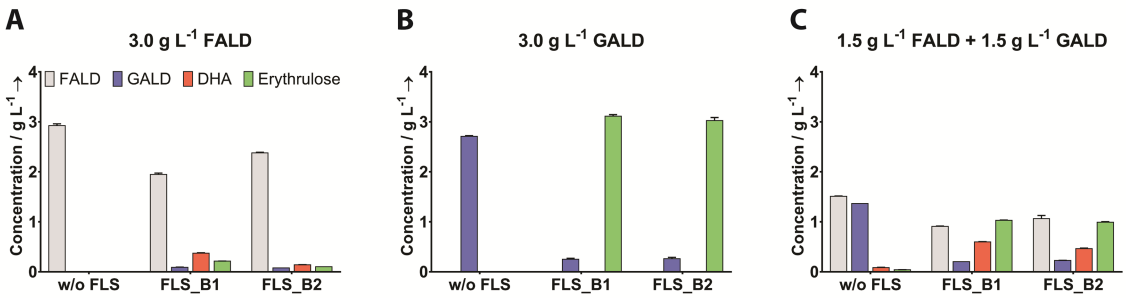

Figure 3.4: Characterization of FLS variants with enhanced four-carbon activity. FLS_B1 or FLS_B2 (40 µM) were applied to **(A)** 3.0 g L^{-1} FALD, **(B)** 3.0 g L^{-1} GALD or **(C)** a mixture of FALD and GALD (1.5 g L^{-1}+ 1.5 g L^{-1}) for 22 h at 30°C. All experiments were performed in duplicates and were analyzed *via* HPLC. FALD is illustrated in gray, GALD in blue, DHA in red and ERY in green.

Figure 3.3 illustrates the docking study of FLS wild type and FLS_B1 with dihydroxyethyl-ThDP intermediate as ligand and either an FALD or a second GALD as acceptor substrate. No notable differences were observed between FLS_B1 and FLS_B2, therefore, only FLS_B1 is illustrated in comparison with the wild type. While coordinating the second GALD in the active center of the wild type is rare, this event was much more frequently observed for FLS_B1. Due to the amino acid substitutions, sufficient space seems to be available for substrate binding and subsequent catalysis. This probably also corresponds to the reduced activity on FALD. Since FALD coordination occurred at a slightly shorter distance for the wild type than was observed for FLS_B1, it might explain the reduced DHA activity for the variants, since it seems that the additional space in the active site has a contrary effect on the DHA activity.

The variants were characterized in more detail, starting with the reaction from FALD, GALD or a 1:1 mixture of both (Figure 3.4). As desired, low levels of activity were detected for FALD alone. A slightly higher FALD consumption was observed for FLS_B1 than for FLS_B2, resulting in more than two times greater DHA production of 0.37 g L^{-1} compared to 0.14 g L^{-1}, respectively. In contrast, a high level of activity was observed for both variants starting with GALD. Thus, the applied 3.0 g L^{-1} GALD were almost completely converted. The behavior of these two biocatalysts in terms of ERY production was equally good. Under mixed conditions, a slightly higher FALD consumption was again observed for FLS_B1, so that more DHA was produced. In both cases, ERY was the major product for FLS_B1 and FLS_B2 with 1.03 g L^{-1} and 0.99 g L^{-1}, respectively. The ratio ERY to DHA was therefore 1.7 for FLS_B1 and 2.1 for FLS_B2. Considering all the data, FLS_B2 seems to be just slightly better suited for the envisioned cascade. Surprisingly, the control reaction without any enzyme also produced DHA and traces of ERY. According to Simonov and coworkers,[196] the aldol condensation can also be catalyzed by phosphates of the buffer. Further studies showed that the formation increased with increasing pH. However, several other products were also measured, which indicated a reaction with low selectivity. Since the background signal was not too strong and the initial screening was performed in this buffer system, the use of phosphate buffer was not changed in later experiments.

3.5 Kinetic characterization with GALD

Prior to the application of the variants tailored for ERY production, we determined kinetic parameters based on GALD compared to the wild type. Here we investigated a substrate range between 2.5 mM and 1 M GALD. Within these concentrations, no typical Michaelis-Menten kinetic could be observed for wild type of FLS. Therefore, the K_m value was estimated based on experimental data. At the highest GALD concentration, a k_{cat} value of 0.32 s^{-1} was measured for the wild type. In contrast, both variants showed typical Michaelis-Menten behavior. As indicated in the docking studies shown in Figure 3.3, the correct coordination of two GALD occurs more efficiently in the case of FLS_B1 and FLS_B2, resulting in a significantly lower K_m value (>30 times lower). Accordingly, the catalytic activity for the variants is increased at lower concentrations, for example, two-fold higher at 15 g L^{-1} GALD and a more than three-fold increase at 6 g L^{-1} GALD. Overall, the catalytic efficiency of these tailored biocatalysts was significantly improved (Table 3.2).

Table 3.2: Kinetic characterization of wild type, FLS_B1 and FLS_B2 with GALD as substrate.

Enzyme	k_{cat} (s^{-1})	K_m (mM)	k_{cat}/K_m (M^{-1} s^{-1})
FLS_wt[a]	1.31 ± 0.90	7565 ± 2425	0.16 ± 0.06
FLS_B1	0.25 ± 0.00	159.8 ± 6.5	1.58 ± 0.04
FLS_B2	0.25 ± 0.00	159.8 ± 9.4	1.54 ± 0.05

Nonlinear regression of the enzyme activity as a function of substrate concentration. Reactions were performed in 50 mM sodium phosphate, pH 8.0. Errors in the table represent standard deviation from two replicates.
[a]: Estimated values, no Michaelis-Menten typical saturation (≤ 1 M GALD).

3.6 Biocatalytic process for the production of ERY from GALD

Highest achieved ERY concentration (*in vitro*) to date is 5.4 g L^{-1}, using a transketolase in a continuous operating enzyme membrane reactor, with a GALD feed of 3 g L^{-1} and a space-time yield (STY) of 1.9 g L^{-1} h^{-1}.[197] ERY is formed by interconverting GALD and β-hydroxypyruvate, followed by concomitant release of CO_2. In contrast, FLS can facilitate ERY production in a fully atom-economic biocatalytic process, avoiding carbon loss. Moreover, it should be noted that β-hydroxypyruvate is a rather expensive compound compared to ERY and GALD has recently been described as a renewable alternative to current fossil-based primary C_2 feedstocks.[198,199] To highlight the greater aldehyde tolerance of FLS and to emphasize the enormous potential of the optimized variants, we decided to start the biocatalysis with 25 g L^{-1} GALD. The time courses of ERY production for wild type and variants are shown in (Figure 3.5). For FLS_B2, the highest ERY concentration of 24.6 g L^{-1} was determined, and it corresponded to a theoretical yield of 98%. Although very similar kinetic parameters were determined for FLS_B1 and FLS_B2, only 21.9 g L^{-1} ERY was measured for FLS_B1. A possible explanation for this might be a slight difference in stability. Nevertheless, both variants surpassed the wild type over the complete time course, which only achieved a theoretical yield of 66%.

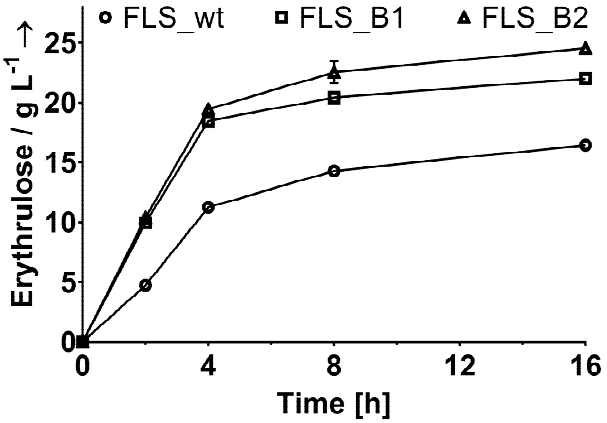

Figure 3.5: Biocatalysis of ERY from GALD by FLS over time. Reactions were performed in duplicates at 30°C and 750 rpm shaking, containing 150 µM of wild type (circle), FLS_B1 (square) or FLS_B2 (triangle) and 25 g L^{-1} GALD. Samples were taken at 0, 2, 4, 8 and 16 h and the ERY concentration was determined by HPLC.

The space-time yield almost doubled within the linear range of 4h for the two variants compared to the wild type from 2.8 g L^{-1} h^{-1} to 4.6 g L^{-1} h^{-1} and 4.9 g L^{-1} h^{-1} for FLS_B1 and FLS_B2, respectively. Since the prolonged presence of reactive aldehydes can have a detrimental effect on proteins, we investigated whether degradation or conformational changes of FLS_B2 occurred during the biocatalytic process. We first checked whether degradation of FLS_B2 occurs during the biocatalysis. For this purpose, an SDS-PAGE was performed (Figure 3.6A). No significant degradation of FLS_B2 was observed. Although the intensity of the protein band appeared somewhat weaker at the end of the process, no fragments could be detected. Instead, a weak protein band at about 120 kDa was observed. This could be homodimers (122.8 kDa) of the enzyme. Since GALD (25 g L^{-1}; 416.3 mM) is clearly in excess compared to the biocatalysts (150 µM) used, the cross-linking of FLS_B2 might somehow be mediated by GALD without removing much substrate from the reaction. However, degradation of the biocatalyst during the process seems to be unlikely. Next, we analyzed the same samples to determine whether conformational changes occurred during the biocatalytic process. Therefore, we investigated protein melting points (T_m) using a thermal shift assay. We assumed that any change of the enzyme during the process would also lead to a significant displacement of the T_m or to lower intensities. Considering the different environments at the respective time points investigated (pre-process start: no aldehyde; process start: GALD in excess; process end: predominantly ERY), the observed marginal differences in protein melting points (Figure 3.6B) are to be neglected. In addition, no loss of intensity (decreased interaction between the dye and hydrophobic regions of the enzyme due to previous degradation) or increased baseline (e.g. due to already unfolded or partially unfolded proteins) could be detected. In addition, we would like to point out that the reaction mixture was clear at any time during the biocatalytic process. Therefore, FLS_B2 seems to be sufficiently stable over the biocatalytic process. In summary, all properties relevant for biocatalysis were successfully improved.

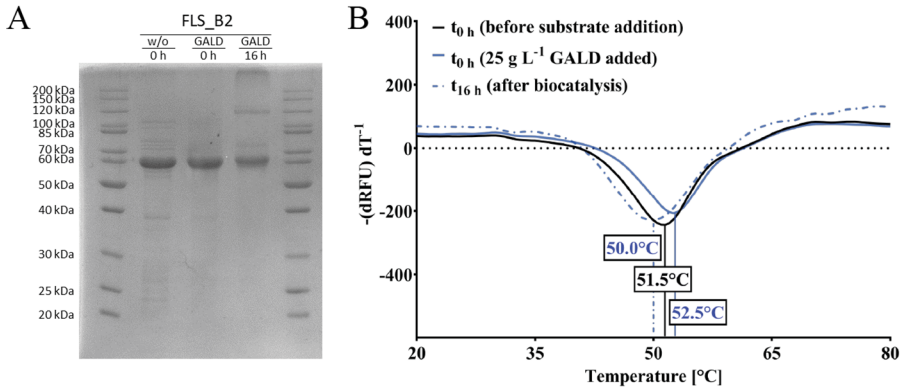

Figure 3.6: Stability of the biocatalyst during the biocatalytic process. (**A**) SDS-PAGE of biocatalysis samples of FLS_B2. Samples from pre-process start (w/o; 0 h), process start (GALD; 0 h) and process end (GALD; 16 h) were proper diluted to 1 mg mL^{-1} total protein and analyzed. FLS_B2 has a size of 61.4 kDa. (**B**) Thermofluor assay of biocatalysis samples of FLS_B2. Samples from pre-process start ($t_{0\,h}$; before substrate addition), process start ($t_{0\,h}$; 25 g L^{-1} GALD added) and process end ($t_{16\,h}$) were proper diluted to 1 mg mL^{-1} total protein and analyzed.

3.7 FLS variants with enhanced two-carbon activity

Once we successfully converted ERY from GALD, we wondered whether it was possible to generate an FLS variant with high activity for GALD formation but reduced activity for DHA. Although the library was designed for variants with increased GALD consumption, we were able to identify suitable candidates for GALD production. This clearly underscores the significance of the screening design. In this case, the identified variants showed different substitutions at both positions. This indicated that a simultaneous exchange at position 29 and 113 was necessary to shift FLS to having a stronger GALD synthase character. The characterization was performed as already described for the other set of FLS variants and is shown in Figure 3.7. For FLS_A1 (H29M/Q113G), no DHA production was detected at all with FALD as the sole substrate, but it also had the lowest GALD production compared to FLS_A2 (H29R/Q113M) or FLS_A3 (H29D/Q113C). Considering the kinetic parameters for FLS_B1 and FLS_B2, high concentration of GALD would still be needed. In the case of FLS_A3, 0.49 g L^{-1} GALD was produced. Starting with GALD, it was noticeable that FLS_A3 consumed almost no additional GALD, whereas the other two variants were able to produce some ERY. Under mixed conditions, lower amounts of DHA were detected for FLS_A3 than were observed for FLS_A1 and FLS_A2.

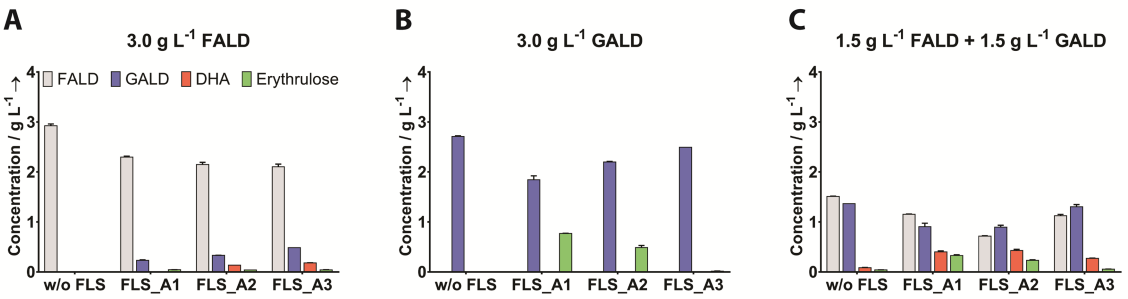

Figure 3.7: Characterization of FLS variants with enhanced two-carbon activity. FLS_A1, FLS_A2 or FLS_A3 (40 µM) were applied to (**A**) 3.0 g L^{-1} FALD, (**B**) 3.0 g L^{-1} GALD or (**C**) a mixture (1.5 g L^{-1} + 1.5 g L^{-1}) of FALD and GALD for 22 h at 30°C. All experiments were performed in duplicates and were analyzed *via* HPLC. FALD is illustrated in gray, GALD in blue, DHA in red and ERY in green.

3.8 Synthetic enzyme cascade for production of ERY from FALD

Based on the characterization of both sets of FLS variants, FLS_A3 and FLS_B2 appeared to be the most promising candidates to combine. To verify that, and as a proof of concept for the synthetic enzyme cascade for *in vitro* fixation of FALD to ERY, we decided to investigate each combination of FLS_A and FLS_B candidates. For this purpose, we applied them in a 1:1 ratio to convert 3.0 g L^{-1} FALD (Table 3.3). Again, the application of FLS wild type under same conditions resulted exclusively in the production of DHA. The highest specificity for ERY was obtained by combining FLS_A2 and FLS_B2, where nearly equal amounts of DHA and ERY were obtained. As already concluded from the variant characterization, the combination of FLS_A3 and FLS_B2 showed the highest conversion at 74%, with an ERY specificity of 33%, meaning that a ratio of ERY to DHA of 0.76 was detected. This ratio falls exactly in the range where both compounds are applied in industry.[200] Accordingly, we were able to demonstrate for the first time the successful production of ERY from a C_1 carbon source, although there still is potential for further developing the cascade reaction. It was noticeable for all investigated combinations that a part of the GALD was not converted further. With respect to the kinetic parameters of FLS_B1 and FLS_B2, the supply of GALD might have been limiting, so that the potential of these variants could not be exploited since it was the case for the production of ERY from GALD alone. This suggested that, although the character of the variant FLS_A3 has been successfully altered, catalytic efficiency still needs to be further tailored. Besides additional FLS engineering, a designed glycolaldehyde synthase that was published with an increased catalytic activity toward GALD (from FALD) could be used in combination with FLS_B2.[87] Here, the glycolaldehyde synthase showed a catalytic efficiency of 9.6 M^{-1} s^{-1} and tolerated substrate concentrations of up to 3.0 g L^{-1} FALD. This might help to contribute to achieve the full potential of the cascade.

Table 3.3: Overview of the *in vitro* fixation of FALD to ERY with combination of FLS variants.

FLS_A		FLS_B	Conversion (%)	GALD (%)	DHA (%)	ERY (%)
A1	+	B1	65.7 ± 0.0	14.5 ± 0.0	53.8 ± 0.0	31.7 ± 0.0
A1	+	B2	57.0 ± 0.0	15.4 ± 0.0	51.9 ± 0.0	32.7 ± 0.0
A2	+	B1	56.9 ± 0.0	20.0 ± 0.0	44.8 ± 0.0	35.2 ± 0.0
A2	+	B2	58.1 ± 0.0	21.3 ± 0.0	41.2 ± 0.0	37.5 ± 0.0
A3	+	B1	59.2 ± 0.2	19.0 ± 0.0	51.1 ± 0.0	29.9 ± 0.0
A3	+	B1	74.3 ± 0.0	23.7 ± 0.0	43.3 ± 0.0	32.9 ± 0.0

For FLS wild type > 99% conversion with DHA specificity of > 99% was overserved under same condition. Combined FLS variants (45 µM each) were applied in a 1:1 ratio to convert 3.0 g L^{-1} FALD at 30°C for 22 h. Errors in the table represent standard deviation from two replicates.

4. DEVELOPMENT OF NEW-TO-NATURE BIOCATALYSTS

Excerpts of this work have been submitted to ChemBioChem and are reproduced herein with permission from S. Güner, P. Lommes, G. Schenk and V. Sieber "Exploring alkylsulfatases as a platform for artificial metalloenzymes to access new-to-nature reactions" ChemBioChem, 2023, submitted, Copyright 2023. Wiley-VCH GmbH, Weinheim.

4.1 Proof of concept

There is great interest from industry in the production of chiral primary amines, as they are among the most valuable and versatile building blocks for the synthesis of a wide range of amine-containing pharmaceuticals and natural products.[89] The chemical production of primary amines is extremely challenging. The amination increases the nucleophilicity of the respective compound, leading to a higher reactivity and the formation of a mixture of primary, secondary and tertiary amines. The control of chemoselectivity is significantly complicated by this.[201] To overcome this problem, the exploitation of enzymatic selectivity might be a promising approach. However, biocatalysts suitable for this reaction also demonstrate shortcomings, requiring the discovery or development of novel enzymes with more viable properties. The aim of this work was to utilize the protein scaffold of the inverting *sec*-alkylsulfatase PISA1 for the development of a new-to-nature biocatalyst that can perform enzymatic amination with ammonia. While the native protein scaffold can provide substrate specificity, stereocontrol or a suitable electronic environment,[128,129,202,203] the idea is to incorporate metal ions with higher affinity for ammonia. As proof of concept, the preparation of the metal-free enzyme, loading with different divalent metal ions and the catalytic activity with a native substrate in the absence and presence of ammonia were investigated. Experiments were performed with an enzyme stock prepared by José Guillermo Ortiz Tena[185,191], which is hereafter identified as $PISA1_{GO}$.

4.1.1 QM/MM Simulations

Initially, *in silico* metal ion exchange studies using QM/MM simulations (quantum mechanics/molecular mechanics) were performed in collaboration with Prof. Iris Antes (Technical University of Munich). In particular, the exchange of the binuclear Zn(II) cluster by Ni(II) and the impact on the stabilization of ammonia in the active site of PISA1 were investigated. These simulations were performed by Okke Melse based on the protein crystal structure (homodimer; PDB ID: 2yhe) with two active sites. The first step was to investigate whether the coordination of Ni(II) still results in a stable system. For this purpose, the interaction energies of the protein scaffold with binuclear Zn(II) or Ni(II) were analyzed. The QM approach was important, since the interactions with metal ions cannot be well described by classical MM methods. The estimated interaction energy for Ni(II) (E_{int} = 38083 kcal mol^{-1}) was about 75% compared to native Zn(II) (E_{int} = 50540 kcal mol^{-1}). However, the binding of both metal ions were clearly beneficial, which indicates stable metal ion coordination by PISA1 in both cases.

Subsequently, the dynamics of these systems were addressed using MM simulations. These simulations were performed with Zn(II) and water as well as with Ni(II) and ammonia. One challenge was that the simulation parameters for metal ions are typically not optimized for two metal ions in close proximity. Due to this artifact, the coordination of the metals changed slightly during the experiment. However, it was more than sufficient for an initial assessment. The distance between both metal ions stabilized at ~5.0 Å for native Zn(II) (3.3 Å in the crystal structure) and at ~4.7 Å for Ni(II). Thereby, the same amino acid residues coordinated the metal ions. The dynamics of the native system showed that the water molecule remained stable between both Zn(II). In consequence of the described artifact, the water molecule directed more strongly to one of the Zn(II) during the simulation. The artificial system indicated that the ammonia molecule can by stabilized by Ni(II) in the active site. Nevertheless, in one of the two simulated active sites, a water molecule replaced the stabilized ammonia during the simulation. Based on QM/MM geometry optimization and molecular dynamics simulations, a metal ion substitution by Ni(II) as well as the stabilization of ammonia in the active site of PISA1 seemed to be achievable, which was further explored experimentally.

4.1.2 Characterization of PISA1$_{GO}$

PISA1 was extensively characterized in previous studies using different alkyl sulfate esters.[169,170,176,178,191] However, the substrate used in this study was not investigated. The enzyme stock PISA1$_{GO}$ was briefly characterized in advance to the metal ion exchange study. Due to the lack of a suitable high-throughput method for a reliable detection of catalytic activity for alkylsulfatases, in most cases endpoint measurements were performed. A colorimetric assay for sulfatases was developed by Ortiz-Tena *et al*. to address this issue by detecting released sulfate *via* a two-step enzymatic cascade.[185] By applying this method, the enzymatic activity of PISA1$_{GO}$ was monitored over the period of 24 h in a resource-saving manner (Figure 4.1).

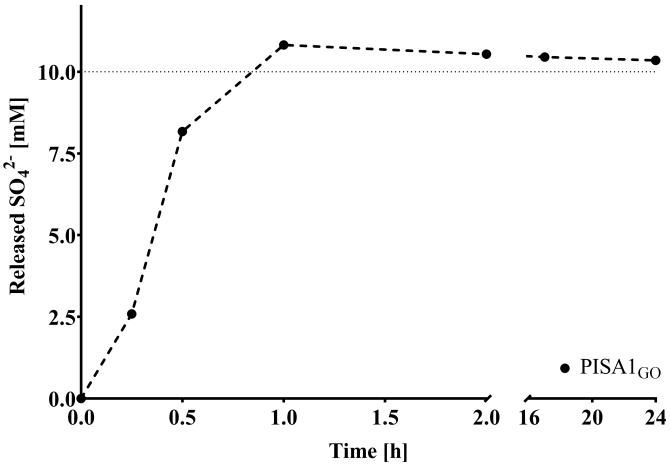

Figure 4.1: Reaction of PISA1$_{GO}$ with *rac*-2-hepyl sulfate over time. Here, 1.82 µM PISA1$_{GO}$ (128.8 µg; 0.129 mg mL^{-1}) was incubated in 100 mM TRIS-HCl (pH 8.20) with 20 mM *rac*-2-heptyl sulfate/K$^+$ at 30°C and 350 rpm shaking. Samples were taken after 0.25, 0.5, 1, 2, 17 and 24 h. Analysis was performed by colorimetric sulfate assay. Released amount of sulfate (in mM) is illustrated over time.

Here, reactions with 20 mM of the racemic substrate were prepared and investigated. It should be noted that PISA1 is a highly enantioselective enzyme and converts only (*R*)-2-heptyl sulfate to (*S*)-2-heptanol, with an equimolar sulfate release. It was observed that PISA1$_{GO}$ converted all of the available substrate (50%) already after 1 h of incubation. The level of released sulfate remained stable over the following time. A short lag phase was observed in the first 15 min, as the reaction mixture was not preheated to 30°C before starting the reaction. Based on this result, the following experiments were performed over a reaction time of 60 min. Subsequently, it was evaluated whether the sulfate assay is also applicable for a kinetic characterization of sulfatases. This was conducted by determining the turnover number (k_{cat}) for PISA1$_{GO}$ with 20 mM of the secondary substrate.

For a reliable calculation of k_{cat}, a linear initial reaction velocity is essential. This kinetic parameter describes the maximum number of conversions of substrate molecules per second at a defined enzyme concentration.[204] To adjust the reaction rate, different concentrations of PISA1$_{GO}$ (0.01 – 9.90 µM) were applied to identify the best condition for k_{cat} determination. While in the preparations with high enzyme amounts a high level of released sulfate was already observed after 5 min and the reaction rate decreased until the next measuring point, sulfate was only detected at all at the end of the reaction with the lowest amount of enzyme applied (Figure 4.2A). Further investigations indicated that, considering a proper preheating of the reaction mixture, the use of 0.28 µM PISA1$_{GO}$ was most suitable for a determination of the k_{cat} value. Accordingly, the initial reaction rate of PISA1$_{GO}$ was successfully determined in both biological and technical triplicates with excellent reproducibility under the specified conditions (Figure 4.2B). Based on the observed slope, a k_{cat} value of 16.19 ± 0.04 s^{-1} was calculated for PISA1$_{GO}$ using 20 mM *rac*-2-heptyl sulfate as substrate. The kinetic characterization of PISA1 was in the past performed using isothermal titration calorimetry (ITC). Here, k_{cat} values of 4.37 ± 1.03 s^{-1} and 5.85 ± 0.80 s^{-1} were described for pure (*R*)-2-octyl sulfate.[170,176]

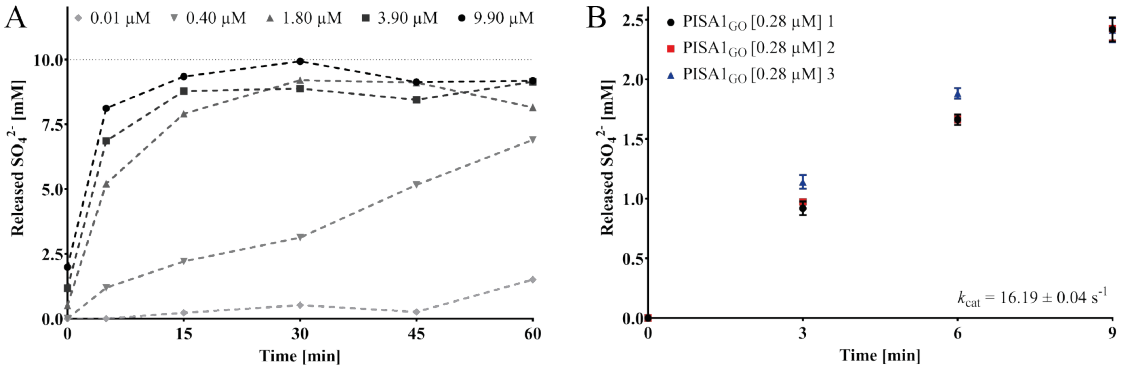

Figure 4.2: Determination of the turnover number (k_{cat}) for PISA1$_{GO}$. (**A**) Identification of optimal enzyme concentration for determination of a linear initial reaction rate. Reactions were prepared with 20 mM of *rac*-2-heptyl sulfate/K^+ and incubated for 1 h at 30°C and 350 rpm shaking. Time points were taken after 0, 5, 15, 30, 45 and 60 min. PISA1$_{GO}$ concentrations of 0.01, 0.40, 1.80, 3.90 and 9.90 µM were investigated. (**B**) Determination of the linear initial reaction rate. Reactions mixture were prepared as biological and technical triplicates using 0.28 µM (0.0196 mg mL^{-1}) of PISA1$_{GO}$ in 100 mM TRIS-HCl (pH 8.20). Reactions were started after preheating for 15 min at 30°C with the addition of preheated 20 mM *rac*-2-heptyl sulfate/K^+. Samples were taken before the reaction was started and after 3, 6 and 9 min. Released amount of sulfate was determined *via* sulfate assay.

These literature values are sufficiently similar to the values determined in this work, considering that the substrates used are slightly different (carbon chain length). However, the observed standard deviation was noticeably lower. As a result, it can be concluded that the sulfate assay is ideally suited for an efficient kinetic characterization of sulfatases.

4.1.3 Metal ion exchange

For a successful exchange of metal ions in the active site of the alkylsulfatase, it was initially necessary to produce the apoenzyme by removing the natively coordinated Zn(II). This can lead to a loss of catalytic activity and can affect as well the folding, aggregation state, and solubility of the protein.[205] For other members of the metallo-β-lactamase (MBL) superfamily, it has already been shown in literature that stripping out the native metal ions is feasible by using a chelating agent.[175,205–207] Hence, it was investigated whether EDTA could be used to remove the metal ions from the active site of $PISA1_{GO}$. Assuming a completely loaded enzyme, each catalytic center is occupied by two Zn(II), and thus one equivalent was defined as two moles of EDTA per mole of enzyme. To prepare the apoenzyme, $PISA1_{GO}$ was treated with 2.5 mM EDTA (90 equivalents). As a control, the protein was treated under the same conditions in the absence of the chelating agent. No significant precipitation was observed in either case. For determination of catalytic activities by means of the sulfate assay, it was essential to first remove the applied EDTA, since the assay is also based on metal ion dependent enzymes. This was achieved by an additional desalting step. Finally, a conversion rate of 94.9% was measured for the control ($PISA1_{control}$), while the putative apoenzyme ($PISA1_{apo}$) converted only 1.4% of the available substrate (Figure 4.3A). Furthermore, protein melting point (T_m) analysis was performed to allow a deeper comparison between $PISA1_{control}$ and $PISA1_{apo}$. Analogous effects were observed here as well. While the T_m of the control (57.0°C) was not affected compared to the untreated enzyme (57.0°C), a significant shift of -10.5°C (T_m = 46.5°C) was detected for the putative apoenzyme (Figure 4.3B). For the holo- and apostate of other metalloenzymes, such significant differences in T_m were also demonstrated.[207,208]

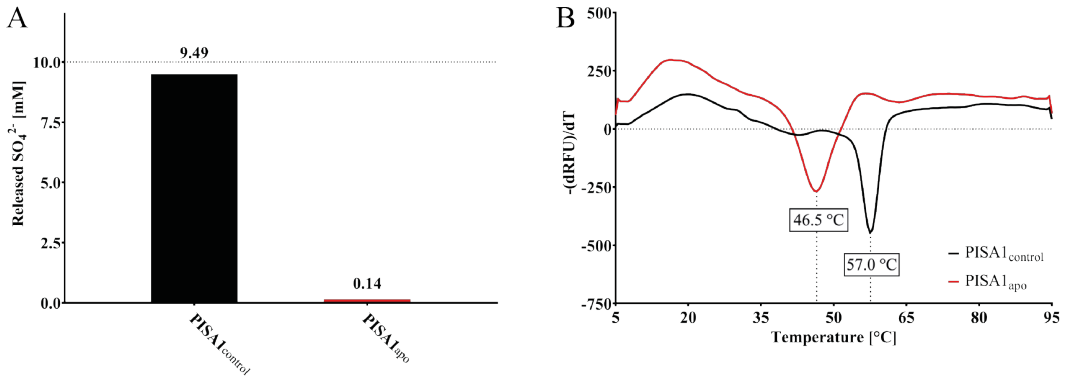

Figure 4.3: Comparison of $PISA1_{control}$ and $PISA1_{apo}$ in terms of activity and protein melting point. (**A**) Residual catalytic activities of $PISA1_{control}$ (black; 94.9% conversion) and $PISA1_{apo}$ (red; 1.40% conversion): 0.40 µM of enzyme were incubated for 1 h at 30°C and 350rpm with 20 mM of *rac*-2-heptyl sulfate/K^+ as substrate (in 100 mM TRIS-HCl, pH 8.20). (**B**) Protein melting points (T_m) of $PISA1_{control}$ (black; T_m = 46.5°C) and $PISA1_{apo}$ (red; T_m = 57.0°C) were measured with thermofluor assay. Each well contained 23 µL enzyme (0.144 mg mL^{-1}) and 2 µL SYPRO Orange working stock.

The experiments showed that the preparation process (24 h) caused only minor effects on the protein scaffold. Both the almost complete loss of catalytic activity and the change in thermodynamic stability indicated a successful removal of Zn(II) from the active site in case of $PISA1_{apo}$. Next, it was validated whether the active conformation of the putative apoenzyme can be recovered by the addition of native metal ions. For this purpose, both $PISA1_{control}$ and $PISA1_{apo}$ were incubated with 1.4 and 1.2 equivalents of Zn(II), respectively. This was performed in analogy to the treatment with the chelating agent. Subsequently, catalytic activities of the preparations were evaluated in comparison to freshly thawed, untreated enzyme. It was found that an additional desalting step was required to remove free zinc ions, as enzymes of the sulfate assay were inhibited by Zn(II). This time, the preheating step (15 min, 30°C) was also used to allow proper protein refolding or adaptation prior to the start of the reaction. Both the untreated enzyme and the control ($PISA1_{control+Zn}$) showed comparable activity, with a k_{cat} (first 15 min) of 19.0 s^{-1} and 16.3 s^{-1}, respectively (Figure 4.4). Almost no turnover was observed for $PISA1_{apo}$ when no metal ions were provided, whereas addition of Zn(II) partially recovered catalytic activity, with a k_{cat} of 6.2 s^{-1} (over 60 min). Kinetic monitoring of the reaction showed also no significant difference between the untreated enzyme and $PISA1_{control+Zn}$. However, while a hyperbolic curve was observed for both controls, $PISA1_{apo+Zn}$ showed a nearly linear slope.

These results underlined the robustness of the protein scaffold, as the preparation process (now 48 h) still showed no harmful effect and a recovery of the catalytic activity was easily possible. This suggested that PISA1 is an excellent platform for the production of artificial metalloenzymes. Thus, it was investigated whether the putative apoenzyme is suitable to be loaded with non-native metal ions. It was assumed that the coordination of elements with similar properties would be more successful and allow more likely a catalytic activity. Therefore, metals were selected based on the periodic table of elements since members of a group or period share certain characteristics.[209,210]

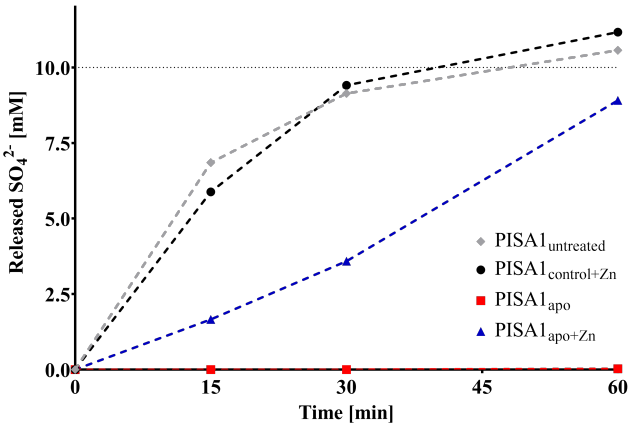

Figure 4.4: Reloading of $PISA1_{apo}$ with native Zn(II). Reactions with 20 mM *rac*-2-heptyl sulfate/K^+ and 0.40 µM of respective enzyme were incubated for 60 min at 30°C and 350 rpm shaking. Released sulfate measured at time points 0, 15, 30 and 60 min. $PISA1_{untreated}$ (grey: 0, 6.85, 9.14 and 10.57 mM) and $PISA1_{control+Zn}$ (black: 0, 5.88, 9.41 and 11.17 mM) showed a hyperbolic reaction curve. For $PISA1_{apo}$ almost no activity was observed (red: 0.03 mM after 60 min). $PISA1_{apo+Zn}$ showed a linear reaction curve (blue: 0, 1.66, 3.59 and 8.91 mM).

Accordingly, Cd(II) was studied as a member of the same group, along with Co(II), Ni(II), Cu(II), and Mn(II) as members of the same period. Since the addition of reducing agents was to be avoided, iron, which is easily oxidized from Fe(II) to Fe(III), was not considered. The loading of $PISA1_{apo}$ was performed identically to the reloading with native Zn(II). However, as a lower binding affinity of the protein scaffold was assumed for non-native metal ions, 3.1 equivalents were added instead of 1.2 equivalents of M(II) chlorides. Another desalting step was necessary to remove non-bonded, free metal ions after loading time of 24 h. This resulted in further dilution of the enzymes, which required a concentration by means of a 10 kDa filter in order to evaluate the catalytic activity of the samples.

First, the natural reaction was investigated in the absence of ammonia under the conditions described. Even after a preparation process of 72 h, $PISA1_{control}$ and $PISA1_{apo}$ showed the previously observed behavior (Figure 4.5). Reloading with native zinc was still successful. Fortunately, for all putative artificial sulfatases, a higher release of sulfate was detected than for $PISA1_{apo}$. Three groups were identified. While treatment with Ni(II) (78.3%) and Cd(II) (66.3%) led to comparable catalytic activity as reloading with Zn(II), a significantly lower release of sulfate was observed for Cu(II) (20.5%) and Mn(II) (16.2%). Loading with Co(II) (3.0%) resulted in only minimal activity. Kinetic monitoring of the reactions revealed further differences (Figure 4.5B). While the protein scaffold treated with Cd(II) showed a hyperbolic curve similar to the untreated enzyme, a similar linear curve was observed for the enzymes loaded with Zn(II) again and Ni(II). Overall, these results underscored that PISA1 is an excellent platform for the generation of artificial metalloenzymes.

For a deeper insight, the protein melting points of the artificial sulfatases were also investigated (Figure 4.6). However, no T_m was detected for $PISA1_{Cu}$. Also in this experiment, the variants formed three groups, whereby no correlation with the catalytic activity was observed. Only the Ni(II) treated variant (57.0°C) recovered the original T_m of the holoenzyme. Loading with Mn(II) (54.5°C) resulted in a slightly lower melting point.

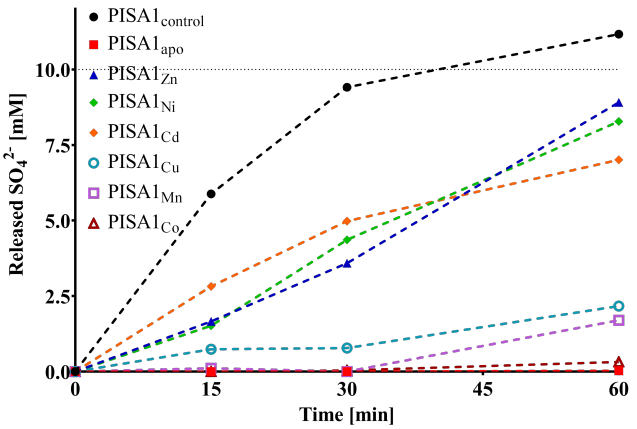

Figure 4.5: Loading of $PISA1_{apo}$ with non-native metal ions. Reactions (20 mM *rac*-2-heptyl sulfate/K^+ and 0.40 µM of enzyme) were incubated for 60 min at 30°C and 350 rpm shaking. Released sulfate, at time points 0, 15, 30 and 60 min. $PISA1_{Ni}$ (green; 1.52, 4.36 and 8.28 mM), $PISA1_{Cd}$ (orange; 2.82, 4.98 and 7.01 mM), $PISA1_{Cu}$ (light blue; 0.74, 0.78 and 2.17 mM), $PISA1_{Mn}$ (purple; 0.11, 0.00 and 1.70 mM) and $PISA1_{Co}$ (red; 0.00, 0.04 and 0.32 mM).

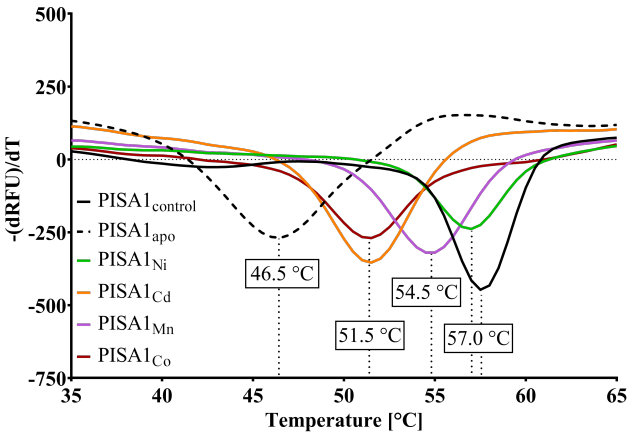

Figure 4.6: Protein melting points of artificial PISA1 variants. Thermofluor assay of $PISA1_{apo}$ (dotted; 46.5°C), $PISA1_{control}$ (black; 57.5°C), $PISA1_{Ni}$ (green; 57.0°C), $PISA1_{Cd}$ (orange; 51.5°C), $PISA1_{Co}$ (red; 51.5°C) and $PISA1_{Mn}$ (purple; 54.5°C).

Although the catalytic activity of $PISA1_{Cd}$ and $PISA1_{Co}$ differed significantly ($\Delta_{conversion}$ = 63.3%), a T_m of 51.5°C was detected for both. Considering the QM/MM simulations, the recovered catalytic activity for the natural reaction, as well as based on the stabilization of the protein scaffold by coordinating Ni(II) in the active site, $PISA1_{Ni}$ was the most promising candidate for the catalysis of the non-natural reaction with ammonia.

4.1.4 Unlocking the biocatalysis of a primary aliphatic amine

Among the enzymes that interact with ammonia are a number of nickel-dependent metalloenzymes, such as urease.[211] This is mainly based on the good affinity of Ni(II) for ammonia.[181–183] Therefore, it was particularly encouraging that the protein scaffold loaded with Ni(II) showed the best performance in comparison to other non-native metal ions. To evaluate whether $PISA1_{Ni}$ holds the potential to be a new biocatalytic tool for selective production of primary aliphatic amines, the non-natural reaction with *rac*-2-heptyl sulfate in presence of equimolar ammonia was investigated. As a control, untreated, freshly thawed enzyme was applied under identical conditions. Since the sulfate assay can only determine the amount of sulfate released and a separation of 2-heptanol and 2-aminoheptane is not possible, GC/MS analysis was performed this time. This required an extraction of the products with ethyl acetate. As expected, the chromatogram for the control reaction showed only a single peak for the production of 2-heptanol. Complete conversion of the substrate was calculated, indicating no inhibitory effect of supplemented ammonia hydroxide. A high production of 2-heptanol was also observed for the reaction with $PISA1_{Ni}$. In addition, a further minor peak was detected in the chromatogram, which was not observed for the control (Figure 4.7). A library search indicated the formation of 2-aminoheptane with high probability. The retention time was identical to the standard. This was a strong indication that coordinated Ni(II) successfully stabilized ammonia in the active site, enabling the biocatalysis of the primary aliphatic amine. Thus, $PISA1_{Ni}$ demonstrated the potential to be a powerful biocatalytic tool. Even if 2-aminoheptane was only produced in minor quantities, this represented an excellent starting point for further optimizations.

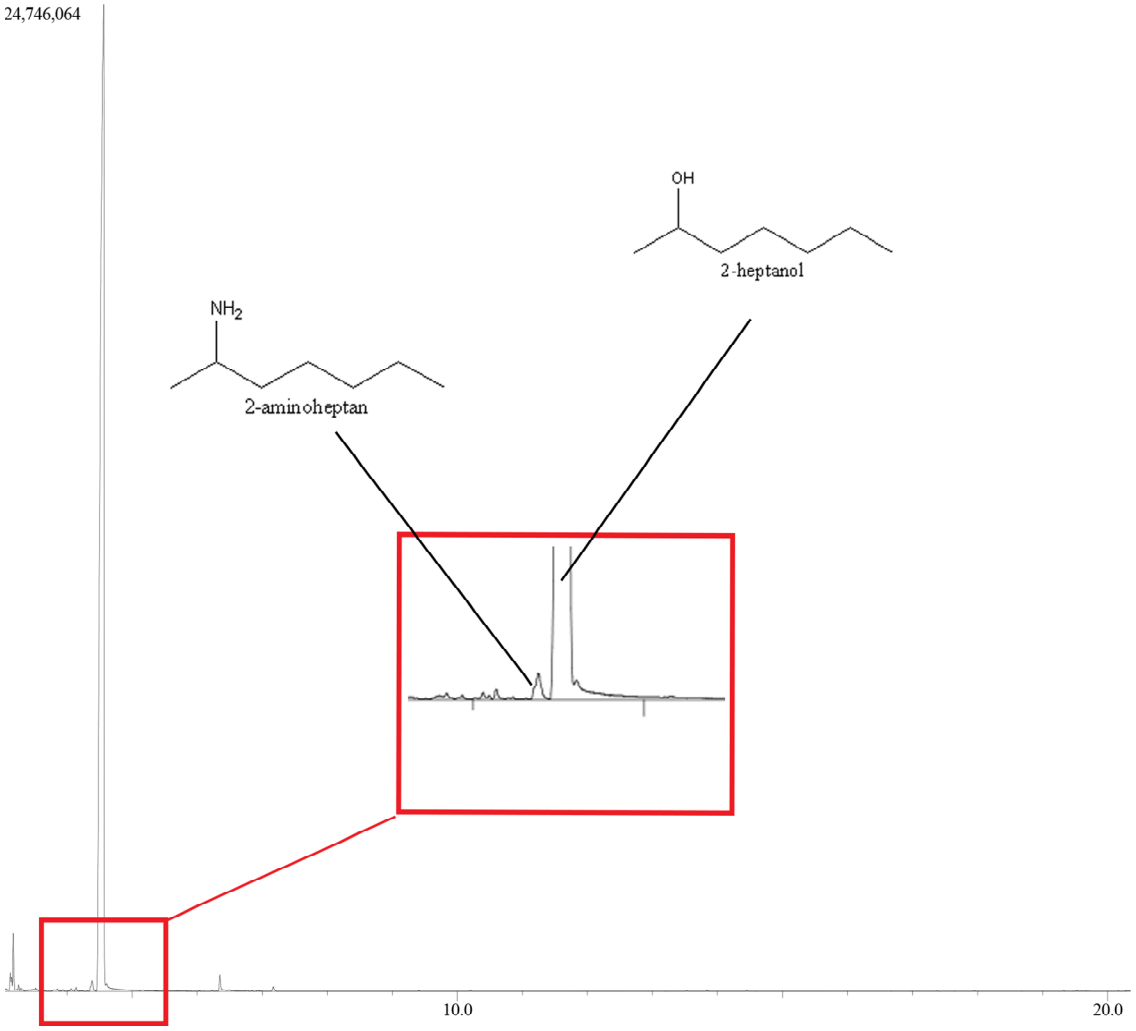

Figure 4.7: GC/MS Chromatogram of the non-natural reaction with PISA1$_{Ni}$. The reaction was prepared in 500 µL of 100 mM TRIS-HCl, pH 8.20 with 0.4 µM PISA1$_{Ni}$, 20 mM *rac*-2-heptyl sulfate/K^+ and 10 mM ammonia hydroxide; Incubated overnight at 30°C and 350 rpm shaking. Products were extracted with 500 µL of ethyl acetate.

4.1.5 Reproducibility

However, first the reproducibility of the results was addressed. Since the preparation of the apoenzyme, using the enzyme stock PISA1$_{GO}$ was successfully demonstrated three times, a new enzyme stock was investigated, which is hereafter identified as PISA1$_{SG}$. Surprisingly, it was not possible to produce the apoenzyme using the PISA1$_{SG}$ stock. To exclude any differences during the preparation process, the preparation of the apoenzymes for both stocks was investigated in comparison, simultaneously under identical conditions. Subsequently, the catalytic activity of both enzymes was determined by sulfate assay (Figure 4.8) and GC/MS analysis. While treatment with EDTA resulted in a significant decrease in conversion for PISA1$_{GO}$ (1.8%), still full conversion was observed for identically treated PISA$_{SG}$.

In the preliminary experiment, the conversion of PISA1$_{GO}$ was decreased to 1.4% by EDTA treatment. The residual activity of 1.8% monitored here indicated a high reproducibility of the experiments, at least for this enzyme stock. Nevertheless, no indications were observed explaining the different behavior of the two enzyme stocks. Therefore, further investigations on PISA1$_{SG}$ were essential.

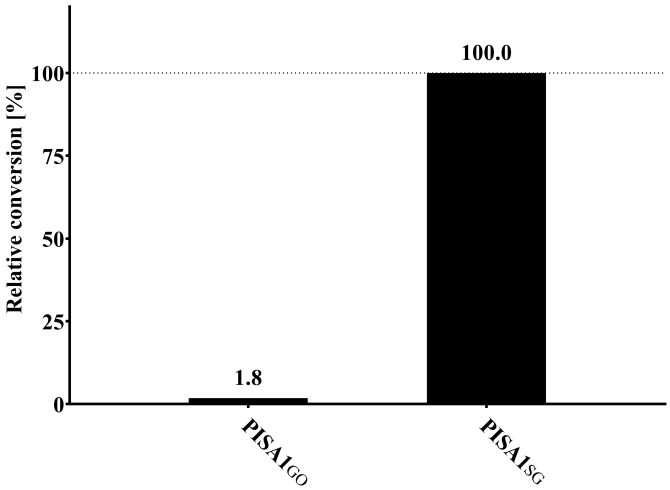

Figure 4.8: Residual activities of PISA1$_{GO}$ and PISA1$_{SG}$ treated with EDTA. Therefore, 14.1 µM of PISA1$_{GO}$ and PISA1$_{SG}$ were incubated with 2.5 mM EDTA (~90 equivalents) overnight in the fridge without shaking. Samples were desalted and 0.40 µM of enzyme was used in both cases to prepare reactions with 20 mM *rac*-2-heptyl sulfate/K^+ (1 h, 30°C, 350 rpm). Analysis performed with sulfate assay.

4.2 Adjustment of the apoenzyme preparation process

Interestingly, utilizing $PISA1_{GO}$, a metal-free protein scaffold could be produced, which enabled a robust loading with non-native metal ions and the production of a primary aliphatic amine. Removal of the metal ions from the active site of $PISA1_{SG}$ was not possible under identical conditions, thus the enzyme was intensively studied in this chapter. With the objective of developing a process that enables the reproducible production of $PISA1_{Ni}$ to unlock this non-natural reaction for biocatalytic applications.

4.2.1 Adaptation of the applied EDTA equivalents

Initially, it was hypothesized that an apoenzyme production could be achieved by varying the applied chelating agent equivalents. Therefore, different amounts of EDTA were added within the described preparation process and the residual activity of the enzymes were determined. Thus, up to 100 mM EDTA was applied (Table 4.1).

Table 4.1: Pipetting scheme for addition of different equivalents of EDTA.

No.	$PISA1_{SG}$[a] [µL]	Buffer[b] [µL]	EDTA[c] [µL]	Total volume [µL]	$PISA1_{SG}$ [mg mL^{-1}]	EDTA [mM]	EDTA [equivalents]
1	250	750	-	1000.0	0.625	-	-
2	250	750	2.5	1002.5	0.623	1.25	~71
3	250	750	10.0	1010.0	0.619	4.95	~284
4	250	750	25.0	1025.0	0.610	12.19	~708
5	250	750	100.0	1100.0	0.568	45.45	~2840
6	250	750	250.0	1250.0	0.500	100.00	~7090

[a]: 2.5 mg mL^{-1} (with 20% (v/v) glycerol); [b]: 100 mM TRIS-HCl, pH 8.20; [c]: 500 mM EDTA/Na^+ pH 7.99.

Precipitation was not observed in any of the samples, indicating that EDTA was not causing destabilization of the protein scaffold. The catalytic activity was investigated by GC/MS analysis, as the reactions could be performed both in presence of EDTA, and after removal of EDTA by means of a desalting step. However, this showed no impact on the catalytic activity of the enzymes. However, since no difference was observed, only the residual activity in presence of EDTA is presented. Without the addition of EDTA, a complete conversion of the available substrate was detected, which was taken as 100% (Figure 4.9). A significant conversion was observed for all samples, indicating that the removal of metal ions from the active site was not possible regardless of the amount of chelator added. Nevertheless, slight differences were observed. The addition of 12.2 mM EDTA (708 equivalents) caused the largest decrease in conversion down to 66.6%. Considering that the biggest impact was observed here, this region was studied in more detail in another experiment. However, no further reduction in activity could be observed. Moreover, it was also postulated that by mitigating the molecular crowding effect[212], a removal of metal ions from the active site would be facilitated. This was addressed by reducing the total amount of protein while maintaining the equivalents of chelating agent. Unfortunately, this approach also failed to reproduce the conducted proof of concept.

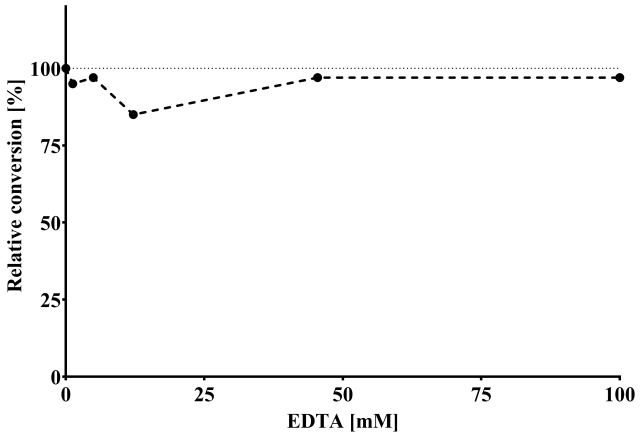

Figure 4.9: Treatment of PISA1$_{SG}$ with different equivalents of EDTA. Relative conversion is shown as a function of the added chelator concentration (Table 4.1). Reactions were prepared with 0.80 µM PISA1$_{SG}$ and 20 mM of *rac*-2-heptyl sulfate/K^+. Samples were incubated for 1 h at 30°C and 350 rpm shaking. Analysis was performed by GC/MS.

Since none of the currently investigations allowed a successful removal of the metal ions and the subsequent loss of catalytic activity, a substantial difference between the two enzyme stocks was apparent.

4.2.2 Adaptation of the applied temperature

Based on the fact, that a successful apoenzyme production was already possible, the initial focus was on optimizing that process for PISA1$_{SG}$. It was presumed that, beside the amount of chelating agent applied, the ambient temperature could also have an important impact. Previously, treatment with EDTA was performed in a refrigerator (~4°C). In order to investigate whether an adaptation of this temperature has an influence, stripping of the metal ions at different temperatures was studied. As demonstrated, the variation of the chelator concentration resulted in limited success, thus it was kept constant at 355 equivalents here. The following conditions were tested: 3 h at (1) 50°C, (2) 30°C (with shaking), and (3) on ice, as well as overnight at (4) room temperature and (5) in a refrigerator. As a control, the enzyme was incubated at 50°C without the addition of EDTA. Precipitation was observed for samples incubated above room temperature. Precipitated proteins were removed using a centrifugation step. Since it was not possible to determine the protein concentration for sample 1, the residual activity was investigated with the same volume added to the control reaction.

Incubation at 50°C resulted in minimal loss of catalytic activity, highlighting the robustness of the enzyme (Figure 4.10). Removal of metal ions was still not possible at room temperature, on ice and in the refrigerator. Interestingly, treatment at 30°C (only sample that was shaken) resulted in a significant reduction in conversion (29.5%). Considering that a T_m of 46.5°C was determined for the apoenzyme, precipitation occurs at this and higher temperatures. This was observed at 50°C, indicating that stripping of the metal ions was successful, but the apoenzyme precipitated immediately. These results indicated that partial unfolding of the protein scaffold could assist the removal of metal ions from the active site.

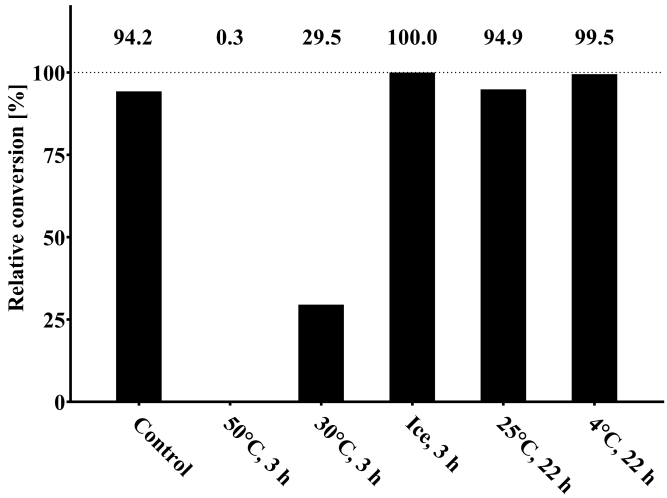

Figure 4.10: Apoenzyme preparation at different temperatures. PISA1$_{SG}$ (3.5 µM) was incubated with 355 equivalents of EDTA for 3 h at 50°C, 30°C and on ice, as well as overnight at room temperature (25°C) and in a refrigerator (4 to 8°C). As control, the enzyme was treated incubated 50°C, without addition of chelator. Reactions were prepared with 0.80 µM enzyme and 20 mM of *rac*-2-heptyl sulfate/K^+. Samples were incubated for 1 h at 30°C and 350 rpm shaking. Analysis was performed by sulfate assay.

4.2.3 Assisting by protein unfolding

The indicated assisting effect of protein unfolding was investigated in more detail in this section. To stabilize protein preparations during storage, glycerol was routinely supplemented. However, since a protein destabilization was to be investigated here, the experiments were performed in the presence and absence of glycerol. Thus, the influence of glycerol was simultaneously investigated. Conditions were adjusted to be slightly below the protein melting point of the apoenzyme. Since it was earlier observed that precipitation occurs at elevated temperatures, a 10-fold higher total protein amount was applied to counteract this by means of a stronger molecular crowding effect. Accordingly, 70 equivalents of chelator were added and partial unfolding was forced for 1 h at 42°C and 750 rpm shaking. The control was conducted without additives. Subsequently, the temperature was decreased to allow potential protein refolding (1 h, 25°C), the added chelating agent was removed by a desalting step, and the residual enzyme activity was analyzed. In the absence of glycerol, only minor precipitation was observed, which was as expected even lower in the presence of glycerol. Reduced protein precipitation supported the assumption of a beneficial molecular crowding effect. Although no turbidity was observed at all for the control, a slightly reduced conversion of 92.5% was monitored (Figure 4.11). The influence of shaking, which was not applied in previous treatments, could be responsible for this. Fortunately, an almost complete loss of catalytic activity was observed under both conditions tested. This indicated that by means of partial protein unfolding, the metal ions could be successfully removed. While a residual activity with 0.27% conversion was observed in the presence of glycerol, it was even lower (0.13%) in the absence of glycerol. Compared to the apoenzyme (1.40%) of the proof of concept, slightly lower conversions were observed here. A possible explanation for this could be that EDTA had an improved access to the binding site as a consequence of the partial unfolding.

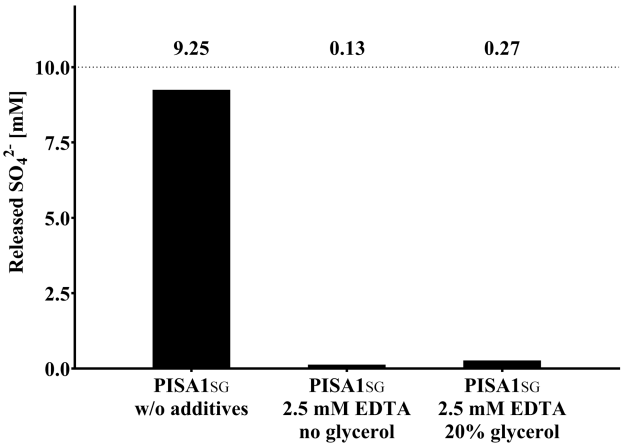

Figure 4.11: Preparation of $PISA1_{SG}$ apoenzymes with partial protein unfolding. Incubation of $PISA1_{SG}$ (35 µM) for 1 h at 42°C and 750 rpm shaking with 70 equivalents of EDTA, in presence and absence of 20% (v/v) glycerol. After recovery for 1 h at room temperature samples were desalted on a PD-10 column. Reactions were prepared with 0.80 µM enzyme and 20 mM of *rac*-2-heptyl sulfate/K^+. Samples were incubated for 1 h at 30°C and 350 rpm shaking. Analysis was performed by sulfate assay.

After the putative apoenzyme was successfully produced with $PISA1_{SG}$ for the first time, reloading with native metal ions was analyzed. Here, the partial unfolding treatment was again used to allow correct refolding of the protein scaffold in presence of the metal ions. Due to the previously performed desalting step, both preparations contained no more glycerol. To avoid further dilution, no additional glycerol was added. Identical to the proof of concept, 1.2 equivalents of Zn(II) were supplemented to recover the catalytic activity. For the control, a remaining conversion of 83.3% was determined, which was again reduced by approximately 10% (Figure 4.12). The repeated shaking of the samples could be considered as the reason for this. Unfortunately, it was not possible to reload both apoenzyme preparations with Zn(II) and recover native alkylsulfatase activity. In both cases, only a minimal conversion was detected. Therefore, the reloading of the protein scaffold was further adjusted. One approach was to perform an additional incubation step, where the applied temperature (30 min, 53.0°C) exceeded the T_m of the apoenzyme (T_m = 46.5°C). It was assumed that only the reconstruction of the holoenzyme (T_m = 57.0°C) could protect the protein scaffold from precipitation, which would simultaneously lead to holoenzyme enrichment. Unfortunately, this approach also failed to recover the catalytic activity, although remaining protein was detected after the treatment. Furthermore, it was evaluated whether a complete protein unfolding by means of a strong chaotropic agent would facilitate the metal ion exchange. In this case, guanidinium chloride (GdmCl) was selected. Proteins lose their ordered structure at high concentrations of GdmCl, thus protein unfolding is initiated.[213] Protein refolding is enabled by removing the chaotropic agent again. In this experiment, $PISA1_{SG}$ was fully unfolded using 4 M GdmCl. Refolding was performed in the presence of EDTA in order to remove released metal ions from the environment and provide the apoenzyme. High catalytic activity was still detected regardless of this treatment, and therefore this approach was not pursued further.

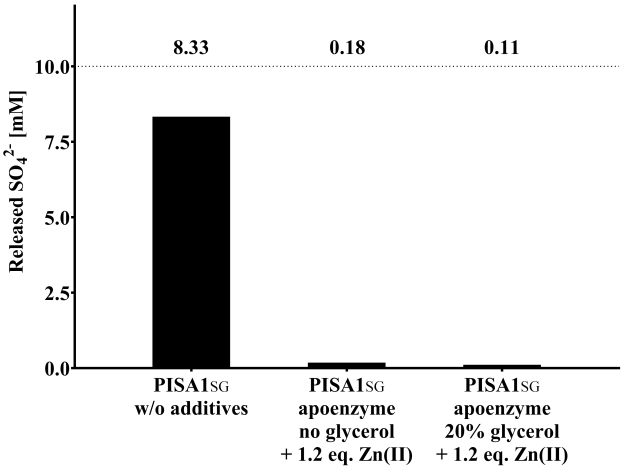

Figure 4.12: Reloading of PISA1$_{SG}$ apoenzymes with partial protein unfolding. Reloading was conducted with 1.2 equivalents of Zn(II). Samples were incubated for 1 h at 42°C and 750 rpm shaking, followed by a recovery step at 25°C and incubation overnight in a refrigerator. The control was treated identical, without additives. After a desalting step, reactions were performed with 0.80 µM enzyme, 20 mM *rac*-2-heptyl sulfate/K^+ for 1 h at 30°C and 350 rpm shaking. The released Sulfate concentration as determined by sulfate assay.

4.2.4 Assisting by additional chelating agents

The question of whether EDTA is the most suitable Zn(II) chelating agent arose after the failure to perform metal ion exchange of the completely unfolded protein scaffold. EDTA (ethylenediaminetetraacetic acid) is a hexadentate chelating agent that coordinates a metal ion centrally *via* 6 bonds. It forms highly stable 1:1 complexes with divalent cations and is therefore particularly suitable for the complexation of Zn(II).[214] However, other chelating agents have been applied in the literature in combination with EDTA to successfully remove metal ions from M(II)-dependent metalloenzymes and produce the respective apoenzyme. For this, an equimolar chelator mixture consisting of EDTA, 1,10-phenanthroline, dimethyl-2,6-pyridinedicarboxylate, and 8-hydroxyquinoline-5-sulfonic acid is frequently used.[164,206,215,216] Therefore, it was investigated whether the application of this chelator mixture resulted in a beneficial effect on the production of PISA1$_{SG}$ apoenzyme. For a deeper assessment, the mixture of the new chelating agents was applied in the presence and absence of equimolar EDTA. Additionally, the influence of the chelating agents was investigated individually. Nevertheless, no positive effect was observed in any of the experiments. Consequently, the additional chelators were not supplemented in the subsequent studies.

4.3 Exploring the divergent behavior of different PISA1 preparations

While metal ion exchange could be performed reliably in a reproducible manner for $PISA1_{GO}$, this was not achieved under identical conditions for $PISA1_{SG}$. Although various parameters of the apoenzyme preparation process were modified, successful replacement of metal ions could not be realized. This suggested the presence of a major difference between both enzymes. To determine the responsible parameter, general properties such as catalytic activity, buffer composition, molecular weight and protein folding were comparatively analyzed.

4.3.1 Catalytic activity

An obvious difference between the two enzyme preparations was their production dates. The first assumption concerning the different behavior was that alteration processes occurred during storage. To address this, the catalytic activities of $PISA1_{GO}$ and $PISA1_{SG}$ were monitored under standard conditions within the first hour. Both of these enzymes converted the substrate completely within the first hour as expected (Figure 4.13). However, a significant difference in reaction velocity was observed. Interestingly, $PISA1_{SG}$ required only a quarter of the time for complete conversion compared to $PISA1_{GO}$. At first sight, this would point to a time-dependent inactivation of $PISA1_{GO}$. However, it is noticeable that the k_{cat} of 8.3 s^{-1} (without preheating) determined for $PISA1_{GO}$ in this experiment was similar to values reported in the literature (4.4 and 5.9 s^{-1} for (*R*)-2-octyl sulfate).[170,176] Therefore, an assumption of time-dependent inactivation of the enzyme is questionable. In contrast, a higher k_{cat} of 28.0 s^{-1} was detected for $PISA1_{SG}$ considering the first 15 min. Since all substrates applied were synthesized in house, variations could not to be excluded. Therefore, it was additionally investigated whether the respective substrate batch showed an influence on the enzymatic activity. Regardless of the batch used, the behavior shown in Figure 4.13 was observed for $PISA1_{GO}$ and $PISA1_{SG}$, with identical turnover numbers. Even with this observation, the different behavior of both preparations could still not be explained. Therefore, further investigations were conducted.

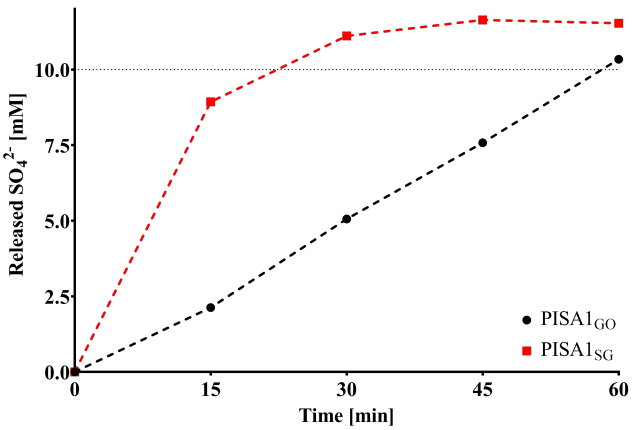

Figure 4.13: Comparison of the catalytic activities of $PISA1_{GO}$ and $PISA1_{SG}$. Reactions were prepared with 0.40 µM of $PISA1_{GO}$ (black) or $PISA1_{SG}$ (red). Samples were incubated for 1 h at 30°C and 350rpm with 20 mM of rac-2-heptyl sulfate/K^+ as substrate (100 mM TRIS-HCl, pH 8.20). Released amounts of sulfate are shown in mM, at time points 0, 15, 30, 45 and 60 min.

4.3.2 Buffer composition

Many enzymatic reactions are strongly influenced by environmental conditions, such as temperature, pH or salinity. While these are rather stable *in vivo*, already minor deviations can cause major effects *in vitro*. Therefore, it was considered that the significant difference in catalytic activity was caused by differences in the environment of the enzymes. Accordingly, this was analyzed in more detail. To investigate the environment, proteins were removed using a 10 kDa filter and the flow trough was analyzed by HPLC. It should be noted that such filters are often stored in glycerol. In order to avoid misleading, filters were washed three times with 500 µL buffer in advance. It was observed that $PISA1_{GO}$ did not contain glycerol. Thus, the addition of glycerol was omitted in subsequent enzyme preparations. Furthermore, the pH of $PISA1_{GO}$ was investigated and a pH of 8.12 was determined. Considering the described dialysis with 100 mM TRIS-HCl (pH 8.20), the measured pH value was in an expected range. The pH of different preparations of $PISA1_{SG}$ were in a very similar range.

4.3.3 Protein mass spectrometry

In addition to environmental factors, changes within the protein primary structure due to random mutations were also considered. Therefore, all in house available PISA1 expression plasmids were first verified by sequencing. However, no mismatch with the original sequence was detected. Nevertheless, since spontaneous mutations could not be excluded, both enzyme preparations were analyzed by protein mass spectrometry (Figure 4.14).

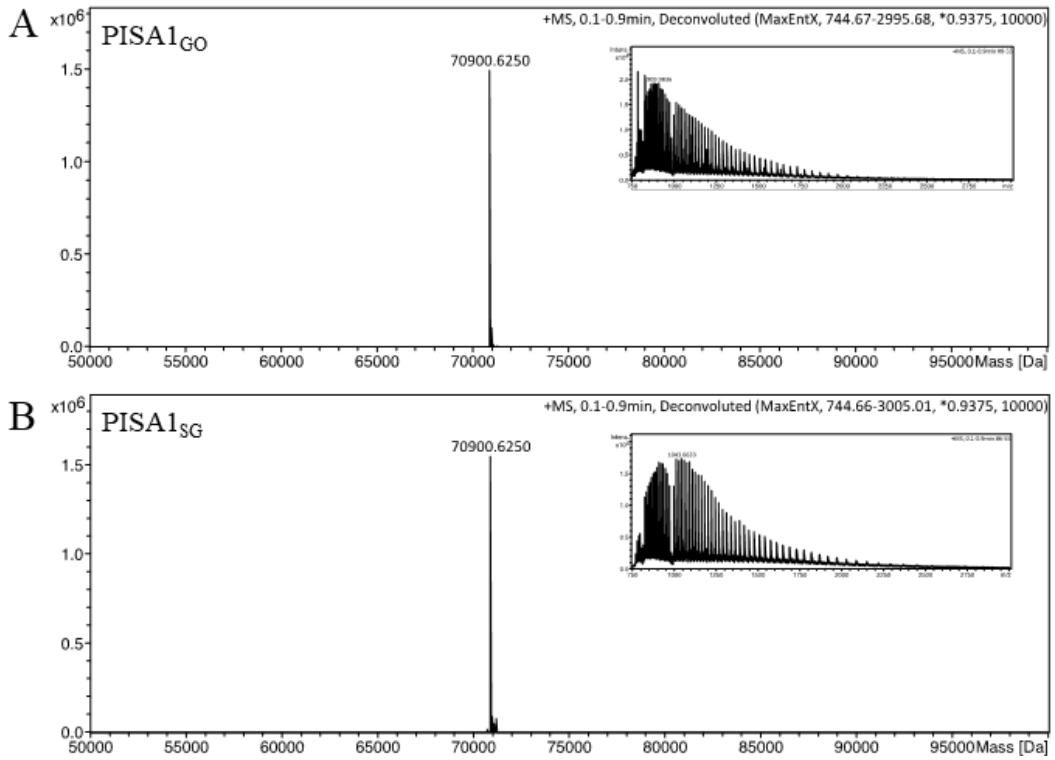

Figure 4.14: Protein mass spectrometry of $PISA1_{GO}$ and $PISA1_{SG}$. Measurements were performed in collaboration with the Chair of Biological Chemistry (TUM) conducted by Christian Deuschle. Protein samples were dialyzed twice against 10 mM ammonium acetate and then mixed 1:1 with methanol and 1% formic acid. Molecular weight of the unfolded amino acid sequence of (**A**) $PISA1_{GO}$ and (**B**) $PISA1_{SG}$ was determined by ESI-TOF-MS analysis.

For this purpose, protein samples were unfolded, and the molecular weight was determined by ESI-TOF-MS analysis. This was realized in collaboration with Prof. Arne Skerra (Technical University of Munich), with experiments performed by Christian Deuschle. Here, no differences could be detected. The identical molecular weight of 70,900.625 Da was measured for both protein samples. Unfortunately, this measurement does not support the assumption of spontaneous mutations without taking into account the difficult distinction between leucine and isoleucine. A theoretical molecular weight of 73,834.06 Da (excluding N-terminal methionine) was calculated in advance based on the amino acid sequence. Nevertheless, a significantly lower molecular weight was observed for both preparations. This indicated that the native signal peptide (28 amino acids) for secretion into the periplasm was also cleaved. For this case, a theoretical molecular weight of 70,899.54 Da (uncharged) was expected. Thus, the theoretical and measured molecular weights were in adequate concordance.

To confirm this experimentally, secretion of $PISA1_{SG}$ into the periplasmic space of *E. coli* was studied. Therefore, the outer cell membrane of *E. coli* was penetrated by cold osmotic shock and periplasm proteins were released into the environment. The intact cells were then separated and lysed using a sonotrode. SDS-PAGE was performed to determine the localization of PISA1 in the cell. Thus, secretion into the periplasmic space was demonstrated. Removal of the native signal peptide resulted in a significant reduction in protein expression, disabling identification of PISA1 by SDS-PAGE.

4.3.4 Circular dichroism spectroscopy

The native folding of a protein is essentially influenced by two aspects, while the first part is rather static and is based on the assembly of the primary structure, the second one is mainly dealing with the dynamics of the folding process itself.[217] On this basis, it was suggested that differently folded species were evolved during the protein folding process. Therefore, the overall protein structure was comparatively analyzed by CD spectroscopy.[218] The experiments were performed in collaboration with Prof. Buchner (Technical University of Munich), under the supervision of Annika Strauch.

Due to the low background signal of the sodium phosphate buffer, it was possible to scan the samples in a range between 180 and 250 nm (Figure 4.15). The enzymes showed highly overlapping CD spectra, suggesting an identical overall protein structure. From the spectra, it could be recognized that PISA1 is a very well folded protein. Here, the intensity of the maxima at 193 nm is related to the ratio of α-helices. Disordered secondary structures, such as a random coil, would reduce the intensity here. Both minima at 209 and 220 nm, showed similar intensity and are related to the ratio of β-sheets. Based on the CD spectra, a high ratio of α-helices can accordingly be identified. These observations are consistent with the crystal structure of PISA1 (PDB ID: 2yhe), where also a high ratio of α-helices can be identified.

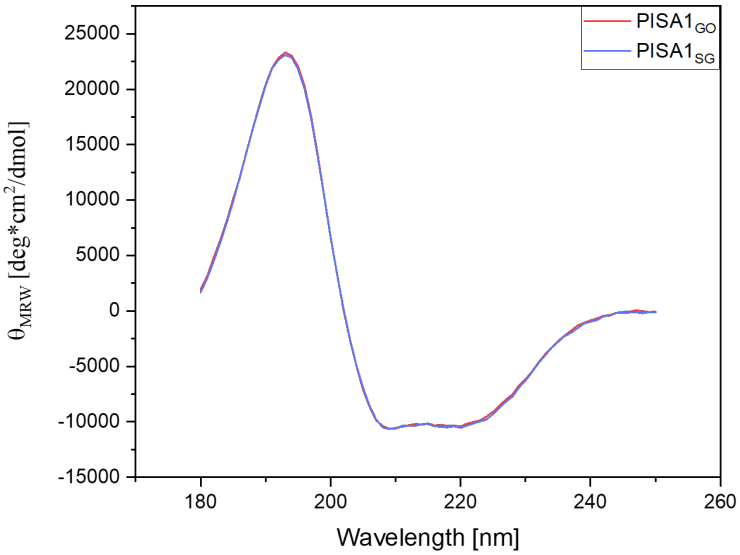

Figure 4.15: Circular dichroism spectroscopy of $PISA1_{GO}$ and $PISA1_{SG}$. Both protein preparations were desalted against 20 mM sodium phosphate buffer, pH 8.20 and diluted to 0.267 mg mL^{-1} (3.8 µM). Measurements were performed at 20°C with 10 repeats and scan between 180 to 250 nm (1 nm steps). $PISA1_{GO}$ illustrated as red line and $PISA1_{SG}$ as blue line.

4.3.5 Protein expression

Surprisingly, despite their different behavior, both enzymes showed consistent characteristics in primary and secondary structure. Thus, the resources to identify the origin of the different behavior were almost exhausted. As a last point, protein expression was addressed. This was performed under described conditions in *E. coli* BL21 (DE3) using the pET expression system.[176,178,185] However, significantly lower total protein yields were achieved for $PISA1_{SG}$ than described for $PISA1_{GO}$, although the conditions, strain and plasmid were identical.

Nevertheless, it was within the scope of possibilities that the expression conditions were different. In addition, it was considered that the use of components from different suppliers for the preparation of complex media could have also an influence. Fortunately, in addition to purified $PISA1_{GO}$ preparation, a harvested *E. coli* expression culture of $PISA1_{GO}$ (stored at -20°C) was also available, produced on the same day under identical conditions. The utilization of these cells allowed concluding about the expression conditions. $PISA1_{GO}$ was purified and dialyzed under conditions described previously, without the supplementation of glycerol. Interestingly, a total protein amount, comparably low to $PISA1_{SG}$ was obtained. Moreover, comparable behavior in the metal ion exchange study was observed, where removal of Zn(II) using EDTA was still not possible. This indicated that the influence of expression was negligible and shifted the focus instead to the purification process. In this case, the standard operating procedure was already followed precisely, eliminating the possibility of understanding what exactly the different behavior was based on. Therefore, the decision was made to exclude the proof of concept results with $PISA1_{GO}$. Instead, a systematic approach was chosen to address the scientific question.

4.4 PISA1 metal ion exchange study

In this and subsequent sections, experiments were performed exclusively with self-produced enzymes, and hence $PISA1_{SG}$ is hereafter identified as PISA1. The objective was to establish a procedure that enables a reliable and reproducible metal ion exchange of PISA1 in order to unlock the biocatalytic production of primary aliphatic amines.

4.4.1 Optimization of protein expression

From an industrial point of view, enzymes utilized for biocatalytic reactions represent one of the major cost driver.[16] Due to the poor total protein yield, optimization of PISA1 expression was essential. Various approaches were applied to realize this. The first attempt was to adapt the conditions described in the literature.[169] Thus, along with different media, such as lysogeny broth, terrific broth and autoinduction medium, also various expression temperatures (16°C, 20°C, 30°C and 37°C) were investigated. While protein expression was not possible in autoinduction media, the highest protein yield of 12 mg PISA1 per liter expression culture was obtained at 30°C in LB media. Although the yield was more than doubled, this was still not sufficient. Next, the utilization of alternative *E. coli* expression hosts, such as Rosetta (DE3), Origami 2 (DE3), and Tuner (DE3) were investigated in comparison to BL21 (DE3). However, this approach was not resulting in an increase in protein yield. Therefore, the expression host was not exchanged.

Furthermore, the strength of bacterial protein expression is significantly influenced by the initiation of translation. This is controlled by various regulatory elements. Crucial among them is the ribosomal binding to the Shine-Dalgarno sequence (hybridization of the 16S rRNA to the ribosome binding site), the binding of the complementary tRNA to the start codon, and the distance between the two binding sites (spacer).[219–221] The original expression plasmid for PISA1 was kindly provided by Prof. Kurt Faber (University of Graz).[169] On detailed evaluation of the applied cloning strategy, it was noticed that the vector's own start codon was removed to allow cloning with the restriction enzymes NheI and XhoI. This resulted in an extension of the spacer by 9 nucleotides (17 nucleotides in total). However, since an optimal spacer length of 7 – 8 nucleotides is reported for *E. coli*, this was identified as an promising target.[219] To reconstruct the original spacer length of 8 nucleotides, PISA1 was recloned. The original vector pET21b (Amp^R) was exchanged for pET24a (Kan^R), which allowed a reduction of the required antibiotic selection pressure. The use of the new expression plasmid increased the total protein yield by more than 30-fold compared to the initial expression. Up to 160 mg of PISA1 was purified from 1 L of expression culture. For this, after reaching an OD_{600} of 0.8 – 1.0, the temperature was lowered to 20°C and protein expression was induced with 0.5 mM IPTG.

4.4.2 Modulation of the enzymatic microenvironment

The development of a robust metal ion exchange process was addressed next. The major challenge so far has been to provide the metal-free protein scaffold, as a high tolerance to chelators was observed for PISA1. Therefore, a different strategy was considered, which was based on the fact that metallo-β-lactamases and other metalloenzymes coordinate metal ions often *via* conserved histidine residues.

The aromatic histidine shows amphoteric properties and consequently can act both as an acid and as a base.[222] Here, the imidazole side chain is characterized by a pK_a of approximately 6.0. Accordingly, the charge state of histidine is essentially influenced by the pH of the environment. While it is neutral under physiological conditions, histidine is protonated in an acidic environment (pH <6) resulting in a cationic property. Deprotonation, on the other hand, occurs at slightly basic conditions, imparting an anionic property. This is enhanced at higher pH or by complexation with metal ions, resulting in the donation of a second proton and the formation of an imidazolate ion.[223] In the case of PISA1, Zn(II)/Zn(II) coordination is mediated by 7 amino acid residues, with a predominant ratio of histidine.[176] Therefore, modulation of the pH of the enzymatic microenvironment was identified as a promising tool for metal ion exchange. It was hypothesized that protonation of the histidine residues in the active site results in electrostatic repulsion of the bivalent metal cations.

To accomplish this, PISA1 was transferred to an acidic environment by means of a desalting step. Here, buffer systems based on citric acid or acetic acid were used, as they provide an additional chelating property with different strength. To determine the most suitable condition, a pH range of 3.0 – 6.5 and 4.0 – 5.5 was screened for citric acid and acetic acid, respectively (Table 4.2). This environment was then replaced with a metal-free, basic environment with a second desalting step to preserve the enzyme in the apostate. Based on the assumption of a low dissociation constant (K_d) of PISA1 for Zn(II).

Table 4.2: Determination of the most suitable environment for metal ion exchange.

No.	PISA1 [mg mL^{-1}]	Volume [mL]	1. Desalting[a,b] [pH]	2. Desalting[c] [pH]	Volume [mL]	PISA1$_{apo}$ [mg mL^{-1}]	PISA1$_{apo}$ [µM]
01	1.0	1.75	3.0[a]	8.49	3.0	0.526	7.42
02	1.0	1.75	4.0[a]	8.49	3.0	0.319	4.50
03	1.0	1.75	4.5[a]	8.49	3.0	0.310	4.37
04	1.0	1.75	5.0[a]	8.49	3.0	0.371	5.23
05	1.0	1.75	6.0[a]	8.49	3.0	0.405	5.71
06	1.0	1.75	6.5[a]	8.49	3.0	0.405	5.71
07	1.0	1.75	4.0[b]	8.49	3.0	0.422	5.95
08	1.0	1.75	4.5[b]	8.49	3.0	0.465	6.56
09	1.0	1.75	5.0[b]	8.49	3.0	0.388	5.47
10	1.0	1.75	5.5[b]	8.49	3.0	0.396	5.59

[a]: 150 mM citric acid sodium phosphate buffer.
[b]: 150 mM sodium acetate acetic acid buffer.
[c]: 100 mM metal-free TRIS-HCl (Chelex®100 treated), pH 8.49.

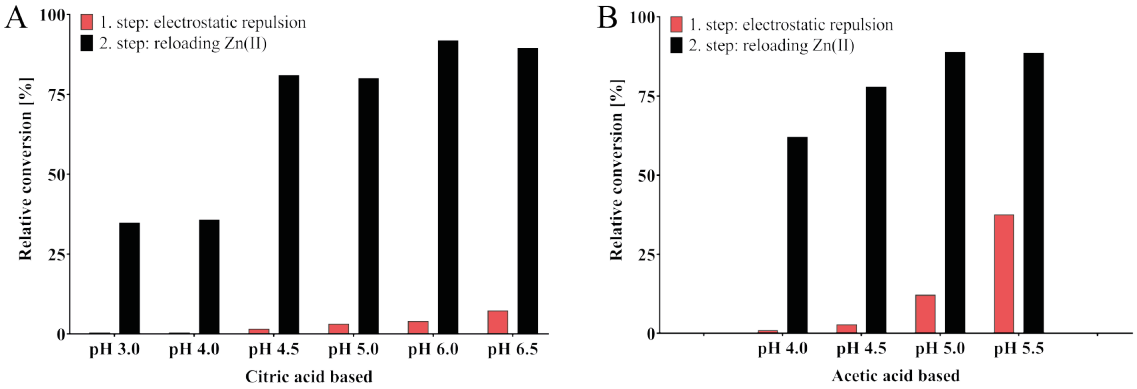

Figure 4.16: Metal ion exchange of PISA1 based on electrostatic repulsion of Zn(II) in the active site. First, the microenvironment of PISA1 was exchanged with respective buffer, based on (**A**) citric acid (pH 3.0 – 6.5) or on (**B**) acetic acid (pH 4.0 – 5.5), to release native Zn(II) by electrostatic repulsion. Released metal ions were removed by an additional desalting step against 100 mM metal-free TRIS-HCl buffer, pH 8.49. In a second step, 3.3 equivalents of Zn(II) were supplemented and free, non-bonded metal ions were subsequently removed again. More details are listed in Table 4.2. Analysis was performed *via* GC/MS.

To evaluate under which conditions the production of the apoenzyme is possible, the residual activities of the enzymes were determined (Figure 4.16). Several conditions enabled the production of the apoenzyme. For both buffer systems, enzymatic activity was observed to be eliminated at pH below 4.5. This indicated that successful electrostatic repulsion of Zn(II) can be achieved by sufficient protonation of the histidine residues in the active site. As expected, the buffer system based on citric acid showed a higher supportive effect on the removal of metal ions.

However, to enable a robust metal ion exchange process, the metal-free protein scaffold also had to be able to be reloaded. To address this property, all samples were incubated with 3.3 equivalents of Zn(II). Here, a partial recovery of enzymatic activity was observed for all samples. Thereby, the citric acid based environment at pH 4.5 was identified as the most suitable. Here, it was possible to almost completely eliminate the enzyme activity, indicating successful removal of metal ions. Moreover, the recovery of the activity was sufficiently accomplished by the addition of metal ions, indicating a successful reloading. These results were reproduced with various PISA1 preparations. Thus, a robust process for metal ion exchange of PISA1 was successfully established.

4.4.3 Preparation of artificial metalloenzymes based on PISA1

Once a method was established that allowed reliable removal and reintroduction of Zn(II), the introduction of non-native metal ions was addressed. Ni(II), Cd(II), Cu(II), Mn(II) and Co(II) were selected, which were already part of the proof of concept. However, the focus was on the preparation of the Ni(II) loaded enzyme. While 81.8% of enzymatic activity was recovered by addition of Zn(II), this was not achieved with any of the non-native metal ions (Figure 4.17). The catalytic activities in each case were identical to the apoenzyme. Instead, a strong degree of protein precipitation was observed immediately after the addition of the metal ions. This effect increased when the applied equivalents were elevated. Apparently, loading the protein scaffold with metal ions other than Zn(II) appeared to be more difficult than expected.

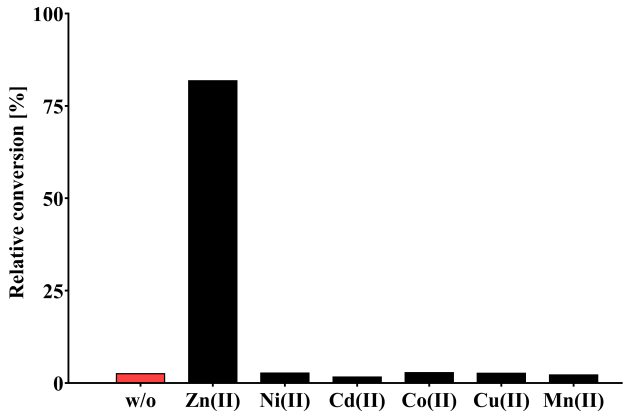

Figure 4.17: Loading of PISA1 apoenzyme with Zn(II) and non-native metal ions. The metal-free protein scaffold of PISA1 was produced by modulation of the enzymatic microenvironment (*via* 150 mM citrate buffer, pH 4.5). Loading with non-native Ni(II), Cd(II), Co(II), Cu(II), and Mn(II) was conducted homologous to reloading with native Zn(II), using 3.3 equivalents of metal ions. Analysis was performed *via* GC/MS.

Consequently, it was important to adjust the metal ion exchange process in order to stabilize the apoenzyme sufficiently for artificial metal ion coordination in the active site. As glycerol showed previously a stabilizing effect on PISA1, the apoenzyme was prepared in the presence of 20% glycerol to facilitate loading with Ni(II). The supplementation of glycerol showed no significant effect on production of the apoenzyme (Figure 4.18). Reloading with Zn(II) was also not affected, as 85.2% of the catalytic activity could be recovered. However, this adjustment allowed a significant reduction of the Ni(II) induced protein precipitation. Finally, a partial recovery of 25.3% catalytic activity was observed with Ni(II) for the natural reaction. This indicated that Ni(II) was successfully coordinated in the active site of PISA1. Next, the biocatalysis of primary aliphatic amines based on ammonia was investigated by using this variant. Initially, the same conditions as for the proof of concept study were conducted. However, the production of 2-aminoheptane could not be demonstrated. Various optimization efforts, including the use of ammonia in excess and the application of alternative nitrogen sources also did not lead to success. Therefore, approaches to enable this non-natural reaction using the PISA1 protein scaffold were terminated.

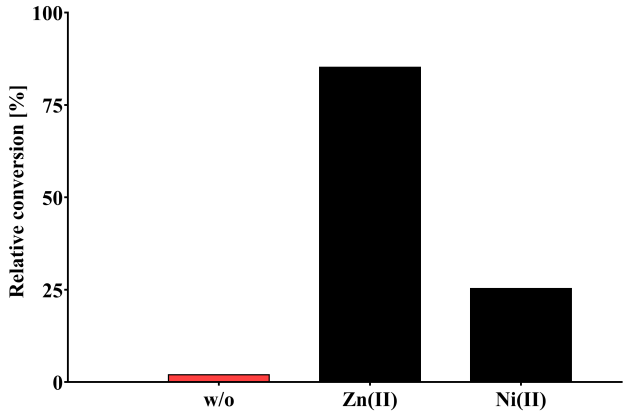

Figure 4.18: Loading of PISA1 apoenzyme with non-native Ni(II) using glycerol stabilization. The metal-free protein scaffold was produced in presence of 20% glycerol (w/v) by modulation of the enzymatic microenvironment (via 150 mM citrate buffer, pH 4.5). Loading of apoenzyme was conducted with 3.3 equivalents of Zn(II) and Ni(II), respectively. Analysis was performed *via* GC/MS.

4.5 Discovery and characterization of new alkylsulfatases

The objective of unlocking a new biocatalytic tool for the selective production of primary aliphatic amines, based on the protein scaffold of the inverting *sec*-alkylsulfatase PISA1, could not be accomplished. Nevertheless, it emerged from the proof of concept study that this new-to-nature reaction can be catalyzed. Crucial for this is a nucleophilic attack (via S_N2) of activated ammonia at the chiral carbon atom of the alkyl sulfate ester to release the corresponding primary aliphatic amine. Consequently, alternative protein scaffolds were searched that could enable this reaction. However, no other *sec*-alkylsulfatase besides PISA1 has been identified so far that exhibits an inverting reaction mechanism. Therefore, a sequence-driven approach was applied to discover sophisticated, new alkylsulfatases and unlock the potential of this non-natural reaction.

4.5.1 Sequence-driven approach for discovery of new alkylsulfatases

Sulfur is an essential element required for growth. When inorganic sulfate is limited, most organisms express a variety of sulfur metabolizing enzymes called sulfatases, which can release inorganic sulfate from organic sulfate esters by hydrolysis. Sulfatases, which are found in all three domains of life, represent a very heterogeneous group of enzymes. Based on substrate spectrum and mechanistic aspects, they are divided into arylsulfatases, Fe(II) α-ketoglutarate dependent sulfatases and alkylsulfatases.

So far, a number of organisms have been described which are able to metabolize alkyl sulfates. However, only very few alkylsulfatases could be identified at DNA level, since in most cases these organisms harbored multiple sulfatases. Apart from the inverting *sec*-alkylsulfatase PISA1, mainly *prim*-alkylsulfatases have been identified so far. Whereby the majority derived from the phylum of Proteobacteria. Distinction between primary and secondary alkylsulfatases based solely on sequence similarities was not feasible. For a more precise identification of PISA1 homologous enzymes, conserved protein motifs should be included as search criteria in addition to the primary structure. Alkylsulfatases are members of the β-lactamases superfamily and can be assigned to metallo-β-lactamase (MBL) subclass B3 based on the binuclear Zn(II) cluster. Four conserved metal ion binding motifs (α-site/β-site) were previously described for this B3-MBL subclass, the canonical HHH/DHH motif, and the rarer motifs QHH/DHH (B3-Q), EHH/DHH (B3-E) and HRH/DQK (B3-RQK).[224] Based on these conserved motifs, individual representatives can be identified.

Three-dimensional structures are available for the *sec*-alkylsulfatase PISA1[176] (PDB: 2yhe) and the *prim*-alkylsulfatases SdsA1[174] (PDB: 2cg3) and SdsAP[225] (PDB: 4nur). While PISA1 shares 45% and 48% sequence identity with SdsA1 and SdsAP, respectively, this is 45% for the two primary alkylsulfatases. The active sites of these enzymes were first analyzed, focusing on the conserved metal ion binding motif (Figure 4.19A).

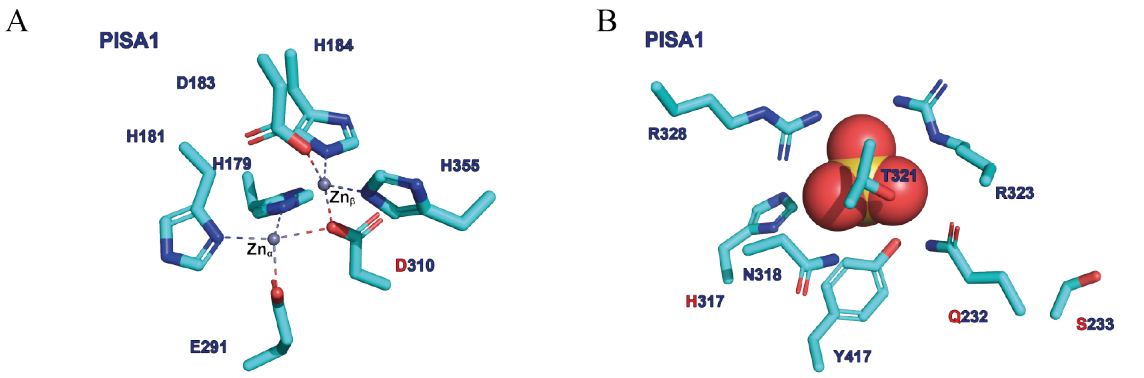

Figure 4.19: Active site of the inverting *sec*-alkylsulfatase PISA1. Conserved amino acid residues of (**A**) Zn(II) binding site and (**B**) sulfate binding site are illustrated as sticks.

Structural analysis of the alkylsulfatases showed that coordination of both Zn(II) occurs *via* a conserved HHE/DHH motif. These alkylsulfatases can thus be assigned to the MBL B3-E motif, with the glutamic acid shifted from position 1 to position 3 of the α-site. A distinction between primary and secondary alkylsulfatase was still not possible. However, it was observed that this motif was extended by a bridging amino acid, which interacted with both Zn(II). This occurred for both primary alkylsulfatases *via* glutamic acid, whereas for PISA1 it was mediated *via* aspartic acid. Utilization of the shorter chain aspartic acid at this position could slightly increase the available space in the active site and shift the preference toward secondary substrates. Therefore, this position was selected as an important criterion.

Such an extended binding motif with bridging amino acid is rather unusual for enzymes with β-lactamase activity, while reported for several MBL type phosphatases. This could be related to the fact that sulfatases and phosphatases present an additional conserved binding site for sulfate and phosphate, respectively. The sulfate binding site (Figure 4.19B) could also significantly influence the acceptance of substrates type. The coordination of the sulfate group occurs *via* 7 amino acid residues, the majority of which are conserved. The SdsA1 binding site showed one variation compared to PISA1 and for SdsAP two variations were observed (Table 4.3). The sequence-based search for homologous PISA1 enzymes, considering the characteristics of the binding sites for Zn(II) and sulfate, resulted in the identification of three promising, uncharacterized annotations. These candidates, which are hereafter termed as CmAS, FtAS, and VpAS, were heterologous expressed, purified, as well as characterized.

Table 4.3: Metal ion binding motifs of B3 MBL subclass and alkylsulfatases.

Enzyme	Type	Zn(II) α-site[a]	Bridging AA[b]	Zn(II) β-site[a]	Sulfate-binding site[c]
PISA1	*sec*	H_{179} H_{181} E_{291}	D_{310}	D_{183} H_{184} H_{355}	Q_{232} H_{317} N_{318} T_{321} R_{323} R_{328} Y_{417}
SdsA1	*prim*	H_{169} H_{171} E_{280}	**E_{299}**	D_{173} H_{174} H_{344}	Q_{222} H_{306} N_{307} T_{310} R_{312} R_{317} **H_{406}**
SdsAP	*prim*	H_{192} H_{194} E_{303}	**E_{322}**	D_{196} H_{197} H_{367}	**M_{245}** H_{329} N_{330} **S_{333}** R_{335} R_{340} Y_{428}
CmAS	new	H_{169} H_{171} E_{280}	**E_{299}**	D_{173} H_{174} H_{344}	**M_{222}** H_{306} N_{307} T_{310} R_{312} R_{317} Y_{407}
FtAS	new	H_{110} H_{112} E_{216}	D_{235}	D_{114} H_{115} H_{277}	**M_{159}** **P_{242}** N_{243} T_{246} R_{248} R_{253} Y_{338}
VpAS	new	H_{174} H_{176} E_{285}	**E_{304}**	D_{178} H_{179} H_{349}	Q_{227} H_{311} N_{312} T_{315} R_{317} R_{322} Y_{410}

Sequence positions are shown in subscript, and variations from PISA1 motif are highlighted in boldface.
[a]: Amino acid residues interacting with first Zn(II) (α-site) or second Zn(II) (β-site).
[b]: Metal ion-bridging amino acid (D, E) extended the conserved motif of alkylsulfatases.
[c]: Amino acid residues interacting with the sulfate group.

4.5.2 Overview of the selected candidates

4.5.2.1 CmAS: an alkylsulfatase from *Cupriavidus metallidurans* Ni-2

To find suitable alternatives to the inverting *sec*-alkylsulfatase PISA1, candidates with different variations in the Zn(II) and sulfate binding site were selected. The first protein (GenBank: AVA36238.1) was identified from *Cupriavidus metallidurans* Ni-2 (β-Proteobacterium), a strain adapted to high levels of Ni(II).[226] This was evaluated as a beneficial feature, with regard to the envisioned metal ion exchange. Annotated as an alkyl/arylsulfatase (659 AA), CmAS showed 57% sequence identity to PISA1 (663 AA). A native secretory signal peptide (21 AA) was also identified for this protein by a prediction tool (SignalP v. 5.0), whereas the signal peptide of PISA1 consists of 28 AA. Overall, two variations to PISA1 were found within both characteristic protein motifs. Identical to primary alkylsulfatases, glutamic acid was noted as the bridging amino acid. However, a slightly altered sulfate-binding site was recognized. Combined with the high sequence identity and the origin from a Ni(II) tolerant strain, CmAS was selected as promising candidate.

4.5.2.2 FtAS: an alkylsulfatase from *Fontimonas thermophila*

The next candidate highlighted the importance of including conserved protein motifs as a search criterion. Although FtAS, which is annotated as BDS1 alkylsulfatase (GenBank: SFF55323.1), was identified from a γ-Proteobacterium as was PISA1, it shared only 32% sequence identity. Interestingly, the protein is significantly truncated (577 AA) compared to all other described alkylsulfatases. Regardless, a secretory signal peptide (26 AA) was also identified. Despite these differences, only 2 variations were observed within the conserved protein motifs. It was the only candidate identified with identical Zn(II) binding site to PISA1, in which aspartic acid served as the bridging amino acid. However, the sulfate binding site showed two variations in contrast. While one variation was homologous to SdsAP, the other was not observed so far.

4.5.2.3 VpAS: an alkylsulfatase from *Variovorax paradoxus* EPS

Annotated as a sterol-binding domain protein (GenBank: ADU34375.1), the alkylsulfatase VpAS was identified from the β-Proteobacterium *Variovorax paradoxus* EPS. Identical to all alkylsulfatases isolated from Gram-negative bacteria, a secretory signal peptide (25 AA) was identified. The sequence identity of the 657 AA sized protein was 52%. VpAS presented a sulfate binding site perfectly consistent with PISA1. Only one variation was observed overall. Therby, homologous to primary alkylsulfatases, VpAS utilized glutamic acid as the bridging amino acid. The selection of suitable candidates was completed with VpAS, as in combination with FtAS (identical Zn(II) binding site) both PISA1 motifs were covered.

4.5.3 Characterization of the new alkylsulfatases

For the identification of new *sec*-alkylsulfatases, the selected candidates were characterized in comparison to PISA1 as a benchmark. Heterologous production of the enzymes was performed using the conditions refined for PISA1 (chapter 4.4.1), which allowed purification of up to 160 mg of PISA1 from 1 L of expression culture. This protein yield could not be realized for CmAS or VpAS, respectively. Nevertheless, up to 80 mg of purified enzyme was produced in each case. This was not the case for FtAS. Only approximately 10 mg of protein could be purified under identical conditions. However, this was sufficient to also characterize FtAS.

4.5.3.1 Thermodynamic stability

A high degree of protein stability is an important characteristic for a robust biocatalyst. Protein stability is divided into thermodynamic stability (protein folding) and kinetic stability (biological functionality).[227] Given that these parameters are not inherently correlated. Interestingly, primary and secondary alkylsulfatases also show differences in their thermodynamic stability. For example, a T_m of 74.5°C was described for SdsA1, and SdsAP is also thermostable, while the protein melting point of PISA1 was detected at 57°C.[170,175,207] This dissimilarity in protein melting point was also observed within the new alkylsulfatases. CmAS and VpAS showed thermostable properties with a T_m of 69.5°C and 81.5°C, respectively (Figure 4.20). For FtAS, two protein melting points were detected at 42.5°C and 52.5°C, both lower than the T_m of PISA1, which was previously determined by CD spectroscopy and was reproducible with the thermofluor assay applied in this study. Such a behavior could be related to a partially Zn(II) loaded FtAS mixture or to the fact that the quaternary structure is dissociated first (42.5°C) followed by unfolding of the monomers (52.5°C). However, supplying additional Zn(II) resulted not in a fusion of both melting points. The presence of 10 mM secondary alkyl sulfate resulted in only minor stabilization of the proteins.

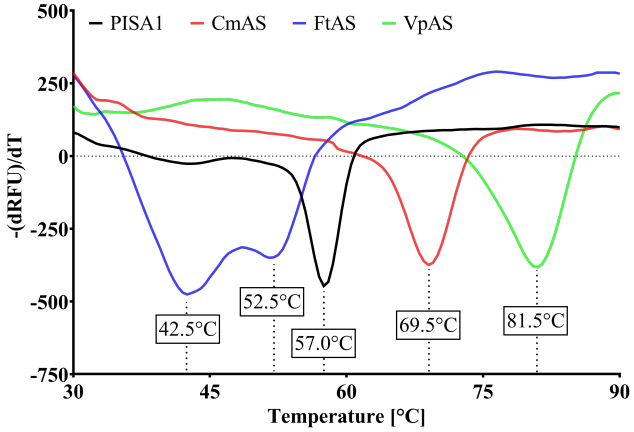

Figure 4.20: Thermodynamic stabilities of PISA1, CmAS, FtAS, and VpAS. Protein melting points were determined by thermofluor assay. Each well contained 2 µL enzyme (1.0 mg mL^{-1}), 21 µL 100 mM TRIS-HCl, pH 8.2 and 2 µL of SYPRO Orange working stock. Measurements were performed in triplicates and here the mean is presented. For PISA1, CmAS, FtAS, or VpAS, the protein melting points of 57.0°C, 69.5°C, 42.5°C/52.5°C and 81.5°C were determined, respectively.

4.5.3.2 Kinetic stability

More crucial than thermodynamic stability will be the kinetic stability, and in particular, secondary alkylsulfatase activity. However, due to the observed wide range in thermodynamic stability, different temperature optima were postulated for CmAS, FtAS and VpAS. Recognizing the strong influence of the environment on PISA1, different preferences for buffer system and pH were also considered. Therefore, the secondary alkylsulfatase activity of the enzymes on 10 mM *rac*-2-octanyl sulfate was investigated overnight in a temperature range of 30 – 75°C along with a pH range of 4 – 11. The required throughput was ensured by the sulfate assay.

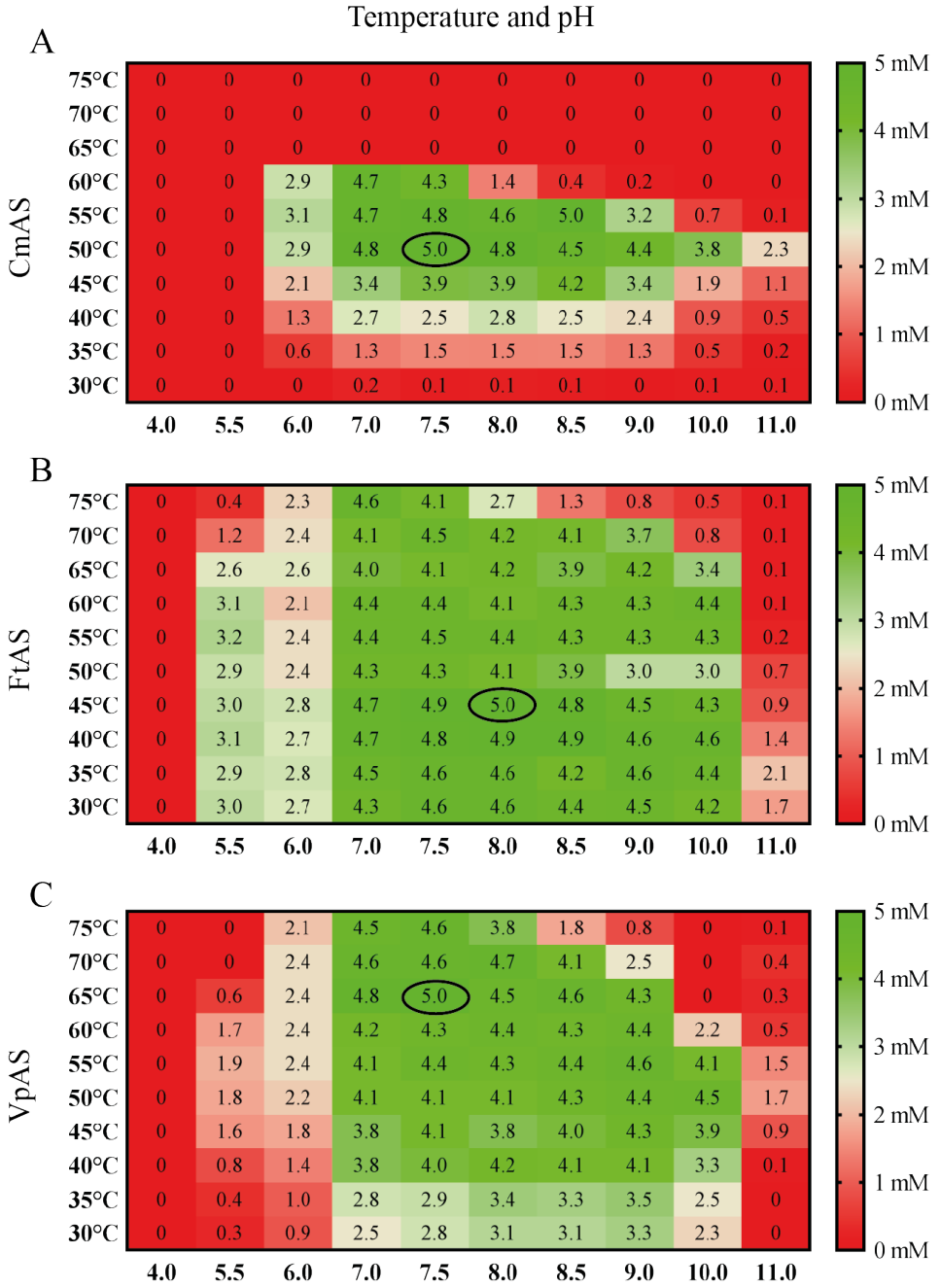

Figure 4.21: Investigation of the preferred reaction conditions of CmAS, FtAS and VpAS. The conversion of 10 mM of *rac*-2-octanyl sulfate was investigated overnight with 7.9 µM of (**A**) CmAS (**B**) FtAS and (**C**) VpAS in a range of 30 – 75°C and a pH of 4.0 – 11.0, respectively. The study was performed based on following buffers: 150 mM citric acid sodium phosphate buffer (pH 4.0 and 5.5), 100 mM potassium phosphate buffer (pH 6.0), 100 mM TRIS-HCl buffer (pH 7.0, 7.5, 8.0, 8.5 and 9.0) and 100 mM ammonium buffer (pH 10.0 and 11.0).

Fortunately, secondary alkylsulfatase activity was detected for all new enzymes (Figure 4.21). Here, the external conditions showed a stronger impact on CmAS than was observed for FtAS or VpAS. It must be noted that all buffers used were calibrated at 25°C and were not adjusted to the increasing temperature. For example, TRIS buffers are known to have a strong dependence on the ambient temperature. Here, the pK_a value decreases by about 0.03 units per degree Celsius elevation in temperature. However, taking into account thermodynamic stability, FtAS should have a significantly constrained activity range. This suggests a high specific enzyme activity, since it can be assumed that the respective turnover was achieved in the time between the start of the reactions (simultaneous mixing of master mix and enzyme, plus a centrifugation step) and reaching the desired temperature. This hypothesis is supported by the fact that the thermodynamic stability of FtAS was not significantly improved in the presence of substrate.

A common characteristic of the three alkylsulfatases was that only half of the racemic substrate was converted as a maximum. This indicates a similar high enantioselectivity, which was already described for PISA1. Furthermore, no enzymatic activity was detected for any biocatalyst at pH 4, suggesting that it is likely that the respective apoenzymes can be produced by modulating the enzymatic microenvironment. Final optimal reaction conditions were identified as 50°C, pH 7.5 (actual pH of 6.7), 45°C, pH 8.0 (actual pH of 7.4), and 65°C, pH 7.5 (actual pH of 6.3) for CmAS, FtAS, and VpAS, respectively. Subsequent experiments were performed under these conditions.

4.5.3.3 Enzyme promiscuity

A broad substrate spectrum has been described for PISA1, including different side chains and varying position of the sulfate group. While only low activity was observed for primary alkyl sulfate esters, the enzyme showed high activities on secondary substrates, with the relative position of the sulfate ester moiety varying from C2 to C4. In contrast, *prim*-alkylsulfatases are predominantly active only on primary alkyl sulfate esters.[170,176] For a deeper evaluation of the new alkylsulfatases, the substrate spectrum was investigated using a primary and various secondary substrates (Table 4.4). As was already apparent, FtAS showed the highest agreement with the substrate spectrum of PISA1 (Table 4.5). Substance 1a was barely accepted, while enzymatic activity was observed across the range of secondary substrates, with lower total turnover compared to PISA1. Thus, all available data indicate that FtAS can be classified as a secondary alkylsulfatase. In contrast, complete conversion of substance 1a was observed for CmAS and VpAS, while substances *rac*-3a, *rac*-4a and *rac*-5a were barely accepted.

Table 4.4: Overview of the selected substrates and the corresponding products.

ID	Substrate	Type	R_1	R_2	ID	Hydrolysis product
1a	dodecyl sulfate	*prim*	-	*n*-undecyl	1b	1-dodecanol
rac-2a	*rac*-2-heptyl sulfate	*sec*	methyl	*n*-pentyl	2b	2-heptanol
rac-3a	*rac*-3-heptyl sulfate	*sec*	ethyl	*n*-butyl	3b	3-heptanol
rac-4a	*rac*-4-heptyl sulfate	*sec*	*n*-propyl	*n*-propyl	4b	4-heptanol
rac-5a	*rac*-4-phenyl-2-butyl sulfate	*sec*	methyl	ethyl phenyl	5b	4-phenyl-2-butanol

Table 4.5: Investigation of the promiscuities of PISA1, CmAS, FtAS and VpAS.

ID	Substrate	Type	Product[a]	PISA1[1]	CmAS[2]	FtAS[3]	VpAS[4]
1	dodecyl sulfate	*prim*	1-dodecanol	0.1%	100%	0.8%	100%
rac-3	*rac*-3-heptyl sulfate	*sec*	3-heptanol	50%	0.9%	20.3%	0.4%
rac-4	*rac*-4-heptyl sulfate	*sec*	4-heptanol	50%	0.3%	22.1%	0.5%
rac-5	*rac*-4-phenyl-2-butyl sulfate	*sec*	4-phenyl-2-butanol	50%	0.5%	33.1%	2.9%

[a]: The analysis was performed by GC/MS, relative conversions are presented in relation to PISA1, except for ID 1.
[b]: Reactions were performed with 20 mM respective substrate and 0.40 µM respective enzyme for 20 h with 750 rpm shaking at (1) 30°C, pH 8.2, (2) 50°C, pH 7.5, (3) 45°C, pH 8.0 or (4) 65°C, pH 7.5.

In this case, the data indicate that both can be classified as *prim*-alkylsulfatases. However, compared to all known representatives, CmAS and VpAS showed a detectable turnover of the secondary alkyl sulfate ester with the functional moiety at position C2 (Figure 4.21).

4.5.3.4 Metal ion exchange

After demonstrating that CmAS, FtAS, and VpAS possess secondary alkylsulfatase activity, it was evaluated how readily the metal ions could be removed from the active site. Treatment with a chelating agent, as well as the protonation of the active site histidines were investigated. Unfortunately, FtAS displayed the same challenges as PISA1. Combined with low protein expression, FtAS was not considered further. In contrast, removal of metal ions from a primary alkylsulfatase was already demonstrated.[207] In the case of CmAS and VpAS, the corresponding apoenzyme was straightforward to produce by both methods. This was confirmed by loss of catalytic activity, along with a significant shift in T_m. Removal of native metal ions and reloading with Zn(II) was exemplarily demonstrated for CmAS *via* modulation of the enzyme microenvironment and for VpAS *via* treatment with EDTA (Figure 4.22). For both apoenzymes, it was observed that the addition of Zn(II) resulted in significantly lower protein precipitation compared to PISA1. The catalytic activity as well as the initial protein melting point could be fully restored in both cases. For CmAS, the supplementation of 10 equivalents of Zn(II) was sufficient, while for VpAS 100 equivalents of metal ions were required. In conclusion, CmAS and VpAS represented promising protein scaffolds for artificial metalloenzymes.

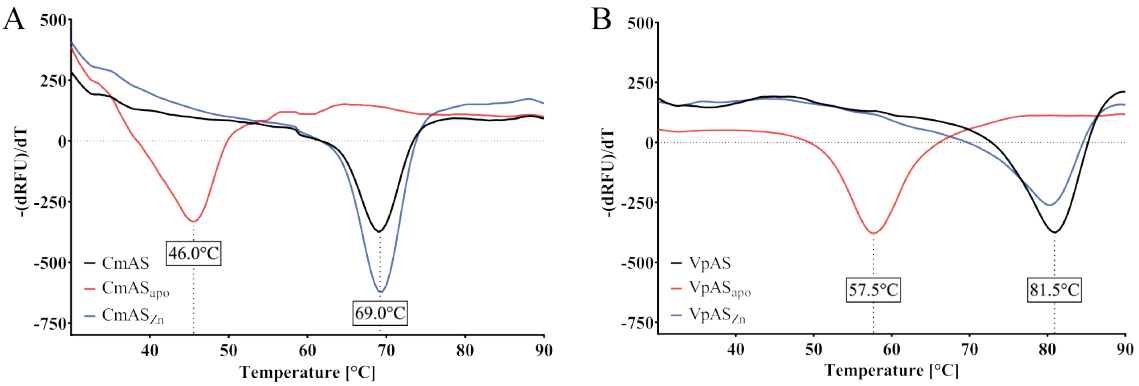

Figure 4.22: Metal ion exchange of new alkylsulfatases CmAS and VpAS. Metal ions were removed in the case of (**A**) CmAS or (**B**) VpAS by modulation of the enzymatic microenvironment (*via* 150 mM citrate buffer, pH 4.5) or by treatment with 100 equivalents of EDTA, respectively. Protein melting points of the respective native alkylsulfatases (black), apoenzymes (red), and protein scaffolds reloaded with Zn(II) (blue) were determined by thermofluor assay.

4.5.3.5 CD spectroscopy

Lastly, CmAS was used as an example to investigate whether the removal of metal ions from the active site resulted in conformational changes of the protein scaffold. For this purpose, both the holoenzyme and the apoenzyme were analyzed by CD spectroscopy. Both forms of the enzyme showed highly overlapping CD spectra (Figure 4.23), suggesting an identical overall protein structure and countering conformational changes as a result of the removal of metal ions. Thus, this protein scaffold is ideally suited for metal ion exchange, since the active site remained structurally stable in the absence of metal ions. Moreover, based on the detected CD spectra, a rather similar protein folding to PISA1 could be deduced.

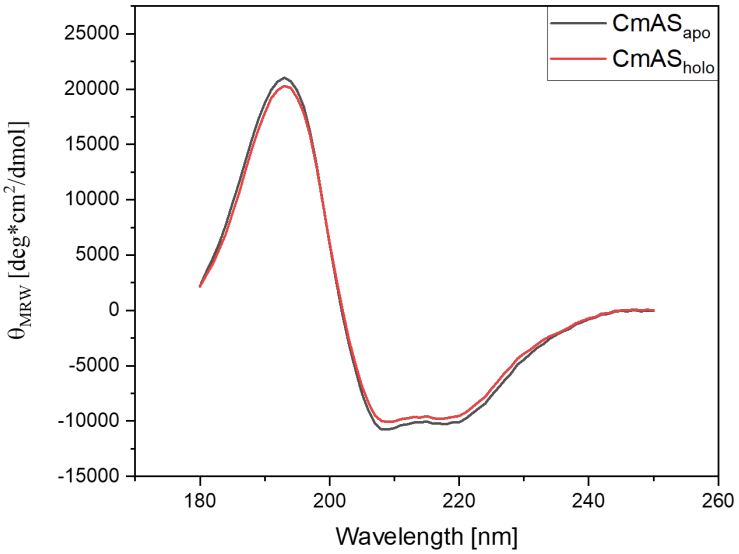

Figure 4.23: Circular dichroism spectroscopy of holo- and apostate of CmAS. Both proteins were desalted against 20 mM sodium phosphate buffer, pH 8.20 and diluted to 0.267 mg mL^{-1} (3.8 µM). Measurements were performed at 20°C with 10 repeats and scan between 180 to 280 nm (1 nm steps). Holoenzyme illustrated as red line and apoenzyme as black line.

4.6 CmAS metal ion exchange study

Once two new alkylsulfatases were identified that showed sufficient agreement with the characteristics of PISA1 but allowed much easier exchange of metal ions, the initial proof of concept study was aimed to be reproduced. Considering that CmAS was originally isolated from a Ni(II) tolerant strain, this protein scaffold was selected for the production of artificial metalloenzymes. The apostate of CmAS was provided using the process developed for PISA1, modulation of the enzyme microenvironment, which is based on electrostatic repulsion.

4.6.1 Preparation of artificial metalloenzymes based on CmAS

The same bivalent metal ions were investigated here as in the initial proof of concept. As previously determined, 10 equivalents of Zn(II) were required for complete reloading of the apoenzyme. Since a lower affinity of the protein scaffold for non-native metal ions was assumed, 50 equivalents of the respective metal ions were used here. This resulted in a higher degree of protein precipitation in the case of Zn(II) than was observed when 10 equivalents were used. In contrast, the metal-free protein scaffold was less sensitive to non-native metal ions, resulting in lower protein precipitation.

First, the influence of these various metal ions on the thermodynamic stability of the protein scaffold was investigated to estimate the respective loading state of the enzymes (Table 4.6). The apoenzyme (T_m = 46.0°C) and the holoenzyme completely loaded with Zn(II) (69.0°C) were included as controls. A stabilizing effect was observed in all cases, with mainly a single protein melting point. Only the treatment with Co(II) caused a stronger stabilization (71.5°C) than was observed with native Zn(II). This was a strong indication that a fully loaded active site was achieved and further that the protein scaffold is suitable for the creation of artificial metalloenzymes.

In contrast, the stabilizing effect for Ni(II) was only half as strong as for Zn(II). Since it could not be excluded that a partial loading of the protein scaffold occurred here, 50 equivalents of Zn(II) were added in a second step. This resulted in additional thermodynamic stabilization of the protein scaffold, with a higher T_m detected than for the native holoenzyme (Table 4.6). That indicated that the treatment with Ni(II) resulted in an artificial metalloenzyme with mononuclear site and consequently a Ni(II)/Zn(II) hetero binuclear site was generated by additional supplementation of Zn(II).

Table 4.6: Protein melting points of CmAS and variants.

$CmAS_{apo}$ loading	**w/o M(II)**	**+ Zn(II)**	**+ Co(II)**	**+ Ni(II)**	**+ Cd(II)**	**+ Cu(II)**	**+ Mn(II)**
1. step[a]	46.0°C	69.0°C	71.5°C	57.5°C	62.5°C	50.0°C	52.5°C
Δ T_m	-	+23.0	+25.5	+11.5	+16.5	+4.0	+6.5
+ Zn(II)[b]	69.5°C	69.0°C	72.0°C	74.0°C	69.0°C	75.5°C	70.5°C
Δ T_m	+23.5	+0.0	+0.5	+16.5	+6.5	+25.5	+18.0

[a]: $CmAS_{apo}$ was incubated without metal ions or with 50 eq. of Zn(II), Co(II), Ni(II), Cd(II), Cu(II) or Mn(II)
[b]: All respective CmAS variants from first step were incubated with 50 eq. of Zn(II)

The same behavior was observed for the apoenzyme treated with Cu(II) in the first step. Since a similar T_m to the native holoenzyme was detected for the enzymes previously treated with Cd(II) and Mn(II), a complete exchange by Zn(II) could not be excluded. In contrast, no effect on the enzyme ($CmAS_{Co}$) loaded in the first step with Co(II) was observed, neither a strong protein precipitation nor a significant shift of the T_m was detected. This indicates that the coordination of Co(II) resulted in a stable system. However, none of these artificial metalloenzymes (mononuclear, binuclear, or hetero-binuclear) achieved the catalysis of primary aliphatic amines, and thus the focus was directed to other non-natural reactions.

4.6.2 Identification of non-natural reactions

Various artificial metalloenzymes could be generated based on the metal-free protein scaffold of CmAS, and the enzyme completely loaded with Co(II) (termed as $CmAS_{Co}$) showed the most promising properties. Therefore, the influence of metal ion exchange on catalytic activity was investigated in depth. The preference of environmental conditions was investigated for the conversion of *rac*-2-heptyl sulfate in a defined range compared to the native holoenzyme (Figure 4.24). Associated with the slightly elevated thermodynamic stability of $CmAS_{Co}$, a shift in kinetic stability toward higher temperatures was observed. Moreover, the artificial metalloenzyme showed a preference for a more basic environment than the native enzyme. The coordination of Co(II) additionally showed an influence on enantioselectivity; while native CmAS, identical to PISA1, FtAS, and VpAS, only converted at most half of the racemic substrate, $CmAS_{Co}$ showed a conversion of up to 60% at 55°C and basic conditions. Having found a significant effect on the enantioselectivity of the biocatalyst, promiscuity was also investigated under standard conditions (Table 4.7). Strikingly, metal ion exchange resulted in an almost complete loss of primary alkylsulfatase activity. The acceptance of *rac*-3a and *rac*-4a was only slightly improved compared to the native enzyme, whereas the conversion of the secondary substrate with aromatic side chain (*rac*-5a) was increased 20-fold.

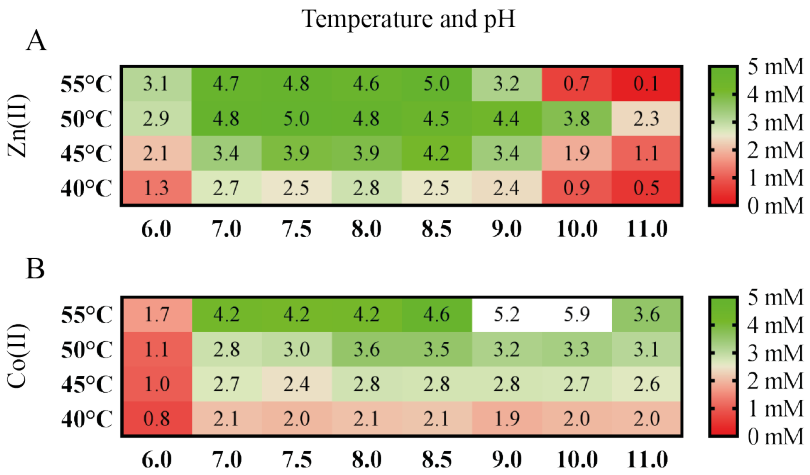

Figure 4.24: Investigation of the preferred external conditions of native CmAS and $CmAS_{Co}$. The conversion of 10 mM of *rac*-2-heptyl sulfate was investigated with 7.9 µM of $CmAS_{Zn}$ (**A**) or $CmAS_{Co}$ (**B**) in a range of 40 – 55°C and a pH of 6.0 – 11.0. The study was performed with the following buffers: 100 mM potassium phosphate buffer (pH 6.0), 100 mM TRIS-HCl (pH 7.0, 7.5, 8.0, 8.5 and 9.0) and 100 mM ammonium buffer (pH 10.0 and 11.0).

Table 4.7: Investigation of the promiscuities of CmAS and $CmAS_{Co}$ in comparison to PISA1.

ID	Substrate	Type	Product[a,b]	PISA1	CmAS	$CmAS_{Co}$
1	dodecyl sulfate	*prim*	1-dodecanol	0.1%	100%	1.0%
rac-3	*rac*-3-heptyl sulfate	*sec*	3-heptanol	50%	0.9%	2.2%
rac-4	*rac*-4-heptyl sulfate	*sec*	4-heptanol	50%	0.3%	3.6%
rac-5	*rac*-4-phenyl-2-butyl sulfate	*sec*	4-phenyl-2-butanol	50%	0.5%	10.1%

[a]: The analysis was performed by GC/MS, relative conversions are presented in relation to PISA1, except for ID 1.
[b]: Reactions were performed for 20 h and 750 rpm shaking with the respective substrate (20 mM) and 0.40 µM of PISA1 at 30°C, pH 8.2 or 0.40 µM of CmAS resp. $CmAS_{Co}$ at 50°C, pH 7.5.

Along with the hydrolytic release of the secondary aryl alcohol (10.1%), $CmAS_{Co}$ also catalyzed the production of various related unbranched alkenyl arenes (1.1%). Alkenyl arenes are primarily used as building blocks for polymerization reactions, often derived from petrochemical resources.[228,229] In addition, they are also used for the production of pharmaceuticals and detergents.[230] These coproducts were not detected for the native alkylsulfatases PISA1, CmAS, FtAS and VpAS. Specifically, 4-phenyl-1-butene (0.4%), 4-phenyl-2-butene (0.3%), and 1-phenyl-1-butene (0.4%) were produced by the artificial metalloenzyme, with a total release of 1.1% of unbranched alkenyl arenes (Figure 4.25).

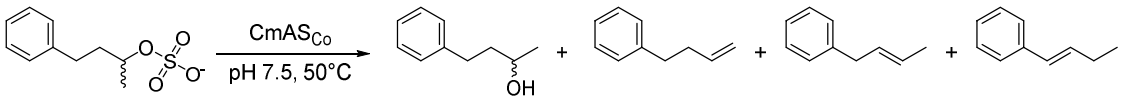

rac-4-phenyl-2-butyl sulfate (*rac*-5a) | 4-phenyl-2-butalol (10.1%) | 4-phenyl-1-butene (0.4%) | 4-phenyl-2-butene (0.3%) | 1-phenyl-1-butene (0.4%)

Figure 4.25: New-to-nature reaction catalyzed by $CmAS_{Co}$. Reaction was performed for 20 h and 750 rpm shaking with 20 mM of *rac*-4-phenyl-2-butyl sulfate (*rac*-5a) and 0.40 µM of $CmAS_{Co}$ in 100 mM TRIS-HCl, pH 7.5 at 50°C. In addition to 10.1% of the natural product (4-phenyl-2-butanol), a total of 1.1% of non-natural products (unbranched alkenyl arenes) were also detected.

4.7 Screening of various metal ions for catalysis of non-natural reactions

The artificial biocatalyst, consisting of the metal-free protein scaffold of CmAS and non-native Co(II), enabled production of promising alkenyl arenes under mild conditions. However, since only a minor side activity was observed here, other combinations of protein scaffolds and metal ions were screened in order to catalyze this non-natural reaction more effectively. For this purpose, VpAS was added to the preselected protein scaffold based on similar characteristics and 58% sequence identity. Moreover, the selection of non-native metal ions was broadened by various bivalent, trivalent and tetravalent metal ions. This expanded set of potential artificial metalloenzymes was simultaneously screened for the production of aliphatic primary amines.

4.7.1 Preparation of metal-free protein scaffolds

The alkylsulfatases CmAS and VpAS (pH 7.5) preferred an environment with lower pH than PISA1 (pH 8.2), hence, both biocatalysts were prepared directly in their favored environment. As part of this, it was found that the thermodynamic stability of CmAS is pH dependent (Figure 4.26). At a pH of 7.5, the enzyme showed a T_m of 75.5°C, which decreased in linear dependence with increasing pH, leading to a melting point of 66.0°C for CmAS at a pH of 9.0, almost 10°C decreased. In contrast, such a strong pH dependence was not observed for VpAS.

Guided by serendipity, it was found that CmAS and VpAS can be targeted expressed in their holo- or apostate, depending on media components from different suppliers. The use of yeast extract and tryptone from the supplier Carl Roth (Karlsruhe, DE) resulted in the production of the biocatalysts in holostate, while the use of the components from the supplier Sigma-Aldrich (St. Louis, USA) caused the production in apostate (Figure 4.27). In contrast, this dependency was not observed for PISA1. This could indicate that PISA1 has a higher affinity for Zn(II) compared to CmAS or VpAS and is thus less influenced by the availability of free metal ions. This assumption is supported by the fact that the removal of metal ions from CmAS and VpAS was much more straightforward.

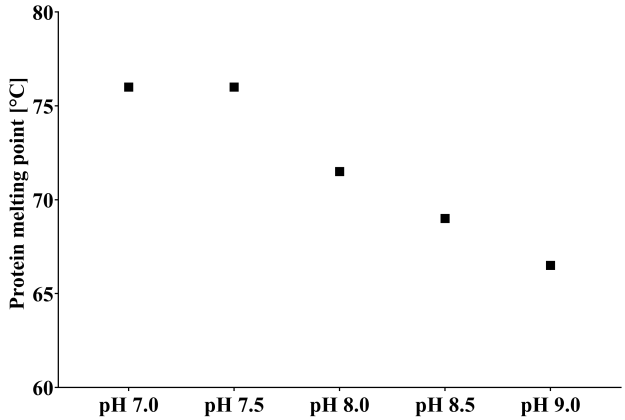

Figure 4.26: Dependence of the thermodynamic stability of native CmAS on ambient pH. CmAS was produced under described conditions. Subsequently, the environment of aliquots was exchanged against 100 mM TRIS-HCl, pH 7.0 – 9.0 by means of a desalting step. Protein melting points (T_m) were measured with thermofluor assay. Each well contained 2 µL of CmAS (1.0 mg mL^{-1}), 21 µL respective buffer and 2 µL SYPRO Orange working stock.

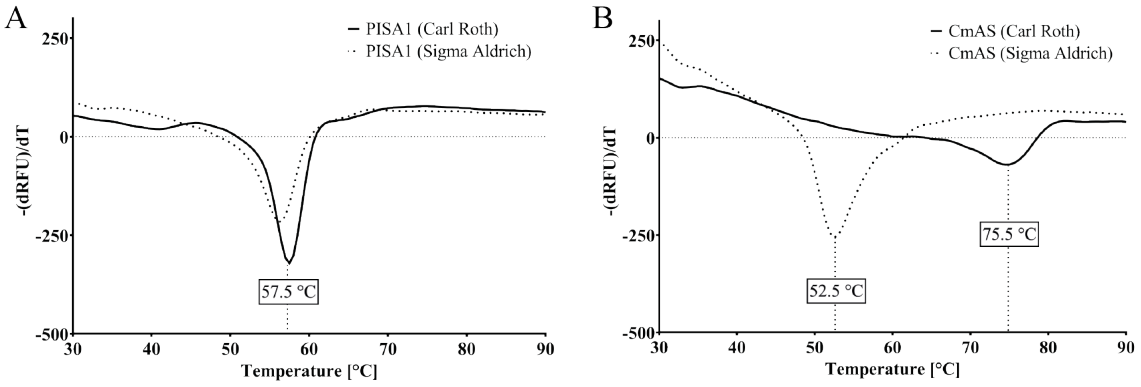

Figure 4.27: Impact of media components on the production of *prim*- and *sec*-alkylsulfatases. The media components used from different suppliers showed no effect on the production of PISA1 (**A**), whereas the production of CmAS (**B**) could be specifically controlled as holo- or apostate, by using media components from Carl Roth or Sigma-Aldrich, respectively.

4.7.2 The expanded set of artificial metalloenzymes

Previously, only bivalent metal ions were studied, specifically zinc, cobalt, nickel, cadmium, copper and manganese. This set of metal ions was broadened by additional 6 bivalent (magnesium, calcium, barium, iron, tin and europium) and 6 trivalent (ruthenium, rhodium, gallium, indium, osmium and cerium) metal ions as well as one tetravalent (platinum). A total of 18 non-native metal ions were screened, whereby Fe(II), Ga(III), Sn(II) and Eu(II) required the addition of a reducing agent (sodium dithionite). In combination with the protein scaffolds of CmAS and VpAS, this resulted in 36 possible artificial metalloenzymes, which were applied in order to determine non-natural reactions with compounds *rac*-2a, *rac*-3a, *rac*-4a and *rac*-5a (Table 4.4). Including all controls, 160 different reactions were prepared and assessed for alkenyl arene and primary amine production, respectively.

In order to achieve a sufficient throughput, the protein scaffolds were produced directly in their apostate and were mixed with 100 equivalents of the respective metal ions. Due to the limited workability, the removal of free, non-bound metal ions after the loading process was omitted. However, the presence of some metal ions compromised the spectroscopic determination of protein concentration (Table 4.8). The analysis of protein melting points indicated that several new artificial metalloenzymes were generated. Both metal-free protein scaffolds often responded rather comparably to the added metal ions. However, the addition of high concentrations of Zn(II) resulted in precipitation of the majority of $CmAS_{apo}$.

Table 4.8: Measured protein concentration of the artificial metalloenzymes.

Scaffold	w/o	Zn(II)	Co(II)	Ni(II)	Cd(II)	Cu(II)	Mn(II)	Mg(II)	Ca(II)	Ba(II)
CmAS	1.76	0.09	3.33	1.62	1.55	1.70	1.57	1.76	1.79	1.78
VpAS	1.76	1.38	1.64	1.65	1.59	1.44	1.36	1.77	1.74	1.77
Scaffold	**Fe(II)[a]**	**Sn(II)[a]**	**Eu(II)[a]**	**Ru(III)**	**Rh(III)**	**Ga(III)[a]**	**In(III)**	**Os(III)**	**Ce(III)**	**Pt(IV)**
CmAS	1.16	1.63	1.14	1.06	n.d.	1.43	0.19	n.d.	n.d.	1.59
VpAS	2.64	1.68	1.36	1.87	0.68	0.99	0.38	n.d.	n.d.	1.55

Protein concentrations (in mg mL^{-1}) were determined by spectrometry (chapter 2.2.4.10). CmAS or VpAS (25 µM; 1.76 mg mL^{-1}) was mixed with 100 equivalents of the respective metal ions (5 mM) and incubated for 20 h at 25°C.
[a]: In presence of 10 mM sodium dithionite as reducing agent.

4.7.3 Impact on the natural alkylsulfatase activity

The metal ion coordination of CmAS already demonstrated a significant influence on the substrate range. Therefore, the natural alkylsulfatase activity was first assessed with 20 mM of the secondary substrates (Table 4.4). For this purpose, reactions were performed with 10% of the respective combination of protein scaffold and metal ions for 16 h at 55°C in a metal-free buffer (treatment caused a pH of 8.5). To also enable the simultaneous production of alkenyl arenes and aliphatic primary amines, one equivalent of ammonia (substrate related) was added.

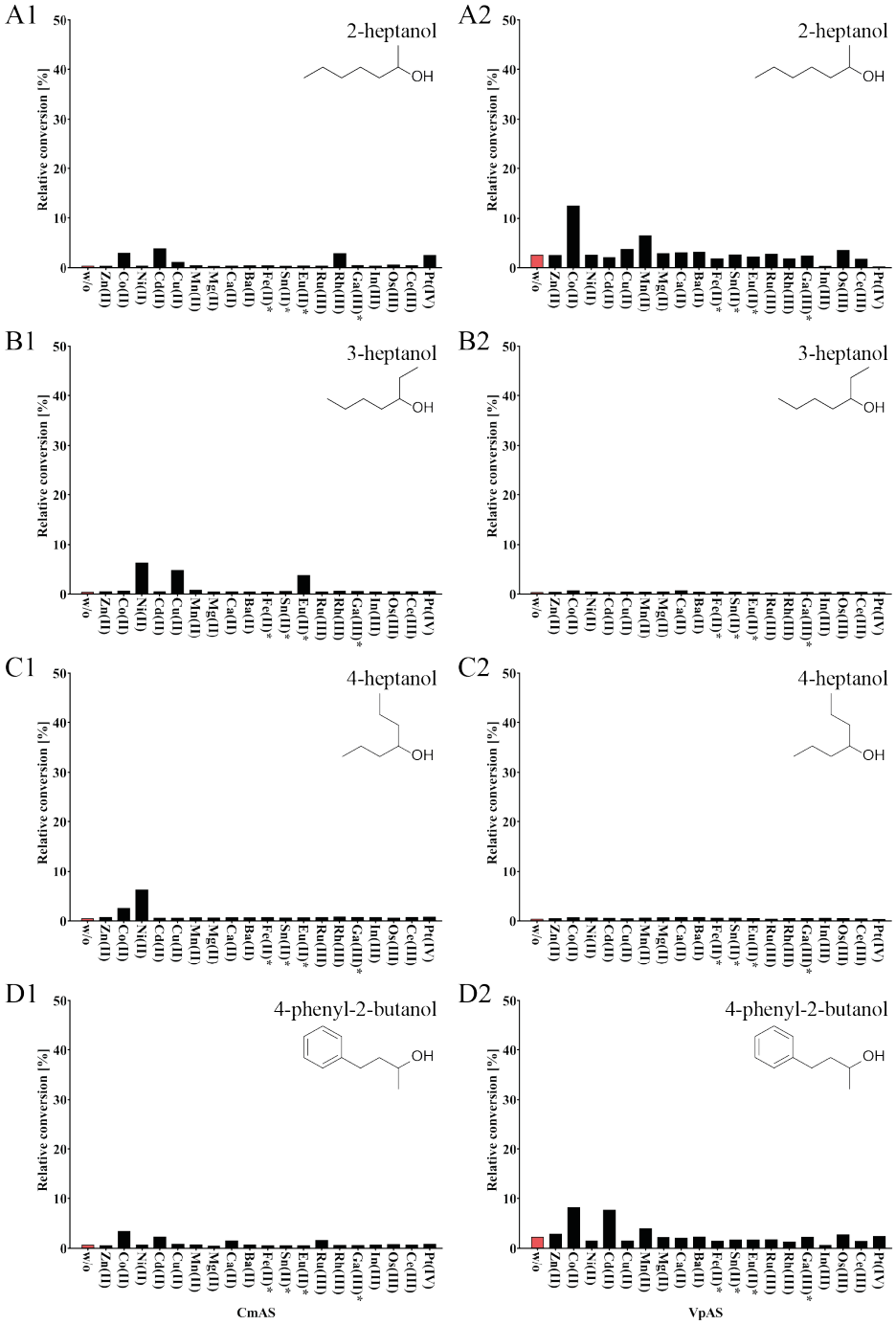

Figure 4.28: Assessment of the expanded set of artificial metalloenzymes – alkylsulfatase activity. Using media components from Sigma-Aldrich, the metal-free protein scaffolds were specifically produced. CmAS (**1**) or VpAS (**2**) were incubated with 100 equivalents of the respective metal ions (Table 4.8). Reactions were performed at 55°C for 16 h using 20 mM *rac*-2a (**A**), *rac*-3a (**B**), *rac*-4a (**C**), or *rac*-5a (**D**) as substrate, 10% enzyme supernatant, and 20 mM ammonia in 100 mM metal-free TRIS-HCl, pH 8.49. Analysis was performed by GC/MS.

Under the selected screening conditions, which represented a compromise for both alkylsulfatases, a lower activity was observed for the hydrolysis of the secondary alkyl sulfate ester at relative position C2 (Figure 4.28A). However, considering that CmAS precipitated almost completely in the presence of 100 equivalents of Zn(II), the significance of this control is missing. Moreover, when VpAS was used as protein scaffold for the biocatalysis of substances with the sulfate moiety at relative position C2 (*rac*-2a and *rac*-5a), an unusually strong background reaction was observed. Subsequent studies showed that the presence of the ammonia equivalent enhanced the pH dependent, base-catalyzed hydrolysis of compounds *rac*-2a and *rac*-5a, although *rac*-5a was significantly less stable. Nevertheless, considering that all combinations of apoenzyme and metal ions were treated under identical conditions, a sufficient intrinsic quality of the screening was reached to initially evaluate the single variants.

Excitingly, significant catalytic activity was observed for the combination of CmAS and Eu(II), which was limited exclusively on substrate with the sulfate group at relative position C3 (*rac*-3a). Europium, which belongs to the group of lanthanides, is one of the rarest elements on earth, without significant biological importance. Because of this, only a few proteins are described that can use europium for the catalysis of enzymatic reactions. Equally exciting to observe was that CmAS combined with Ni(II) showed enzymatic activity when the sulfate group was at position C3 or C4. This represented a valuable platform to investigate the biocatalytic production of aliphatic primary amines based on the protein scaffold of CmAS. Apart from that, the already known characteristic of CmAS was observed for the incorporation of Co(II), even if in a weakened degree. In contrast, the protein scaffold of VpAS showed no considerable catalytic activity when the sulfate group was at position C3 or C4. The addition of Co(II) otherwise showed a similar influence on VpAS as already observed for CmAS, whereby a stronger catalytic activity was mediated. A comparable activity for compound *rac*-5a was also observed with Cd(II).

4.7.4 Biocatalysis of aliphatic primary amines

For none of the 160 analyzed reactions a release of primary aliphatic amines was observed. Treatment of CmAS with Ni(II) resulted in significant native activity with *rac*-3a and *rac*-4a, however, no amination was detected here. Since the metal-free protein scaffolds of CmAS and VpAS possessed almost no catalytic activity, at least partial loading with Ni(II) can be assumed. Accordingly, it indicated that these protein scaffolds are not suitable for catalysis of this new-to-nature reaction. Therefore, efforts to implement this non-natural reaction were finally terminated.

4.7.5 Biocatalysis of alkenyl arenes

A sophisticated performance of the artificial metalloenzymes was observed for the other non-natural reaction based on the substrate with aromatic side chain. Although background activity was observed, which can be attributed to the slightly higher pH of the metal-free buffer and the presence of ammonia, a significant release of alkenyl arenes were detected by artificial

metalloenzymes based on both protein scaffolds. In contrast, the production of olefins starting from the various alkyl sulfates was not observed at all, neither enzymatically nor base-catalyzed. Therefore, the focus was on the reaction with *rac*-4-phenyl-2-butyl sulfate (*rac*-5a).

For CmAS, in addition to treatment with Co(II), conversion of the compound *rac*-5a to alkenyl arenes was also observed with Ca(II), Ru(II) and Cd(II). Although a reduced release of 4-phenyl-2-butanol from previously 10.1% to 3.4% was detected in the screening for the Co(II)-loaded enzyme, the production of the various related unbranched alkenyl arenes (1.0%) remained almost unchanged. Responsible for this was the newly observed background activity of about 0.4%. For Ca(II), Ru(II) and Cd(II), an identical non-natural reactivity was observed, with a substantially reduced secondary alcohol release of 1.5%, 1.6% and 2.3%, respectively. Accordingly, the ratio of these variants was shifted more toward the co-activity.

A more promising behavior was observed for VpAS based variants. Interestingly, strong natural activity could be detected with Co(II), but without additional production of alkenyl arenes. The Pt(IV) based variant showed a contrary behavior, while the natural activity only slightly exceeded the background activity, a similarly strong non-natural reactivity of 1.8% was detected. Loading of the metal-free protein scaffold with Cd(II) resulted in a combination of both activities. Comparable to the behavior with Co(II), 7.7% of the secondary alcohol was detected. In addition, 4-phenyl-1-butene (1.1%), 4-phenyl-2-butene (1.0%), and 1-phenyl-1-butene (1.1%) were detected, which combined corresponded to a production of 3.2% of unbranched alkenyl arenes. This represents a three-fold improvement over the previously observed non-natural reactivity, although screening was performed under non-optimal conditions. Assuming that this artificial metalloenzyme acts similar to CmAS loaded with Co(II), a significantly stronger production of alkenyl arenes can be assumed under optimal conditions.

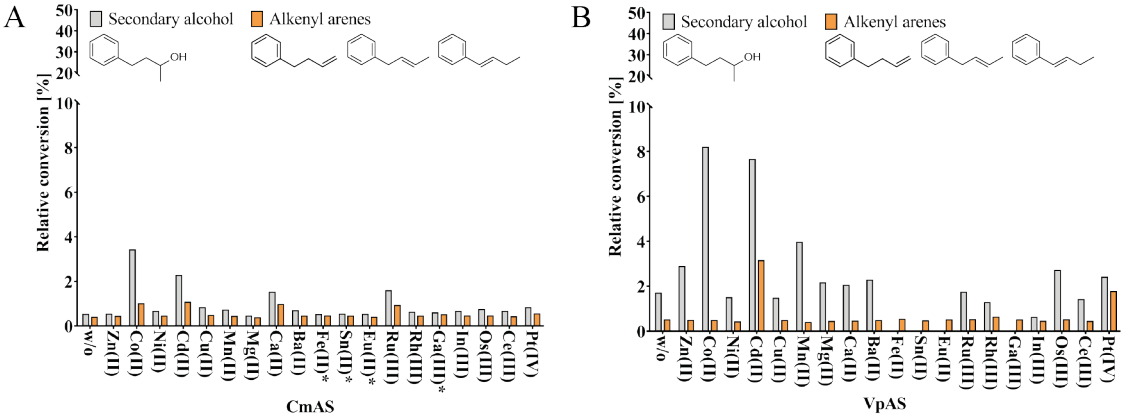

Figure 4.29: Assessment of the expanded set of artificial metalloenzymes – non-natural activity. All combinations of CmAS (**A**) or VpAS (**B**) and respective metal ions were subsequently screened for the biocatalysis of alkenyl arenes. For this purpose, reactions with *rac*-5a as substrate (Figure 4.28D1-2) were investigated with respect to the production of various alkenyl arenes (4-phenyl-1-butene, 4-phenyl-2-butene and 1-phenyl-1-butene) in addition to the natural release of the secondary alcohol (4-phenyl-2-butanol).

5. DISCUSSION, CONCLUSION AND FUTURE PERSPECTIVES

5.1 Enzymatic oligomerization of formaldehyde

This work was previously published and is reproduced herein with permission from S. Güner, V. Wegat, A. Pick and V. Sieber "Design of a synthetic enzyme cascade for the *in vitro* fixation of a C_1 carbon source to a functional C_4 sugar" Green Chemistry, 2021, 23(17), 6583 – 6590.[141] Copyright 2021. The Royal Society of Chemistry.

The author, André Pick and Volker Sieber conceived and designed the study. The author performed *in silico* studies, design and cloning of the library, screening development, screening, selection of variants, characterization, applying suitable variants, determination of kinetic parameters and data analysis. Vanessa Wegat produced library supernatant and performed GDH assay. The author wrote the initial draft of the manuscript. The co-authors critically reviewed the manuscript.

We successfully developed a high-throughput combinatorial screening design and identified variants with different properties from the same library. Altogether, 48 plates were investigated, and every variant was evaluated in terms of GALD, DHA and ERY activity. It should be highlighted that *in silico* and *in vitro* results were mostly consistent. This was underscored by determining the kinetic parameters with GALD, where it was shown that the tailored variants had a >30 times lower K_m value and significantly optimized catalytic efficiency compared to the wild type. The two most promising variants (FLS_A3 and FLS_B2) were combined in a cell-free synthetic cascade and the production of ERY from the C_1 carbon source was shown for the first time. In this setting, the variant catalyzing FALD fusion to GALD was identified as a bottleneck in achieving complete conversion of FALD; thus, the catalytic activity of FLS_A3 must be further optimized. As the primary objective of the *in silico* investigation being ERY formation from GALD (second reaction), it was more plausible that highly suitable variants (FLS_B1 and FLS_B2) were found for this reaction. The potential of these variants was demonstrated in comparison to the wild type in a biocatalytic process starting from 25.0 g L^{-1} GALD, which was recently described as a promising renewable C_2 platform molecule.[198,199] FLS_B2 allowed the production of 24.6 g L^{-1} ERY with a theoretical yield of 98%. This represents the highest ERY concentration achieved *in vitro* reported to date. Furthermore, we were able to show that this biocatalyst does not undergo significant degradation or conformational change during the biocatalysis. This additionally highlights the robustness of the FLS.

5.2 Development of new-to-nature biocatalysts

5.2.1 Biocatalytic primary amination with ammonia

The discovery of the enzyme PISA1 in 2011 represented the first identification of an inverting *sec*-alkylsulfatase at sequence level.[169,176] Following an comprehensive characterization,[170] the potential of PISA1 for deracemization of *sec*-alcohols in an enantioconvergent process was demonstrated in 2013.[178] Apart from the development of an assay for the detection of released sulfate in 2018,[185] no further scientific publication based on PISA1 followed. Therefore, it seemed that the potential of this enzymatic reaction was already exhausted. The underlying mechanism for inversion of configuration remains intriguing. The inversion is achieved by a nucleophilic attack (via S_N2) of an activated water molecule on the chiral carbon atom of the sulfate ester, breaking the C-O bond and releasing the inverted alcohol.[176] In this work, the replacement of the attacking nucleophile was investigated to enable entry into a new class of products and thus impart new potential to the *sec*-alkylsulfatase PISA1.

Ammonia, as a sophisticated target nucleophile was selected to unlock the product class of primary aliphatic amines. Chemical catalysis of these building blocks is costly and requires the use of unsustainable transition metal catalysts and harsh reaction conditions.[92] Whenever chemocatalysis reaches its limits, the competitiveness of biocatalysis for industrial processes is strengthened. Implementation of this novel catalytic activity in PISA1 required functional coordination of ammonia in the active site, which enabled its utilization as an attacking nucleophile for the inverting mechanism. The successful biocatalysis of 2-aminoheptane demonstrated that this new-to-nature reaction is feasible in principle. Nucleophilic substitution is most likely still mediated *via* S_N2 by the artificial metalloenzyme using ammonia instead of water. Since the native enzyme was not able to catalyze this reaction, the functional incorporation of Ni(II) into the active site of PISA1 appears to be crucial. Which is presumably based on a higher affinity of Ni(II) for ammonia.[181–183] This is also supported by the fact that the natural activity was not significantly affected by the metal ion exchange. Unfortunately, it was not possible to reproduce these results despite excessive efforts. The circumstances behind this are discussed in more depth in the following section. Nevertheless, it remains unclear whether the metal-free protein scaffold provided also the desired stereocontrol of the reaction in addition to substrate specificity and an apparently promiscuous reaction mechanism. To conclude, the implementation of a novel catalytic activity is highly challenging. Only a minor side activity can be expected initially, which means that a low detection limit is required for successful identification. However, the GC/MS analysis used in this work should have been sufficient, as the production of 2-aminoheptane was detected in the proof of concept. The real challenge was the restricted feedback (yes/no response), whereby convergences to functional conformations could not be detected. Therefore, the optimization of an already detectable catalytic activity is a comparatively straightforward issue.

5.2.2 The unsolved mystery of PISA1

This work is hallmarked by the different functional properties observed depending on the preparation of the inverting *sec*-alkylsulfatase PISA1. Thus, despite intensive efforts, it was not possible to reproduce the sophisticated findings based on $PISA1_{GO}$ with other preparation of the enzyme. Along with physicochemical characteristics, environmental factors that can affect the functional behavior of enzymes were also considered.[231] However, no significant dissimilarity was identified that could explain this unequal behavior.

An attempt is nevertheless presented to narrow down the fundamental origin. Although the molecular weight and folding properties of $PISA1_{GO}$ and $PISA1_{SG}$ were identical, both preparations showed substantial variations in terms of turnover number, stability, tolerance to chelating agents and acceptance of non-native metal ions. Therefore, neither randomly occurred alterations of the primary structure nor a divergent folding process appear to be responsible. Fortunately, non-processed, harvested cells from a duplicate $PISA1_{GO}$ expression culture were available and stored under identical conditions. Subsequent preparation resulted an enzyme with similar properties to $PISA1_{SG}$. Consequently, the preparation of PISA1 after successful heterologous expression appears to be a critical factor. This sensitivity toward the preparation conditions might even be true for metalloenzymes in general. Amino acid residues that are essential for enzymatic activity and are not directly involved in metal coordination are referred to as the second coordination sphere. Their biological function is mainly based on non-covalent interactions, such as hydrogen bonding, electrostatic interactions, hydrophobic effects and van der Waals forces. These rather weak interactions are directly influenced by the enzymatic microenvironment and can have an impact on the physical and chemical properties of the active site.[232] In addition, purified proteins can undergo chemical modifications, oxidation and hydrolysis reactions even during long-term storage as a frozen solution.[233–235] During the freezing process, also the buffer system can show an influence. For instance, the use of sodium phosphate buffer can cause crystallization of the dibasic salt, while the acidic salt remains soluble for a longer time.[236] This can lead to a temporary drop in pH and thus influence the respective enzyme. However, the maturation of $PISA1_{SG}$ under comparable conditions has not resulted in the desired success either. Furthermore, the oligomerization state of an protein can be affected by pH and ionic strength of the buffer used during purification.[237] This was investigated by size exclusion chromatography without the identification of different species. Lastly, environmental conditions such as buffer system, pH, temperature, and salinity were addressed. Still no plausible explanation could be found. The binding of Zn(II) occurred much more strongly in the case of $PISA1_{SG}$. The tolerance to a variety of chelating agents that work perfectly for other Zn(II)-dependent enzymes remains remarkable.[238] Thus, although the mycotoxin-degrading metalloenzyme ochratoxinase also showed a higher tolerance to EDTA (tested up to 20 mM), Zn(II) was easily removed by applying 1,10-phenanthroline, one of the other chelating agents used in this work.[239] Even the

application of guanidinium chloride to PISA1, which causes (partial) unfolding of the protein scaffold, failed to produce the apoenzyme. Similar behavior was described for the metallo-ß-lactamase L1, where complete unfolding could not be achieved in the presence of 6 M guanidinium chloride and refolded enzyme still contained significant amounts of Zn(II).[240] This may also have been the case here.

The scientific issue was readdressed in an unbiased approach. Similar to the members of the second coordination sphere, the residues directly involved in metal ion coordination (first coordination sphere) are also affected by the enzymatic microenvironment. Modulation of the pH of this microenvironment resulted in successful protonation of the first coordination sphere histidines, causing release of the bivalent metal cations due to electrostatic repulsion.[222,223] Based on the apparent strong affinity of the protein scaffold for Zn(II), the environment was exchanged with a metal free buffer to keep PISA1 in apostate. The catalytic activity of the protein scaffold was easily recovered by the addition of Zn(II), while this time non-native metal ions were not accepted. In addition, supplementation of those caused strong protein precipitation. This effect could be significantly reduced in the presence of 20% glycerol, so that finally loading with Ni(II) was achieved. However, this variant showed significant differences compared to the one from the proof of concept. For the natural reaction, a reduced catalytic activity was detected, while the non-natural reaction was not catalyzed at all. CD spectroscopy is an excellent method to study secondary structures of proteins and to monitor conformational changes due to changes in environmental conditions, such as pH, temperature, and ionic strength.[241] However, unlike nuclear magnetic resonance (NMR) and X-ray crystallography, detailed residue specific information is not provided.[218] Thus, CD spectroscopy was used to detect a Ca(II)-induced change in secondary and tertiary structure for the Ca(II)-dependent enzyme cadmodulin.[242] In contrast, no structural changes were observed for the enzyme glyoxylase I, which is inactivated by Zn(II) and activated by Ni(II) or Co(II), after metal ion exchange. Crystal structure analysis revealed slight differences in the active site and that in the inactive form, Zn(II) is trigonal bipyramidal coordinated, while in the active form the coordination of Ni(II) or Co(II) possesses an octahedral geometry.[243]

In addition, CD spectroscopy could not distinguish between the holo- and apostate of the new alkylsulfatase CmAS, which was first described in this work. In case of PISA1, members of the first and second coordination spheres of the protein scaffold may have been affected by a different microenvironment, resulting in slight alterations in residue orientation that could not be detected. Already minor differences can lead to a significant influence on the catalytic activity. To verify this, the protein structures needed to be analyzed using a higher resolution method. However, since $PISA1_{GO}$ was consumed in the course of this work, the divergent behavior remains an unsolved mystery.

5.2.3 Classification of alkylsulfatases

To date, only a few alkylsulfatases have been identified at the sequence level, and the limited availability of structural information constrains the elucidation of general relationships between structure and function. Therefore, it has not been possible to discriminate between primary and secondary alkylsulfatases based on their structure. In this work, due to the conserved Zn(II) binding site, alkylsulfatases are generally assigned to the metallo-β-lactamase subgroup B3-E. With the addition of a bridging amino acid, which interacts with both Zn(II). The application of a sequence-driven approach with additional consideration of conserved protein motifs, such as the Zn(II) and sulfate binding site, resulted in the identification of the new alkylsulfatases CmAS, FtAS and VpAS. Subsequent characterization using PISA1 as a benchmark revealed interesting properties as well as structure-function relationships. Based on functional characteristics, it appears that FtAS can be assigned as *sec*-alkylsulfatase, whereas CmAS and VpAS belong rather to the group of *prim*-alkylsulfatases. Structural comparison of conserved protein motifs of PISA1 and VpAS provided insights that could facilitate the identification of primary and secondary alkylsulfatases based on the primary structure. Here, a sequence identity of 52% was observed between PISA1 and VpAS, and in terms of conserved protein motifs, only a variation in the bridging amino acid of the Zn(II) binding site was observed. It appeared that SDS hydrolyzing alkylsulfatases, including SdsA1, SdsAP, CmAS, and VpAS, utilize the longer chain glutamic acid at this position. In contrast, PISA1 and FtAS, which utilize the shorter chain aspartic acid, showed only minor activity on the primary substrate. For secondary substrates, on the other hand, high conversions were observed. Thus, it seemed that the bridging amino acid is a crucial characteristic to discriminate alkylsulfatases. However, compared to other *prim*-alkylsulfatases, CmAS and VpAS showed an unusually high conversion of 2-heptyl sulfate. For instance, a turnover number (k_{cat}) of 0.01 s^{-1} (2-octyl sulfate) was determined for SdsA1 with an inhibition constant (K_i) of 1.4 mM.[176] Therefore, in the case of CmAS and VpAS, a reduced level of inhibition could explain the observed turnover.

Based on this classification, neither the enantioselectivity (for a given substrate enantiomer) nor the stereoselectivity (in context of reaction mechanism) can be deduced.[172] Both selectivities were not identifiable for *prim*-alkylsulfatases so far, since primary alkyl sulfates such as SDS are achiral molecules.[169] However, since *sec*-alkylsulfatases enantioselectively hydrolyze chiral molecules such as *rac*-2a, *rac*-3a, *rac*-4a, and *rac*-5a, both preferences are apparent. Hydrolysis can proceed *via* retention (attack on the S-O bond) or inversion (attack on the C-O bond) of the configuration at the chiral carbon center, depending on the underlying mechanism.[171,244] Interestingly, in addition to FtAS, the two *prim*-alkylsulfatases CmAS and VpAS also showed a maximum conversion of 50% of *rac*-2-heptyl sulfate in their native state. Therefore, both enzymes can provide initial insights into the enantioselectivity and stereoselectivity of *prim*-alkylsulfatases.

5.2.4 Artificial metalloenzymes based on CmAS and VpAS

In this work, several approaches were presented that enabled production of metal free alkylsulfatase scaffolds. Successful removal of metal ions based on modulation of the enzymatic microenvironment to allow electrostatic repulsion was previously demonstrated for PISA1. Assuming a higher affinity of this protein scaffold for Zn(II) compared to CmAS and VpAS, it was not surprising that this method also is applicable here. The preparation of both apoenzymes was even more straightforward by application of 100 equivalents (equals 10 mM) of EDTA. This is also true in comparison with the behavior of other *prim*-alkylsulfatases. SdsA1 required treatment with 200 mM of the chelating agent (protein concentration not specified) for a period of 48 h in presence of Chelex® 100 to provide the corresponding apoenzyme.[207] The catalytic activity of SdsAP, on the other hand, was only reduced to 25% in the presence of 10 mM chelator (protein concentration also not specified).[175] Although this could be based on a more accessible active site, it seems more likely that the binding of Zn(II) is not as strong for CmAS and VpAS as for other alkylsulfatases. This is supported by the observation that both were more sensitive to the availability of metal ions in complex media during heterologous expression. Consequently, this characteristic property was exploited to allow direct expression of CmAS and VpAS as apoenzymes, thus simplifying and reducing the cost of subsequent metal ion screening for non-natural reactions. Thereby it was possible to extend the spectrum of the selected metal ions from 6 to 18 and to include trivalent and tetravalent metal cations in addition to bivalent ones. For a comprehensive evaluation of the artificial metalloenzymes, both natural activity and possible non-natural activities were investigated using *rac*-2a, *rac*-3a, *rac*-4a and *rac*-5a as substrates. For this purpose, an equivalent of ammonia (substrates related) was added to all reactions, resulting in an enhanced autocatalytic hydrolysis of the substrates with the sulfate moiety at relative position C2 (*rac*-2a and *rac*-5a). Interestingly, it appeared that the utilization of the VpAS protein scaffold enhanced this effect. Further studies showed that this background can be decreased by an additional treatment with EDTA to ensure metal free preparation. Accordingly, traces of Zn(II) could be responsible for the intensified occurrence of this background reaction. Non-enzymatic hydrolysis of secondary sulfate esters are documented in the literature and can be suppressed by the addition DMSO.[167] However, since the influence of such co-solvents on alkylsulfatases was not studied in this work, the use of DMSO was omitted. In terms of the hydrolytic alkylsulfatase activity, it emerged that the incorporated metal ions directly affect the catalytic activity and the range of accepted molecules. Such behavior was previously observed for other metalloenzymes. The substitution with non-native metal ions, even if they share similar chemical characteristics such as ionic charge, size, mass, redox potential, electronic configuration or allowed coordination geometry, often leads to significant changes in catalytic activity.[131] However, the responsible circumstances at the atomic level often remain unclear. The geometry of metal ion coordination was studied in detail for the single Zn(II) dependent carbonic anhydrase II. Replacement of native

Zn(II) with Co(II), Ni(II), Cu(II), Cd(II) and Mn(II) resulted in different active and inactive variants. The catalytic activity was directly modulated by the geometry of the metal ion coordination (tetrahedral for Zn(II), tetrahedral to octahedral for Co(II), octahedral for Ni(II) and trigonal bipyramidal for Cu(II)).[245] Another example is the Mg(II) dependent catechol-*O*-methyltransferase (COMT), which catalyzes the transfer of the methyl group of the cofactor *S*-adenosyl-L-methionine (SAM) to catechol. The native Mg(II) can be exchanged with a broad range of non-native metal ions, resulting in changes in catalytic activity and the structure of the enzyme.[246,247] These structural changes can affect the second coordination sphere, which as previously mentioned, are primarily based on rather weak non-covalent interactions and affect the physical and chemical properties of the active site.[232] A highlight of the metal ion screening was that the active site of CmAS was natively configured to be able to utilize Eu(II) for the enzymatic hydrolysis of a sulfate ester bond. In the past decade, lanthanides emerged as more widespread in biology and environmentally more important to bacteria (especially methylotrophs) than initially assumed.[248] In the aftermath of the *Deepwater Horizon* blowout in 2010, there was an increased proliferation of methanotrophic bacteria (a class of methylotrophic bacteria that use methane), resulting in the depletion of abundant lanthanides (La, Ce, Pr, and Nd) from ocean water in this area.[249] The majority of already discovered lanthanide dependent proteins predominantly utilize Ln(III) or Ce(III).[250] In contrast, the biological function of the rarer europium is less understood. Growth experiments with methanotrophic organisms showed that Eu(III) moderately stimulated growth in one case, while other more abundant lanthanides showed a stronger effect.[251,252] However, there are good reasons for biocatalysts to use lanthanides.[253] In any case, it should be taken into account that TRIS buffers are preferred when studying lanthanides, since many of the Good's buffers showed a non-negligible interaction.[254] Lanthanides generally possess increased Lewis acidity, which makes them catalysts that are more robust.[255] The charge-to-radius ratio is higher than other common biological Lewis acids and increases even further in the lanthanide series from left to right.[256] In addition, lanthanides can reach unusually high coordination numbers (8 – 12),[253] which could enable hitherto undiscovered new-to-nature reactions. However, the primary focus of the metal ion screening was on the production of various unbranched alkenyl arenes starting from *rac*-4-phenyl-2-butyl sulfate (*rac*-5a). Preliminary experiments based on $CmAS_{Co}$ enabled the release of cumulated 1.1%. Using the Cd(II) loaded protein scaffold of VpAS, this was further increased to 3.2%. Alkenyl arenes are typically versatile compounds that can be used as precursor for detergents, plastics, elastomers or pharmaceuticals.[257] In industry, such compounds are often produced *via* acid-based C–C bond formation between arenes and olefins. However, these processes also have limitations. More recently, processes based on transition metal catalysts have been reported that overcome some of the shortcomings of conventional approaches.[230] Accordingly, the development of a new-to-nature biocatalyst for the production of alkenyl arenes seems to be as reasonable.

5.3 Future perspectives

The work presented in this thesis contributed to the expansion of the biocatalytic toolbox with respect to the elongated oligomerization of formaldehyde and a new-to-nature reaction to the versatile compounds of alkenyl arenes.

On the horizon, the use of C_1 carbon sources for the synthesis of value-added products is emerging as a major trend in biocatalysis. The utilization of carbon dioxide, a key characteristic of third-generation biorefinery concepts, will decouple the manufacturing process from fossil and plant-based feedstocks, reducing greenhouse gas emissions and enable a circular economy.[258,259] The chemo-enzymatic cascade for the synthesis of starch from CO_2, also using the FLS catalyzed fixation of FALD to DHA, has been a significant breakthrough recently.[260] This highlights the power of this biocatalytic tool, even if the kinetic parameters still need to be optimized.[261] The approach of high-throughput combinatorial screening proved to be an excellent strategy to tailor FLS variants with desired properties. Since only a single library with theoretically 225 variants was screened, the potential for further optimization is far from exhausted. A possible field of application could also be the production of rare sugars. Recently, the food and pharmaceutical industries showed great interest in these compounds.[262] It seems reasonable to assume that the ThDP dependent umpolung is also suitable for the formation of a C–C bond between two glyceraldehyde molecules. This would provide biocatalytic access to a rare 3-ketohexose.[263,264] In initial experiments, no catalytic activity of the FLS wild type was detected with glyceraldehyde. However, both FLS_B variants, which provide additional space in the active site, might be applicable for this reaction.

An ambitious long-term goal of biocatalysis research is to develop efficient biocatalysts with desired functions from scratch to enable fully programmable protein catalysis in the future.[265] Today, it is already feasible to design biocatalysts with properties that do not occur in nature. It appeared that alkylsulfatases provide an excellent platform for the development of new-to-nature biocatalysts. For 3 of the 4 alkylsulfatases studied, a non-natural reaction was observed when the strategy of metal substitution was followed. This suggests that artificial metalloenzymes based on alkylsulfatases harbor the potential for additional novel functions. At this stage, it seems possible that this is also true for other members of the metallo-β-lactamase superfamily. Despite extensive attempts, the primary amination with ammonia based on PISA1 could not be reproduced. The divergent behavior of different protein preparations remains an unsolved mystery. Due to the lack of robustness and although such a biocatalytic tool would harbor great potential, this approach should not be pursued further. In contrast, the discovery of the second new-to-nature reaction, which enables the synthesis of alkenyl arenes, represents a solid starting point. As mentioned elsewhere, the optimization of an already detectable catalytic activity is a comparatively straightforward issue.

6. APPENDIX

6.1 Supporting information: Enzymatic oligomerization of formaldehyde

This work was previously published and is reproduced herein with permission from S. Güner, V. Wegat, A. Pick and V. Sieber "Design of a synthetic enzyme cascade for the *in vitro* fixation of a C_1 carbon source to a functional C_4 sugar" Green Chemistry, 2021, 23(17), 6583 – 6590.[141]

The author, André Pick and Volker Sieber conceived and designed the study. The author performed *in silico* studies, design and cloning of the library, screening development, screening, selection of variants, characterization, applying suitable variants, determination of kinetic parameters and data analysis. Vanessa Wegat produced library supernatant and performed GDH assay. The author wrote the initial draft of the manuscript. The co-authors critically reviewed the manuscript.

Conversion of glycolaldehyde to erythrulose

To determine whether the FLS "wild type" is capable of converting GALD to ERY, 10 µM (0.61 mg mL^{-1}) of FLS was applied to 20 mM GALD solely. Reaction mixtures (200 µL) were prepared in 50 mM sodium phosphate, pH 8.2 and supplemented with 2 mM $MgSO_4$ and 0.1 mM ThDP. As a control, enzyme addition was omitted. The samples were incubated for 60 h at room temperature, without shaking. Analysis was performed *via* HPLC. No change was determined for the control reaction. FLS showed partial consumption of GALD and a new peak appeared that overlaid with the standard for erythrulose.

Evaluation of the active site of FLS

The thiamine diphosphate-dependent (ThDP) benzaldehyde lyase was redesigned by protein engineering for the production of DHA from FALD. Therefore, several positions within the active pocket of the FLS have already been modified. In order to identify promising target positons, the focus was on amino acid residues in the active center that had not yet been investigated. The active site of the enzyme is formed at the interface of the monomers of the homodimer. The cofactor ThDP is thereby embedded (Figure 6.1-1A/B). A major part of the positions has already been investigated in the context of increased DHA production. Marked in green (Figure 6.1-2A/B) are I29, G394, N419 and W480 which showed a significant impact for the production of DHA. Marked in blue (Figure 6.1-3A/B) are non-investigated positions including H29 and Q113. Certain parts of secondary structure elements, in particular glycines, were also not changed. These are highlighted in magenta (Figure 6.1-4A/B).

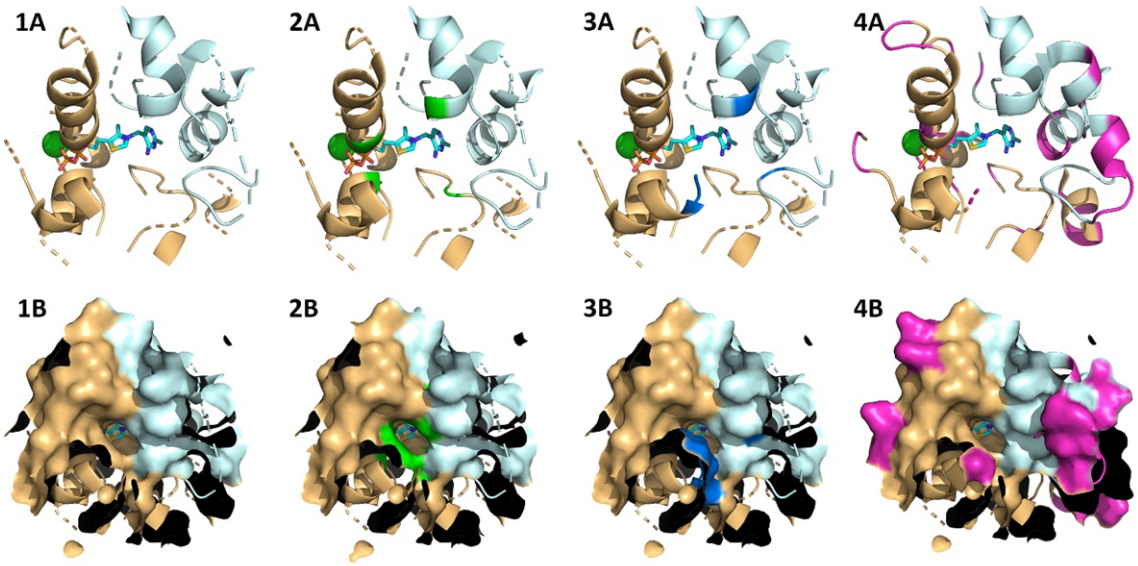

Figure 6.1: Preliminary *in silico* investigation of FLS. The active site of the enzyme is formed at the interface of the monomers (light brown and blue). The active center is illustrated as (**A**) cartoon or as (**B**) surface. (**1**) shows all surrounding amino acids within a radius of 12 Å. (**2**) marked in green are all positions with significant improvement in DHA production (**3**) marked in blue are all non-investigated positons in close proximity to the cofactor and (**4**) marked in magenta are further non-investigated positions.

Investigation of the buffer system

The formation of DHA were observed in control reactions (without enzyme addition), when FALD and GALD was used as mixed substrates. Simonov *et al*., already described a catalytic activity of phosphate-based buffer systems in 2007.[196] Therefore, the influence of the buffer system was investigated in more detail, with special regard to the production of ERY. The buffer capacity used was increased 10-fold for this experiment. Furthermore, the influence of the pH value was also investigated. Accordingly, 4.5 g L^{-1} DHA in combination with 1.5 g L^{-1} FALD was incubated in 0.5 M sodium phosphate buffer (pH range 7.0 - 8.0; 0.2 steps) for 22 h at 30°C. As a control, the buffer system was replaced by water. The samples were then analyzed *via* HPLC, especially with regard to ERY formation (Figure 6.2). No formation of ERY or other products were observed in the water control.

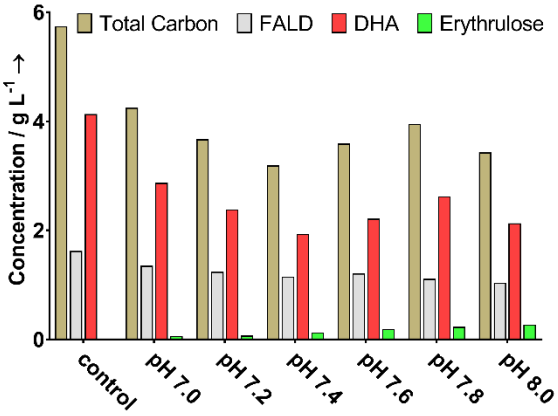

Figure 6.2: Catalytic activity of the sodium phosphate buffer (pH Range: 7.0 – 8.0). Total carbon is illustrated in black, FALD in grey, DHA in red and ERY in green.

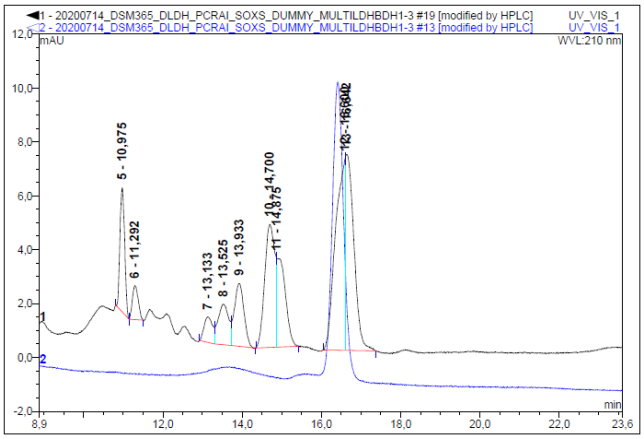

Figure 6.3: HPLC chromatogram (UV signal) of buffer-catalyzed reaction. Buffer-catalyzed reaction (0.5 M sodium phosphate, pH 8.0) in black compared to water control (blue). 4.5 g L^{-1} DHA was incubated in combination with 1.5 g L^{-1} FALD for 22 h at 30°C in water or 0.5 M sodium phosphate buffer, pH 8.0. For the control only the signal for DHA was detected, for the buffer reaction a lot of unidentified peaks were observed.active site of the enzyme is formed at the interface of the monomers (light brown and blue).

In addition, no consumption of DHA and FALD were found here. Using 0.5 M sodium phosphate, a formation of ERY was detected instead. The formation increased with increasing pH. However, several other products were also measured (Figure 6.3), which indicated a reaction with low selectivity. No standards for this side products were available. When only FALD, DHA and ERY are considered, a significant carbon loss was observed. At lower buffer capacities, the influence of the buffer was minimal. Nevertheless, an inert buffer system should be considered in future to further increase the selectivity.

Kinetic characterization of FLS "wild type" and variants

For kinetic characterization with GALD, approximately one-month-old purified FLS_wt, FLS_B1 and FLS_B2 (stored at -80°C) were thawed at room temperature. Reactions were prepared in a 96-MTP, containing 30 µM of respective FLS (1.84 mg mL^{-1}), 2 mM $MgSO_4$, 0.1 mM ThDP and varying GALD concentrations in 50 mM sodium phosphate buffer, pH 8.0. Thereby, GALD concentrations of 2.5, 5, 7.5, 10, 25, 50, 75, 100, 250, 500, 750 and 1000 mM were investigated. After pre-incubation of reaction mixture and enzymes separately for 10 min at 30°C, reactions were started with addition of enzyme.

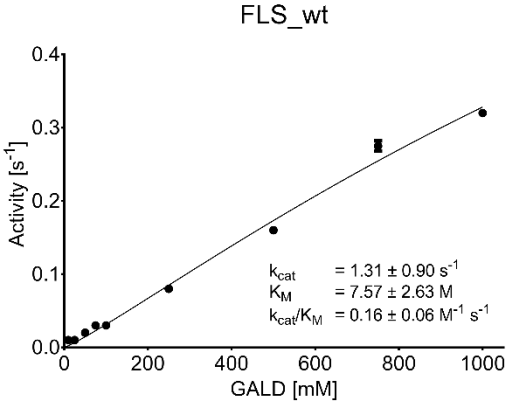

Figure 6.4: Michaelis-Menten kinetic of FLS_wt.

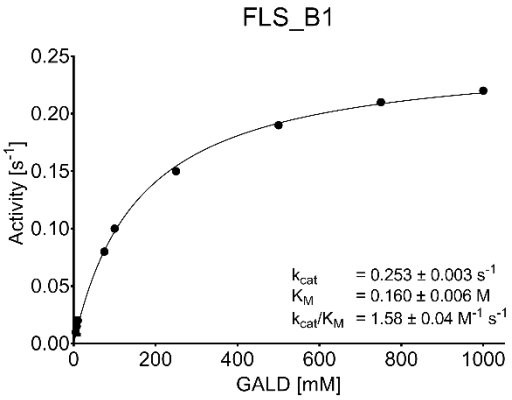

Figure 6.5: Michaelis-Menten kinetic of FLS_B1.

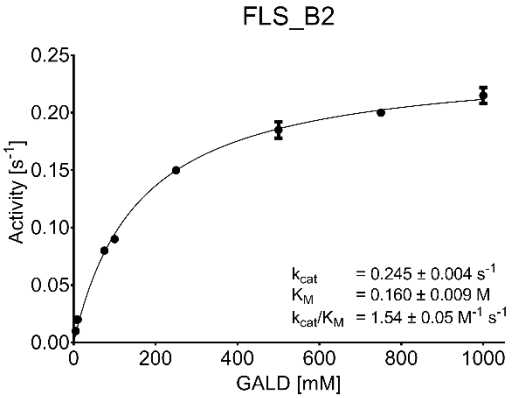

Figure 6.6: Michaelis-Menten kinetic of FLS_B2.

After mixing by pipetting directly t_0 samples were taken, proper diluted and prepared for HPLC analysis. After further 90 min incubation at 30°C and 750 rpm shaking in a MTP-Shaker, again samples were taken. The initial slope based on ERY production was used to determine catalytic activities. Subsequently, the data were fitted to determine the kinetic parameters.

Chromatograms of standards

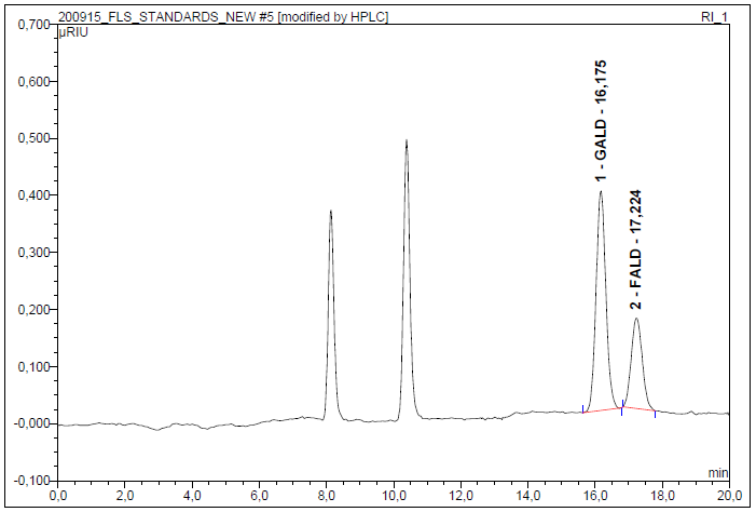

Figure 6.7: HPLC chromatogram of 1 mM standard 1 (FALD and GALD) with RI detector. GALD retention time of 16.2 min and FALD retention time of 17.2 min.

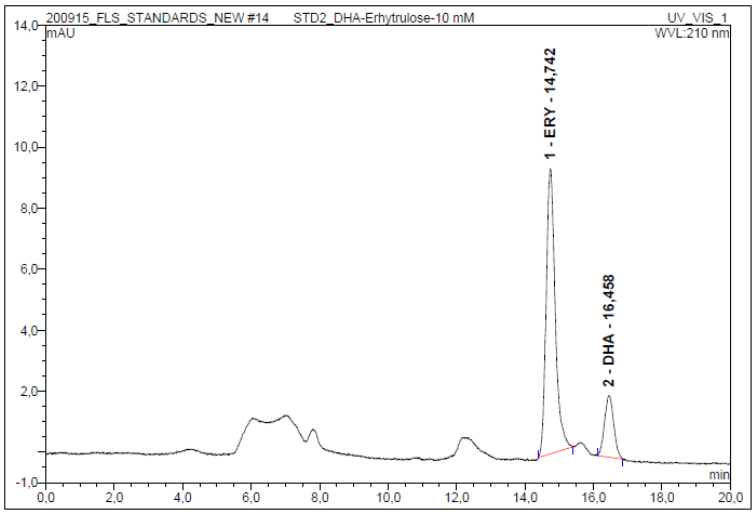

Figure 6.8: HPLC chromatogram of 1 mM standard 2 (DHA and ERY) with UV detector. ERY retention time of 14.7 min and DHA retention time of 16.5 min.

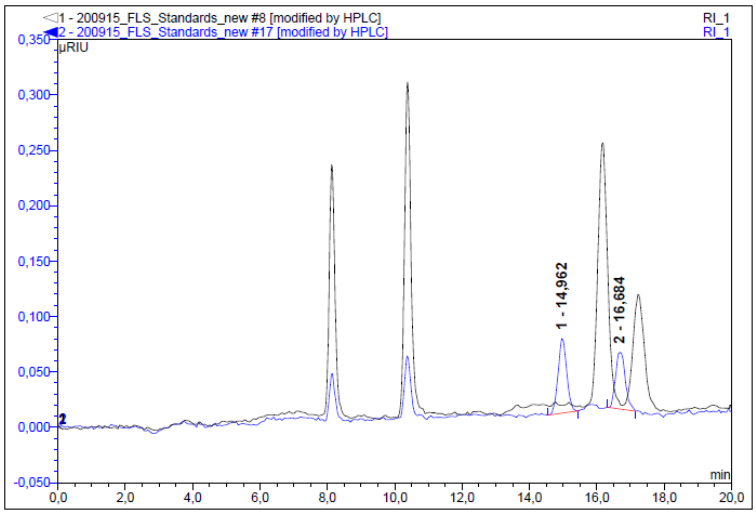

Figure 6.9: Overlay of chromatograms (RI detector). Overlay of chromatograms for standard 1 (Black) and 2 (Blue) to demonstrate successful separation of the corresponding peaks.

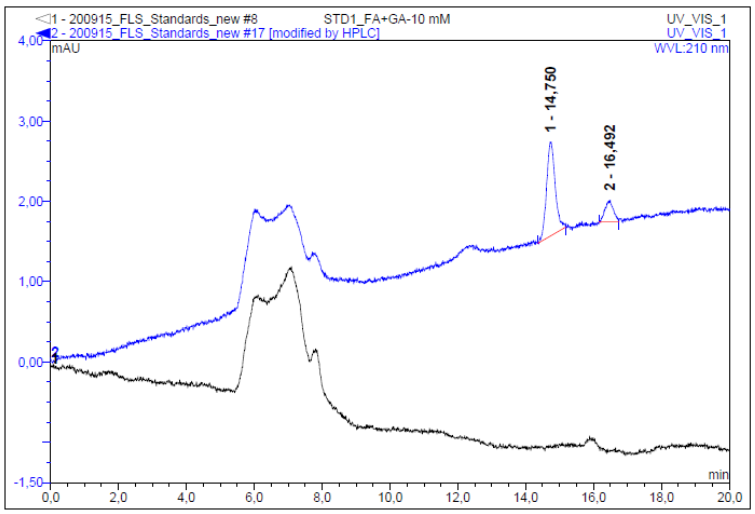

Figure 6.10: Overlay of chromatograms (UV detector). Overlay of chromatograms for standard 1 (Black) and 2 (Blue) to demonstrate successful separation of the corresponding peaks.

Calibration

All calibration samples were prepared in a range between 1.0 and 100 mM and analyzed *via* HPLC. HPLC sample preparation required a 10-fold dilution, resulting in determined range of 0.1 – 10.0 mM. FALD and GALD were determined based on the signal of the RI detector. DHA and ERY were determined based on the signal of the UV detector.

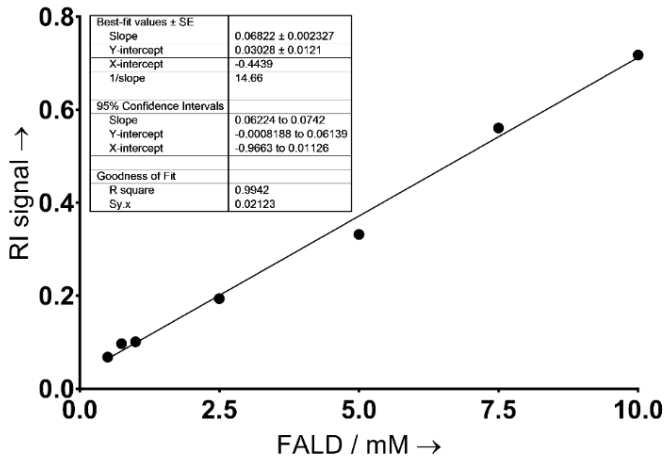

Figure 6.11: Measured calibration curve of formaldehyde in a range of 0.1 – 10.0 mM FALD.

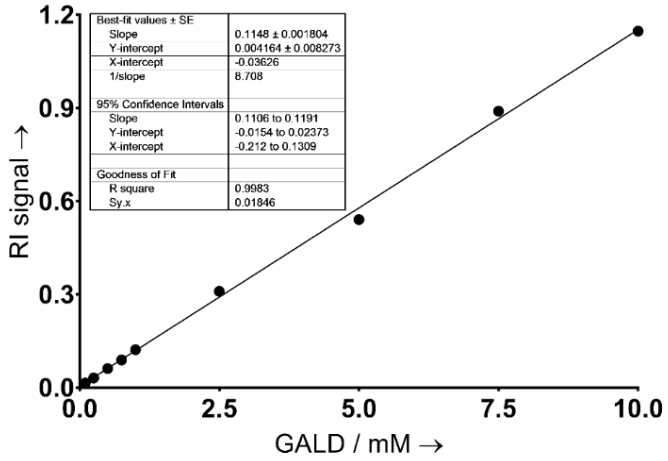

Figure 6.12: Measured calibration curve of glycolaldehyde in a range of 0.1 – 10.0 mM GALD.

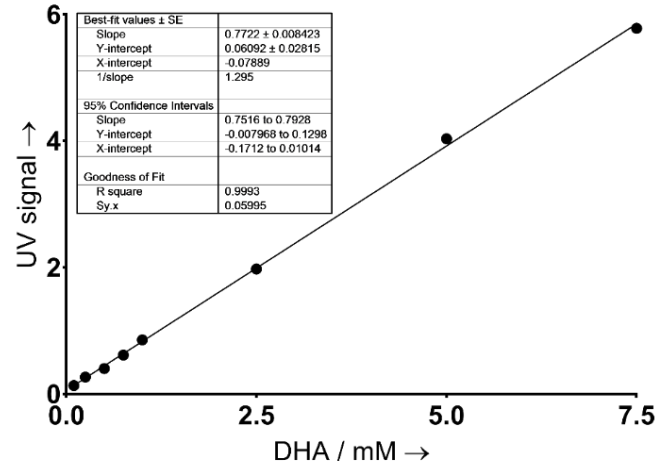

Figure 6.13: Measured calibration curve of dihydroxyacetone in range of 0.1 – 7.5 mM DHA.

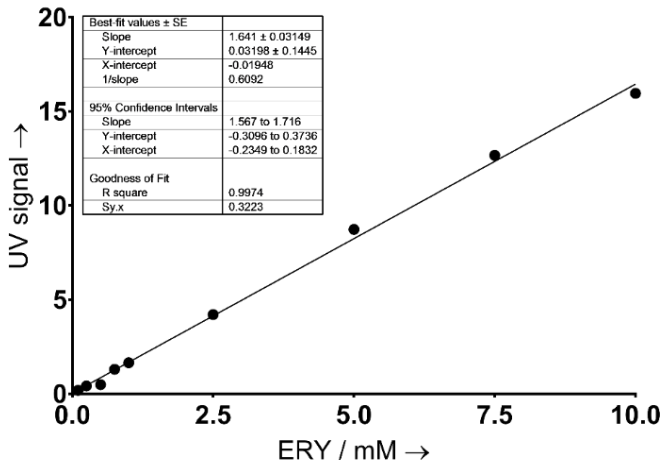

Figure 6.14: Measured calibration curve of erythrulose in range of 0.1 – 10.0 mM ERY.

6.2 Supporting information: Development of new-to-nature biocatalysts

Covalent modification of PISA1$_{SG}$ by aldehydes

In the context of another project in which the tolerance of various enzymes against formaldehyde and glyceraldehyde was studied, the aldehyde tolerance of PISA1$_{SG}$ was investigated as well. Treatment with 2.5 M formaldehyde resulted in immediate turbidity, and analysis by thermofluor assay indicated a complete protein precipitation. This effect was weaker with decreasing formaldehyde concentration, so that at 180 mM formaldehyde a splitting of the initial protein melting point was observed. In addition to the T_m for the native holoenzyme at 56.5°C, additional one was detected at 39°C. Again, the pronounced effect reduced with decreasing formaldehyde concentration, to the extent that no splitting could be observed at 1.8 mM formaldehyde anymore. A higher sensitivity was observed towards glyceraldehyde, where similar effects occurred at lower aldehyde concentrations. Unexpectedly, the initial protein melting point was stabilized instead of remaining unchanged, resulting in a higher T_m. This stabilizing effect was investigated subsequently in more detail.

The addition of 100 mM glyceraldehyde resulted in a shift of the initial T_m from 56.5°C to 61.5°C, which corresponded to a stabilization by 5°C (Figure 6.15A). To investigate this partial stabilization in more detail, two scientific questions were addressed. First, it was investigated whether this was a covalent or non-covalent effect. Therefore, free, non-protein bonded glyceraldehyde was removed from the environment by means of a desalting step. The subsequent investigation showed only a slight reduction in stabilization in the absence of free aldehyde (59.5°C), so that a covalent effect seems to be mainly responsible. In addition, a gradient (range of 0 – 100 mM glyceraldehyde) was used to investigate the dependence of the strength of this effect on the applied aldehyde concentration (Figure 6.15B). A linear dependence was observed, where the increase of glyceraldehyde resulted in a stronger shift of the initial T_m. However, it should be mentioned here that with higher stabilization, the ratio of splitting and thus the second T_m also elevated.

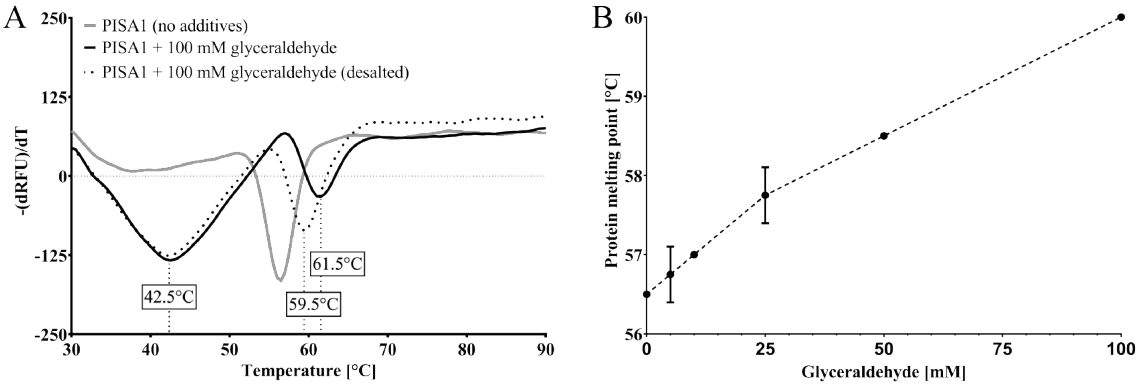

Figure 6.15: Investigation of the stabilizing effect of glyceraldehyde on PISA1$_{SG}$. **(A)** The effect of 100 mM glyceraldehyde on the thermodynamic stability of PISA1 was studied in the presence of free glyceraldehyde (black line) and after removal of non-bound glyceraldehyde (dotted line). Control without additives is shown in gray. (**B**) In addition, a glyceraldehyde gradient of 0 – 100 mM was used to investigate the dependence of the stabilizing effect on the aldehyde concentration applied.

NMR spectra of alkyl sulfate esters

^{1}H of *rac*-3-heptyl sulfate/NH_4^+ (*rac*-3a)

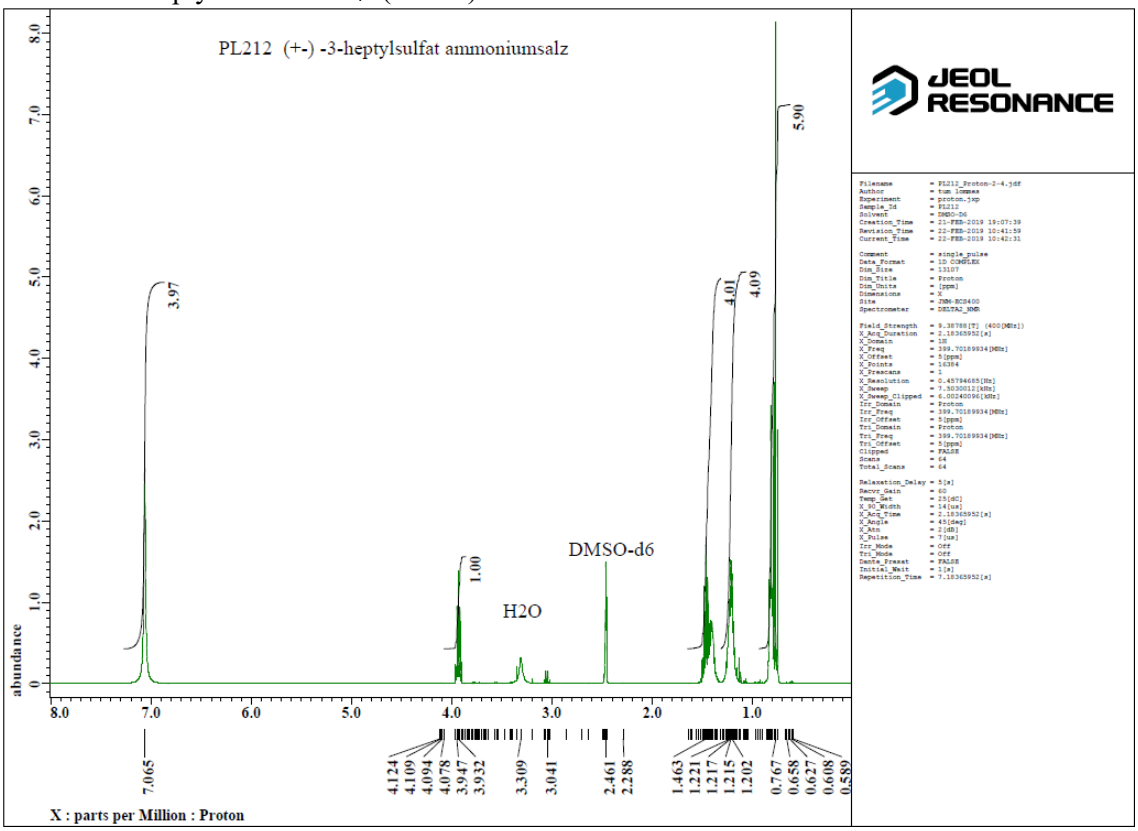

^{13}C of *rac*-3-heptyl sulfate/NH_4^+ (*rac*-3a)

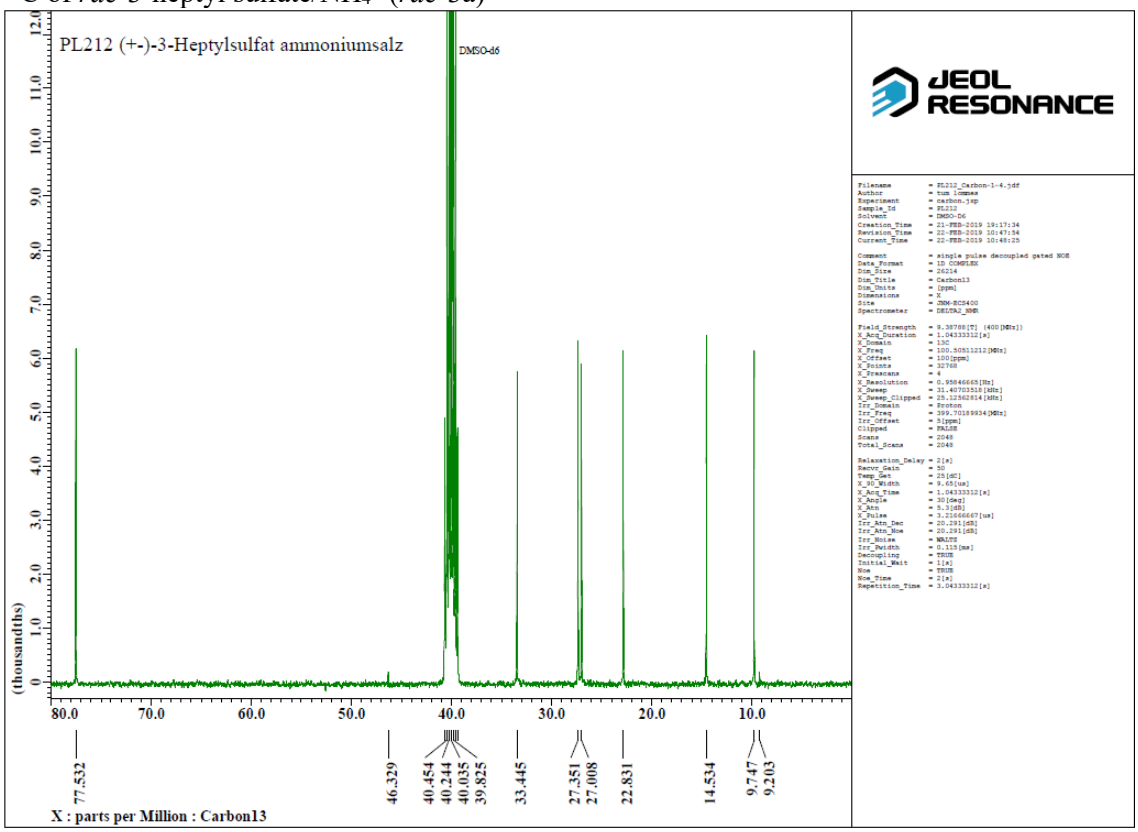

^{1}H of *rac*-4-heptyl sulfate/NH_4^+ (*rac*-4a)

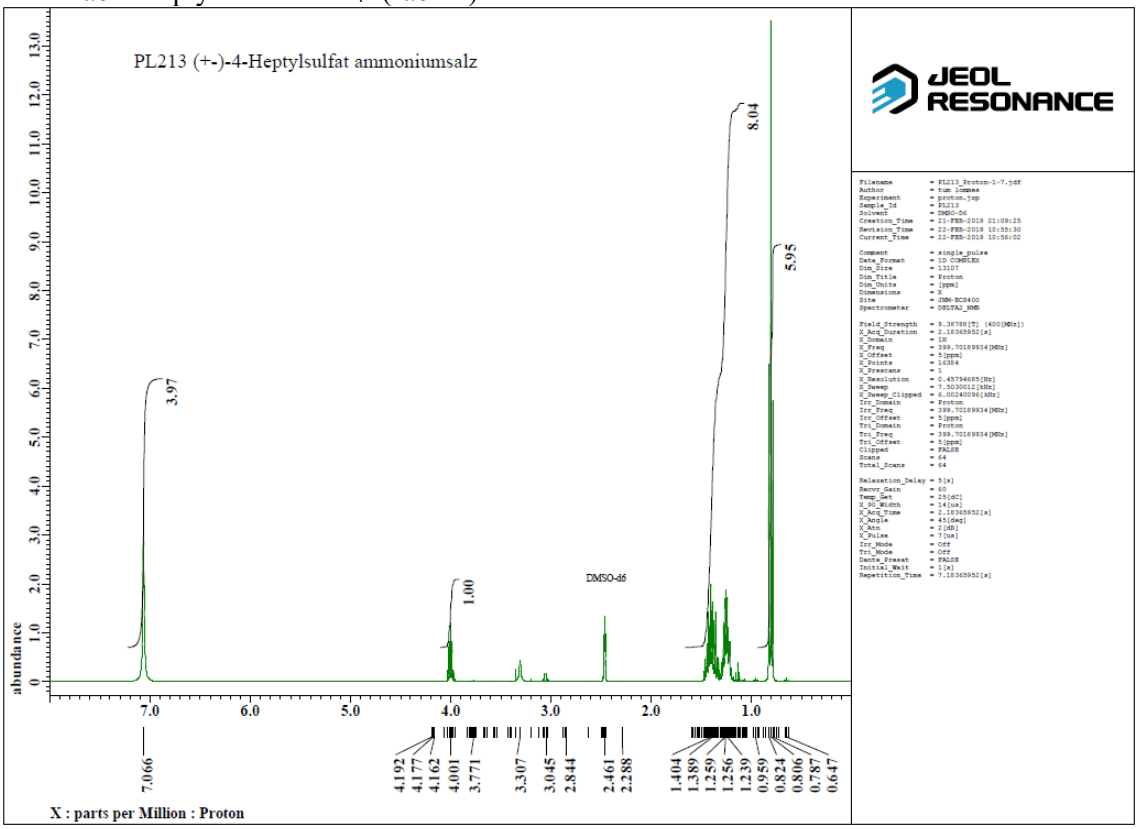

^{13}C of *rac*-4-heptyl sulfate/NH_4^+ (*rac*-4a)

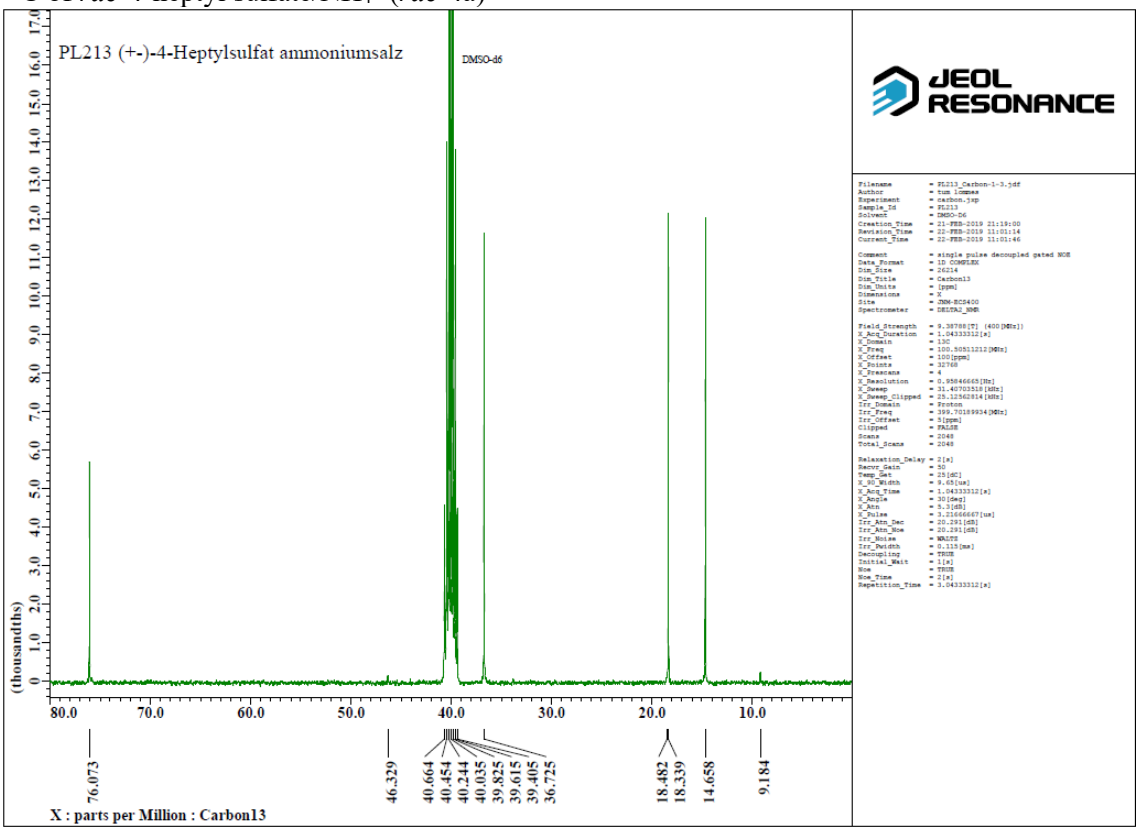

[1]H of *rac*-4-phenyl-2-butyl sulfate (*rac*-5a)

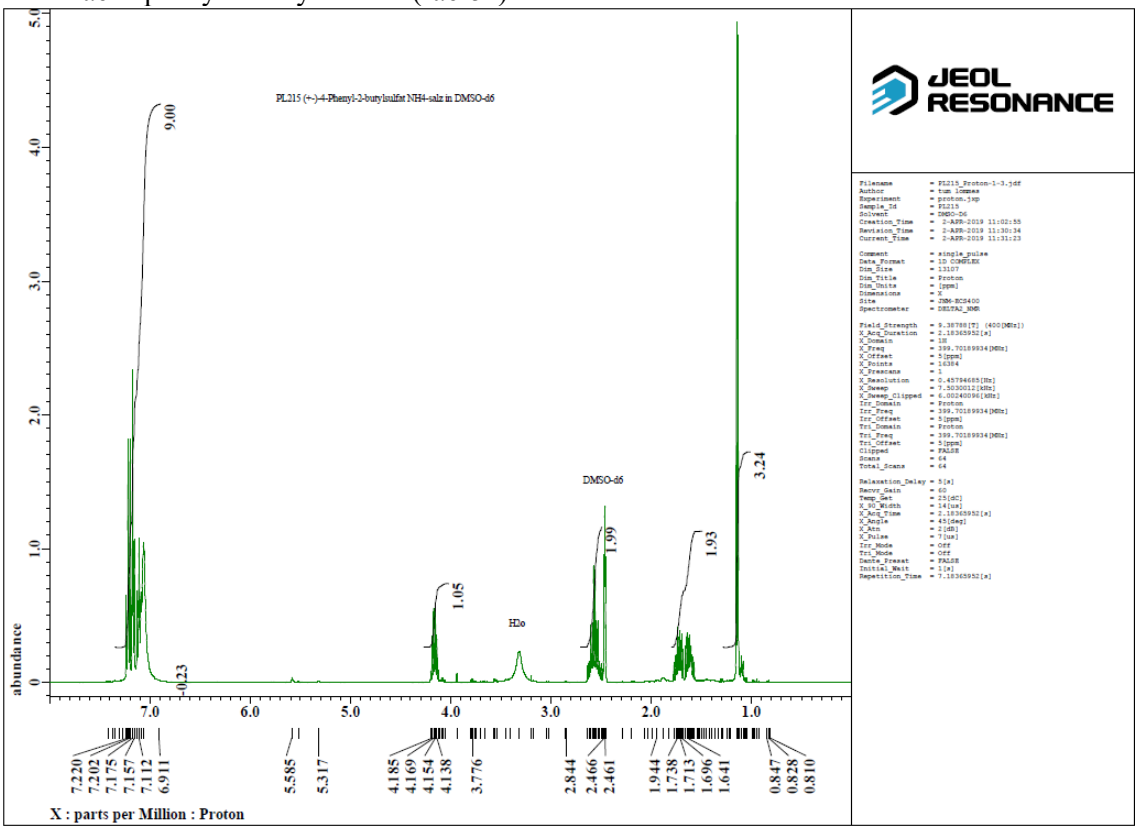

[13]C of *rac*-4-phenyl-2-butyl sulfate (*rac*-5a)

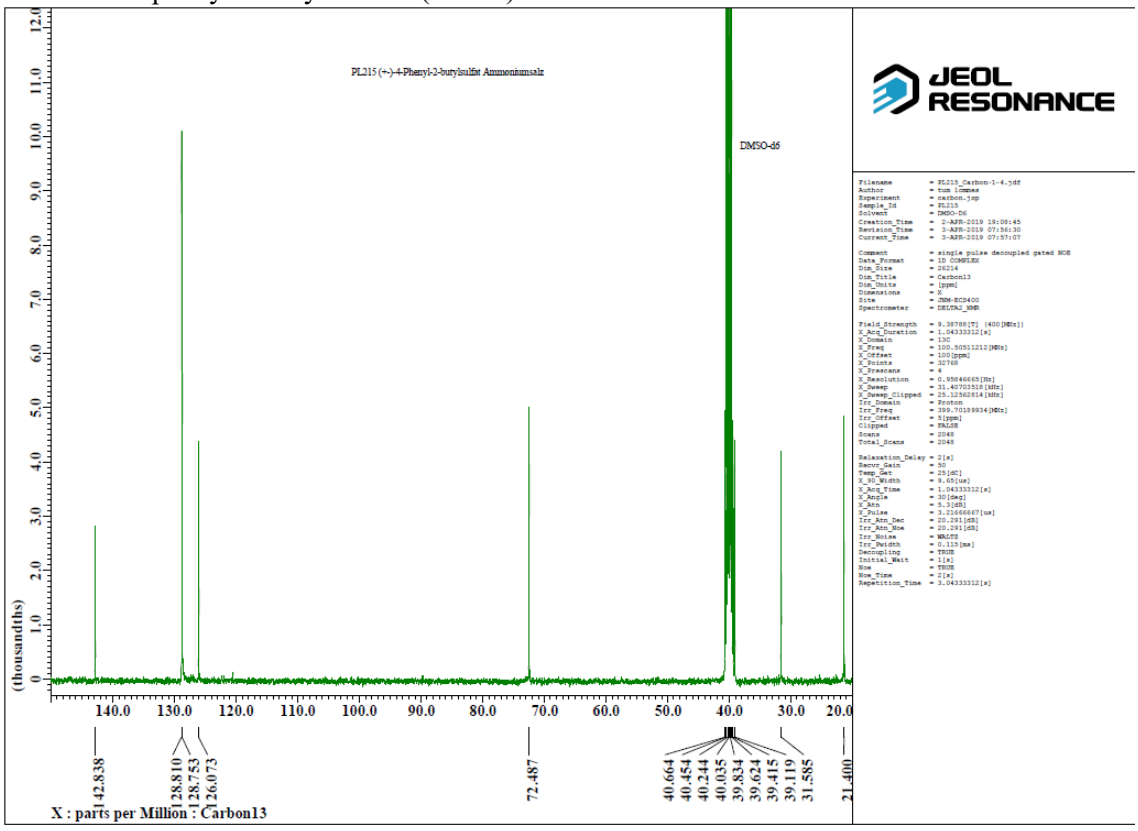

REFERENCES

[1] U. Hanefeld, F. Hollmann and C. E. Paul. Biocatalysis making waves in organic chemistry. *Chemical Society reviews* **2022**, *51*, 594–627, DOI: 10.1039/d1cs00100k.

[2] N. J. Turner and R. Kumar. Editorial overview: Biocatalysis and biotransformation: The golden age of biocatalysis. *Current opinion in chemical biology* **2018**, *43*, A1-A3, DOI: 10.1016/j.cbpa.2018.02.012.

[3] E. L. Bell, W. Finnigan, S. P. France, A. P. Green, M. A. Hayes, L. J. Hepworth, S. L. Lovelock, H. Niikura, S. Osuna and E. Romero et al. Biocatalysis. *Nature Reviews Methods Primers* **2021**, *1,* DOI: 10.1038/s43586-021-00044-z.

[4] R. A. Sheldon and P. C. Pereira. Biocatalysis engineering: the big picture. *Chemical Society reviews* **2017**, *46*, 2678–2691, DOI: 10.1039/c6cs00854b.

[5] U. T. Bornscheuer, G. W. Huisman, R. J. Kazlauskas, S. Lutz, J. C. Moore and K. Robins. Engineering the third wave of biocatalysis. *Nature* **2012**, *485*, 185–194, DOI: 10.1038/nature11117.

[6] U. T. Bornscheuer. The fourth wave of biocatalysis is approaching. *Philosophical transactions. Series A, Mathematical, physical, and engineering sciences* **2018**, *376,* DOI: 10.1098/rsta.2017.0063.

[7] V. G. Zuin, I. Eilks, M. Elschami and K. Kümmerer. Education in green chemistry and in sustainable chemistry: perspectives towards sustainability. *Green Chemistry* **2021**, *23*, 1594–1608, DOI: 10.1039/d0gc03313h.

[8] R. A. Sheldon and D. Brady. Green Chemistry, Biocatalysis, and the Chemical Industry of the Future. *ChemSusChem* **2022**, e202102628, DOI: 10.1002/cssc.202102628.

[9] T. Anastas Paul and J. C. Warner. The Twelve Principles of Green Chemistry. *Green Chemistry: Theory and Practice* **1998**, *29*.

[10] R. A. Sheldon and J. M. Woodley. Role of Biocatalysis in Sustainable Chemistry. *Chemical reviews* **2018**, *118*, 801–838, DOI: 10.1021/acs.chemrev.7b00203.

[11] R. A. Sheldon. The E factor 25 years on: the rise of green chemistry and sustainability. *Green Chemistry* **2017**, *19*, 18–43, DOI: 10.1039/C6GC02157C.

[12] K. Faber in *Biotransformations in Organic Chemistry: A Textbook*, Springer International Publishing, Cham, **2018**, pp. 1–30.

[13] J. M. Woodley. Ensuring the Sustainability of Biocatalysis. *ChemSusChem* **2022**, e202102683, DOI: 10.1002/cssc.202102683.

[14] R. A. Sheldon, D. Brady and M. L. Bode. The Hitchhiker's guide to biocatalysis: recent advances in the use of enzymes in organic synthesis. *Chemical science* **2020**, *11*, 2587–2605, DOI: 10.1039/c9sc05746c.

[15] J. M. Sperl and V. Sieber. Multienzyme Cascade Reactions—Status and Recent Advances. *ACS Catalysis* **2018**, *8*, 2385–2396, DOI: 10.1021/acscatal.7b03440.

[16] S. Wu, R. Snajdrova, J. C. Moore, K. Baldenius and U. T. Bornscheuer. Biocatalysis: Enzymatic Synthesis for Industrial Applications. *Angewandte Chemie (International ed. in English)* **2021**, *60*, 88–119, DOI: 10.1002/anie.202006648.

[17] A. S. Bommarius. Biocatalysis: A Status Report. *Annual review of chemical and biomolecular engineering* **2015**, *6*, 319–345, DOI: 10.1146/annurev-chembioeng-061114-123415.

[18] R. A. Sheldon, A. Basso and D. Brady. New frontiers in enzyme immobilisation: robust biocatalysts for a circular bio-based economy. *Chemical Society reviews* **2021**, *50*, 5850–5862, DOI: 10.1039/d1cs00015b.

[19] S. Kara and A. Liese in *Industrial enzyme applications* (Eds.: A. Vogel, O. May), Wiley-VCH, Weinheim, **2019**, pp. 71–94.

[20] S. Mordhorst and J. N. Andexer. Round, round we go - strategies for enzymatic cofactor regeneration. *Natural product reports* **2020**, *37*, 1316–1333, DOI: 10.1039/D0NP00004C.

[21] I. Zachos, C. Nowak and V. Sieber. Biomimetic cofactors and methods for their recycling. *Current opinion in chemical biology* **2019**, *49*, 59–66, DOI: 10.1016/j.cbpa.2018.10.003.

[22] I. Zachos, S. Güner, A. Essert, P. Lommes and V. Sieber. Boosting artificial nicotinamide cofactor systems. *Chemical communications (Cambridge, England)* **2022**, *58*, 11945–11948, DOI: 10.1039/D2CC03423A.

[23] E. M. M. Abdelraheem, H. Busch, U. Hanefeld and F. Tonin. Biocatalysis explained: from pharmaceutical to bulk chemical production. *Reaction Chemistry & Engineering* **2019**, *4*, 1878–1894, DOI: 10.1039/c9re00301k.

[24] M. L. Metzker. Sequencing technologies - the next generation. *Nature reviews. Genetics* **2010**, *11*, 31–46, DOI: 10.1038/nrg2626.

[25] Z. Sun, Y. Wikmark, J.-E. Bäckvall and M. T. Reetz. New Concepts for Increasing the Efficiency in Directed Evolution of Stereoselective Enzymes. *Chemistry–A European Journal* **2016**, *22*, 5046–5054, DOI: 10.1002/chem.201504406.

[26] J. B. Pyser, S. Chakrabarty, E. O. Romero and A. R. H. Narayan. State-of-the-Art Biocatalysis. *ACS central science* **2021**, *7*, 1105–1116, DOI: 10.1021/acscentsci.1c00273.

[27] R. A. Sheldon and D. Brady. Streamlining Design, Engineering, and Applications of Enzymes for Sustainable Biocatalysis. *ACS Sustainable Chemistry & Engineering* **2021**, *9*, 8032–8052, DOI: 10.1021/acssuschemeng.1c01742.

[28] H. Renata, Z. J. Wang and F. H. Arnold. Expanding the enzyme universe: accessing non-natural reactions by mechanism-guided directed evolution. *Angewandte Chemie (International ed. in English)* **2015**, *54*, 3351–3367, DOI: 10.1002/anie.201409470.

[29] D. C. Miller, S. V. Athavale and F. H. Arnold. Combining chemistry and protein engineering for new-to-nature biocatalysis. *Nature Synthesis* **2022**, *1*, 18–23, DOI: 10.1038/s44160-021-00008-x.

[30] M. T. Reetz. Biocatalysis in organic chemistry and biotechnology: past, present, and future. *Journal of the American Chemical Society* **2013**, *135*, 12480–12496, DOI: 10.1021/ja405051f.

[31] L. Jaenicke. Centenary of the award of a Nobel prize to Eduard Buchner, the father of biochemistry in a test tube and thus of experimental molecular bioscience. *Angewandte Chemie (International ed. in English)* **2007**, *46*, 6776–6782, DOI: 10.1002/anie.200700390.

[32] L. Rosenthaler. Durch Enzyme bewirkte asymmetrische Synthesen. 2. Mitteilung. *Biochemische Zeitschrift* **1909**, *17*, 257.

[33] D. Yi, T. Bayer, C. P. S. Badenhorst, S. Wu, M. Doerr, M. Höhne and U. T. Bornscheuer. Recent trends in biocatalysis. *Chemical Society reviews* **2021**, *50*, 8003–8049, DOI: 10.1039/d0cs01575j.

[34] S. N. Cohen, A. C. Chang, H. W. Boyer and R. B. Helling. Construction of biologically functional bacterial plasmids in vitro. *Proceedings of the National Academy of Sciences* **1973**, *70*, 3240–3244, DOI: 10.1073/pnas.70.11.3240.

[35] F. Sanger, S. Nicklen and A. R. Coulson. DNA sequencing with chain-terminating inhibitors. *Proceedings of the National Academy of Sciences* **1977**, *74*, 5463–5467, DOI: 10.1073/pnas.74.12.5463.

[36] R. K. Saiki, S. Scharf, F. Faloona, K. B. Mullis, G. T. Horn, H. A. Erlich and N. Arnheim. Enzymatic amplification of beta-globin genomic sequences and restriction site analysis for diagnosis of sickle cell anemia. *Science* **1985**, *230*, 1350–1354, DOI: 10.1126/science.2999980.

[37] M. C. Feiten, M. Di Luccio, K. F. Santos, D. de Oliveira and J. V. Oliveira. X-Ray Crystallography as a Tool to Determine Three-Dimensional Structures of Commercial Enzymes Subjected to Treatment in Pressurized Fluids. *Applied biochemistry and biotechnology* **2017**, *182*, 429–451, DOI: 10.1007/s12010-016-2336-9.

[38] C. M. Heckmann and F. Paradisi. Looking Back: A Short History of the Discovery of Enzymes and How They Became Powerful Chemical Tools. *ChemCatChem* **2020**, *12*, 6082–6102, DOI: 10.1002/cctc.202001107.

[39] M. Smith. Synthetic DNA and Biology (Nobel Lecture). *Angewandte Chemie (International ed. in English)* **1994**, *33*, 1214–1221, DOI: 10.1002/anie.199412141.

[40] F. H. Arnold. Innovation by Evolution: Bringing New Chemistry to Life (Nobel Lecture). *Angewandte Chemie (International ed. in English)* **2019**, *58*, 14420–14426, DOI: 10.1002/anie.201907729.

[41] F. H. Arnold. Design by directed evolution. *Accounts of chemical research* **1998**, *31*, 125–131.

[42] A. A. Beaudry and G. F. Joyce. Directed evolution of an RNA enzyme. *Science* **1992**, *257*, 635–641, DOI: 10.1126/science.1496376.

[43] T. S. Wong, K. L. Tee, B. Hauer and U. Schwaneberg. Sequence saturation mutagenesis (SeSaM): a novel method for directed evolution. *Nucleic acids research* **2004**, *32*, e26, DOI: 10.1093/nar/gnh028.

[44] W. P. Stemmer. Rapid evolution of a protein in vitro by DNA shuffling. *Nature* **1994**, *370*, 389–391, DOI: 10.1038/370389a0.

[45] H. Zhao, L. Giver, Z. Shao, J. A. Affholter and F. H. Arnold. Molecular evolution by staggered extension process (StEP) in vitro recombination. *Nature biotechnology* **1998**, *16*, 258–261, DOI: 10.1038/nbt0398-258.

[46] M. C. Ebert and J. N. Pelletier. Computational tools for enzyme improvement: why everyone can - and should - use them. *Current opinion in chemical biology* **2017**, *37*, 89–96, DOI: 10.1016/j.cbpa.2017.01.021.

[47] S. Lutz. Beyond directed evolution--semi-rational protein engineering and design. *Current opinion in biotechnology* **2010**, *21*, 734–743, DOI: 10.1016/j.copbio.2010.08.011.

[48] S. Lutz and U. T. Bornscheuer. Protein engineering handbook, John Wiley & Sons, **2012**.

[49] S. Mazurenko, Z. Prokop and J. Damborsky. Machine Learning in Enzyme Engineering. *ACS Catalysis* **2020**, *10*, 1210–1223, DOI: 10.1021/acscatal.9b04321.

[50] J. Jumper, R. Evans, A. Pritzel, T. Green, M. Figurnov, O. Ronneberger, K. Tunyasuvunakool, R. Bates, A. Žídek and A. Potapenko et al. Highly accurate protein structure prediction with AlphaFold. *Nature* **2021**, *596*, 583–589, DOI: 10.1038/s41586-021-03819-2.

[51] S. Neun, P. J. Zurek, T. S. Kaminski and F. Hollfelder. Ultrahigh throughput screening for enzyme function in droplets. *Methods in enzymology* **2020**, *643*, 317–343, DOI: 10.1016/bs.mie.2020.06.002.

[52] A. R. Alcántara, P. Domínguez de María, J. A. Littlechild, M. Schürmann, R. A. Sheldon and R. Wohlgemuth. Biocatalysis as Key to Sustainable Industrial Chemistry. *ChemSusChem* **2022**, e202102709, DOI: 10.1002/cssc.202102709.

[53] R. Wohlgemuth. Biocatalysis - Key enabling tools from biocatalytic one-step and multi-step reactions to biocatalytic total synthesis. *New biotechnology* **2021**, *60*, 113–123, DOI: 10.1016/j.nbt.2020.08.006.

[54] P. N. Devine, R. M. Howard, R. Kumar, M. P. Thompson, M. D. Truppo and N. J. Turner. Extending the application of biocatalysis to meet the challenges of drug development. *Nature Reviews Chemistry* **2018**, *2*, 409–421, DOI: 10.1038/s41570-018-0055-1.

[55] L. E. Zetzsche and A. R. H. Narayan. Broadening the scope of biocatalytic C-C bond formation. *Nature Reviews Chemistry* **2020**, *4*, 334–346, DOI: 10.1038/s41570-020-0191-2.

[56] N. J. Turner and E. O'Reilly. Biocatalytic retrosynthesis. *Nature chemical biology* **2013**, *9*, 285–288, DOI: 10.1038/nchembio.1235.

[57] J. Mlynarski and J. Paradowska. Catalytic asymmetric aldol reactions in aqueous media. *Chemical Society reviews* **2008**, *37*, 1502–1511, DOI: 10.1039/B710577K.

[58] S. R. Marsden, L. Mestrom, D. G. G. McMillan and U. Hanefeld. Thermodynamically and Kinetically Controlled Reactions in Biocatalysis – from Concepts to Perspectives. *ChemCatChem* **2020**, *12*, 426–437, DOI: 10.1002/cctc.201901589.

[59] S. R. Marsden, L. Mestrom, H. J. Wijma, S. J. Noordam, D. G. G. McMillan and U. Hanefeld. Thermodynamics Determine the Diastereochemical Outcome of Catalytic Reactions. *ChemCatChem* **2021**, *13*, 2530–2536, DOI: 10.1002/cctc.202100178.

[60] M. Brovetto, D. Gamenara, P. S. Méndez and G. A. Seoane. C-C bond-forming lyases in organic synthesis. *Chemical reviews* **2011**, *111*, 4346–4403, DOI: 10.1021/cr100299p.

[61] R. Kluger. Ionic intermediates in enzyme-catalyzed carbon-carbon bond formation: patterns, prototypes, probes, and proposals. *Chemical reviews* **1990**, *90*, 1151–1169, DOI: 10.1021/cr00105a005.

[62] W.-D. Fessner, A. Schneider, H. Held, G. Sinerius, C. Walter, M. Hixon and J. V. Schloss. The Mechanism of Class II, Metal-Dependent Aldolases. *Angewandte Chemie (International ed. in English)* **1996**, *35*, 2219–2221, DOI: 10.1002/anie.199622191.

[63] T. D. Machajewski and C.-H. Wong. The Catalytic Asymmetric Aldol Reaction. *Angewandte Chemie (International ed. in English)* **2000**, *39*, 1352–1375, DOI: 10.1002/(SICI)1521-3773(20000417)39:8<1352::AID-ANIE1352>3.0.CO;2-J.

[64] F. W. Alexander, E. Sandmeier, P. K. Mehta and P. Christen. Evolutionary relationships among pyridoxal-5'-phosphate-dependent enzymes. Regio-specific alpha, beta and gamma families. *European journal of biochemistry* **1994**, *219*, 953–960, DOI: 10.1111/j.1432-1033.1994.tb18577.x.

[65] S. Desmons, R. Fauré and S. Bontemps. Formaldehyde as a Promising C 1 Source: The Instrumental Role of Biocatalysis for Stereocontrolled Reactions. *ACS Catalysis* **2019**, *9*, 9575–9588, DOI: 10.1021/acscatal.9b03128.

[66] C. F. Barbas, Y. F. Wang and C. H. Wong. Deoxyribose-5-phosphate aldolase as a synthetic catalyst. *Journal of the American Chemical Society* **1990**, *112*, 2013–2014, DOI: 10.1021/ja00161a064.

[67] M. Dick, R. Hartmann, O. H. Weiergräber, C. Bisterfeld, T. Classen, M. Schwarten, P. Neudecker, D. Willbold and J. Pietruszka. Mechanism-based inhibition of an aldolase at high concentrations of its natural substrate acetaldehyde: structural insights and protective strategies. *Chemical science* **2016**, *7*, 4492–4502, DOI: 10.1039/c5sc04574f.

[68] G. DeSantis, J. Liu, D. P. Clark, A. Heine, I. A. Wilson and C.-H. Wong. Structure-Based mutagenesis approaches toward expanding the substrate specificity of d-2-Deoxyribose-5-phosphate aldolase. *Bioorganic & Medicinal Chemistry* **2003**, *11*, 43–52, DOI: 10.1016/S0968-0896(02)00429-7.

[69] A. Vogel, O. May (Eds.) *Industrial enzyme applications*, Wiley-VCH, Weinheim, **2019**.

[70] M. Schurmann and G. A. Sprenger. Fructose-6-phosphate aldolase is a novel class I aldolase from Escherichia coli and is related to a novel group of bacterial transaldolases. *Journal of Biological Chemistry* **2001**, *276*, 11055–11061, DOI: 10.1074/jbc.M008061200.

[71] D. Güclü, A. Szekrenyi, X. Garrabou, M. Kickstein, S. Junker, P. Clapés and W.-D. Fessner. Minimalist Protein Engineering of an Aldolase Provokes Unprecedented Substrate Promiscuity. *ACS Catalysis* **2016**, *6*, 1848–1852, DOI: 10.1021/acscatal.5b02805.

[72] J. A. Castillo, C. Guérard-Hélaine, M. Gutiérrez, X. Garrabou, M. Sancelme, M. Schürmann, T. Inoue, V. Hélaine, F. Charmantray and T. Gefflaut et al. A Mutant D-Fructose-6-Phosphate Aldolase (Ala129Ser) with Improved Affinity towards Dihydroxyacetone for the Synthesis of Polyhydroxylated Compounds. *Advanced Synthesis & Catalysis* **2010**, *352*, 1039–1046, DOI: 10.1002/adsc.200900772.

[73] J. Yang, S. Sun, Y. Men, Y. Zeng, Y. Zhu, Y. Sun and Y. Ma. Transformation of formaldehyde into functional sugars *via* multi-enzyme stepwise cascade catalysis. *Catalysis Science & Technology* **2017**, *7*, 3459–3463, DOI: 10.1039/C7CY01062A.

[74] P. Bracco, H. Busch, J. von Langermann and U. Hanefeld. Enantioselective synthesis of cyanohydrins catalysed by hydroxynitrile lyases - a review. *Organic & biomolecular chemistry* **2016**, *14*, 6375–6389, DOI: 10.1039/C6OB00934D.

[75] M. Santi, L. Sancineto, V. Nascimento, J. Braun Azeredo, E. V. M. Orozco, L. H. Andrade, H. Gröger and C. Santi. Flow Biocatalysis: A Challenging Alternative for the Synthesis of APIs and Natural Compounds. *International journal of molecular sciences* **2021**, *22,* DOI: 10.3390/ijms22030990.

[76] M. P. van der Helm, P. Bracco, H. Busch, K. Szymańska, A. B. Jarzębski and U. Hanefeld. Hydroxynitrile lyases covalently immobilized in continuous flow microreactors. *Catalysis Science & Technology* **2019**, *9*, 1189–1200, DOI: 10.1039/C8CY02192A.

[77] T. Purkarthofer, K. Gruber, M. Gruber-Khadjawi, K. Waich, W. Skranc, D. Mink and H. Griengl. A biocatalytic Henry reaction--the hydroxynitrile lyase from Hevea brasiliensis also catalyzes nitroaldol reactions. *Angewandte Chemie (International ed. in English)* **2006**, *45*, 3454–3456, DOI: 10.1002/anie.200504230.

[78] H. C. Hailes, D. Rother, M. Müller, R. Westphal, J. M. Ward, J. Pleiss, C. Vogel and M. Pohl. Engineering stereoselectivity of ThDP-dependent enzymes. *The FEBS journal* **2013**, *280*, 6374–6394, DOI: 10.1111/febs.12496.

[79] K. Faber, N. J. Turner and W.-D. Fessner. Science of Synthesis: Biocatalysis in Organic Synthesis, Georg Thieme Verlag, **2015**.

[80] R. Westphal, C. Vogel, C. Schmitz, J. Pleiss, M. Müller, M. Pohl and D. Rother. A tailor-made chimeric thiamine diphosphate dependent enzyme for the direct asymmetric synthesis of (S)-benzoins. *Angewandte Chemie (International ed. in English)* **2014**, *53*, 9376–9379, DOI: 10.1002/anie.201405069.

[81] X. Bugaut and F. Glorius. Organocatalytic umpolung: N-heterocyclic carbenes and beyond. *Chemical Society reviews* **2012**, *41*, 3511–3522, DOI: 10.1039/C2CS15333E.

[82] R. Kluger and K. Tittmann. Thiamin diphosphate catalysis: enzymic and nonenzymic covalent intermediates. *Chemical reviews* **2008**, *108*, 1797–1833, DOI: 10.1021/cr068444m.

[83] S. R. Marsden, L. Gjonaj, S. J. Eustace and U. Hanefeld. Separating Thermodynamics from Kinetics-A New Understanding of the Transketolase Reaction. *ChemCatChem* **2017**, *9*, 1808–1814, DOI: 10.1002/cctc.201601649.

[84] J. Martin, L. Eisoldt and A. Skerra. Fixation of gaseous CO2 by reversing a decarboxylase for the biocatalytic synthesis of the essential amino acid l-methionine. *Nature Catalysis* **2018**, *1*, 555–561, DOI: 10.1038/s41929-018-0107-4.

[85] M. Nattermann, S. Burgener, P. Pfister, A. Chou, L. Schulz, S. H. Lee, N. Paczia, J. Zarzycki, R. Gonzalez and T. J. Erb. Engineering a Highly Efficient Carboligase for Synthetic One-Carbon Metabolism. *ACS Catalysis* **2021**, *11*, 5396–5404, DOI: 10.1021/acscatal.1c01237.

[86] J. B. Siegel, A. L. Smith, S. Poust, A. J. Wargacki, A. Bar-Even, C. Louw, B. W. Shen, C. B. Eiben, H. M. Tran and E. Noor et al. Computational protein design enables a novel one-carbon assimilation pathway. *Proceedings of the National Academy of Sciences* **2015**, *112*, 3704–3709, DOI: 10.1073/pnas.1500545112.

[87] X. Lu, Y. Liu, Y. Yang, S. Wang, Q. Wang, X. Wang, Z. Yan, J. Cheng, C. Liu and X. Yang et al. Constructing a synthetic pathway for acetyl-coenzyme A from one-carbon through enzyme design. *Nature communications* **2019**, *10*, 1378, DOI: 10.1038/s41467-019-09095-z.

[88] H.-J. Jo, J.-H. Kim, Y.-N. Kim, P.-W. Seo, C.-Y. Kim, J.-W. Kim, H. Yu, H. Cheon, E. Y. Lee and J.-S. Kim et al. Glyoxylate carboligase-based whole-cell biotransformation of formaldehyde into ethylene glycol *via* glycolaldehyde. *Green Chemistry* **2022**, *24*, 218–226, DOI: 10.1039/D1GC03549E.

[89] Q. Yin, Y. Shi, J. Wang and X. Zhang. Direct catalytic asymmetric synthesis of α-chiral primary amines. *Chemical Society reviews* **2020**, *49*, 6141–6153, DOI: 10.1039/C9CS00921C.

[90] M. Höhne and U. T. Bornscheuer. Biocatalytic Routes to Optically Active Amines. *ChemCatChem* **2009**, *1*, 42–51, DOI: 10.1002/cctc.200900110.

[91] H. Gröger. Biocatalytic concepts for synthesizing amine bulk chemicals: recent approaches towards linear and cyclic aliphatic primary amines and ω-substituted derivatives thereof. *Applied microbiology and biotechnology* **2019**, *103*, 83–95, DOI: 10.1007/s00253-018-9452-0.

[92] T. C. Nugent. Chiral Amine Synthesis. *Methods, Developments and Applications*, John Wiley & Sons Incorporated, Weinheim, **2009**.

[93] D. J. C. Constable, P. J. Dunn, J. D. Hayler, G. R. Humphrey, J. J. L. Leazer, R. J. Linderman, K. Lorenz, J. Manley, B. A. Pearlman and A. Wells et al. Key green chemistry research areas—a perspective from pharmaceutical manufacturers. *Green Chemistry* **2007**, *9*, 411–420, DOI: 10.1039/B703488C.

[94] G. A. Aleku, S. P. France, H. Man, J. Mangas-Sanchez, S. L. Montgomery, M. Sharma, F. Leipold, S. Hussain, G. Grogan and N. J. Turner. A reductive aminase from Aspergillus oryzae. *Nature chemistry* **2017**, *9*, 961–969, DOI: 10.1038/NCHEM.2782.

[95] F. Steffen-Munsberg, C. Vickers, H. Kohls, H. Land, H. Mallin, A. Nobili, L. Skalden, T. van den Bergh, H.-J. Joosten and P. Berglund et al. Bioinformatic analysis of a PLP-dependent enzyme superfamily suitable for biocatalytic applications. *Biotechnology advances* **2015**, *33*, 566–604, DOI: 10.1016/j.biotechadv.2014.12.012.

[96] H. Yamada, T. Kimura, A. Tanaka and K. Ogata. Amine Transaminase. *Agricultural and Biological Chemistry* **1964**, *28*, 443–450, DOI: 10.1080/00021369.1964.10858262.

[97] J. S. Shin and B. G. Kim. Comparison of the omega-transaminases from different microorganisms and application to production of chiral amines. *Bioscience, biotechnology, and biochemistry* **2001**, *65*, 1782–1788, DOI: 10.1271/bbb.65.1782.

[98] A. Gomm and E. O'Reilly. Transaminases for chiral amine synthesis. *Current opinion in chemical biology* **2018**, *43*, 106–112, DOI: 10.1016/j.cbpa.2017.12.007.

[99] S. A. Kelly, S. Mix, T. S. Moody and B. F. Gilmore. Transaminases for industrial biocatalysis: novel enzyme discovery. *Applied microbiology and biotechnology* **2020**, *104*, 4781–4794, DOI: 10.1007/s00253-020-10585-0.

[100] C. K. Savile, J. M. Janey, E. C. Mundorff, J. C. Moore, S. Tam, W. R. Jarvis, J. C. Colbeck, A. Krebber, F. J. Fleitz and J. Brands et al. Biocatalytic asymmetric synthesis of chiral amines from ketones applied to sitagliptin manufacture. *Science* **2010**, *329*, 305–309, DOI: 10.1126/science.1188934.

[101] A. A. Desai. Sitagliptin manufacture: a compelling tale of green chemistry, process intensification, and industrial asymmetric catalysis. *Angewandte Chemie (International ed. in English)* **2011**, *50*, 1974–1976, DOI: 10.1002/anie.201007051.

[102] M. J. Abrahamson, E. Vázquez-Figueroa, N. B. Woodall, J. C. Moore and A. S. Bommarius. Development of an amine dehydrogenase for synthesis of chiral amines. *Angewandte Chemie (International ed. in English)* **2012**, *51*, 3969–3972, DOI: 10.1002/anie.201107813.

[103] L. J. Ye, H. H. Toh, Y. Yang, J. P. Adams, R. Snajdrova and Z. Li. Engineering of Amine Dehydrogenase for Asymmetric Reductive Amination of Ketone by Evolving Rhodococcus Phenylalanine Dehydrogenase. *ACS Catalysis* **2015**, *5*, 1119–1122, DOI: 10.1021/cs501906r.

[104] D.-H. Wang, Q. Chen, S.-N. Yin, X.-W. Ding, Y.-C. Zheng, Z. Zhang, Y.-H. Zhang, F.-F. Chen, J.-H. Xu and G.-W. Zheng. Asymmetric Reductive Amination of Structurally Diverse Ketones with Ammonia Using a Spectrum-Extended Amine Dehydrogenase. *ACS Catalysis* **2021**, *11*, 14274–14283, DOI: 10.1021/acscatal.1c04324.

[105] C. Wong, D. G. Drueckhammer and H. M. Sweers. Enzymatic vs. fermentative synthesis: thermostable glucose dehydrogenase catalyzed regeneration of NAD(P)H for use in enzymatic synthesis. *Journal of the American Chemical Society* **1985**, *107*, 4028–4031, DOI: 10.1021/ja00299a044.
[106] F. G. Mutti, T. Knaus, N. S. Scrutton, M. Breuer and N. J. Turner. Conversion of alcohols to enantiopure amines through dual-enzyme hydrogen-borrowing cascades. *Science* **2015**, *349*, 1525–1529, DOI: 10.1126/science.aac9283.
[107] F.-F. Chen, G.-W. Zheng, L. Liu, H. Li, Q. Chen, F.-L. Li, C.-X. Li and J.-H. Xu. Reshaping the Active Pocket of Amine Dehydrogenases for Asymmetric Synthesis of Bulky Aliphatic Amines. *ACS Catalysis* **2018**, *8*, 2622–2628, DOI: 10.1021/acscatal.7b04135.
[108] T. Knaus, W. Böhmer and F. G. Mutti. Amine dehydrogenases: efficient biocatalysts for the reductive amination of carbonyl compounds. *Green Chemistry* **2017**, *19*, 453–463, DOI: 10.1039/C6GC01987K.
[109] O. Mayol, K. Bastard, L. Beloti, A. Frese, J. P. Turkenburg, J.-L. Petit, A. Mariage, A. Debard, V. Pellouin and A. Perret et al. A family of native amine dehydrogenases for the asymmetric reductive amination of ketones. *Nature Catalysis* **2019**, *2*, 324–333, DOI: 10.1038/s41929-019-0249-z.
[110] A. Pushpanath, E. Siirola, A. Bornadel, D. Woodlock and U. Schell. Understanding and Overcoming the Limitations of Bacillus badius and Caldalkalibacillus thermarum Amine Dehydrogenases for Biocatalytic Reductive Amination. *ACS Catalysis* **2017**, *7*, 3204–3209, DOI: 10.1021/acscatal.7b00516.
[111] K. Mitsukura, M. Suzuki, K. Tada, T. Yoshida and T. Nagasawa. Asymmetric synthesis of chiral cyclic amine from cyclic imine by bacterial whole-cell catalyst of enantioselective imine reductase. *Organic & biomolecular chemistry* **2010**, *8*, 4533–4535, DOI: 10.1039/C0OB00353K.
[112] J. Mangas-Sanchez, M. Sharma, S. C. Cosgrove, J. I. Ramsden, J. R. Marshall, T. W. Thorpe, R. B. Palmer, G. Grogan and N. J. Turner. Asymmetric synthesis of primary amines catalyzed by thermotolerant fungal reductive aminases. *Chemical science* **2020**, *11*, 5052–5057, DOI: 10.1039/d0sc02253e.
[113] F. Parmeggiani, N. J. Weise, S. T. Ahmed and N. J. Turner. Synthetic and Therapeutic Applications of Ammonia-lyases and Aminomutases. *Chemical reviews* **2018**, *118*, 73–118, DOI: 10.1021/acs.chemrev.6b00824.
[114] F. G. Mutti and T. Knaus in *Biocatalysis for Practitioners* (Eds.: G. de Gonzalo, I. Lavandera), Wiley, **2021**, pp. 143–180.
[115] K. Chen and F. H. Arnold. Engineering new catalytic activities in enzymes. *Nature Catalysis* **2020**, *3*, 203–213, DOI: 10.1038/s41929-019-0385-5.
[116] B. Hauer. Embracing Nature's Catalysts: A Viewpoint on the Future of Biocatalysis. *ACS Catalysis* **2020**, *10*, 8418–8427, DOI: 10.1021/acscatal.0c01708.
[117] C. K. Winkler, J. H. Schrittwieser and W. Kroutil. Power of Biocatalysis for Organic Synthesis. *ACS central science* **2021**, *7*, 55–71, DOI: 10.1021/acscentsci.0c01496.
[118] S. C. Hammer, A. M. Knight and F. H. Arnold. Design and evolution of enzymes for non-natural chemistry. *Current Opinion in Green and Sustainable Chemistry* **2017**, *7*, 23–30, DOI: 10.1016/j.cogsc.2017.06.002.
[119] K. F. Biegasiewicz, S. J. Cooper, X. Gao, D. G. Oblinsky, J. H. Kim, S. E. Garfinkle, L. A. Joyce, B. A. Sandoval, G. D. Scholes and T. K. Hyster. Photoexcitation of flavoenzymes enables a stereoselective radical cyclization. *Science* **2019**, *364*, 1166–1169, DOI: 10.1126/science.aaw1143.
[120] V. B. Urlacher and M. Girhard. Cytochrome P450 Monooxygenases in Biotechnology and Synthetic Biology. *Trends in biotechnology* **2019**, *37*, 882–897, DOI: 10.1016/j.tibtech.2019.01.001.
[121] P. C. E. Moody and E. L. Raven. The Nature and Reactivity of Ferryl Heme in Compounds I and II. *Accounts of chemical research* **2018**, *51*, 427–435, DOI: 10.1021/acs.accounts.7b00463.
[122] M. P. Doyle. Catalytic methods for metal carbene transformations. *Chemical reviews* **1986**, *86*, 919–939, DOI: 10.1021/cr00075a013.
[123] G. Dequirez, V. Pons and P. Dauban. Nitrene chemistry in organic synthesis: still in its infancy? *Angewandte Chemie (International ed. in English)* **2012**, *51*, 7384–7395, DOI: 10.1002/anie.201201945.
[124] Z. Liu and F. H. Arnold. New-to-nature chemistry from old protein machinery: carbene and nitrene transferases. *Current opinion in biotechnology* **2021**, *69*, 43–51, DOI: 10.1016/j.copbio.2020.12.005.
[125] P. S. Coelho, E. M. Brustad, A. Kannan and F. H. Arnold. Olefin cyclopropanation *via* carbene transfer catalyzed by engineered cytochrome P450 enzymes. *Science* **2013**, *339*, 307–310, DOI: 10.1126/science.1231434.
[126] J. A. McIntosh, P. S. Coelho, C. C. Farwell, Z. J. Wang, J. C. Lewis, T. R. Brown and F. H. Arnold. Enantioselective intramolecular C-H amination catalyzed by engineered cytochrome P450 enzymes in vitro and in vivo. *Angewandte Chemie (International ed. in English)* **2013**, *52*, 9309–9312, DOI: 10.1002/anie.201304401.
[127] M. Jeschek, S. Panke and T. R. Ward. Artificial Metalloenzymes on the Verge of New-to-Nature Metabolism. *Trends in biotechnology* **2018**, *36*, 60–72, DOI: 10.1016/j.tibtech.2017.10.003.
[128] F. Schwizer, Y. Okamoto, T. Heinisch, Y. Gu, M. M. Pellizzoni, V. Lebrun, R. Reuter, V. Köhler, J. C. Lewis and T. R. Ward. Artificial Metalloenzymes: Reaction Scope and Optimization Strategies. *Chemical reviews* **2018**, *118*, 142–231, DOI: 10.1021/acs.chemrev.7b00014.
[129] H. J. Davis and T. R. Ward. Artificial Metalloenzymes: Challenges and Opportunities. *ACS central science* **2019**, *5*, 1120–1136, DOI: 10.1021/acscentsci.9b00397.
[130] Y. Lu, N. Yeung, N. Sieracki and N. M. Marshall. Design of functional metalloproteins. *Nature* **2009**, *460*, 855–862, DOI: 10.1038/nature08304.
[131] C. E. Valdez, Q. A. Smith, M. R. Nechay and A. N. Alexandrova. Mysteries of metals in metalloenzymes. *Accounts of chemical research* **2014**, *47*, 3110–3117, DOI: 10.1021/ar500227u.
[132] R. B. Leveson-Gower, C. Mayer and G. Roelfes. The importance of catalytic promiscuity for enzyme design and evolution. *Nature Reviews Chemistry* **2019**, *3*, 687–705, DOI: 10.1038/s41570-019-0143-x.
[133] K. Okrasa and R. J. Kazlauskas. Manganese-substituted carbonic anhydrase as a new peroxidase. *Chemistry–A European Journal* **2006**, *12*, 1587–1596, DOI: 10.1002/chem.200501413.
[134] Q. Jing, K. Okrasa and R. J. Kazlauskas. Stereoselective hydrogenation of olefins using rhodium-substituted carbonic anhydrase--a new reductase. *Chemistry–A European Journal* **2009**, *15*, 1370–1376, DOI: 10.1002/chem.200801673.
[135] Q. Jing and R. J. Kazlauskas. Regioselective Hydroformylation of Styrene Using Rhodium-Substituted Carbonic Anhydrase. *ChemCatChem* **2010**, *2*, 953–957, DOI: 10.1002/cctc.201000159.
[136] T. Haas, R. Krause, R. Weber, M. Demler and G. Schmid. Technical photosynthesis involving CO2 electrolysis and fermentation. *Nature Catalysis* **2018**, *1*, 32–39, DOI: 10.1038/s41929-017-0005-1.
[137] C. Mesters. A Selection of Recent Advances in C1 Chemistry. *Annual review of chemical and biomolecular engineering* **2016**, *7*, 223–238, DOI: 10.1146/annurev-chembioeng-080615-034616.
[138] G. Chen, G. I. N. Waterhouse, R. Shi, J. Zhao, Z. Li, L.-Z. Wu, C.-H. Tung and T. Zhang. From Solar Energy to Fuels: Recent Advances in Light-Driven C1 Chemistry. *Angewandte Chemie (International ed. in English)* **2019**, *58*, 17528–17551, DOI: 10.1002/anie.201814313.

[139] L. V. Teixeira, L. F. Moutinho and A. S. Romão-Dumaresq. Gas fermentation of C1 feedstocks: commercialization status and future prospects. *Biofuels, Bioproducts and Biorefining* **2018**, *12*, 1103–1117, DOI: 10.1002/bbb.1912.
[140] J. T. Fabarius, V. Wegat, A. Roth and V. Sieber. Synthetic Methylotrophy in Yeasts: Towards a Circular Bioeconomy. *Trends in biotechnology* **2021**, *39*, 348–358, DOI: 10.1016/j.tibtech.2020.08.008.
[141] S. Güner, V. Wegat, A. Pick and V. Sieber. Design of a synthetic enzyme cascade for the in vitro fixation of a C 1 carbon source to a functional C 4 sugar. *Green Chemistry* **2021**, *23*, 6583–6590, DOI: 10.1039/D1GC02226A.
[142] H. He, C. Edlich-Muth, S. N. Lindner and A. Bar-Even. Ribulose Monophosphate Shunt Provides Nearly All Biomass and Energy Required for Growth of E. coli. *ACS synthetic biology* **2018**, *7*, 1601–1611, DOI: 10.1021/acssynbio.8b00093.
[143] S. Bontemps, L. Vendier and S. Sabo-Etienne. Ruthenium-catalyzed reduction of carbon dioxide to formaldehyde. *Journal of the American Chemical Society* **2014**, *136*, 4419–4425, DOI: 10.1021/ja500708w.
[144] L. E. Heim, H. Konnerth and M. H. G. Prechtl. Future perspectives for formaldehyde: pathways for reductive synthesis and energy storage. *Green Chemistry* **2017**, *19*, 2347–2355, DOI: 10.1039/C6GC03093A.
[145] A. Butlerow. Bildung einer zuckerartigen Substanz durch Synthese. *European Journal of Organic Chemistry* **1861**, *120*, 295–298, DOI: 10.1002/jlac.18611200308.
[146] R. Breslow. On the mechanism of the formose reaction. *Tetrahedron Letters* **1959**, *1*, 22–26, DOI: 10.1016/S0040-4039(01)99487-0.
[147] S. Poust, J. Piety, A. Bar-Even, C. Louw, D. Baker, J. D. Keasling and J. B. Siegel. Mechanistic Analysis of an Engineered Enzyme that Catalyzes the Formose Reaction. *ChemBioChem* **2015**, *16*, 1950–1954, DOI: 10.1002/cbic.201500228.
[148] S. EYMUR. Umpolung strategy: Advances in catalytic C-C bond formations. *Turkish Journal of Chemistry* **2013,** DOI: 10.3906/kim-1303-85.
[149] L. Zhang, R. Singh, S. D, Z. Guo, J. Li, F. Chen, Y. He, X. Guan, Y. C. Kang and J.-K. Lee. An artificial synthetic pathway for acetoin, 2,3-butanediol, and 2-butanol production from ethanol using cell free multi-enzyme catalysis. *Green Chemistry* **2018**, *20*, 230–242, DOI: 10.1039/C7GC02898A.
[150] T. Li, Z. Tang, H. Wei, Z. Tan, P. Liu, J. Li, Y. Zheng, J. Lin, W. Liu and H. Jiang et al. Totally atom-economical synthesis of lactic acid from formaldehyde: combined bio-carboligation and chemo-rearrangement without the isolation of intermediates. *Green Chemistry* **2020**, *22*, 6809–6814, DOI: 10.1039/D0GC02433C.
[151] J. E. Hodge. Dehydrated Foods, Chemistry of Browning Reactions in Model Systems. *Journal of Agricultural and Food Chemistry* **1953**, *1*, 928–943, DOI: 10.1021/jf60015a004.
[152] R. Jermann, M. Toumiat and D. Imfeld. Development of an in vitro efficacy test for self-tanning formulations. *International journal of cosmetic science* **2002**, *24*, 35–42, DOI: 10.1046/j.0412-5463.2001.00123.x.
[153] Combination of erythrulose and a reducing sugar with self-tanning properties, **2002**.
[154] C. Burger, C. Kessler, S. Gruber, A. Ehrenreich, W. Liebl and D. Weuster-Botz. L-Erythrulose production with a multideletion strain of Gluconobacter oxydans. *Applied microbiology and biotechnology* **2019**, *103*, 4393–4404, DOI: 10.1007/s00253-019-09824-w.
[155] F. Carly and P. Fickers. Erythritol production by yeasts: a snapshot of current knowledge. *Yeast* **2018**, *35*, 455–463, DOI: 10.1002/yea.3306.
[156] J. Bongs, D. Hahn, U. Schörken, G. A. Sprenger, U. Kragl and C. Wandrey. Continuous production of erythrulose using transketolase in a membrane reactor. *Biotechnology letters* **1997**, *19*, 213–216.
[157] I. A. Sevostyanova, O. N. Solovjeva and G. A. Kochetov. A hitherto unknown transketolase-catalyzed reaction. *Biochemical and biophysical research communications* **2004**, *313*, 771–774, DOI: 10.1016/j.bbrc.2003.11.164.
[158] R. K. Mitra, J. M. Woodley and M. D. Lilly. Escherichia coli transketolase-catalyzed carbon-carbon bond formation: biotransformation characterization for reactor evaluation and selection. *Enzyme and Microbial Technology* **1998**, *22*, 64–70, DOI: 10.1016/S0141-0229(97)00106-3.
[159] M. Gyamerah and A. J. Willetts. Kinetics of overexpressed transketolase from Escherichia coli JM 107/pQR 700. *Enzyme and Microbial Technology* **1997**, *20*, 127–134, DOI: 10.1016/S0141-0229(96)00106-8.
[160] F. Baier and N. Tokuriki. Connectivity between catalytic landscapes of the metallo-β-lactamase superfamily. *Journal of molecular biology* **2014**, *426*, 2442–2456, DOI: 10.1016/j.jmb.2014.04.013.
[161] K. Bush and G. A. Jacoby. Updated functional classification of beta-lactamases. *Antimicrobial agents and chemotherapy* **2010**, *54*, 969–976, DOI: 10.1128/AAC.01009-09.
[162] C. Bebrone. Metallo-beta-lactamases (classification, activity, genetic organization, structure, zinc coordination) and their superfamily. *Biochemical pharmacology* **2007**, *74*, 1686–1701, DOI: 10.1016/j.bcp.2007.05.021.
[163] M. W. Crowder, J. Spencer and A. J. Vila. Metallo-beta-lactamases: novel weaponry for antibiotic resistance in bacteria. *Accounts of chemical research* **2006**, *39*, 721–728, DOI: 10.1021/ar0400241.
[164] F. Ely, K. S. Hadler, L. R. Gahan, L. W. Guddat, D. L. Ollis and G. Schenk. The organophosphate-degrading enzyme from Agrobacterium radiobacter displays mechanistic flexibility for catalysis. *The Biochemical journal* **2010**, *432*, 565–573, DOI: 10.1042/BJ20101054.
[165] L. J. Daumann, B. Y. McCarthy, K. S. Hadler, T. P. Murray, L. R. Gahan, J. A. Larrabee, D. L. Ollis and G. Schenk. Promiscuity comes at a price: catalytic versatility vs efficiency in different metal ion derivatives of the potential bioremediator GpdQ. *Biochimica et biophysica acta* **2013**, *1834*, 425–432, DOI: 10.1016/j.bbapap.2012.02.004.
[166] M. M. Pedroso, J. A. Larrabee, F. Ely, S. E. Gwee, N. Mitić, D. L. Ollis, L. R. Gahan and G. Schenk. Ca(II) Binding Regulates and Dominates the Reactivity of a Transition-Metal-Ion-Dependent Diesterase from Mycobacterium tuberculosis. *Chemistry–A European Journal* **2016**, *22*, 999–1009, DOI: 10.1002/chem.201504001.
[167] M. Toesch, M. Schober, R. Breinbauer and K. Faber. Stereochemistry and Mechanism of Enzymatic and Non-Enzymatic Hydrolysis of Benzylic sec-Sulfate Esters. *European Journal of Organic Chemistry* **2014**, *2014*, 3930-3034, DOI: 10.1002/ejoc.201402211.
[168] M. Toesch, M. Schober and K. Faber. Microbial alkyl- and aryl-sulfatases: mechanism, occurrence, screening and stereoselectivities. *Applied microbiology and biotechnology* **2014**, *98*, 1485–1496, DOI: 10.1007/s00253-013-5438-0.
[169] M. Schober, P. Gadler, T. Knaus, H. Kayer, R. Birner-Grünberger, C. Gülly, P. Macheroux, U. Wagner and K. Faber. A stereoselective inverting sec-alkylsulfatase for the deracemization of sec-alcohols. *Organic letters* **2011**, *13*, 4296–4299, DOI: 10.1021/ol201635y.
[170] M. Schober, T. Knaus, M. Toesch, P. Macheroux, U. Wagner and K. Faber. The Substrate Spectrum of the Inverting sec-Alkylsulfatase Pisa1. *Advanced Synthesis & Catalysis* **2012**, *354*, 1737–1742, DOI: 10.1002/adsc.201100864.
[171] P. Gadler and K. Faber. New enzymes for biotransformations: microbial alkyl sulfatases displaying stereo- and enantioselectivity. *Trends in biotechnology* **2007**, *25*, 83–88, DOI: 10.1016/j.tibtech.2006.11.006.
[172] P. Gadler and K. Faber. Highly Enantioselective Biohydrolysis ofsec-Alkyl Sulfate Esters with Inversion of Configuration Catalysed byPseudomonas spp. *European Journal of Organic Chemistry* **2007**, *2007*, 5527–5530, DOI: 10.1002/ejoc.200700637.

[173] M. Schober and K. Faber. Inverting hydrolases and their use in enantioconvergent biotransformations. *Trends in biotechnology* **2013**, *31*, 468–478, DOI: 10.1016/j.tibtech.2013.05.005.
[174] G. Hagelueken, T. M. Adams, L. Wiehlmann, U. Widow, H. Kolmar, B. Tümmler, D. W. Heinz and W.-D. Schubert. The crystal structure of SdsA1, an alkylsulfatase from Pseudomonas aeruginosa, defines a third class of sulfatases. *Proceedings of the National Academy of Sciences* **2006**, *103*, 7631–7636, DOI: 10.1073/pnas.0510501103.
[175] M. Long, L. Ruan, F. Li, Z. Yu and X. Xu. Heterologous expression and characterization of a recombinant thermostable alkylsulfatase (sdsAP). *Extremophiles : life under extreme conditions* **2011**, *15*, 293–301, DOI: 10.1007/s00792-011-0357-4.
[176] T. Knaus, M. Schober, B. Kepplinger, M. Faccinelli, J. Pitzer, K. Faber, P. Macheroux and U. Wagner. Structure and mechanism of an inverting alkylsulfatase from Pseudomonas sp. DSM6611 specific for secondary alkyl sulfates. *The FEBS journal* **2012**, *279*, 4374–4384, DOI: 10.1111/febs.12027.
[177] D. R. Edwards, D. C. Lohman and R. Wolfenden. Catalytic proficiency: the extreme case of S-O cleaving sulfatases. *Journal of the American Chemical Society* **2012**, *134*, 525–531, DOI: 10.1021/ja208827q.
[178] M. Schober, M. Toesch, T. Knaus, G. A. Strohmeier, B. van Loo, M. Fuchs, F. Hollfelder, P. Macheroux and K. Faber. One-pot deracemization of sec-alcohols: enantioconvergent enzymatic hydrolysis of alkyl sulfates using stereocomplementary sulfatases. *Angewandte Chemie (International ed. in English)* **2013**, *52*, 3277–3279, DOI: 10.1002/anie.201209946.
[179] T. A. Hamlin, M. Swart and F. M. Bickelhaupt. Nucleophilic Substitution (SN 2): Dependence on Nucleophile, Leaving Group, Central Atom, Substituents, and Solvent. *Chemphyschem : a European journal of chemical physics and physical chemistry* **2018**, *19*, 1315–1330, DOI: 10.1002/cphc.201701363.
[180] I. Fleming. Grenzorbitale und Reaktionen organischer Verbindungen, VCH, Weinheim, Basel (Schweiz), Cambridge, New York, NY, **1990**.
[181] X.-Y. Shang, H.-Y. An, T. Zhang, J.-H. Lin, F. Hao, D.-H. Yu, J.-C. Xiao and T.-D. Li. Evaluating and understanding the affinity of metal ions to water and ammonia using density functional theory calculation. *Chemical Physics Letters* **2021**, *768*, 138398, DOI: 10.1016/j.cplett.2021.138398.
[182] D. Walter and P. B. Armentrout. Sequential Bond Dissociation Energies of M + (NH 3) x (x = 1−4) for M = Ti−Cu. *Journal of the American Chemical Society* **1998**, *120*, 3176–3187, DOI: 10.1021/ja973202c.
[183] D. E. Clemmer and P. B. Armentrout. Ammonia activation by cobalt(1+), nickel(1+) and copper(1+): metal(1+)-amidogen bond energies and metal(1+)…ammonia adduct lifetimes. *The Journal of Physical Chemistry* **1991**, *95*, 3084–3090, DOI: 10.1021/j100161a025.
[184] R. Machielsen, A. R. Uria, S. W. M. Kengen and J. van der Oost. Production and characterization of a thermostable alcohol dehydrogenase that belongs to the aldo-keto reductase superfamily. *Applied and environmental microbiology* **2006**, *72*, 233–238, DOI: 10.1128/AEM.72.1.233-238.2006.
[185] J. G. Ortiz-Tena, B. Rühmann and V. Sieber. Colorimetric Determination of Sulfate *via* an Enzyme Cascade for High-Throughput Detection of Sulfatase Activity. *Analytical chemistry* **2018**, *90*, 2526–2533, DOI: 10.1021/acs.analchem.7b03719.
[186] C. Mülhardt. Der Experimentator: Molekularbiologie, Genomics, Springer, **2009**.
[187] F. M. Ausubel, R. Brent, R. E. Kingston, D. D. Moore, J. G. Seidman, J. A. Smith and K. Struhl. Current protocols in molecular biology, vol. 1 John Wiley & Sons. *Inc., Hoboken, NJ* **2003**.
[188] Agilent Technologies. QuikChange site-directed mutagenesis kit Instruction manual for research use only **2005**.
[189] S. Cheng, C. Fockler, W. M. Barnes and R. Higuchi. Effective amplification of long targets from cloned inserts and human genomic DNA. *Proceedings of the National Academy of Sciences* **1994**, *91*, 5695–5699.
[190] E. M. Williams, J. N. Copp and D. F. Ackerley. Site-saturation mutagenesis by overlap extension PCR. *Methods in molecular biology* **2014**, *1179*, 83–101, DOI: 10.1007/978-1-4939-1053-3_6.
[191] J. G. Ortiz Tena, *Dissertation*, Technische Universität München, München, **2019**.
[192] C. N. Pace, F. Vajdos, L. Fee, G. Grimsley and T. Gray. How to measure and predict the molar absorption coefficient of a protein. *Protein science* **1995**, *4*, 2411–2423.
[193] S. Boivin, S. Kozak and R. Meijers. Optimization of protein purification and characterization using Thermofluor screens. *Protein expression and purification* **2013**, *91*, 192–206, DOI: 10.1016/j.pep.2013.08.002.
[194] G. F. White, V. Lillis and D. J. Shaw. An improved procedure for the preparation of alkyl sulphate esters suitable for the study of secondary alkylsulphohydrolase enzymes. *Biochemical Journal* **1980**, *187*, 191–196, DOI: 10.1042/bj1870191.
[195] Y. P. Liu, H. Li, Y. Sun and Z. S. Zhou. Determination of 1, 3-dihydroxyacetone in fermentation broth by spectrophotometry. *Chin J Pharm* **2011**, *42*, 834–837.
[196] A. N. Simonov, L. G. Matvienko, O. P. Pestunova, V. N. Parmon, N. A. Komandrova, V. A. Denisenko and V. E. Vas'kovskii. Selective synthesis of erythrulose and 3-pentulose from formaldehyde and dihydroxyacetone catalyzed by phosphates in a neutral aqueous medium. *Kinetics and Catalysis* **2007**, *48*, 550–555, DOI: 10.1134/S0023158407040118.
[197] J. Bongs, D. Hahn, U. Schörken, G. A. Sprenger, U. Kragl and C. Wandrey. Continuous production of erythrulose using transketolase in a membrane reactor. *Biotechnology letters* **1997**, *19*, 213–216.
[198] W. H. Faveere, S. van Praet, B. Vermeeren, K. N. R. Dumoleijn, K. Moonen, E. Taarning and B. F. Sels. Toward Replacing Ethylene Oxide in a Sustainable World: Glycolaldehyde as a Bio-Based C2 Platform Molecule. *Angewandte Chemie (International ed. in English)* **2021**, *60*, 12204–12223, DOI: 10.1002/anie.202009811.
[199] W. Faveere, T. Mihaylov, M. Pelckmans, K. Moonen, F. Gillis-D'Hamers, R. Bosschaerts, K. Pierloot and B. F. Sels. Glycolaldehyde as a Bio-Based C 2 Platform Chemical: Catalytic Reductive Amination of Vicinal Hydroxyl Aldehydes. *ACS Catal.* **2020**, *10*, 391–404, DOI: 10.1021/acscatal.9b02437.
[200] T. Schreier, R. Jermann. Combination of erythrulose and a reducing sugar with self-tanning properties, **2002**, Google Patents.
[201] T. Gross, A. M. Seayad, M. Ahmad and M. Beller. Synthesis of primary amines: first homogeneously catalyzed reductive amination with ammonia. *Organic letters* **2002**, *4*, 2055–2058, DOI: 10.1021/ol0200605.
[202] U. Markel, D. F. Sauer, J. Schiffels, J. Okuda and U. Schwaneberg. Towards the Evolution of Artificial Metalloenzymes-A Protein Engineer's Perspective. *Angewandte Chemie (International ed. in English)* **2019**, *58*, 4454–4464, DOI: 10.1002/anie.201811042.
[203] B. Höcker. Protein design: A metalloenzyme reloaded. *Nature chemical biology* **2012**, *8*, 224–225, DOI: 10.1038/nchembio.800.
[204] S. Kozuch and J. M. L. Martin. "Turning Over" Definitions in Catalytic Cycles. *ACS Catalysis* **2012**, *2*, 2787–2794, DOI: 10.1021/cs3005264.
[205] C. J. Jackson, C. W. Coppin, P. D. Carr, A. Aleksandrov, M. Wilding, E. Sugrue, J. Ubels, M. Paks, J. Newman and T. S. Peat et al. 300-Fold increase in production of the Zn2+-dependent dechlorinase TrzN in soluble form *via* apoenzyme stabilization. *Applied and environmental microbiology* **2014**, *80*, 4003–4011, DOI: 10.1128/AEM.00916-14.
[206] R. Paul-Soto, M. Hernandez-Valladares, M. Galleni, R. Bauer, M. Zeppezauer, J.-M. Frère and H.-W. Adolph. Mono- and binuclear Zn-β-lactamase from Bacteroides fragilis : catalytic and structural roles of the zinc ions. *FEBS Letters* **1998**, *438*, 137–140, DOI: 10.1016/s0014-5793(98)01289-7.

[207] C. Aguirre, Y. Goto and M. Costas. Thermal and chemical unfolding pathways of PaSdsA1 sulfatase, a homo-dimer with topologically interlinked chains. *FEBS Letters* **2016**, *590*, 202–214, DOI: 10.1002/1873-3468.12041.
[208] A. R. Palacios, M. F. Mojica, E. Giannini, M. A. Taracila, C. R. Bethel, P. M. Alzari, L. H. Otero, S. Klinke, L. I. Llarrull and R. A. Bonomo et al. The Reaction Mechanism of Metallo-β-Lactamases Is Tuned by the Conformation of an Active-Site Mobile Loop. *Antimicrobial agents and chemotherapy* **2019**, *63,* DOI: 10.1128/AAC.01754-18.
[209] J. Reedijk and N. Tarasova. The International Year of the Periodic Table 2019. *Chemistry International* **2019**, *41*, 2–5, DOI: 10.1515/ci-2019-0101.
[210] P. Schwerdtfeger, O. R. Smits and P. Pyykkö. The periodic table and the physics that drives it. *Nature Reviews Chemistry* **2020**, *4*, 359–380, DOI: 10.1038/s41570-020-0195-y.
[211] N. E. Dixon, T. C. Gazzola, R. L. blakeley and B. Zermer. Letter: Jack bean urease (EC 3.5.1.5). A metalloenzyme. A simple biological role for nickel? *Journal of the American Chemical Society* **1975**, *97*, 4131–4133, DOI: 10.1021/ja00847a045.
[212] B. van den Berg, R. J. Ellis and C. M. Dobson. Effects of macromolecular crowding on protein folding and aggregation. *The EMBO journal* **1999**, *18*, 6927–6933, DOI: 10.1093/emboj/18.24.6927.
[213] C. N. Pace, G. R. Grimsley and J. M. Scholtz in *Protein Science Encyclopedia* (Ed.: A. R. Fersht), Wiley-VCH Verlag GmbH & Co. KGaA, Weinheim, Germany, **2008**.
[214] R. J. Kula, D. T. Sawyer, S. I. Chan and C. M. Finley. Nuclear Magnetic Resonance Studies of Metal-Ethylenediaminetetraacetic Acid Complexes. *Journal of the American Chemical Society* **1963**, *85*, 2930–2936, DOI: 10.1021/ja00902a016.
[215] K. S. Hadler, E. A. Tanifum, S. H.-C. Yip, N. Mitić, L. W. Guddat, C. J. Jackson, L. R. Gahan, K. Nguyen, P. D. Carr and D. L. Ollis et al. Substrate-promoted formation of a catalytically competent binuclear center and regulation of reactivity in a glycerophosphodiesterase from Enterobacter aerogenes. *Journal of the American Chemical Society* **2008**, *130*, 14129–14138, DOI: 10.1021/ja803346w.
[216] S. Tadrowski, M. M. Pedroso, V. Sieber, J. A. Larrabee, L. W. Guddat and G. Schenk. Metal Ions Play an Essential Catalytic Role in the Mechanism of Ketol-Acid Reductoisomerase. *Chemistry–A European Journal* **2016**, *22*, 7427–7436, DOI: 10.1002/chem.201600620.
[217] M. Karplus and D. L. Weaver. Protein-folding dynamics. *Nature* **1976**, *260*, 404–406, DOI: 10.1038/260404a0.
[218] N. J. Greenfield. Using circular dichroism spectra to estimate protein secondary structure. *Nature protocols* **2006**, *1*, 2876–2890, DOI: 10.1038/nprot.2006.202.
[219] R. L. Vellanoweth and J. C. Rabinowitz. The influence of ribosome-binding-site elements on translational efficiency in Bacillus subtilis and Escherichia coli in vivo. *Molecular microbiology* **1992**, *6*, 1105–1114, DOI: 10.1111/j.1365-2958.1992.tb01548.x.
[220] H. M. Salis, E. A. Mirsky and C. A. Voigt. Automated design of synthetic ribosome binding sites to control protein expression. *Nature biotechnology* **2009**, *27*, 946–950, DOI: 10.1038/nbt.1568.
[221] B. S. Laursen, H. P. Sørensen, K. K. Mortensen and H. U. Sperling-Petersen. Initiation of protein synthesis in bacteria. *Microbiology and molecular biology reviews* **2005**, *69*, 101–123, DOI: 10.1128/MMBR.69.1.101-123.2005.
[222] F. Schneider. Histidine in enzyme active centers. *Angewandte Chemie (International ed. in English)* **1978**, *17*, 583–592, DOI: 10.1002/anie.197805831.
[223] S. Li and M. Hong. Protonation, tautomerization, and rotameric structure of histidine: a comprehensive study by magic-angle-spinning solid-state NMR. *Journal of the American Chemical Society* **2011**, *133*, 1534–1544, DOI: 10.1021/ja108943n.
[224] L. A. Wilson, E. G. Knaven, M. T. Morris, M. Monteiro Pedroso, C. J. Schofield, T. B. Brück, M. Boden, D. W. Waite, P. Hugenholtz and L. Guddat et al. Kinetic and Structural Characterization of the First B3 Metallo-β-Lactamase with an Active-Site Glutamic Acid. *Antimicrobial agents and chemotherapy* **2021**, *65*, e0093621, DOI: 10.1128/AAC.00936-21.
[225] L. Sun, P. Chen, Y. Su, Z. Cai, L. Ruan, X. Xu and Y. Wu. Crystal structure of thermostable alkylsulfatase SdsAP from Pseudomonas sp. S9. *Bioscience reports* **2017**, *37,* DOI: 10.1042/BSR20170001.
[226] S. Lee, A. Khanal, A.-H. Cho, H. Lee, M.-S. Kang, T. Unno, H.-G. Hur and J.-H. Lee. Cupriavidus sp. strain Ni-2 resistant to high concentration of nickel and its genes responsible for the tolerance by genome comparison. *Archives of microbiology* **2019**, *201*, 1323–1331, DOI: 10.1007/s00203-019-01700-5.
[227] J. M. Sanchez-Ruiz. Protein kinetic stability. *Biophysical chemistry* **2010**, *148*, 1–15, DOI: 10.1016/j.bpc.2010.02.004.
[228] F. J. Golemba, J. E. Guillet and S. C. Nyburg. Synthesis and crystal structure of isotactic poly-4-phenyl-1-butene. *Journal of Polymer Science Part A-1: Polymer Chemistry* **1968**, *6*, 1341–1349, DOI: 10.1002/pol.1968.150060525.
[229] K. Endo and T. Otsu. Monomer-isomerization polymerization. XV. Monomer-isomerization polymerization of 4-phenyl-2-butene with Ziegler-Natta catalyst. *Journal of Polymer Science: Polymer Chemistry Edition* **1976**, *14*, 2083–2085, DOI: 10.1002/pol.1976.170140825.
[230] W. Zhu and T. B. Gunnoe. Advances in Group 10 Transition-Metal-Catalyzed Arene Alkylation and Alkenylation. *Journal of the American Chemical Society* **2021**, *143*, 6746–6766, DOI: 10.1021/jacs.1c01810.
[231] Y. Chen, J. Chen, C. Chang, J. Chen, F. Cao, J. Zhao, Y. Zheng and J. Zhu. Physicochemical and functional properties of proteins extracted from three microalgal species. *Food Hydrocolloids* **2019**, *96*, 510–517, DOI: 10.1016/j.foodhyd.2019.05.025.
[232] M. Zhao, H.-B. Wang, L.-N. Ji and Z.-W. Mao. Insights into metalloenzyme microenvironments: biomimetic metal complexes with a functional second coordination sphere. *Chemical Society reviews* **2013**, *42*, 8360–8375, DOI: 10.1039/c3cs60162e.
[233] M. C. Manning, K. Patel and R. T. Borchardt. Stability of protein pharmaceuticals. *Pharmaceutical Research* **1989**, *6*, 903–918, DOI: 10.1023/A:1015929109894.
[234] D. B. Volkin, H. Mach and C. R. Middaugh. Degradative covalent reactions important to protein stability. *Molecular Biotechnology* **1997**, *8*, 105–122, DOI: 10.1007/bf02752255.
[235] R. Jaenicke. Stability and stabilization of globular proteins in solution. *Journal of Biotechnology* **2000**, *79*, 193–203, DOI: 10.1016/S0168-1656(00)00236-4.
[236] T. J. Anchordoquy and J. F. Carpenter. Polymers protect lactate dehydrogenase during freeze-drying by inhibiting dissociation in the frozen state. *Archives of Biochemistry and Biophysics* **1996**, *332*, 231–238, DOI: 10.1006/abbi.1996.0337.
[237] T. Burgdorf, E. van der Linden, M. Bernhard, Q. Y. Yin, J. W. Back, A. F. Hartog, A. O. Muijsers, C. G. de Koster, S. P. J. Albracht and B. Friedrich. The soluble NAD+-Reducing NiFe-hydrogenase from Ralstonia eutropha H16 consists of six subunits and can be specifically activated by NADPH. *Journal of bacteriology* **2005**, *187*, 3122–3132, DOI: 10.1128/JB.187.9.3122-3132.2005.
[238] Z. Kiss. The zinc chelator 1,10-phenanthroline enhances the stimulatory effects of protein kinase C activators and staurosporine, but not sphingosine and H2O2, on phospholipase D activity in NIH 3T3 fibroblasts. *The Biochemical journal* **1994**, *298 (Pt 1)*, 93–98, DOI: 10.1042/bj2980093.
[239] D. Dobritzsch, H. Wang, G. Schneider and S. Yu. Structural and functional characterization of ochratoxinase, a novel mycotoxin-degrading enzyme. *The Biochemical journal* **2014**, *462*, 441–452, DOI: 10.1042/BJ20140382.
[240] Z. Hu, G. R. Periyannan and M. W. Crowder. Folding strategy to prepare Co(II)-substituted metallo-beta-lactamase L1. *Analytical biochemistry* **2008**, *378*, 177–183, DOI: 10.1016/j.ab.2008.04.007.
[241] S. R. Martin and M. J. Schilstra in *Methods in Cell Biology*, Elsevier, **2008**, pp. 263–293.

[242] J. F. Maune, K. Beckingham, S. R. Martin and P. M. Bayley. Circular dichroism studies on calcium binding to two series of Ca2+ binding site mutants of Drosophila melanogaster calmodulin. *Biochemistry* **1992**, *31*, 7779–7786, DOI: 10.1021/bi00149a006.
[243] U. Suttisansanee, K. Lau, S. Lagishetty, K. N. Rao, S. Swaminathan, J. M. Sauder, S. K. Burley and J. F. Honek. Structural variation in bacterial glyoxalase I enzymes: investigation of the metalloenzyme glyoxalase I from Clostridium acetobutylicum. *The Journal of biological chemistry* **2011**, *286*, 38367–38374, DOI: 10.1074/jbc.M111.251603.
[244] I. Boltes, H. Czapinska, A. Kahnert, R. von Bülow, T. Dierks, B. Schmidt, K. von Figura, M. A. Kertesz and I. Usón. 1.3 Å Structure of Arylsulfatase from Pseudomonas aeruginosa Establishes the Catalytic Mechanism of Sulfate Ester Cleavage in the Sulfatase Family. *Structure* **2001**, *9*, 483–491, DOI: 10.1016/S0969-2126(01)00609-8.
[245] J. K. Kim, C. Lee, S. W. Lim, A. Adhikari, J. T. Andring, R. McKenna, C.-M. Ghim and C. U. Kim. Elucidating the role of metal ions in carbonic anhydrase catalysis. *Nature communications* **2020**, *11*, 4557, DOI: 10.1038/s41467-020-18425-5.
[246] J. Axelrod and R. Tomchick. Enzymatic O-Methylation of Epinephrine and Other Catechols. *Journal of Biological Chemistry* **1958**, *233*, 702–705, DOI: 10.1016/s0021-9258(18)64731-3.
[247] M. Sparta and A. N. Alexandrova. How metal substitution affects the enzymatic activity of catechol-o-methyltransferase. *PloS one* **2012**, *7*, e47172, DOI: 10.1371/journal.pone.0047172.
[248] E. R. Featherston and J. A. Cotruvo. The biochemistry of lanthanide acquisition, trafficking, and utilization. *Biochimica et biophysica acta. Molecular cell research* **2021**, *1868*, 118864, DOI: 10.1016/j.bbamcr.2020.118864.
[249] A. M. Shiller, E. W. Chan, D. J. Joung, M. C. Redmond and J. D. Kessler. Light rare earth element depletion during Deepwater Horizon blowout methanotrophy. *Scientific reports* **2017**, *7*, 10389, DOI: 10.1038/s41598-017-11060-z.
[250] R. Friedman. Preferential Binding of Lanthanides to Methanol Dehydrogenase Evaluated with Density Functional Theory. *The journal of physical chemistry. B* **2021**, *125*, 2251–2257, DOI: 10.1021/acs.jpcb.0c11077.
[251] C. Hogendoorn, P. Roszczenko-Jasińska, N. C. Martinez-Gomez, J. de Graaff, P. Grassl, A. Pol, H. J. M. Op den Camp and L. J. Daumann. Facile Arsenazo III-Based Assay for Monitoring Rare Earth Element Depletion from Cultivation Media for Methanotrophic and Methylotrophic Bacteria. *Applied and environmental microbiology* **2018**, *84,* DOI: 10.1128/AEM.02887-17.
[252] L. J. Daumann. Essential and Ubiquitous: The Emergence of Lanthanide Metallobiochemistry. *Angewandte Chemie (International ed. in English)* **2019**, *58*, 12795–12802, DOI: 10.1002/anie.201904090.
[253] J. A. Cotruvo. The Chemistry of Lanthanides in Biology: Recent Discoveries, Emerging Principles, and Technological Applications. *ACS central science* **2019**, *5*, 1496–1506, DOI: 10.1021/acscentsci.9b00642.
[254] P. Mandal, J. Kretzschmar and B. Drobot. Not just a background: pH buffers do interact with lanthanide ions-a Europium(III) case study. *Journal of biological inorganic chemistry* **2022**, *27*, 249–260, DOI: 10.1007/s00775-022-01930-x.
[255] S. Lim and S. J. Franklin. Lanthanide-binding peptides and the enzymes that Might Have Been. *Cellular and molecular life sciences* **2004**, *61*, 2184–2188, DOI: 10.1007/s00018-004-4156-2.
[256] J. Rumble. CRC handbook of chemistry and physics (100th ed.). Boca Rotan, FL, **2019**, CRC Press, Taylor and Francis Group.
[257] Z. Luo, C. A. Whitcomb, N. Kaylor, Y. Zhang, S. Zhang, R. J. Davis and T. B. Gunnoe. Oxidative Alkenylation of Arenes Using Supported Rh Materials: Evidence that Active Catalysts are Formed by Rh Leaching. *ChemCatChem* **2021**, *13*, 260–270, DOI: 10.1002/cctc.202001526.
[258] Z. Liu, K. Wang, Y. Chen, T. Tan and J. Nielsen. Third-generation biorefineries as the means to produce fuels and chemicals from CO2. *Nature Catalysis* **2020**, *3*, 274–288, DOI: 10.1038/s41929-019-0421-5.
[259] P. Intasian, K. Prakinee, A. Phintha, D. Trisrivirat, N. Weeranoppanant, T. Wongnate and P. Chaiyen. Enzymes, In Vivo Biocatalysis, and Metabolic Engineering for Enabling a Circular Economy and Sustainability. *Chemical reviews* **2021**, *121*, 10367–10451, DOI: 10.1021/acs.chemrev.1c00121.
[260] T. Cai, H. Sun, J. Qiao, L. Zhu, F. Zhang, J. Zhang, Z. Tang, X. Wei, J. Yang and Q. Yuan et al. Cell-free chemoenzymatic starch synthesis from carbon dioxide. *Science* **2021**, *373*, 1523–1527, DOI: 10.1126/science.abh4049.
[261] N. Massad and S. Banta. Development of a kinetic model and figures of merit for formaldehyde carboligations catalyzed by formolase enzymes. *Biotechnology and bioengineering* **2022,** DOI: 10.1002/bit.28217.
[262] W. Zhang, T. Zhang, B. Jiang and W. Mu. Enzymatic approaches to rare sugar production. *Biotechnology advances* **2017**, *35*, 267–274, DOI: 10.1016/j.biotechadv.2017.01.004.
[263] G. U. YUEN and J. M. SUGIHARA. Crystalline D,L-xylo-3-Hexulose, A New Hexose 1. *The Journal of Organic Chemistry* **1961**, *26*, 1598–1601, DOI: 10.1021/jo01064a070.
[264] Y. Xu, P. Chi, J. Lv, M. Bilal and H. Cheng. L-Xylo-3-hexulose, a new rare sugar produced by the action of acetic acid bacteria on galactitol, an exception to Bertrand Hudson's rule. *Biochimica et biophysica acta* **2021**, *1865*, 129740, DOI: 10.1016/j.bbagen.2020.129740.
[265] S. L. Lovelock, R. Crawshaw, S. Basler, C. Levy, D. Baker, D. Hilvert and A. P. Green. The road to fully programmable protein catalysis. *Nature* **2022**, *606*, 49–58, DOI: 10.1038/s41586-022-04456-z.